Sheffield Hallam University

A Sheffield Hallam University thesis

217

Finite Element Model of a Tennis Ball Impact with a Racket

Thomas Bruce Allen

A thesis submitted in partial fulfilment of the requirements of

Sheffield Hallam University

for the degree of Doctor of Philosophy

April 2009

Collaborating Organisation: Prince

Abstract

Previous authors have produced analytical models which accurately simulate tennis impacts. However, currently there are few published studies on the simulation of tennis impacts using finite-element (FE) technique. The purpose of this study was to produce accurate FE models of tennis impacts, which will serve as design tools as well as aid in furthering the understanding of how the ball, string-bed and racket behave during play.

An FE model of a pressurised tennis ball was produced in Ansys/LS-DYNA 10.0 and validated against experimental data. The ball model was updated to simulate the extreme playing temperatures of 10 and 40°C and validated against experimental data, obtained inside a climate chamber. Following validation of the ball model, an FE model of a head-clamped racket was produced and validated against experimental data. The validation included a range of inbound velocities, angles and spin rates, for impacts at a number of nominal locations on the string-bed. Finally, an FE model of a freely suspended racket was constructed and validated against experimental data. Impacts were simulated at a number of nominal impact locations on the string-bed, with a range of ball inbound velocities, angles and spin rates. The impacts were recorded using two *Phantom v4.2* high-speed cameras and analysed in 3D. The FE models were all in good agreement with the experimental data, for the individual stages of the validation.

A parametric modelling program was produced to be used in conjunction with the model. This program enables the user to adjust a variety of parameters, such as the inbound velocity of the ball, impact location and mass of the racket, and run simulations without any specialist knowledge of the FE model. This program was used to analyse the model against ball to racket impact data obtained during player testing. There was relatively good agreement between the model and player testing data.

Finally, the model was used to determine the influence of racket structural stiffness, mass and the position of the balance point, when performing a typical topspin forehand. It was found that using a head-heavy racket, with high structural stiffness and mass, will increase the rebound velocity and topspin of the ball, for a shot of this type at the centre of the string-bed.

Keywords: tennis ball, tennis racket, high speed cinematography, finite-element modelling.

Acknowledgements

Contents

List of figures

XVII

List of tables

Nomenclature

Roman letters

A	Cross sectional area	$[m^2]$
E	Young's Modulus	$[N \cdot m^{-2}]$
f_n	Natural frequency	$[Hz]$
G	Shear Modulus	$[N \cdot m^{-2}]$
I	Moment of inertia	$[kg \cdot m^{-2}]$
K	Dynamic modulus of strings	$[N \cdot m^{-1}]$
k	Structural stiffness of racket	$[N \cdot m^{-1}]$
L	Length	$[m]$
m	Racket mass	$[kg]$
P	Pressure	$[N \cdot m^{-2}]$
T	Period of torsional vibration	$[s]$
V	Volume	$[m^3]$

Greek letters

ν	Poisson's ratio	
θ	Inbound angle relative to racket normal	
μ	Coefficient of friction	

XXI

1. Introduction

The following chapters contain a three year study into the creation and validation of a finite element (FE) model of an impact between a tennis ball and racket.

1.1. Motivation for the Research

Over the years, tennis technology has developed, which has had an enormous impact on the way the game is played. Racket materials have changed from wood to aluminium, to the oversized, more exotic composite ones used today (Haake *et al.,* 2007). These advances have allowed players to hit shots faster and with greater accuracy (Brody, 1997a), effectively increasing the speed of the game (Brody, 1997b). However, this is also believed to have increased the dominance of the server and there is growing apprehension that this is resulting in a reduction in spectator appeal (Kotze *et al.,* 2000). The International Tennis Federation (ITF) is concerned with maintaining public and commercial interest, in order to prevent the demise of the sport through lack of financial support. To successfully regulate a sport, such as tennis, the governing body needs a full understanding of the physical principles and technologies within the game. Thus, the ITF set up a Technical Department in 1997 in order to monitor and direct scientific advances in the sport (ITF Technical Department, 2009).

As a scientific subject area, tennis is well publicised with advances in knowledge and technology coming from within academia and industry. Researchers, scientists and engineers have simulated the various aspects of the game through conventional laboratory investigations, which can be both costly and time consuming. A large number of published studies have been concerned with creating analytical models. Discrepancies between publications have arisen due to errors and assumptions in both experimental and modelling techniques.

The sponsors of this project are *Prince* whose principal aim is to design and manufacture tennis rackets, for use by both amateur and professional players. *Prince* require a tool which can be used to aid the design of their next generation of rackets, which must conform to the current rules of the ITF. This tool should be straightforward and easy to use to enable it to fit seamlessly into their existing design process. FE models have been successfully applied to

1

increase the physical understanding of other sports and aid in the design of equipment. This project is concerned with constructing an accurate FE model to form the basis of a tennis racket design tool. The intention of this project is to highlight and explain areas of disagreement between previous studies and also to evaluate the suitability of FE technique for modelling tennis ball impacts.

1.2. Aim and objectives

The aim of this thesis is to create an FE model which accurately simulates tennis ball to racket impacts.

The main objectives are as follows;

1. To review existing literature in the field of tennis ball to court and ball to racket impacts.

2. To produce and validate a realistic FE model of a pressurised tennis ball.

3. To produce and validate a realistic FE model of a pressurised tennis ball impacting a freely suspended racket.

4. To produce a parametric modelling program which enables key parameters of a tennis ball to racket model to be easily adjusted and simulations run without the requirement of using an FE interface.

5. To produce a tool that can aid in the design and development of tennis rackets.

6. To use an FE model of a ball to racket impact to further the scientific understanding of tennis.

1.3. Thesis structure

This project is concerned with the construction of a realistic FE model of a tennis ball impacting with a freely suspended racket. This will involve obtaining the key physical properties of the ball, strings and racket which will be used in

the model. The first stage will be to construct a realistic FE model of a tennis ball impacting on a rigid surface. This ball model will be developed into a ball to racket model which can simulate the full range of tennis shots encountered during play. A parametric modelling program will also be constructed alongside the FE model. This program will enable a wide variety of simulations, encompassing different tennis shots, to be undertaken efficiently. Finally the applications of the model with regard to the design of tennis rackets will be discussed.

It is imperative that an FE model is validated against experimental data to assess its accuracy and validity. This thesis is documented in chapters, the majority of which are concerned with the detailed validation of each of the main parts of the FE model against experimental data.

2. Literature Review

2.1.   Introduction

There is a large amount of literature on the physics of tennis, dating back as far as 1877 (Raleigh, 1877). Previous research has sought to find a greater scientific understanding of the interaction of the ball with both the court and the racket. Work has often been duplicated, which has led to the establishment of certain conclusions. However, there have also been areas of contradiction. The intention of this literature review is to highlight well established conclusions and attempt to explain the reasons for areas of discrepancy and misunderstanding.

This project is concerned with the creation and experimental validation of a finite element (FE) model of an impact between a tennis ball and racket. The most logical method of approaching this problem is to separate it into three stages, as detailed below;

1. Model the interaction of the ball with a rigid surface.

2. Model the interaction of the ball with a string–bed.

3. Model the interaction of the ball with a complete racket.

This literature review aims to follow the same course.

The sponsors of this project are **Prince**, who are concerned with the manufacture of a wide range of different tennis rackets. The intention of this project is to create a tool which can be used to aid the design of their next generation of rackets. It is therefore important to provide them with an overview of how tennis equipment has changed since the origins of the modern game, as well as how these changes have affected play.

This chapter will analyse existing literature on the physics of tennis. The FE model will be built and validated in stages to ensure the highest possible accuracy. Therefore, the literature review contains separate sections on the ball, string-bed and racket. The impacts simulated in the model must be representative of actual play; hence a section on player testing has been included. The final sections are on previous tennis models and the effects of technological advances on the game.

2.2. The ball

2.2.1.   The history of the tennis ball

The modern game of tennis or 'lawn tennis' evolved from real tennis in the 1870's, partly due to the invention of the lawn mower. Initially, solid vulcanised rubber balls were used. Improvements quickly followed, including making the ball hollow and pressurising it, as well as stitching a flannel cover around the core to prevent wear (ITF Technical Department, 2009). Originally, the hollow cores were manufactured from a single clover leaf shaped piece of rubber; this procedure was later replaced with the bonding of two compression moulded half shells. The flannel cover was also replaced by specialist cloth, which was bonded to the cores (ITF Technical Department, 2009). Pressureless or unpressurised balls, which had butadiene rubber (synthetic) cores, came into existence in the 1960's (Haines, 1993). However, the pressureless balls failed to gain popularity and were never widely used. In 1972 the International Tennis Federation (ITF) introduced yellow balls to the rules; this was followed by the high altitude ball in 1989. In 2002 the original ball was replaced by a faster type 1 ball, a type 2 ball which was identical to the original and a slower type 3 ball (ITF Technical Department, 2009).

2.2.2.   Rules of tennis balls as set by the ITF

In order to regulate the game of tennis and ensure consistency, any balls used in tournament play must be approved by the ITF. This involves passing a number of assessments, which are mass, size, deformation and rebound. Prior to these assessments, the ball must be acclimatised for 24 hours, at 20 ± 2°C and 60 ± 5% humidity and then compressed. The approval procedures are documented in detail by the ITF (ITF Technical Department, 2009).

Downing (2007a) found no correlation between the static and dynamic stiffness of tennis balls, concluding that rebound is the most important test with regard to the ball's impact characteristics during play. When dropped from a height of 2.54 m, standard balls (type 1-3), must rebound between 1.35 and 1.47 m. High altitude balls must bounce to a height of 1.22 -1.35 m, to compensate for the lower pressure at which they are intended to operate. The ITF test limits for

balls are summarised in Table 2.1. This study will concentrate on type 2 balls as they are the most commonly used.

Table 2.1 Test limits for ITF approved balls (ITF Technical Department, 2009)

	TYPE 1 (FAST)	TYPE 2 (MEDIUM)[1]	TYPE 3 (SLOW)[2]	HIGH ALTITUDE[3]
WEIGHT (MASS)	56.0-59.4 grams (1.975-2.095 ounces)	56.0-59.4 grams (1.975-2.095 ounces)	56.0-59.4 grams (1.975-2.095 ounces)	56.0-59.4 grams (1.975-2.095 ounces)
SIZE	6.54-6.86 cm (2.57-2.70 inches)	6.54-6.86 cm (2.57-2.70 inches)	7.00-7.30 cm (2.76-2.87 inches)	6.54-6.86 cm (2.57-2.70 inches)
REBOUND	135-147 cm (53-58 inches)	135-147 cm (53-58 inches)	135-147 cm (53-58 inches)	122-135 cm (48-53 inches)
FORWARD DEFORMATION[4]	0.495-0.600 cm (0.195-0.236 inches)	0.560-0.740 cm (0.220-0.291 inches)	0.560-0.740 cm (0.220-0.291 inches)	0.560-0.740 cm (0.220-0.291 inches)
RETURN DEFORMATION[4]	0.670-0.915 cm (0.264-0.360 inches)	0.800-1.080 cm (0.315-0.425 inches)	0.800-1.080 cm (0.315-0.425 inches)	0.800-1.080 cm (0.315-0.425 inches)

2.2.3. *The manufacture of tennis balls and their material properties*

This study will focus on pressurised tennis balls as they are much more widely used, particularly in tournament play. Detailed descriptions of the current manufacturing process of pressurised tennis balls have been undertaken by both the ITF Technical Department (2009) and Penn (2008). The first stage is to combine natural rubber with additional chemicals and extrude the mixture into pellets. Each of these pellets is compression moulded into a half shell with a wall thickness of approximately 3 mm; pairs of shells are bonded together to form a core. The cores are pressurised to approximately 8.3×10^{-4} N·m^2 during the bonding process. The cover consists of two dumb-bell shaped pieces of felt, which are bonded to the core under elevated temperature and pressure using a mould. The white seal is caused by a vulcanised solution, which is applied around the edge of each of the separate pieces of felt before they are bonded to the core.

There is very little published data on the material properties of tennis balls. Although, it is predicted that each manufacturer will use slightly different materials and manufacturing procedures, resulting in small variations in impact characteristics (Miller and Messner, 2003). A range of balls can have different dynamic stiffness values even though they have passed the ITF rebound test. This can cause variation in their dynamic properties at high impact velocities (>10 m·s^{-1}) (Cross, 1999; Haake *et al.,* 2003a) (Figure 2.1). The ratio of the rebound to inbound velocity of the ball is defined as the coefficient of restitution

(COR). With regard to play, a higher COR would result in an increased speed off the court or racket, whilst dynamic stiffness has been stated to affect the ball's rebound angle (Cross, 1999). Miller and Messner (2003) raised concern that with the current approval procedures, a ball could be introduced with the potential to change the fundamental nature of the game. A possible solution for raising consistency between different balls would be to undertake additional rebound tests at higher impact speeds, as suggested by Cross (1999) and Miller and Messner (2003). Further research would be required to support the introduction of a new standard. A representative ball to surface impact model could be used to accurately predict a ball's rebound characteristics at a range of velocities. Such a model could be used for determining the influence of individual parameters on the game.
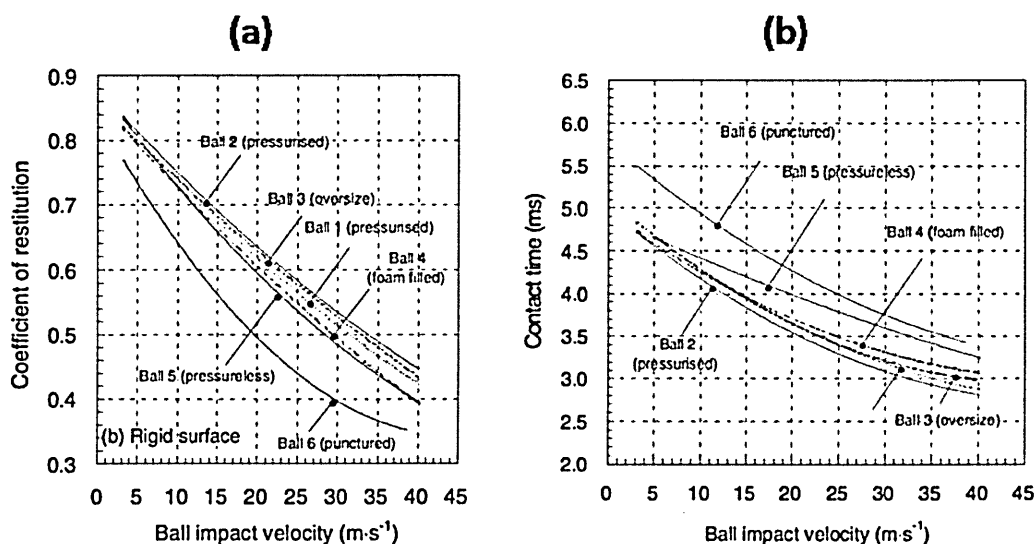
Figure 2.1 Variation in a) COR and b) contact time, between different balls for perpendicular impacts on a rigid surface (Haake *et al.,* 2003a).

A number of authors have found that the rebound characteristics of tennis balls change with temperature (Rose *et al.,* 2000; Downing, 2007b). The internal pressure of a tennis ball will change with temperature in accordance with the combined gas law ($p_1V_1/T_1 = p_2V_2/T_2$). It is predicted that this change in internal pressure will affect the structural stiffness and hence rebound characteristics of the tennis ball. The variation in dynamic properties with temperature could also be partly due to a change in the material properties of the ball, as predicted by Downing (2007b). Undertaking the ITF approval tests across a range of

temperatures could potentially increase consistency when playing under different atmospheric conditions.

Goodwill *et al.,* (2005) performed materials testing on the rubber core and felt cover, which is used in the construction of a tennis ball. A Hounsfield tensometer was used to obtain the quasi-static stress/strain relationship of the rubber in both tension and compression. The maximum load applied to the rubber samples was 150 N for tension and 450 N for compression (Figure 2.2a). The quasi-static stress/strain relationship of the felt cover was obtained for compression, up to a load of 500 N (Figure 2.2b). Testing the material properties of the rubber and felt from a range of balls would provide an indication of the amount of variation between manufacturers. Testing at a range of temperatures would provide an indication as to how the material properties of tennis balls change with temperature. Dynamic mechanical analysis (DMA) could be used to obtain the viscoelastic properties of the rubber core of a tennis ball (Menard, 2008).
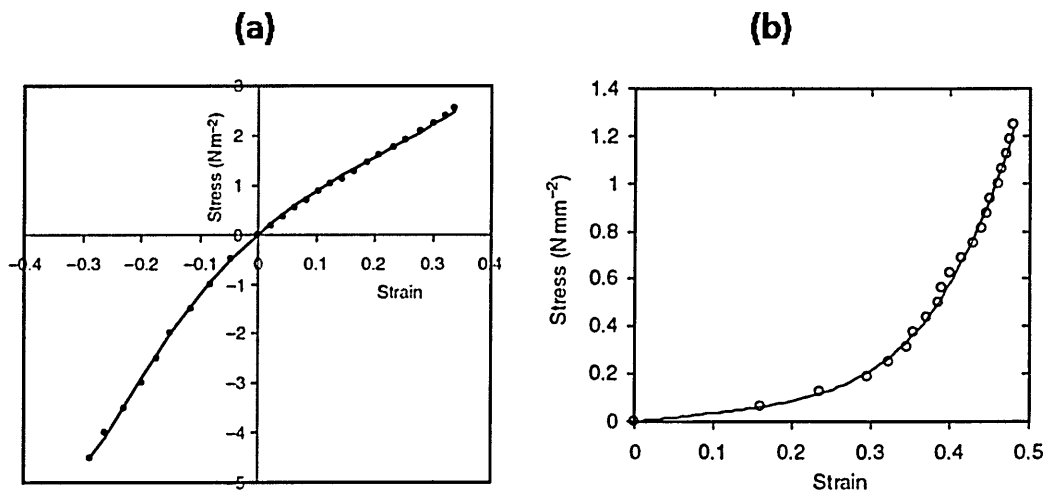
Figure 2.2 Quasistatic material properties of the a) rubber core and b) felt cover of a tennis ball (Goodwill *et al.,* 2005).

Rubber is viscoelastic, which means its properties are both time and temperature dependent. Increasing the strain rate and/or decreasing the temperature results in an increase in the Young's modulus (Menard, 2008). Mase and Kersten (2004) undertook stress relaxation testing on samples taken from the cores of golf balls, in order to obtain their viscoelastic properties. Stress relaxation testing involves measuring the time dependent stress in a

sample held at constant strain, following rapid loading (Menard, 2008). Three point flexure tests were undertaken using a DMA test machine. As the contact time of a golf ball is very small a series of tests were undertaken from -90°C to room temperature. A master curve referenced at room temperature was constructed by undertaking time-temperature superposition on the data obtained from the individual tests. Time-temperature superposition assumes time-temperature equivalence and is used to combine data collected at different temperatures in order to predict the behaviour at a wider frequency range (Menard, 2008). The master curve was fitted to a Prony series and implemented into a model of a golf ball, which was constructed in LS-DYNA. The viscoelastic properties of a tennis ball core could be obtained by undertaking a series of stress relaxation tests across a wide temperature range. However, the contact time of a tennis ball (Goodwill, 2002; Haake *et al.,* 2003a) is approximately 10 times longer than that of a golf ball (Mase and Kersten, 2004). This indicates that the temperature range would not need to be as wide as used by Mase and Kersten (2004).

Ismail and Stronge (2008) measured the viscoelastic properties of the mantle layer (*between core and cover*) of a golf ball using a DMA technique. Forced vibration testing was undertaken on a cantilever specimen in a frequency sweep from 0-20 Hz. The tests were undertaken at different temperatures and time-temperature superposition was used to extend the frequency range. The results were fitted to a Prony series and used to create a golf ball model in Abaqus. Price *et al.* (2008) used DMA to obtain the viscoelastic properties of the materials used in two different soccer balls. Forced vibration testing was undertaken at room temperature (23°C), at a range of frequencies from 0.1-100 Hz. The results were fitted to a Prony series and used to construct soccer ball models in Abaqus EXPLICIT. It is likely that DMA could be used to obtain the viscoelastic properties of tennis ball rubber. However, the contact time of a soccer ball (Price *et al.* 2008) is longer than that of a tennis ball (Goodwill, 2002; Haake *et al.,* 2003a). Therefore, assuming a minimum contact time of 3 ms, (Goodwill, 2002; Haake *et al.,* 2003a) it is likely that the maximum frequency would have to be around 350 Hz. This could be obtained by using a wide frequency range or by testing at different temperatures and applying time-temperature superposition (Menard, 2008).

2.2.4.   Tennis ball properties

Downing (2007a) investigated the relationship between static and dynamic tennis ball stiffness. The static stiffness was determined as the amount of forward deformation from an ITF deformation test. The dynamic properties were obtained by projecting balls onto a force plate at velocities in the range from 15 - 30 $m·s^{-1}$. A higher contact time was stated to indicate a lower dynamic stiffness, as concluded by Dignall and Haake (2000). Downing concluded that there was no relationship between the contact times of tennis balls during dynamic impacts and the amount of forward deformation during a static test. This highlighted that the dynamic properties of tennis balls are more relevant to actual play.

Miller and Messner (2003) measured the COR of tennis balls impacting perpendicular to a rigid surface, for inbound velocities in the range from 7 - 45 $m·s^{-1}$. They concluded that COR decreases with inbound velocity. Although, the decrease in COR, for a set increase in inbound velocity, becomes less pronounced with increasing inbound velocity. COR was stated to decrease from 0.75 at 7 $m·s^{-1}$, to 0.4 at 45 $m·s^{-1}$. Miller and Messer also analysed the effect of 'simulated' wear on COR. Wear was simulated by impacting balls obliquely onto a rough block. They concluded that for an inbound velocity of 40 $m·s^{-1}$, COR decreased significantly at higher numbers of simulated impacts ($\geq$100). One hundred impacts were stated to be high, but possibly achievable by a single ball during a match. Measuring additional parameters, such as contact time, deformation and contact force, would have provided a better indication as to how the dynamic properties of a tennis ball change with impact velocity and wear. Other authors have found wear to affect the aerodynamics and hence flight characteristics of tennis balls (Chadwick and Haake, 2000; Goodwill *et al.,* 2004). Further research should be undertaken to determine the typical and maximum amount of wear which a tennis ball will experience when used during match play.

Goodwill (2002) analysed the perpendicular impact of a tennis ball on both a rigid surface and a force plate, for a range of inbound velocities up to 30 $m·s^{-1}$. Goodwill measured a large range of parameters, including rebound velocities, deformations, centre of mass (COM) displacements, contact times and force plots. COR was found to decrease with inbound velocity, in agreement with

Miller and Messner (2003). Contact time was also found to decrease with inbound velocity, while contact force increased (Figure 2.3a). The peak in contact force at approximately 0.2 ms into the impact has been well reported by numerous authors, and is understood to be due to the walls of the ball buckling (Cross, 1999; Dignall & Haake, 2000; Goodwill *et al.,* 2005; Haake *et al.,* 2005, Hubbard & Stronge, 2001; Pratt, 2000). The maximum deformation of the balls was found to increase with inbound velocity (Figure 2.3b). For an inbound velocity of 30 m·s^{-1} the maximum deformation is approximately equal to the radius of the ball. Goodwill also compared contact times measured with a force plate, with those measured using a high speed video camera. It was difficult to identify the end of contact using the camera, as the balls were still deformed when they left the surface. This led to a discrepancy in the two sets of results and the force plate was stated to be more accurate at measuring contact times.
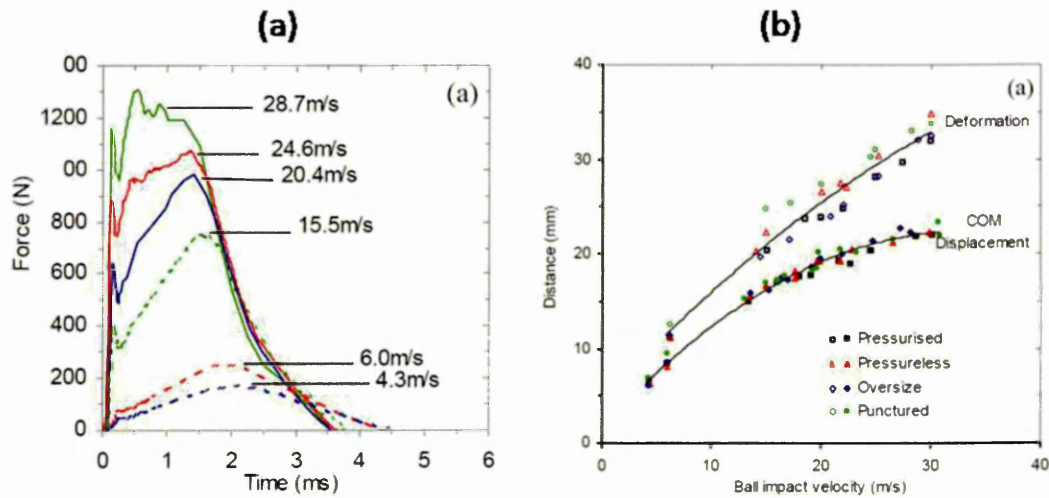
Figure 2.3 Ball impact properties for a perpendicular impact on a rigid surface a) Force plot and b) COM displacement and maximum deformation (Goodwill, 2002).

Rose *et al.* (2000) analysed the effect of temperature on the properties of tennis balls. ITF deformation and rebound tests were undertaken in the temperature range of 0-40°C. The static stiffness of the tennis balls was found to remain effectively constant with temperature. The COR of the balls used in the rebound test was found to increase with temperature. They established the same trend at higher inbound velocities up to 45 m·s^{-1}. The discrepancy between the results obtained for static deformation and impact testing indicates that the dynamic

11

properties of tennis balls cannot be predicted from static tests, in agreement with Downing (2007a).

Downing (2007b) also analysed the effects of temperature, in the range from 10-40°C, on the dynamic properties of tennis balls. COR was found to increase with temperature, in agreement with Rose *et al.* (2000). Downing also measured contact times, which were found to increase with temperature. This increase in contact time indicates a reduction in the ball's structural stiffness (Dignall and Haake, 2000; Brody *et al.,* 2002; Cross and Lindsey, 2005; Goodwill *et al.,* 2005), which was concluded to be due to a change in the rubber core material properties. The change in the internal pressure of a tennis ball with temperature will also have an effect on its rebound characteristics. Testing punctured balls would remove the effect of the internal pressure. Testing punctured balls and cores would have provided further insight into how the properties of both the rubber and felt change with temperature. However, materials testing would provide the best indication of how the properties of the rubber and felt change with temperature. The change in the internal pressure of a tennis ball with temperature can be calculated if the enclosed volume is assumed to remain constant. Physically measuring the internal pressure at each temperature would be more accurate as it would account for any changes in the diameter of the ball; however, this was neglected by both Rose *et al.* (2000) and Downing (2007b). Despite using a force plate to measure contact times, Downing did not publish any results for impact forces.

Bridge (1998) examined the effects of changing internal pressure, in the range from 17-98 kPa, on the bounce characteristics of a 'play' ball dropped from a height of 1 m. Contact area and contact time both decreased with increasing internal pressure, whilst COR increased. Bridge concluded that the increase in COR was due to more energy being stored in the compression of the air inside the ball. A similair experiment was undertaken using a squash ball; the change in pressure was replaced with a change in temperature, in the range from 30-80°C. The contact area, contact time and COR of the squash ball all increased with temperature. Bridge stated that the increase in the flexibility of the rubber with increasing temperature was the dominant factor in determining the rebound characteristics of the ball, rather than the change in internal pressure. This was in agreement with the findings of Downing (2007b) for tennis balls.

During play a tennis ball will impact obliquely to the court surface. When a tennis ball impacts obliquely on a rigid surface the contacting region deforms and flattens, allowing the friction force to reverse if the rotational velocity exceeds the horizontal velocity (Cross, 1999; Haake *et al.,* 2003b). If the reaction force is large enough, the walls of the ball will buckle shortly into the impact, resulting in a cap inverting inside (Dignall & Haake, 2000; Goodwill *et al.,* 2005; Haake *et al.,* 2005, Hubbard & Stronge, 2001; Pratt, 2000), leaving an annulus-contacting region (Cross, 2002). The annulus slides across the surface with a decreasing horizontal speed until the sliding and static friction becomes equal. At this instance the surface tangential velocity of the ball equals its horizontal velocity. This causes the ball to vibrate horizontally, at a frequency determined by its stiffness. In turn, this results in the outer perimeter of the annulus slipping backwards, thus reversing the rotational direction of the ball and creating a higher spin than allowed by the conditions of rolling (Cross, 2002).

Tennis is played on a variety of surfaces, including clay, acrylic and grass. These all affect the balls rebound characteristics in different ways. For example, clay generates high rebound angles, whilst acrylic courts produce lower angles (Haake *et al.,* 2000). The coefficient of friction (COF) is the main factor, which causes the discrepancy in the balls rebound characteristics between individual court surfaces (Brody, 1988).

Downing (2007c) examined the effect of temperature in the range from 10-40°C on surface pace rating (SPR), for an acrylic and synthetic carpet surface. SPR is defined as 100(1- μ), where μ is the COF of the surface. SPR was found to decrease with temperature, indicating an increase in COF. A decrease in SPR equates to the ball losing a higher proportion of its horizontal velocity during the impact. Player testing may also help to provide an insight into how temperature affects the speed of the game on different court surfaces.

The other property that distinguishes different court surfaces, besides COF, is stiffness; clay and grass deform more on impact, in comparison to a hard court such as acrylic. Holmes & Bell (1986) concluded rebound resilience increased linearly with court hardness, up to a maximum of approximately 58%. At this point no further rise in court hardness would affect the deformation of the ball. Therefore, any errors may be negligible if the impacting surface is at least an

13

order of magnitude stiffer than the ball. FE is a suitable tool that could be used to address this hypothesis, by analysing ball rebound characteristics on surfaces of varying stiffness, corresponding to clay, grass and acrylic.

2.2.5.   Summary of the ball

Tennis balls consist of a pressurised rubber core and felt cover. The viscoelastic properties of the rubber core result in a decrease in COR and contact time with increasing inbound velocity. To accurately simulate a tennis ball using FE the viscoelastic properties of the rubber and the internal pressure of the core must be included in the model. The internal pressure and the material properties of the rubber core are dependent on temperature. This means the rebound characteristics of a tennis ball are also dependent on temperature. Therefore, the material properties and the internal pressure used in the model must correspond to the temperature the response of the ball is intended to simulate.

2.3. The string-bed

2.3.1.   The history of tennis strings

In the early days of lawn tennis in the 1870's strings were manufactured from sheep intestines or serosa. Sheep intestines were replaced by those of cows, following World War Two (ITF Technical Department, 2009). The relatively high cost of natural gut combined with its poor durability, led to manufacturers using synthetic materials from the 1950's (Haines, 1993). There are now a range of synthetic strings available, including nylon, polyester and Kevlar. The tension at which strings are strung has also changed. In the 1920's the average string tension was 196 N (44 lbs), in comparison to the larger value of 245 N (55 lbs) used today. Professional players have been reported to use string tensions of up to 343 N (77 lbs) (ITF Technical Department, 2009). The width and length of racket heads has also increased considerably since the 1870's, resulting in larger string-beds (Haake *et al.,* 2007). For the same string tension a larger string-bed will have a lower structural stiffness. Therefore, players may have increased the tension of their strings in order to counteract the effects of the larger string-bed.

2.3.2.   Rules

The first rule to be introduced by the ITF concerning the string-bed and arguable the most important, was in 1978 and is stated below;

"The hitting surface of the racket shall be flat and consist of a pattern of crossed strings connected to a frame and alternately interlaced or bonded where they cross." (ITF Technical Department, 2009)

This rule was introduced following a novel invention labelled the 'spaghetti strings' or 'spaghetti racket', where the strings were not interlaced. The 'spaghetti racket' allowed a player to produce very high spin rates due to large horizontal displacements of the strings during oblique impacts (Goodwill and Haake, 2002).

2.3.3.   The manufacture of tennis strings and their material properties

When manufacturing natural gut strings, the first stage is to remove any contaminants from the intestines. This is done using a chemical bath. The strands are then spun, dried and polished to produce a string with the required diameter. The final stage is to apply a protective polyurethane coating (ITF Technical Department, 2009). Synthetic strings are usually constructed by winding hundreds of filaments around a central core (Haines, 1993; ITF Technical Department, 2009). The filaments are constructed with an extrusion mould. The core can either be extrusion moulded as a solid section or constructed by winding together a number of larger diameter filaments. It is widely accepted that the mechanical properties of tennis strings will be determined by the process used to construct them and the choice of materials (Haines, 1993; ITF Technical Department, 2009).

Cross (2000a) used an Instron machine to measure the static properties of tennis strings. The strings were tensioned at a rate of 100 mm/min (0.0017 m·s^{-1}) up to a maximum load of 700 N. The section of the elongation versus tension curve between 200 and 300 N was stated to be the most important, as this determines the increase in string plane stiffness during a typical tennis shot. There was no experimental verification of this range. Natural gut was found to have the highest elasticity within the range of 200 to 300 N.

Although the results obtained are useful for comparing different strings, it is predicted that an impact between a tennis ball and racket will result in higher strain rates than those tested by Cross (2000a). Assuming an initial length of 0.3 m, a contact time of 5 ms (Brody *et al.*, 2002; Cross & Lindsey, 2005) and the perpendicular displacement of the string-bed in the range from 0.015 to 0.030 m (Goodwill, 2002), the time-averaged strain rate will be 0.6-2.4 $m·s^{-1}$. This is in agreement with the approximate strain rate of 40 000 mm/min (0.67 $m·s^{-1}$) stated by Cross *et al.* (2000).

Calder *et al.*, (1987) analysed both the static and dynamic properties of a range of tennis strings. A mid-sized tennis racket was strung at 220 N (50 lbs), with a load cell fitted in-line with a central main string. No information regarding the string type or gauge was provided. When the racket was head-clamped and subjected to an impact with a tennis ball, the string tension increased by 90 N and the contact time was approximately 3.5 ms. The inbound velocity of the ball was not stated, and there was no mention as to how this may influence the results. The static properties of the strings were obtained using an Instron machine, with the crosshead speed set to 20 mm/min. A rig was constructed for the dynamic tests, which was capable of applying a load of 90 N to a tensioned string, over a period of 3.5 ms. A large amount of hysteresis was observed, for both the static and dynamic tests, when the strings were loaded to 90 N without any preload. Hysteresis is observed as a difference between a loading and unloading stress-strain curve and is due to the sample softening as a result of stretching (Mullins, 1969). The hysteresis decreased to a negligible amount when the pre-load was increased to 270 N. The stiffness of the synthetic strings increased with both the strain rate and the amount of preload, while the stiffness of the natural gut strings remained virtually constant. The stiffness of all the strings was found to be linearly elastic, under the conditions which Calder *et al.* obtained from impacting a ball onto a head-clamped racket. Synthetic strings were concluded to be stiffer than natural gut strings under these conditions. The effect of adjusting the applied load was not analysed.

Cross *et al.* (2000) used a bespoke impact rig to determine the dynamic properties of tennis strings (Figure 2.4a). They stated that a typical impact between a ball and string-bed will have a maximum force of approximately 1500 N and a contact time of around 5 ms. Assuming this load is evenly distributed

over the ten central strings, the maximum force on each of them will be approximately 150 N. This is comparable to the value of 90 N found by Calder *et al.,* (1987). Cross *et al.* replicated this by impacting a string tensioned to 275 N with a 0.29 kg hammer on a pendulum. The inbound velocity of the hammer was 2.63 m·s^{-1} and the string had an initial length of 0.32 m, prior to being tensioned. The velocity of the hammer changed from 2.63 to -2.5 m·s^{-1}, resulting in a load of 120 - 200 N and a contact time of approximately 30 ms. This was stated to be equivalent to a number of ball impacts on a string-bed, each with a duration of 5 ms. Impacting the string at a higher velocity with a lower mass, would be more representative of the impact between a ball and string-bed. A dynamic stiffness was calculated for each string, using the change in tension and elongation during impact. The change in tension for gut, nylon and polyester strings was in the approximate range of 100 - 250 N. The change in the length of the string was calculated from its perpendicular displacement, which was measured using a laser and grid (Figure 2.4a). The change in tension was measured using an s-type load cell (Figure 2.4a). Figure 2.4b shows the contact force increases with dynamic stiffness, while contact duration decreases. The large variation in contact duration for different values of dynamic stiffness indicates that there may be errors as a result of using an unrealistically high mass at low velocity. Natural gut strings were found to have the lowest dynamic stiffness at 20 kN·m^{-1}, although only two strings of this type were tested. There may be errors in the results due to the frequency response of the s-type load cell, which is more suitable for measuring static loads than dynamic loads.

(a)   **(b)**
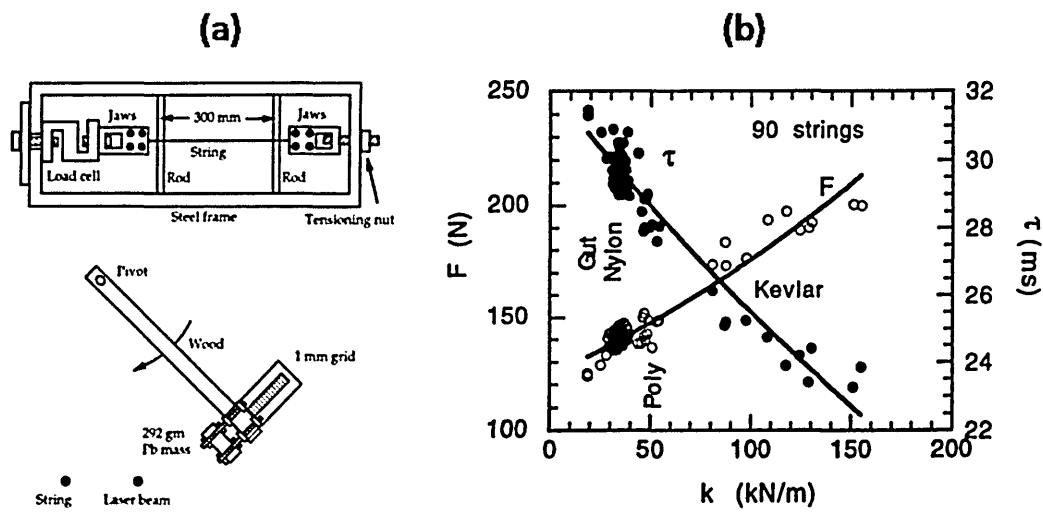
Figure 2.4 a) Dynamic string tester and b) Dynamic stiffness and contact duration results for a selection of strings (Cross *et al.* 2000).

Cross (2001a) derived a method for obtaining the dynamic stiffness of tennis strings within their operational range, using an Instron machine. The first stage is to load a string with a gauge length of 20 mm to 280 N (63 lbs), at a rate of 50 mm/min (0.00083 m·s^{-1}) and hold it for 100s. This is intended to replicate stringing a racket. Following this the string is loaded to 380 N (85.5 lbs) and held for a further 10 s. This is intended to replicate 2000 impacts between a ball and string-bed, each with a contact time of 5 ms. The final stage is to unload the string at a rate of 100 mm/min (0.0017 m·s^{-1}). The unloading step is stated to produce a curve without any significant creep effects. This is claimed to be the reason why it is possible to obtain dynamic string properties using an Instron machine. Figure 2.5 shows the load extension curves obtained for a range of different strings. The dynamic stiffness is calculated from the unloading curve by dividing the change in load between 311 and 222 N (70 and 50 lbs) with the change in length. The range of 311 - 222 N is used to obtain the dynamic stiffness as this is stated to be the typical operational range of the strings. However, Cross loaded the strings to 380 N to replicate an impact between a ball and string-bed; this indicates inconsistencies in the method.
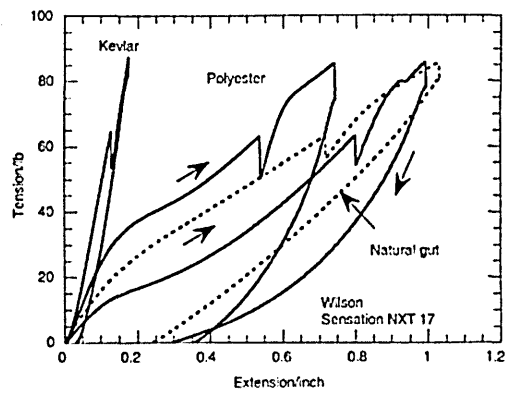
Figure 2.5 Typical material curves which are used for obtaining the dynamic stiffness of different strings (Jenkins, 2003).

The other property besides structural stiffness, which is believed to distinguish individual tennis strings, is friction. There are currently no published studies on string to string friction. Cross *et al.* (2000) measured the COF between tennis strings and the felt used to cover the ball. He glued tennis ball felt onto a pipe with a diameter of 60 mm, wrapped a 1 m length of string around twice and attached a 0.15 kg mass to the end. The force required to lift the mass at a constant velocity, which was not declared, was recorded with a spring balance. The COF for most of the strings was 0.15 - 0.18, while the lowest and highest obtained values were 0.11 and 0.36, respectively. Cross (2000b) analysed the COF of friction between a ball and string-bed. He experimentally obtained sliding and rolling COF's for five different strings, which were 0.27 - 0.42 and 0.05, respectively. However, he calculated sliding friction by placing masses up to 10 kg on a ball and dragging it across the string-bed, a method not representative of a typical high momentum collision. It is predicted that the ball will deform around the strings due to the applied load; meaning that Cross was actually measuring a traction force rather than a friction force. The relationship between the applied load and coefficient of friction was not investigated. The deformation of the ball around the strings may explain the discrepancy between the COF values obtained by Cross *et al.* (2000).

2.3.4.   Ball to string-bed impacts

Ball to head-clamped racket impacts are not representative of an actual tennis shot; however they are commonly used for analysing the effect of string-bed properties, such as string type and tension. Unlike a court impact, where the

majority of the energy is assumed to be stored in the deformation of the ball; when a ball collides with a string-bed the energy is equally divided between both objects (Cross & Lindsey, 2005). During a collision between a ball and a string-bed, the ball loses around 45% of its energy and the string-bed loses around 5% of its energy (Brody et al., 2002; Cross & Lindsey, 2005). Therefore, the ball to string-bed collision is more efficient than a rigid surface impact (Jenkins, 2003; Brody et al., 2002; Cross & Lindsey, 2005). Although there are no set rules, the COR for a tennis ball dropped onto a head-clamped racket from a height of 2.54 m is about 0.75 - 0.8, compared to around 0.74 for a rigid surface (Brody et al., 2002). Reducing string-bed stiffness has the effect of increasing both the rebound velocity of the ball and the contact time, which is approximately 5 ms (Brody et al., 2002; Cross & Lindsey, 2005). The two main factors that determine string-bed stiffness are the string material and tension.

The Babolat Racquet Diagnostic Center (RDC) is commonly used as a tool for measuring the quasi-static stiffness of a string-bed (Babolat, 2009). The RDC displaces the centre of the string-bed using a small disk and provides a stiffness value between 0 and 100 in RDC units. The higher the RDC value the stiffer the string-bed.

Stiffness is considered to be the principal factor that separates the different string materials. Polyester strings have high stiffness, causing them to lose tension at an accelerated rate, unlike highly elastic strings, such as natural gut. Tension increases more during impact with polyester strings, resulting in shorter contact times and a "controlled feel". Natural gut on the other hand, produces a more comfortable feel, due to longer contact times (Cross et al., 2000). FE could be use to analyse the variation in contact times and reaction forces for different string types.

String tension, which typically ranges from 220 - 310 N (Brody et al., 2002), affects both rebound velocity (Haake et al., 2003a; Goodwill and Haake, 2004a; Cross & Lindsey, 2005; Brody et al., 2002) and angle (Goodwill and Haake, 2004a & b). However, decreasing tension by 44 N only results in approximately a 2% rise in the rebound velocity of the ball for a ground stroke (Jenkins, 2003; Brody et al., 2002; Cross & Lindsey, 2005). Obtaining an exact string tension may seem irrelevant, particularly when building an FE model which will have an

inevitable margin of error, but it will have a large effect on the ball's rebound angle for oblique impacts.

Cross (2003) experimentally analysed the friction force between a tennis ball and string-bed for oblique impacts. The friction force was measured using a piezoelectric accelerometer glued to the side of the racket frame, which was positioned on two rollers. Balls were thrown by hand onto the centre of the string-bed at low speed. The time averaged sliding COF between the ball and string-bed was 0.43 ± 0.02 when the inbound angle was 25° to the string plane. Cross concluded that when the ball impacted on the string-bed with no spin or backspin, the friction force initially acted in the opposite direction to the horizontal velocity of the ball (Figure 2.6). Hence, the friction force caused the horizontal velocity of the ball to decrease and the rotational velocity at the circumference to increase. When the horizontal velocity equalled the rotational velocity at the circumference, the ball momentarily gripped the strings. During this gripping period the ball deformed forward until it lost its grip with the strings and started over-spinning. It was stated that impacts around the centre of the string-bed were included in the analysis, although there was no reference as to how the impact positions were calculated. The velocities and spin rates used were also lower than those measured during play (Goodwill *et al.*, 2007a; Kelley *et al.*, 2008; Choppin *et al.*, 2008) and there was noise in the force signals obtained from the piezoelectric accelerometer, as a result of racket frame vibrations. It is likely that if the inbound velocity of the balls was increased to give a better representation of typical playing impacts the racket frame vibrations and hence the noise in the signal would increase. It is very difficult to accurately measure and analyse certain parameters, such as the friction force acting between a ball and surface, using a conventional laboratory experiment. However, this can be achieved using an FE model, as done by Goodwill *et al.* (2005) for an oblique impact between a tennis ball and rigid surface.
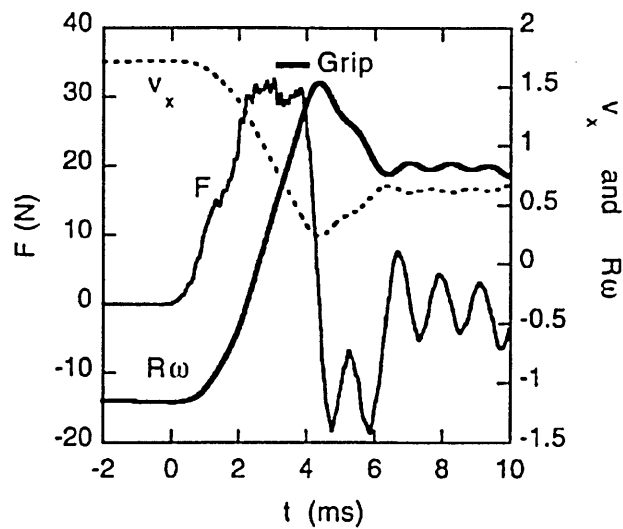
Figure 2.6 Analysis of an impact of a ball on a string-bed with an inbound velocity, angle to the racket plane and backspin of 3.27 m·s⁻¹, 58.5° and 34.9 rad·s⁻¹, respectively (Cross, 2003).

Goodwill and Haake (2004a) experimentally analysed the impact of an oblique spinning tennis ball on a head-clamped racket. They tested inbound velocities of 23 and 31 m·s⁻¹ at an angle of 39° to the normal, with backspin in the range from 0-420 rad·s⁻¹. These conditions were stated to be representative of a topspin forehand. The balls had backspin prior to impact due to a change in the Newtonian frame of reference from the court to the racket. A head-clamped racket was used to isolate the string-bed and eliminate the effect of racket parameters, such as stiffness and mass. A range of natural gut and synthetic strings, were tested. Each string was tested at a tension of 40 and 70 lbs (178 and 311 N). The racket type, which remained constant across all the tests, had a head size of 632 cm². The balls were fired using a modified BOLA (BOLA, 2009) and the impacts were stated to be at the centre of the string-bed. However, there was no evidence to suggest that the impact positions were actually calculated. The impacts were recorded with a high-speed video camera and manually analysed using the bespoke software *Richimas V3*. The standard deviation in inbound velocity and angle for all the impacts was 0.4 m·s⁻¹ and 0.7°, respectively. The standard deviation obtained from a manual tracking repeatability study was 0.2 m·s⁻¹ for velocity, 0.3° for angle and 25 rad·s⁻¹ for spin. The results showed that the rebound velocity, angle and spin of the ball, all decreased with increasing inbound backspin. The vertical rebound velocity of the ball was virtually independent of inbound backspin (Figure 2.7). The horizontal rebound velocity decreased significantly with inbound backspin

(Figure 2.7). This decrease in horizontal velocity is the main cause of the decrease in the resultant rebound velocity and angle with increasing inbound backspin. Rebound velocity was generally higher for the impacts on the rackets strung at the lower tension of 40 lbs (178 N), in agreement with other authors (Jenkins, 2003; Brody *et al.*, 2002; Cross & Lindsey, 2005). The results indicated that string-bed stiffness does not have an effect on rebound spin. This was in contradiction to the belief of many players. However, there was a large amount of scatter in the experimental data making it difficult to justify a solid conclusion. The horizontal rebound velocity remained effectively constant for the two string tensions, while vertical rebound velocity increased with string tension (Figure 2.7). The rebound angle of the balls (*relative to the string-bed normal*) was also smaller for the rackets strung at lower tension, in agreement with Goodwill and Haake (2004b). The stiffness of the string-bed had different effects on the horizontal and vertical rebound velocity of the ball. Testing at a range of different inbound angles would provide further insight into the effect of string-bed stiffness on the rebound characteristics of the ball.
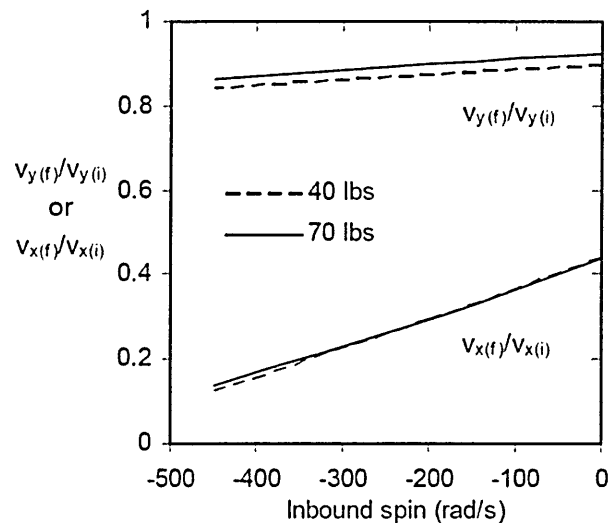
Figure 2.7 Horizontal and vertical coefficient of restitution of balls incident at 39° on a head-clamped racket (Goodwill and Haake, 2004a).

Ball to string and string to string friction, are predicted to affect the rebound velocity, angle and spin of the ball, for oblique impacts. However, there are currently no published investigations where laboratory experiments have been used to determine the effect of changing ball to string or string to string friction.

This is predicted to be due to the difficulty in accurately measuring and adjusting COF.

2.3.5.   Summary of the string-bed

The structural stiffness of a tennis racket string-bed, which is determined by the string material and tension, affects the rebound velocity and angle of the ball. Therefore, a method for simulating a tensioned string-bed in an FE model must be developed. The string-bed must consist of interwoven strings with the correct material properties. As tennis strings are viscoelastic dynamic materials testing must be undertaken. However, previous research indicates that tennis strings have linear material properties within their operational range.

2.4. The racket

2.4.1.   The history of the tennis racket

This sub-section will summarise the evolution of the tennis racket, as detailed by numerous authors (Haines, 1993; Jenkins, 2003; Haake *et al.,* 2007; ITF Technical Department, 2009). Initially, at the end of the 19th century, lawn tennis rackets were key hole shaped and manufactured from a single piece of ash. The ash was boiled to make it pliable and bent into shape whilst still hot. These early rackets had weak throats and were prone to warping when wet; the issues were overcome by using additional materials, such as canvas and metal, to reinforce the problematic areas. As tennis grew in popularity manufacturers began to mass produce their rackets, using the latest materials and production techniques. 1931 saw the introduction of the first multi-ply wood racket, the Dunlop Maxply which was in production for 50 years (Figure 2.8a). Despite its earlier use in other sports equipment, metal was not seen as a practical alternative to wood until the 1960's. This was due to the difficulty in stringing a metal racket, an issue which was overcome by using grommets. In 1974 Howard Head invented the aluminium Prince Oversize racket (Figure 2.8b) (Head, 1975). The racket had a 50% larger strung area, which increased the size of the 'sweet' spot and reduced twisting in the hand as a result of off-centre impacts. Manufacturers also began experimenting with composite materials in the 1970's, mainly due to their higher stiffness to weight ratio in comparison to metals. A significant early composite racket was the Dunlop Max 200G, which

was introduced in 1980 and remained in production for 10 years. The Max 200G was manufactured by injection moulding nylon with short carbon fibres (Haines *et al.,* 1983). Despite its many production advantages, the manufacturers were unable to use the injection moulding process to produce rackets with the same mass and head size as those produced using composite lay-ups. Currently, the majority of rackets are manufactured from composite lay-ups as this allows materials to be precisely placed for optimum stiffness and weight distribution. Modern composite rackets are around 30% lighter and three times stiffer than their state of the art wooden counterparts. A lighter racket can be swung faster, whilst stiffness increases impact efficiency; both of these factors allow the player to increase the rebound velocity of the ball (Haake *et al.,* 2007). The head size of these modern composite rackets is also around 40% larger, which increases ease of play.
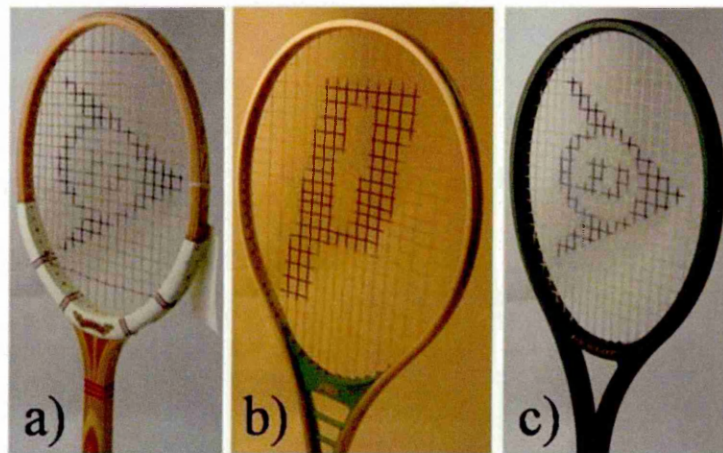
Figure 2.8 A selection of tennis rackets a) 1981 Dunlop Maxply, b) 1977 Prince oversize and c) 1980 Dunlop Max 200G.

Haake *et al.* (2007) measured various properties of 150 tennis racket from the 1870's to 2007. The natural frequency of tennis rackets have increased dramatically since the 1870's while the mass has decreased, as a result of improvements in both materials and manufacturing techniques (Figure 2.9). The largest changes in both the frequency and mass of the rackets have come about since the 1970's.
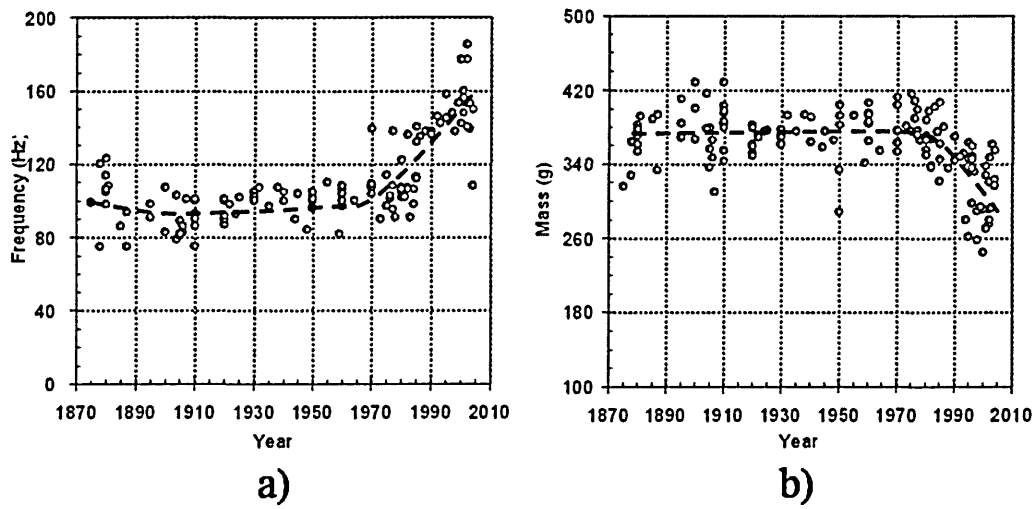
Figure 2.9 Racket properties from 1870 to 2007 a) frequency and b) mass (Haake *et al.*, 2007).

2.4.2. Rules

The Prince Oversize racket resulted in the ITF implementing restrictions on the size of tennis rackets. The extract from the ITF rules regarding the size of the tennis racket is given below (ITF Technical Department, 2009);

> *"The frame of the racket shall not exceed 29.0 inches (73.7 cm) in overall length, including the handle. The frame of the racket shall not exceed 12.5 inches (31.7 cm) in overall width. The hitting surface shall not exceed 15.5 inches (39.4 cm) in overall length, and 11.5 inches (29.2 cm) in overall width."*

The rules also prohibit the use of a racket with external energy sources or the ability to change its properties during a point, as detailed below (ITF Technical Department, 2009);

> *"The frame, including the handle, and the strings, shall be free of any device which makes it possible to change materially the shape of the racket, or to change the weight distribution in the direction of the longitudinal axis of the racket which would alter the swing moment of inertia, or to change deliberately any physical property which may affect the performance of the racket during the playing of a point. No energy source that in any way changes or affects the playing characteristics of a racket may be built into or attached to a racket."*

26

2.4.3.   The manufacture of tennis rackets and their material properties

The current manufacturing process for tennis rackets is described by the ITF Technical Department (2009) and Jenkins (2003). The majority of modern tennis rackets are manufactured from thermoset carbon fibre composites, as they provide a good combination of both strength and manufacturability. The manufacturing process is labour intensive and is often undertaken in the Far East. The first stage is to create a lay-up by bonding together sheets of carbon fibre prepreg on a flat heated bench. The prepreg sheets are placed at different angles to provide specific bending and torsional stiffness. Once complete the lay-up is wrapped around a plastic tube and assembled on a template to produce the basic racket shape (Figure 2.10). Extra prepreg is placed in specific areas to provide the required strength and mass distribution. The ends of the racket shape are pressed together and wrapped in prepreg to form the handle. The throat is assembled separately and placed in a mould along with the main part of the racket frame. The mould is then heated to around 150°C while the plastic tube is pressurised to create a hollow racket. Following moulding the plastic tube is removed and the racket is trimmed to the correct length. The racket is then sanded, painted in an electrostatic process and any graphics and transfers are applied.

Pre-preg layers	Parts	Material	Fibre angle direction
	1	PA Foil	
	2	Glass	±20°
	3	Carbon	±30°
	4	Carbon	0
	5	Glass	0
	6	Carbon	±30°
	7	Carbon	0
	8	Carbon	±30°
	9	Carbon	0
	10	Glass	±30°
	11	Carbon	±30°
The main tube			
	12	Carbon	±30°
	13	Carbon	±30°
	14	Carbon	±30°
	15	Glass	±20°
	16	Carbon	±30°
	17	Carbon	90°
	18	Glass	±30°
	19	Glass	±30°
The throat piece and reinforcements			
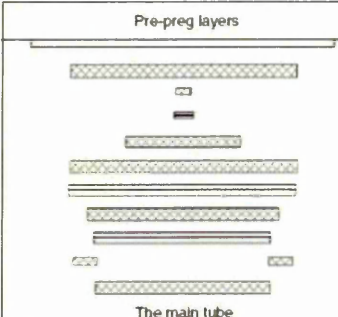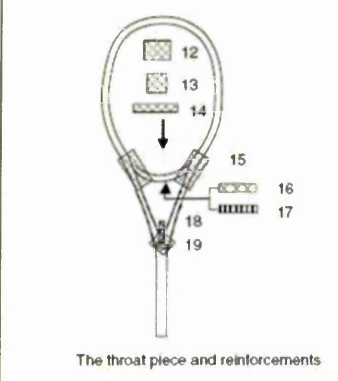
Figure 2.10 Typical lay-up for a composite tennis racket (Jenkin, 2003).

Currently there is limited published data on the material properties of tennis rackets. Gu and Li (2007) used a value of 30.5 GPa in an FE model of a tennis racket, which was obtained from bending and resonance experiments. Specific materials testing would be required to obtain the material properties of the different sections of a tennis racket.

2.4.4.   Simulating a player's grip on a tennis racket

Simulating the impact between a tennis ball and racket is a complex task for a number of reasons. The ball, string and racket material properties are all very intricate and difficult to simulate. Additionally, it is replicating a typical shot which escalates the complexity; especially as all players have individual hitting techniques, incorporating various racket angles and orientations (Choppin *et al.*, 2007b). However, the single most difficult task can be considered to be in experimentally or analytically replicating the grip of a human hand.

Brody (1979) undertook an experiment to determine how grip conditions affect the rebound velocity of a ball from a racket. A ball was dropped from a height of 1 m onto a number of different rackets. The contact time of the impact was in the range from 4.5 - 6.8 ms, which was less than the time required for the racket to complete an oscillation of the fundamental mode of vibration, which is the

dominant mode. This indicates that the player's grip has no influence on the rebound velocity of the ball.

The handle clamping method is an area of much discussion when simulating ball to racket impacts. The main debate is concerned with which method best simulates a players grip. Brody (1987) undertook an investigation to compare the frequency response of a tennis racket when the handle was rigidly clamped and hand held. It was stated that when struck at the geometric string-bed centre (GSC), a handle-clamped racket will oscillate in a manner resembling a diving board with a frequency of 25 - 40 Hz (Figure 2.11). The frequency increases to 100 - 175 Hz if the impact is away from the GSC. This is similar to the lowest frequency of a freely suspended racket (Figure 2.11). A Wilson T2000 racket was impacted on the string-bed with a tennis ball at both the centre and throat area, when hand held and handle-clamped. The frequency response of the racket was significantly lower when the handle was rigidly clamped as opposed to hand held. Hence, findings from any investigations which use handle clamped rackets cannot be taken as representative of a typical collision encountered during play.
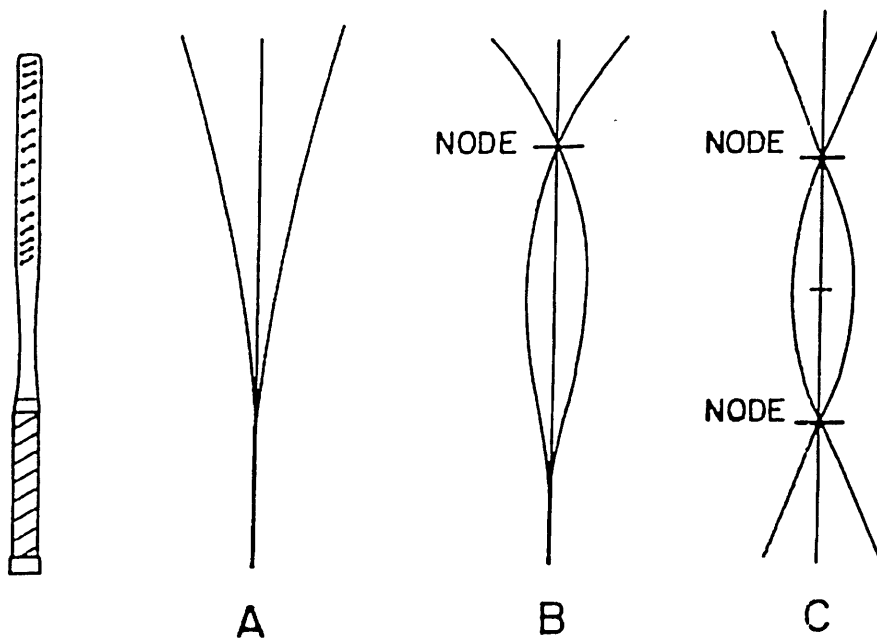
Figure 2.11 Racket frequency response A & B) low frequency handle clamped and c) freely suspended (Brody, 1987).

Cross (1998) undertook an investigation to determine whether a player's grip affects the impact between a ball and racket. A 1990 vintage Wilson graphite composite racket, with piezoelectric disks fitted along the frame and handle, was used to measure the frequency response following a low speed impact with a ball. The racket was found to have a fundamental mode of vibration of 102 Hz when hand held and 109 Hz when freely suspended. Adding a 40g mass to the handle of the freely suspended racket reduced the fundamental frequency to 103 Hz; indicating a better representation of a hand held racket. However, Cross also found that the node in the handle moved closer to the butt when the racket was hand held (Figure 2.12). This was stated to be due to the hand lowering the amplitude of the vibrations in the handle. An 80g mass was required to shift the node into the required position; although this caused the fundamental frequency to drop to 100 Hz. The discrepancy in the amount of mass required to produce the correct fundamental frequency and node position, indicates that further research needs to be undertaken. Cross also found higher frequency vibrations reached the handle before the ball left the racket, indicating that the hand has an influence on the impact. However, the amplitude of these vibrations was considered to be too low to affect the rebound velocity of the ball. Haake *et al.* (2007) found the fundamental frequency of rackets manufactured in 2007 to be approximately 160 Hz, when freely suspended. The higher fundamental frequency, in comparison to the value found by Cross, provides evidence for testing the effect of a player's grip on a variety of rackets from different eras.

Free racquet   Hand
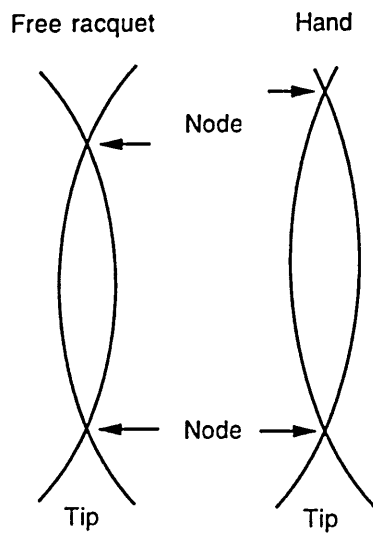
Figure 2.12 Vibration modes of a free and hand held tennis racket (Cross, 1998).

2.4.5.   Ball to racket impacts

Brody (1997a) analysed the effect of changing the impact location along the longitudinal axis of a freely suspended racket. The racket was a prototype and had a mass of 0.278 kg, a length of 0.685 m, a balance point 0.372 from the butt and a moment of inertia of 0.01297 kg·m^{-2}. This was representative of a typical racket from this period (Haake *et al.*, 2007). Brody measured the apparent coefficient of restitution (ACOR), which is the ratio of the rebound to inbound velocity of the ball. For an inbound velocity of 20 m·s^{-1}, ACOR was found to be dependent on impact location (Figure 2.13). The rebound velocity of the ball was lowest at the tip and highest in an area near the throat. Testing at a range of speeds would provide an insight into the relationship between ACOR, inbound velocity and impact location. Brody stated that for an impact between a ball and head-clamped racket, COR will decrease with increasing string tension. However, the string tension of the freely suspended racket used by Brody was not provided.
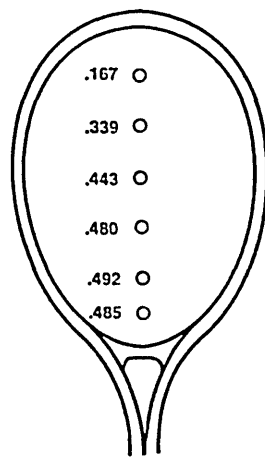
Figure 2.13 Variation of ACOR with impact location for a perpendicular impact between a tennis ball and freely suspended racket (Modified from Brody, 1997a).

Spurr and Downing (2007) undertook an investigation to determine the relationship between racket 'power' and fundamental frequency. Power is measured as the velocity of the ball after impact with a racket. A ball will rebound at a higher velocity from a more powerful racket. The fundamental frequencies of 47 rackets manufactured from 2001-2007 were obtained using an accelerometer. The rackets were hung from a thread and impacted at the 'dead spot' using a rubber hammer. The fundamental frequency of all the rackets was in the range from 130-180 Hz. This was in agreement with values measured by Haake *et al.* (2007) for this period. An impact was simulated at three locations on each of the rackets using the ITF racket power machine. Goodwill *et al.* (2007b) successfully validated the racket power machine using a high-speed video camera, demonstrating that it provides comparable results to a freely suspended racket. The velocity of the rackets in Spurr and Downing's (2007) investigation was 35 m·s^{-1} and the impact positions were 75 mm (tip), 150 mm (centre) and 225 (throat) mm from the tip. The velocity of the racket is defined at the location on the string-bed which has a radius 700 mm from the pivot Goodwill *et al.* (2007b). Therefore, the resultant velocity between the ball and racket would have been highest for the impacts at the tip and lowest for those at the throat. The rebound velocity of the balls was highest for the impacts at the centre and lowest for those at the tip. This indicates that the higher resultant pre-impact velocity at the centre of the racket, overcompensates the greater efficiency of impacts in the throat region (Brody, 1997a; Goodwill and Haake, 2001), in agreement with Goodwill *et al.* (2007b). The correlation

32

between the fundamental frequency of the rackets and the rebound velocity of the balls was weak, however it became stronger as the impact positioned moved closer to the throat. The lower velocity of the impacts at the throat could be the reason for there being less scatter in the experimental data. Overall, the results showed that there was no correlation between the rebound velocity of the ball and the fundamental frequency of the racket. This was in line with Haake *et al.'s* (2007) conclusion, that racket stiffness has only a small effect on serve speed. Haake *et al.* concluded that the mass and balance point of a racket have a larger influence on serve speeds. Testing a selection of rackets with a wider range of natural frequencies may have resulted in a stronger correlation with ball rebound velocity.

Goodwill and Haake (2001) analysed perpendicular impacts between a ball and freely suspended Spalding Heat 90 tennis racket, which was strung at 267 N (60 lbs). The inbound velocity of the balls was in the range from 14 - 32 $m \cdot s^{-1}$. Three discrete impact locations on the long axis of the string-bed were used in the investigation; the GSC and 50 mm above and below the GSC. The rebound velocity of the balls was highest in the throat region and lowest at the tip, in agreement with Brody (1997a). Analysing oblique impacts would be more representative of a typical tennis shot (Choppin *et al.*, 2007).

Goodwill and Haake (2004b) analysed the oblique impact of a tennis ball with no inbound spin on a freely suspended racket. Two string tensions were used in the investigation, 178 and 311 N (40 & 70 lbs). The inbound angle of the balls was set at 36° to the string-bed normal and the velocity was in the range from 15-40 $m \cdot s^{-1}$. All of the impacts were reported to be at the GSC, as this was stated to be where players typically hit the ball during play. However, there was no indication as to whether the precise impact location on the string-bed was measured. String tension was found to have no effect on the rebound velocity or spin of the balls. The rebound angle relative to the string-bed normal was found to increase with string tension, whilst contact distance, contact time and lateral string displacement all decreased. The reduced distance that the ball will travel across the string-bed was predicted to be the reason why professional players choose to string their rackets at high tensions. The conclusion that string tension has no effect on the rebound velocity of a ball was in contradiction to the common belief that lower string-bed stiffness provides more "power".

Goodwill and Haake used a large inbound angle relative to the racket normal; hence the perpendicular velocity component of the ball would have been relatively small. It is predicted that if a significantly smaller inbound angle was used, the lower string tension would have produced a slightly higher rebound velocity. A smaller inbound angle would also have a similar effect on the horizontal velocity of the ball and hence may reduce the discrepancy in rebound angle for the two string tensions. Testing a range of inbound angles would have provided a better indication of the effects of string tension on the rebound characteristics of a tennis ball. Player testing has highlighted that the ball can have spin rates of around 300-550 rad·s^{-1} prior to impact with the racket (Goodwill *et al.,* 2007a; Kelley *et al.,* 2008). Therefore, the impacts would have been more representative of a typical tennis shot if the balls had been incident with initial spin.

2.4.6. Summary of the tennis racket

The majority of tennis rackets are now manufactured from advanced composite materials, with highly specific lay-ups. The use of advanced materials has allowed an increase in racket length, width and fundamental frequency, in combination with a decrease in mass. As rackets become more advanced so must the scientific methods used in their understanding and design. Currently, a freely suspended racket is considered to be the best representation of a players grip. Therefore, any racket simulated in an FE model should be freely suspended. The rebound velocity of the ball off a racket is dependent on the impact location. Therefore, the impact location must be recorded when undertaking experimental work and FE simulations.

2.5. Player testing

When undertaking experiments or producing models of tennis ball impacts, it is imperative that the conditions are representative of play. Player testing is widely considered to be a suitable method for determining ball and racket movements during actual play. This sub-section will summarise existing literature on player testing.

Bower and Cross (2005) undertook player testing to determine the effect of string tension. Three identical rackets were used for the testing; strung at 180,

230 and 280 N (40 lb, 51 lb and 62 lb). The players returned balls fed to them from a tennis ball machine. It is difficult to quantify the extent to which this actually replicates competitive play. The mean rebound velocity of the ball which was measured using a radar gun was 110.1±10.3 and 103.6±8.6 km·h^{-1} (30.1±2.9 and 28.9±2.4 m·s^{-1}) for males and females, respectively. The rebound velocity of the balls was slightly lower for the rackets strung at higher tension. This was in agreement with the findings of other authors for laboratory based experiments (Haake *et al.*, 2003a; Goodwill and Haake, 2004a; Cross & Lindsey, 2005; Brody *et al.*, 2002). Using a static racket at lower tension, under experimental conditions, also causes the ball to rebound at a smaller angle relative to the racket normal (Cross & Lindsey, 2005; Goodwill & Haake, 2004b; Haake *et al.*, 2003). Bower and Cross predicted that during play, the ball will leave a racket strung at lower tension at a greater angle, travelling further and giving the impression of increased power. Their player testing results highlighted that the greater velocities and angles resulting from lower tension strings increased the number of shots landing beyond the base line of the court. The opposite was found for high tension, where there were more cases of the ball failing to clear the net (Bower & Cross, 2005). Therefore, it is imperative to accurately simulate string tension when producing an FE model for oblique impacts.

Knudson and Blackwell (2005) analysed the forehand topspin shots of seven players; all ranked 5.0 or above on the United States Tennis Association National Tennis Ranking Program. The players rallied to simulate play and their shots were recorded with a high-speed camera recording at 180 Hz. The mean racket velocity before impact was 24.3 ± 1.5 m·s^{-1}, at an angle of 27.5 ± 3.5° above horizontal. The players were also tilting their racket heads forward of vertical by a mean value of 4.2 ± 2.8°. The mean rebound velocity of the balls was 29.7 ± 1.7 m·s^{-1}, at 6.6 ± 1.4° above horizontal. Unfortunately, Knudson and Blackwell (2005) did not record ball spin rates.

Choppin *et al.* (2007a & 2007b) developed a method for using a pair of synchronised high-speed video cameras for capturing tennis ball and racket movements in 3D. The method was used to obtain data for the ball and racket movements during practice play at the 2006 Wimbledon Qualifying Tournament. 19 players were tested. Ball and racket movements were recorded within a 2 ×

2 × 2 m calibration volume located at the centre of the baseline. The 3D calibration was undertaken using a checker board (Zhang, 1999). To achieve an accurate calibration at least 15 images should be obtained, with a checkerboard at orientations approximately 20-50° to the image plane (Zhang, 1999). Choppin *et al.* (2007a & 2007b) calibrated the 3D space from the checkerboard images using a readily available Matlab Toolbox, produced by Bouguet (2008). Unfortunately the method developed by Choppin *et al.* required markers to be attached to racket; hence it could not be directly applied to match play. The ideal point of impact was defined as the location on the string-bed that results in the highest rebound ball velocity, whilst the efficiency of a shot was expressed as the ratio of the useful energy out to energy in. Efficiency was found to increase as the impact location moved closer to the ideal point. Slow shots with low spin were found to have the highest efficiency. This was concluded to be due to the large amount of energy which goes into the generation of spin. These results were only obtained for practice at a single tournament which is played on grass. Testing at different tournaments would allow comparisons to be made between different surfaces and players.

Choppin *et al.* (2008) undertook further analysis of the player testing data collected at the 2006 Wimbledon Qualifying Tournament. The mean resultant velocities of the balls before and after impact for males were 9.4 ± 3.4 m·s^{-1} and 33.6 ± 6.6 m·s^{-1}, respectively. The higher rebound velocity of the ball in comparison to Knudson and Blackwell (2005) is predicted to be due to the players being a superior standard in conjunction with lower errors in Choppin *et al.'s* method. Choppin *et al.* (2008) also concluded that the players aimed to hit the ball on the rise, although the vertical velocity at the point of impact was very low in comparison to the horizontal velocity. The mean racket COM and angular velocity before impact for males was 17.7 m·s^{-1} and 31.3 rad·s^{-1}, respectively. The mean rebound topspin was 1125 ± 1122 rev·s^{-1} (118 ± 117 rad·s^{-1}) for males and 1036 ± 812 rev·s^{-1} (108 ± 85 rad·s^{-1}) for females.

Goodwill *et al.* (2007a) used a pair of non-synchronised high-speed video cameras to measure ball spin rates during practise and match play at a Davis Cup match, which was played on Taraflex carpet. The cameras were positioned to film opposite ends of the court and hence capture different shots. The ball spin off the bounce was similar for both match play and practise with a mean

value of 3344 rpm (350 rad·s^{-1}) and a maximum of 5200 rpm (545 rad·s^{-1}). The mean topspin for forehand shots was 2300 rpm (241 rad·s^{-1}) during match play in comparison to 1700 rpm (178 rad·s^{-1}) during practise. This highlights the importance of obtaining data during match play, which indicates limitations in the results obtained by Knudson and Blackwell (2005) and Choppin *et al.* (2007a, 2007b & 2008). The maximum recorded topspin off the racket was 3800 rpm (398 rad·s^{-1}). As with Choppin *et al.* (2007a), further testing is required to determine the effect of playing on different surfaces. The importance of testing at different tournaments was stated in the paper.

Kelley *et al.* (2008) used the same method as Goodwill *et al.* (2007a) to measure ball spin rates during match play at the 2007 Wimbledon Qualifying Tournament. The investigation was focused on female players. The measured spin rates were comparable to those found by Goodwill *et al.* (2007a). The mean spin off the ground was 3104 ± 1208 rpm (325 ± 127 rad·s^{-1}) for males and 3024 ± 721 rpm (316 ± 76 rad·s^{-1}) for females. The mean topspin for female forehand shots was 1552 ± 431 rpm (163 ± 45 rad·s^{-1}) and the maximum was 2727 rpm (286 rad·s^{-1}). The results for ball spin rates from the different publications are summarised in Table 2.2.

Table 2.2 Comparison of ball spin rates from different publications *(mean ± SD)*.

	Mean spin off bounce (rad·s^{-1})	Maximum spin off bounce (rad·s^{-1})	Mean spin off racket (rad·s^{-1})	Maximum spin off racket (rad·s^{-1})
Choppin *et al.*, (2008) - practise male	-	-	118 ± 117	-
Choppin *et al.*, (2008) - practise female	-	-	108 ± 85	-
Goodwill et al., (2007a) - practise	~350	-	178	-
Goodwill et al., (2007a) - match play	~350	545	241	398
Kelley *et al.*, (2008) - match play male	325 ± 127	524	-	-
Kelley *et al.*, (2008) - match play female	316 ± 76	483	163 ± 45	286 ± 117

2.5.1.   Summary of player testing

Player testing can be used to obtain ball and racket movements during simulated, practice and competitive play. At present, the most accurate method is to use two synchronised high-speed video cameras to obtain results in 3D. The results obtained from player testing are required for ensuring realistic conditions when conducting experiments and producing models. In order to

obtain the most realistic range of ball and racket movements the testing should be undertaking during match play.

2.6. Modelling

A number of studies have focused on producing models of tennis ball impacts. These models vary in both accuracy and complexity. This literature review will cover ball to surface, ball to string-bed and ball to racket models.

2.6.1. Ball modelling

Brody (1984) attempted to model an oblique impact on a tennis surface, based on Newtonian mechanics, which assumed that the COR was constant and the ball was rigid. This assumption was based on a typical shot having a drop height of approximately 1 m, with a resultant deformation of less than 10% of the ball's diameter. He concluded that at low incident angles *(relative to the horizontal)* the ball will slide with a decreasing horizontal velocity; whilst at high incident angles the ball will still slide with a decreasing horizontal velocity but then roll at a constant speed. The COF that initiates rolling decreases with the increasing angle of incidence, at constant values of COR. Neglecting the balls deformation means the model would decrease in accuracy for impact velocities above that of a 1 m drop height.

Capel-Davies (2007) examined how the SPR of different court surfaces, was influenced by inbound horizontal velocity. Brody's (1984) model was used to calculate SPR, which was found to be independent of both inbound horizontal velocity and angle of incidence, in the range from 11-31 m·s^{-1} and 11-25°, respectively. This indicates that, assuming the COF to remain constant in an FE model which is used to simulate a range of ball-surface impacts is a realistic representation of reality (Goodwill *et al.,* 2005). Capel-Davies found the horizontal COR to remain proportional to the angle of incidence for the entire range of impacts tested. This demonstrates that a tennis ball does not go into a rolling phase for angles of incidence up to 25°. This was in contradiction to Brody (1984) and was stated to be due to the deformation of the ball during impact (Capel-Davies, 2007). Capel-Davies concluded, that testing at larger angles of incidence should be undertaken to determine if it is possible to cause

38

a tennis ball with no inbound spin to roll during an oblique impact. It may be possible to answer this uncertainty using an FE model.

Dignall and Haake (2000) incorporated deformation into a model by simulating a ball to rigid surface impact as a spring damper system. The spring stiffness and damping coefficient, which are assumed constant throughout the impact, are calculated from experimentally obtained contact times and COR's. Including this deformation of the ball into the computational analysis increased its rebound spin, thus improving the models agreement with experimental results (Dignall & Haake, 2000; Pratt, 2000). However, this type of model produces an unrealistic force-time curve as the constant damping led to a negative force at the end of the impact.

Haake *et al.* (2003b) improved the model, incorporating the viscoelastic properties of the rubber core, by making the spring damper system non-linear. They also included non-symmetrical impulsive forces as well as allowing the friction between the ball and surface to reverse direction during the impact. Haake *et al.* (2005) enhanced how the model simulated the buckling of the walls of the ball by assuming the felt to have very low stiffness. Thus, the COM of the ball was allowed to displace 2 mm before the stiffness of the rubber was incorporated into the calculation. A momentum flux term was also included to account for the energy loss in the ball as it deforms. They concluded that the ball's deformation during impact was proportional to its stiffness, while the contact area was a function of the damping coefficient. Conversely, the model assumed the deformation of the ball to be symmetrical throughout an oblique impact, which didn't agree with their high-speed video cinematography. Excluding this non-symmetrical deformation, caused the model to underestimate the horizontal COM displacement of the ball by around 5%. They suggested that an FE model might lead to a better understanding of how the ball deforms during impact.

Hubbard and Stronge (2001) produced an FE model of the impact of a table tennis ball on a rigid surface, obtaining deformations which were comparable with high-speed video footage. Goodwill *et al.* (2005) applied FEA to tennis, producing a realistic model of a ball using Ansys/LS-DYNA 8.0. The model consisted of separate parts for the rubber core and felt cover. The quasi-static material properties of the rubber and felt where obtained experimentally

(Figure 2.2, page 8). The viscoelastic or rate dependent material properties of rubber where estimated in an interactive process. This technique has been used by numerous other authors when creating FE models for simulating sports ball impacts (Calder and Sandmeyer, 1997; Price *et al.,* 2006 & 2007; Biesen and Smith, 2007; Smith and Singh, 2008). The internal pressure of a selection of tennis balls was measured as 76 kPa, using a bespoke pressure gauge. The internal pressure to volume relationship of the ball was assumed to be isentropic and was simulated in the model using an air-bag, which was assigned to the internal surface of the core. The pressurised ball model was validated against experimental data for both quasi-static compression and dynamic impacts. A punctured ball model was also produced and validated against experimental data for quasi-static compression. This was to provide a separate validation of the method used to simulate the internal pressure of the ball. The punctured and pressurised ball models were both in good agreement with the experimental data for quasi-static compression. Pressurised core and ball models were both validated against experimental data for perpendicular impacts. This was to provide an independent validation of both the rubber core and felt cover. Extending the experimental validation to include punctured balls and cores, would have provided further insight into the accuracy of the air-bag. The rubber core model was in good agreement with the experimental data for the entire range of inbound velocities used in the investigation. The complete ball model over-predicted rebound velocity at inbound velocities greater than 15 $m \cdot s^{-1}$. This over-prediction was attributed to errors in the felt model. The force plots for the pressurised ball model were in good agreement with those obtained experimentally using a force plate. In particular the model accurately simulated a peak in force close to the start of the impact, which has been noted by numerous other authors (Cross, 1999; Dignall and Haake 2000; Goodwill, 2002). Measuring more parameters such as contact time and ball deformation would provide a more rigorous validation of the model. Experimental data showed that the vertical COR of oblique impacts was higher than for normal impacts. The FE model was used to conclude that friction in the contact region produced an unbalanced horizontal force during an oblique impact, causing the ball to deform forwards. This caused a 10% decrease in the volume of the ball in relation to a normal impact, resulting in a higher internal pressure and

40

elevated rebound velocity. Experimental data also indicated that tennis balls incident at an oblique angle to a rigid surface with no inbound spin were rebounding with a spin rate greater than associated with rolling. The FE model was used to show that high spin is due to a lag occurring before the friction force acting on the ball changes direction, as a result of shearing of the felt in the contact region (Figure 2.14). Goodwill *et al.* stated that it would be difficult to come to these conclusions using conventional laboratory experiments. Extending the validation to include oblique spinning impacts would provide a better representation of a typical impact between a ball and court during play. The effects of temperature could also be analysed to determine the influence of different ambient conditions in relation to play.
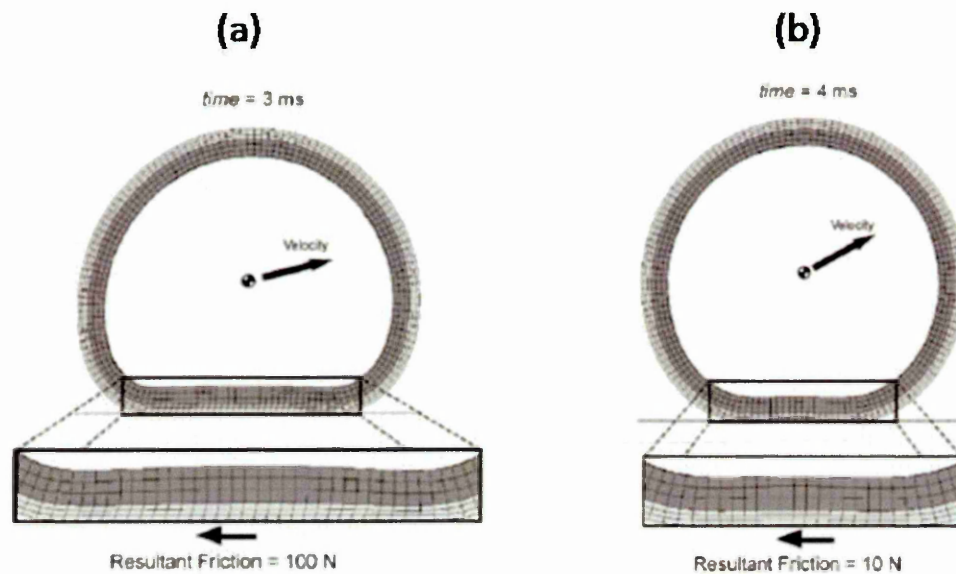
Figure 2.14 Shearing of the felt during an oblique impact on a rigid surface at 15 m·s^{-1} and 30° with no initial spin (Goodwill *et al.*, 2005).

The buckling of the ball during impact indicates the importance of applying a nonlinear FE model (Becker, 2004; Kurowski, 2004; Goodwill *et al.*, 2005). This gives a totally independent investigation, separating FE from analytical models, which rely on experimental results. Therefore, allowing full analysis of the ball's structural stiffness and deformation during an impact. An accurate FE model can be easily modified to simulate different materials, which is particularly useful for manufacturers. FE has been found to underestimate the energy lost in the ball during impacts (Goodwill *et al.*, 2005; Hubbard & Stronge, 2001). However,

this should be easily rectified by enhancing the accuracy of the material models. The principal advantage of an FE model, over conventional experiments, is the ability to make fine adjustments to parameters, such as the COF, in order to determine their effect on the motion of the ball throughout impact and rebound. This can be undertaken whilst keeping all other variables constant; effectively eliminating any inaccuracy of the data that occurs as a result of natural experimental errors, such as variations in impact velocity and angle. Modelling the rebound characteristics of a range of balls on different surfaces can be undertaken efficiently, once the corresponding values of COF have been obtained experimentally.

2.6.2. *String-bed modelling*

Goodwill and Haake (2004a) produced a rigid body and a flexible body mathematical model of an impact between a tennis ball and head-clamped racket. An impact with an inbound velocity of 31 m·s^{-1}, angle of 39° and backspin of 200 rad·s^{-1} was analysed. It was concluded that a rigid body mathematical model under-predicted the rebound spin of the ball, which was found to be higher than that associated with rolling. A flexible body mathematical model was used to show that the ball starts to over-spin at the mid-point of the impact. Over-spinning results in the friction force reversing direction, which causes an increase in the horizontal velocity of the ball. This reversal of the friction force acting on the ball was in agreement with the findings of numerous authors for oblique impacts on a rigid surface (Cross, 2002; Haake *et al.,* 2003b; Haake *et al.,* 2005; Goodwill *et al.,* 2005). However, Goodwill and Haake's (2004a) flexible body model did not have the capacity to calculate the rebound spin of the ball. Further testing including higher spin rates and a range of angles is required to gain further insight into the ball's characteristics when impacting with a string-bed.

Cross (2000b) produced a model of a ball impacting on a string-bed at 10 m·s^{-1}, to analyse the effect of the sliding friction between the ball and the strings. A resultant velocity of 10 m·s^{-1} is considerably lower than values measured during play (Choppin *et al.* 2008). The critical value of sliding friction coefficient between the ball and string-bed was found to be 0.3; below this it was stated that the balls rebound angle and range drops significantly, which would result in

42

a detrimental effect on the player's performance. As well as not validating the model against experimental data, Cross made a number of assumptions and simplifications. His results were based on the assumption that the ball impacts at the centre of the string-bed, which is not representative of a shot during play (Choppin *et al.* 2007b). He also did not consider the effects of friction between strings and their movements. Currently there are no publications on the subject of string-to-string fiction. An FE model, incorporating the correct, ball-to-string and string-to-string friction, could be used to analyse the full effects of varying these parameters on the entire range of impacts encountered during play.

A number of authors have attempted to include a string-bed in an FE model of a tennis racket with varying success (Widing and Moeinzadeh, 1989; Widing and Moeinzadeh, 1990; Kanda *et al.,* 2002). Widing and Moeinzadeh (1989 & 1990) used a static FE model to examine the effect of string tension on the frame stiffness, of a wooden racket clamped at the handle. The ball was simulated by applying a static force of 88.96 N over an area with a radius of 2 cm, at the centre of the string-bed. This is useful for determining the static stiffness of a tennis racket, but it is limited in terms of predicting how a racket will perform during an impact with a ball. They used string tensions of 222.4 and 311.3 N, concluding that the latter reduced the magnitude of frame deformation, hence increasing its stiffness. This was in contradiction to Cross (2001b) who found the fundamental frequency of a racket to decrease by 8.5% when strung. However, as previously mentioned they ignored the sliding of the strings by fixing them at their intercepts. Also, as the handle clamping method was not representative of a player's grip (Brody, 1987), their results do not characterize how string tension may affect frame stiffness during playing conditions. No experimental validation of the model was undertaken, making it difficult to determine the reliability of their findings. An experimentally validated, FE model of a composite racket, could be used to analyse the full effect of string tension, material and geometry on ball rebound and frame stiffness.

A dynamic FE model that incorporates the movement of the strings will allow the racket vibrations and response over time to be examined. Calder *et al.,* (1987) found tennis strings to have relatively linear properties within their operational range. Hence, when building a FE model of a tennis racket it should be possible to use a linear material model for the strings. A range of strings can

be simulated once their corresponding material properties have been obtained experimentally. Perhaps the main advantage of using an FE model would be to allow manufacturers to design strings to an exact specification, as parameters such as COF and string-bed stiffness can be easily adjusted until the results correlate with required targets (Becker, 2004; Kurowski, 2004).

2.6.3. Racket modelling

Brody (1997a) produced a mathematical model of an impact between a tennis ball and freely suspended racket. The model was based on the conservation of linear and angular momentum and the racket was assumed to be rigid. Brody used a value of 0.85 in the model for COR, which was stated to be typical for an impact at the centre of a head-clamped racket. The model was validated against experimental data for perpendicular impacts at 20 $m \cdot s^{-1}$. The rebound velocity of the ball was slightly over-predicted for impacts at the throat and tip, but the model showed good agreement with the experimental data for impacts at the centre of the string-bed. This is because the centre of the string-bed corresponds to one of the node points and is not affected by the stiffness of the racket. The errors at the throat and tip were because the rigid body model was unable to account for energy losses as a result of racket deformations. It is predicted that the errors would be larger if the resultant inbound velocity was increased. Despite its limitations Brody's model can be used to simulate a range of rackets of known mass and moment of inertia.

Goodwill and Haake (2001) created a ball to racket impact model based on a spring damper system, which was validated against experimental data. The ball stiffness and damping coefficients were assumed to be constant throughout the impact; a linear spring was used to model the string-bed and the racket was assumed to be rigid. Head-clamped and freely suspended racket models were both validated experimentally for impacts at the GSC. The freely suspended racket was also impacted at other locations along the longitudinal axis. The models produced realistic results, concluding that a 50% change in string-bed stiffness only correlated to a 3.3% difference in ball rebound velocity, which agreed with other publications (Jenkins, 2003; Brody et al., 2002; Cross & Lindsey, 2005). However, as the racket was assumed to be rigid the model

44

underestimated its rebound velocity; this error was more pronounced for impacts away from the string-bed centre.

Cross (2000c) created an analytical model of a tennis ball impacting on a flexible freely suspended racket, based on a spring damper system. Initially the impact of a tennis ball on a constant cross section aluminium beam was modelled and validated against experimental data. Cross found that for a freely suspended beam the ACOR remains virtually constant with impact position, although it is lower for impacts close to the tip and throat. The same results were found when the model was applied to a freely suspended tennis racket, although there was no experimental validation. In order to gain a better representation of reality a model of a racket with a pivot at the handle was constructed. This updated model showed very similar results to those described previously for impacts at the throat and centre, whilst ACOR increased at the tip. Cross concluded that ACOR decreases with increasing string tension but the effects were stated to be negligible. The stiffness of the racket frame was found to have a larger effect on ACOR. An increase in frame stiffness was found to raise the ACOR for impacts at the tip, whilst having no effect for impacts at the vibration node. Cross's model assumed the material properties of the racket to remain constant along its length. In reality a tennis racket will have varying stiffness along its length which may affect Cross's conclusions. Validating the racket model against experimental data would also provide a better indication of the reliability of the findings.

Goodwill and Haake (2003) improved the spring damper model published by Goodwill and Haake (2001), by replacing the rigid racket with a flexible one. The racket was modelled as a one dimensional beam consisting of N segments. The mass of each of the segments was adjusted until the mass and balance point of the beam corresponded to an actual tennis racket. The required stiffness of the beam was determined from the natural frequency of the racket. The individual segments of the beam all had the same flexural rigidity. The flexible beam model showed stronger agreement with the experimental data in comparison to a rigid body model in terms of ball rebound velocity, for impacts offset from the geometric centre of the string-bed along the longitudinal axis (Figure 2.15). A model that can simulate impacts which are offset from the longitudinal axis of the string-bed would provide a better representation of an actual tennis shot

(Choppin *et al.,* 2008). The vibration response of the racket was in good agreement with the experimental data. However, the model failed to account for the large vibrations experienced by the racket when the ball impacted near the tip. This error is believed to be a consequence of the model assuming the stiffness of the racket to be constant along the entire length.
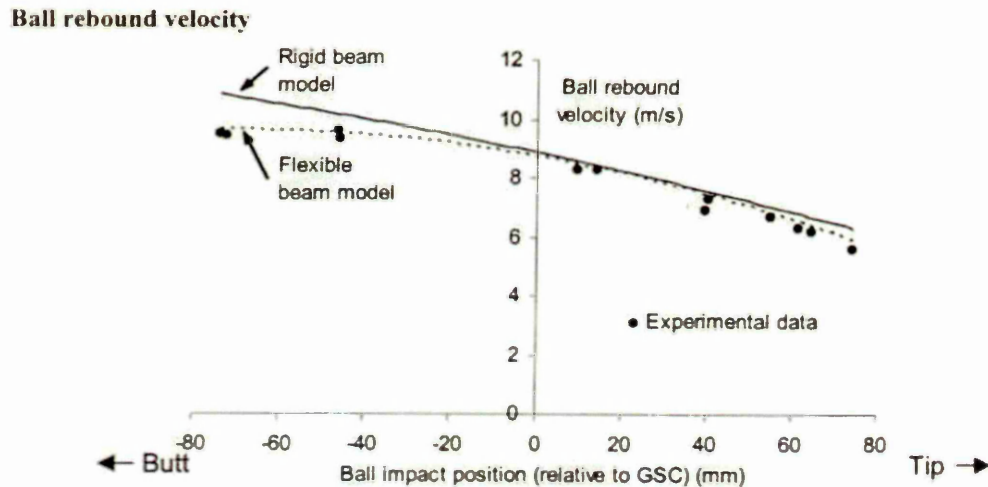
Figure 2.15 Comparison of a flexible and rigid body model for simulating impacts between a tennis ball and freely suspended racket (Goodwill and Haake, 2003).

The material properties of a racket determine its stiffness, and hence bending characteristics. Therefore, the material model is vital when undertaking a dynamic FE simulation. Calder and Sandmeyer (1997) produced FE models of the impact between softball and baseball bats and their corresponding balls. It was possible to model the aluminium bats using readily available material properties, due to their homogeneous nature. The balls were assumed to be isotropic, homogeneous and viscoelastic, to simplify the model. Their viscoelastic properties were adjusted until the COR, deformation and contact time correlated with expected results, for an impact with a bat. A more versatile method would have been to obtain the material properties experimentally. The ball models could then have been validated by simulating an impact with a rigid plate, as done by Goodwill *et al.* (2005). This would eliminate any discrepancy as a result of errors in the bat. Although they claimed the results to reliable, this was based on expected results from published data as opposed to experimental validation using the exact conditions within their model.

46

Jenkins and Calder (1990) produced an FE model of a tennis racket. The tennis strings were not modelled as it was stated that they would have made the problem size too large. As the racket was symmetrical only half of it was modelled. The bending stiffness and fundamental frequency of the racket were found to be in good agreement with experimental data when handle-clamped. Brody (1987) found that a handle-clamped racket has an unrealistically low fundamental frequency in comparison to a hand held racket. Therefore, the method used by Jenkins and Calder (1990) to simulate the racket is not representative of how a player will hold a racket. This makes it difficult to determine how their results relate to match play.

Gu and Li (2007) produced an FE model of tennis racket using ANSYS 10.0. The geometry was created in Solidworks 2005. The material properties of the racket frame were obtained using bending and resonance experiments. The Young's modulus of the racket was 30.5 GPa and the density was 2150 $kg \cdot m^{-3}$. There was no explanation as to how the material properties of the strings were obtained. The Young's modulus of the strings was 2.5 GPa and the density was 1140 $kg \cdot m^{-3}$. This is within the expected range of 2-4 GPa for the quasi-static Young's modulus of nylon. The dominant fundamental frequency of the racket was obtained when it was rigidly clamped at the handle. The authors justified clamping the handle because during an impact the ball will have left the string-bed before the racket has completed an oscillation. This was in agreement with Brody (1979). The dominant frequency was 80 Hz in bending. It was stated that this is less than values of over 100 Hz found by other authors for freely suspended rackets, so is likely to be incorrect.

Kanda *et al.* (2002) produced an FE model of a tennis ball impacting perpendicular to a freely suspended strung tennis racket. The ball was modelled as a pressurized rubber core, with linear material properties. There was no reference to the material properties of the ball or how they were obtained. The felt cover, which has been found to influence rebound spin for impacts on a rigid surface (Goodwill *et al.,* 2005), was not included in the model. The ball had only a single element through the thickness, which is predicted to have resulted in low accuracy. It is not possible to determine the accuracy of the ball model as it was not independently validated, as done by Goodwill *et al.* (2005). As with the ball, the material properties of the racket frame or the method used to obtain

47

them were not provided. A number of impacts were simulated at different locations on the string-bed. The inbound velocity for the ball was 27.8 m·s^{-1} for all of the impacts. ACOR was found to decrease with increasing string tension and to be highest between the GSC and the throat, in agreement with other authors (Brody *et al.*, 2002; Goodwill and Haake, 2001 & 2003). ACOR was also found to decrease as the impact position moved away from the GSC towards the side of the racket. The results were shown to be in agreement with experimental data. However, there was no explanation of the uncertainty in the experimental values or how they were obtained. The results showed that increasing the stiffness of the frame resulted in an increase in ACOR for the impacts at the throat and tip, while having no noticeable effect on those at the node (*approx. GSC*), in agreement with Goodwill and Haake (2003). The variation in ACOR with racket stiffness was more pronounced for impacts at the throat, which was also in agreement with Goodwill and Haake (2003). As with previous publications (Widing and Moeinzadeh, 1989; Widing and Moeinzadeh, 1990), the strings were assumed to be fixed at their intercepts, effectively ignoring the effect of string to string friction. Goodwill and Haake (2004b) measured horizontal string displacement of up to 12 mm for an oblique impact on a freely suspended tennis racket. Hence, Kanda *et al.'s* model is clearly not a realistic representation of reality and subsequent errors would become apparent if simulating an oblique impact. This investigation has shown that FE can be used to accurately simulate impacts between a tennis ball and racket. However, full details of any material properties and experimental validation should be included to enhance the value of the model.

A composite tennis racket is non-homogenous, resulting in anisotropic material properties. Consequently, to produce an accurate FE model of a non-rigid racket, the material properties must be obtained experimentally. These must then be built into a full material model incorporating both layer position and orientation. However, as the deformation of the racket is relatively small it should be possible to use linear material properties for the individual layers (Becker, 2004; Kurowski, 2004; Widing & Moeinzadeh, 1989; Widing & Moeinzadeh, 1990). It is also essential that the model be validated against experimental results. Once the FE model has been successfully validated the effect of altering dimensions and material properties can be analysed without

the cost and time associated with producing numerous prototypes. It would also be possible to simulate oblique spinning impacts. Such a tool would have the potential to be very beneficial to racket manufacturers.

2.6.4. Summary of modelling

A number of different analytical models have been applied to tennis ball-rigid surface impacts. Rigid body models are unrealistic as they don't account for the deformation of the ball observed in high speed video footage. Similarly at present, deformable spring-damper models don't account for the deformation of the ball in the horizontal plane during an oblique impact. FE is an effective tool for simulating the 3D deformation of a ball throughout an impact with a rigid surface. The ability to simulate 3D deformation results in better agreement with experimental data, in comparison to analytical models. At present, there are no dynamic FE models of a tennis racket with a realistic interwoven tensioned string-bed. An FE model should be produced which can accurately simulate the 3D deformation of the ball, string-bed and frame during an oblique spinning impact. Such a model should be extensively validated against experimental data.

2.7. The influence of technological advances on tennis

Advances in both material and manufacturing techniques have led to an increase in racket performance, allowing players to serve at ever increasing velocities (Brody *et al.,* 2002; Haake *et al.,* 2007; Miller, 2007). A number of authors have stated that advances in racket technology have resulted in the server developing a significant advantage over their opponent, identified by an increase in the number of tie breaks (Brody, 1990; Haake *et al.,* 2000). However, Miller (2007) indicated this not to be the case. He published results from Grand Slam tournaments, which showed that the number of aces in the men's game peaked around the year 2000 and have since dropped. This suggests that the players' ability to return serve has improved, compensating for the advantage of the faster serve (Miller, 2007). As the governing body, the ITF are concerned with ensuring fair play, whilst keeping spectator appeal and commercial interest at a maximum. Implementing rule changes or applying regulations on the court surface or racket properties is expensive and could be

damaging to the game if they do not have the desired effect. Therefore, it is imperative that research is undertaken to ensure the highest accuracy when predicting how advances in equipment impact the game, before implementing rule changes.

A large amount of research is undertaken on the physics of tennis. Studies are predominantly involved with impact and aerodynamic analysis and often result in predictive models. In order for these models to be used to analyse the effects of different parameters relative to play, they can be combined into a single trajectory model. Dignall *et al.* (2004) produced a program, labelled *Tennis GUT,* for simulating different tennis shots. *Tennis GUT* was produced by combining ball to racket and ball to rigid surface impact models with a trajectory model. The individual models were considered to be state of the art at the time of publication. However, the ball to racket impact model was only capable of simulating perpendicular non-spinning impacts.

Haake *et al.* (2007) used the bespoke analysis software *Tennis GUT* to determine how the evolution of the tennis racket has affected serve speeds. They composed data from around 150 rackets, dating from the 1870's to 2007, from the Wimbledon Museum and the ITF collection. It was suggested that a player from the current era could serve 17.5% faster using equipment from 2007 in comparison to what was available in the 1870's. The lower mass of a 2007 racket was concluded to be the main contributing factor to the increased serve speeds, followed by the balance point moving closer to the tip. Racket stiffness was concluded to have only a minor effect on serve velocity. However, as the ball to racket model used in *Tennis GUT* was based on the one published by Goodwill and Haake (2003), it has the same limitations and errors. An accurate FE model would provide a better understanding of the impact between a tennis ball and racket.

Haake *et al.* (2000) investigated the effect of using a 6.5% larger and 3% heavier ball to decrease the speed of the game. Standard and oversized balls were projected onto head-clamped and freely suspended tennis rackets, at the centre of the string-bed. The impacts were perpendicular and the balls were projected with no spin at a range of velocities from 15-60 $m·s^{-1}$. The ACOR was the same for both sized balls on the freely suspended rackets. However, the COR was slightly higher for the impacts between the larger balls and head-

50

clamped racket. Haake *et al.* (2000) used Brody's (1997a) model, in which the racket is assumed to be rigid, to predict the rebound velocity of both balls when simulating a serve. It was concluded that the oversized ball will rebound slightly faster from the racket. This was in contradiction to the experimental data where both balls rebounded from the freely suspended racket with effectively the same velocity. The discrepancy is predicted to be due to the model using the COR from the head-clamped racket impacts. Haake *et al.* (2000) undertook experiments and found that the drag coefficient at 0.55 and the rebound velocity off the court were effectively identical for both sized balls. Due to its increased frontal area the larger ball was subject to a greater drag force. The results from the three investigations were combined into a single trajectory model. It was found that although the larger ball would leave the player's racket at a higher velocity it would have an increased flight time, hence impacting the court later. This corresponds to a 10 and 16 ms increase in the time to reach the base line for the 1st and 2nd serve, respectively. Although this provides evidence that the larger ball has the ability to reduce the dominance of the serve, the calculated times are based on a mathematical model. Player testing with the two ball sizes could prove an effective method for validating the results. A fully validated FE model could be used to accurately assess the effect of ball mass and size for impacts on both a freely suspended racket and court surface. This would not require balls to be specially manufactured as in Haake *et al.'s* (2000) investigation.

A realistic FE model, of a ball to freely suspended racket impact, could be used to enhance the understanding of the collision and the effect of individual parameters, such as ball or racket mass, size and structural stiffness. The results obtained can then be applied to the different aspects of the game, including the serve. However, as with any other experiment, the results must be applied to a model encompassing other factors, such as aerodynamics, to determine the full effect on the tennis game (Haake *et al.,* 2007).

2.7.1.   Summary of technological advances

Advances in racket technology over the last century have led to increased service speeds and reduced receiver reaction times. Advances in technology are likely to continue, hence the ITF must be able to monitor and predict how

they will affect the game. An FE model which can accurately simulate a range of tennis shots could be used to predict the effect of changing different ball and racket parameters. Such a model could also function as an effective design tool for racket manufactures.

2.8. Overview of Ansys/LS-DYNA

There are essentially two types of FE solver; implicit and explicit. Implicit solvers are used for analysing static structural problems ($\Sigma F = 0$). Explicit solvers are used for analysing dynamic impact problems ($\Sigma F = ma$). Both types of solver can also be applied to quasistatic problems ($\Sigma F \approx 0$), such as metal forming. As the aim of this project is to create an FE model of a dynamic impact between a tennis ball and racket, an explicit solver is required. Ansys/LS-DYNA is an explicit FE solver which can be applied to a variety of different impact scenarios, including sporting applications (Mase and Kersten, 2004; Goodwill *et al.*, 2005; Biesen and Smith, 2007, Peterson and McPhee, 2008). Ansys/LS-DYNA was selected for this project following an evaluation exercise with other FE solvers, ABAQUS and MSC Nastran. The main reason for selecting Ansys/LS-DYNA was because it has already been successfully applied to tennis ball impacts, by Goodwill *et al.* (2005). The following subsection will highlight some of the key features of Ansys/LS-DYNA, which are required for modelling the impact between a tennis ball and racket.

Elements

The two types of elements in Ansys/LS-DYNA which could be required for this project are, solid and shell. Goodwill *et al.* (2005) used SOLID164 elements with single point integration to model a tennis ball. Fully integrated solid elements do not experience hourglassing but they are approximately four times more computationally expensive in terms of CPU time. Hourglassing modes are zero-energy modes of deformation, which are not physically possible. Shell elements are designed for modelling thin walled structures, such as the frame of a composite tennis racket. There are twelve different formulations of shell elements, for all of which the number of integration points can be specified.

Material models

There are over forty material models in Ansys/LS-DYNA. Models used previously by Goodwill *et al.,* (2005) were MAT_RIGID, MAT_LOW-DENSITY_FOAM and MAT_OGDEN_RUBBER. MAT_RIGID was used by Goodwill *et al.,* to simulate an impact between a tennis ball and rigid surface. MAT_RIGID materials are computationally efficient and can be used to simulate the properties of infinitely stiff parts. Realistic values of Young's modulus should be used when simulating rigid parts to ensure the correct contact behaviour. MAT_LOW-DENSITY_FOAM was used by Goodwill *et al.* to simulate the felt cover of the ball because it is capable of simulating large deformations. Non-linear behaviour is modelled using a quasi-static stress-strain curve. MAT_OGDEN_RUBBER was the material model used by Goodwill *et al.* for the rubber core. This model is based on the Ogden (1984) material model, which is designed for simulating rubbers. The model is capable of simulating non-linear rubber like properties through the use of a quasi-static stress/strain curve. Linear viscoelasticity can also be simulated using a stress relaxation curve. The simplest and most computationally efficient non-rigid material model is MAT_ELASTIC. It is capable of simulating linear material properties at a single temperature through the use of a Young's modulus, Poisson's ratio and density.

Contact

In order to model impacts, contact must be defined between any interacting parts. There are a range of different contact types in Ansys/LS-DYNA. It is possible to define coefficients of static and sliding friction and birth and death times for all types of contact. Goodwill *et al.* (2005) used CONTACT_AUTOMATIC_SURFACE_TO_SURFACE to define contact between the felt cover of a tennis ball and a rigid surface. Surface to surface contact is very efficient for defining contact between parts which experience a larger amount of relative sliding. TIED_CONTACT can be used to glue two surfaces together. Slave nodes are forced to follow the deformation of the master surface.

Loads

All loads in Ansys/LS-DYNA are time dependent. This means they must have a pair of parameters, corresponding to the time and the load. All load definitions can be assigned a birth and death time within the analysis. Special types of loads include constraints and initial velocities. The INTIAL_VELOCITY command can be used to apply an initial velocity to an object, such as a tennis ball (Goodwill *et al.,* 2005). Ansys/LS-DYNA is normally used to run dynamic simulations, within the transient phase of the analysis. However, dynamic relaxation can be used to apply static preloads to a body, e.g. internal air pressure, before the transient phase of the analysis which starts at time zero. The solver will apply damping and monitor the kinetic energy until it is dissipated. The dynamic relaxation phase ends when the current distortional kinetic energy is less than the maximum distortional kinetic energy multiplied by the convergence tolerance. Goodwill *et al.* (2005) simulated the internal pressure of a tennis ball, using an AIRBAG_SIMPLE_PRESSURE_VOLUME command. This involved defining a pressure-volume relationship for the ball and assigning it to a segment created from the interior surface of the rubber core. The airbag command had to be assigned during the dynamic relaxation phase to prevent excessive oscillations of the ball at the start of transient phase of the analysis.

2.8.1. Summary of Ansys/LS-DYNA

Ansys/LS-DYNA is an explicit FE solver which can be applied to tennis ball impacts. A wide range of features such as, solid and shell elements, contact, advanced material models, initial velocity and dynamic relaxation, are likely to be required for this project.

2.9. Discussion

Previous investigations have highlighted discrepancies in the results obtained by different researchers. This is mainly due to the inherent errors that occur when simulating and modelling the dynamic properties of tennis ball impacts, combined with a lack of detailed visual representation. FEA allows investigations to be undertaken in a very controlled environment, allowing for fine adjustments to be made to each researched variable, whilst keeping the

others set at a predetermined value, eliminating unpredictability in the results. The exact details and specifications of the simulation can then be obtained and stored electronically, making them easily accessible for follow-up work. This effectively allows for academic knowledge to be shared, passed on and implemented into further scientific development of tennis or other sports.

A complete visual image can be obtained from a dynamic FE model. This provides the researcher with a superior tool, in comparison to high-speed video, for understanding, presenting and explaining the motion of the ball, strings and racket during impact. High-speed video, whilst excellent for validation work, is effectively only captured in two dimensions, whereas an FE model can be completely revolved and viewed in all planes. In addition, unlike high-speed video footage, sections of an FE model can be blanked, allowing hidden areas to be seen. Perhaps the main advantage of an FE model, over high-speed video, is that the required results can be obtained almost immediately, once the simulation has finished, without the requirements for interpolation. Thus, effectively making FE a more effective and efficient tool for both academia and industry.

A fully validated FE model of a ball to court impact will provide the researcher with a better understanding of how the ball deforms throughout the collision. This can then be used to comprehend and describe how high spin is obtained from oblique impacts. Variables, such as the COF between the ball and court surface, can be adjusted relatively easily in an FE model to determine their effect on an impact. Analysing the effect of a COF is not easily accomplished using conventional experimental methods. An FE model could also be used to evaluate how alterations to parameters of the ball, such as mass and size, would affect the speed of the game. This could be undertaken without the requirement for producing numerous prototypes. A more in depth understanding of the effect of temperature on a tennis ball could also be obtained using an FE model. The additional understanding obtained from an FE model could then be used by the ITF, to implement changes to the rules in order to improve uniformity between different balls.

Previous research has indicated that the structural stiffness of a string-bed affects both the rebound velocity and angle of the ball but not its spin. An accurate FE model of an impact between a ball and string-bed could be used to

analyse the precise effects of varying parameters, such as the structural stiffness of the string-bed. However, accurately modelling a string-bed using FE is a very difficult task, for a number of reasons. First of all the stiffness of a string-bed is dependent on the string tension. Therefore, an efficient and reliable method for modelling tension must be developed. In order for the strings to behave realistically when the required tension is applied to them, they must have the correct material properties and coefficients of static and sliding fiction. As an accurate method for obtaining string friction is not yet available, a procedure for obtaining this would need to be developed. The most difficult task is likely to be physically modelling an interwoven string-bed, with strings that move independently at their intercepts. There are currently no published studies where this has been achieved. Once an accurate model has been produced and validated it will be possible to analyse the ball and string-bed deformations and movements, for a variety of different impacts. The model could potentially be used to enhance the understanding of how ball spin is generated during an oblique impact.

There are two main issues when creating a realistic FE model of a ball to racket impact. These issues are how to simulate a player's grip on the racket and model the different materials. Previous research has shown that a freely suspended racket is a good representation of a player's grip. A model of a freely suspended racket can also be more easily validated than one with a 'simulated' grip. Previous research has shown that a rigid body model of a freely suspended racket over-predicts the rebound velocity of the ball for impacts offset from the GSC and hence node point. Although mathematical models are now incorporating ball and string-bed deformations, the issue that the tennis racket deforms during impact, remains a fairly understudied area. A dynamic FE model of a freely suspended racket, with realistic material properties, will aid the researcher to understand its displacement and vibration response, when colliding with a tennis ball. It will also be possible to obtain an accurate force-time plot for the impact, which would be very difficult using conventional experimental techniques. There are not currently any published analytical or FE models which are capable of simulating an oblique spinning impact, at any location on the string-bed of a tennis racket. This means that there are not currently any models available which can be used to replicate and analyse

realistic tennis shots. An FE model should be developed which can accurately simulate oblique spinning impacts at any location on the string-bed of a tennis racket. Such a model could be used to determine the racket's response to altering different parameters such as the momentum of the collision or impact location. It may also be possible to determine the range of clamping forces exerted on the racket handle by a player's grip, by analysing an FE model against player testing data. An accurate racket model could be extremely beneficial to manufacturers. It would allow manufacturers to gain further insight into the physics of a tennis shot and allow them to produce rackets to exact specifications. This would reduce costs, in both terms of time and capital, associated with producing numerous prototypes. It may also be possible for manufacturers to improve customisation by designing rackets specifically for individual players.

Producing accurate models to represent all the different materials is predicted to be one of the most difficult processes when simulating a ball to racket impact with FE. The ball will require a non-linear material model to simulate its rubber like properties. It is predicted that it will be possible to simulate the strings with a linear material model, as their deformation during impact is fairly small. It should be possible to produce a model for the strings relatively easily once the material properties have been obtained experimentally. Due to the anisotropic nature of the composite materials used in a racket frame, modelling this will be a far more in-depth task. The properties of the individual layers and their orientations must be simulated accurately. Although it may be possible to use linear material models, which reduce computation time, as the racket deformation during impact is relatively low. Full material testing will need to be undertaken, followed by the production of a complex material model.

It is vital that any FE models which simulate different tennis impacts are rigorously validated against experimental data. Previous studies have shown that high-speed video cameras are very effective for measuring ball movements during experiments. Therefore, high-speed video cameras will be used to obtain the experimental data which will be used to validate the FE model. However, analysis using high speed video cameras is subjected to repeatability errors when undertaken manually. The repeatability error in the experimental results must be stated. The validation of the model will be one of the most important

stages of the project. In order for this validation to be fully valid and enable the model to be used to design equipment and monitor the game, it must be undertaken for impacts which are representative of match play. If testing with an initially stationary racket the inbound trajectory of the ball must be converted to the racket's frame of reference. At present, player testing during match simulations (Goodwill *et al.,* 2007a) is the most appropriate method for obtaining the correct pre and post impact velocities, angles and spin rates.

2.10. Chapter summary

In conclusion, an accurate FE model will not only allow manufacturers to produce rackets to exact specifications with reduced prototype costs and timelines, but it will also give the ITF a better understanding of different technologies; thus providing them with a better means by which to regulate them. Researchers will also be able to use FE to aid their understanding of the physical principles which determine the ball's behaviour in the game of tennis.

3. Tennis ball model

3.1. Introduction

The aim of this project is to build and experimentally validate an FE model of a tennis ball to racket impact. The first stage of this process is to construct and independently validate an FE model of an impact between a tennis ball and rigid surface. In order to construct an FE model of a tennis ball, certain properties must be obtained such as the dimensions, material properties and internal pressure. As the properties of a tennis ball change with impact speed, the model will be validated for a range of inbound velocities. A tennis ball consists of three separate parts; a felt cover, a rubber core and an enclosed pressurised volume. In order to provide a rigorous validation, the separate parts of the model will all be independently validated. Following validation at ambient conditions the model will be updated to simulate a range of temperatures. The main objectives of this chapter are:

1. To obtain the properties which are required to construct an FE model of a tennis ball.

2. To build an FE model of a tennis ball.

3. To validate an FE model of a tennis ball against experimental data for room temperature.

4. To validate an FE model of a tennis ball against experimental data for a range of temperatures.

The model which is to be constructed and validated in this chapter will be based on a Prince Tour ball.

3.2. Pressurised tennis ball properties

3.2.1.   Internal pressure

The internal gauge pressure of seven balls and eight cores was measured using a bespoke pressure gauge. The mean internal gauge pressure of all the samples was 85×10^3 N·m^{-2} and the standard deviation (SD) was 3.6×10^3 N·m^{-2}.

3.2.2.   Rubber core properties

MAT_OGDEN_RUBBER is the material model which will be used to simulate the core in Ansys/LS-DYNA 10.0 (Goodwill *et al.,* 2005). The requirements for the Ogden model are density, shear modulus, Poisson's ratio, a stress-strain curve for both tension and compression and a stress relaxation curve. Eight hemispherical rubber cores were provided by the manufacturer as material samples (Figure 3.1). The dimensions of these cores were measured using digital vernier callipers. The mean internal and external diameters of the cores were 0.05254 m (SD 3.49×10^{-4} m) and 0.05942 m (SD 1.55×10^{-4} m), respectively. The mean density of the cores was measured as 1254 kg·m^{-3} (SD 68 kg·m^{-3}).

Figure 3.1 Hemispherical rubber cores provided for material testing.

The stress-strain properties of the rubber were measured using an Instron machine (Figure 3.2). Tensile data was obtained using dog-bone test pieces with the strain recorded using a clip-on extensometer (Figure 3.2a & b). Ideally a non-contacting extensometer would have been used as they have no influence on the test piece; however, there was not one available for this project. In order to achieve a state of simple tensile strain the test pieces were

60

at least ten times longer than their width (Miller, 2006). Ideally the compression testing would have been undertaken using a biaxial test machine as they produce a state of simple compression (Miller, 2006). However, a biaxial tester was not available for this project. Therefore, compression testing was undertaken using cylindrical buttons compressed between a pair of plates (Figure 3.2c). Cylindrical test pieces were used to produce the smallest possible contact area and the plates were lubricated, both these factors help to lower the overall frictional forces and hence reduce the impact of shear stresses (Miller, 2006).
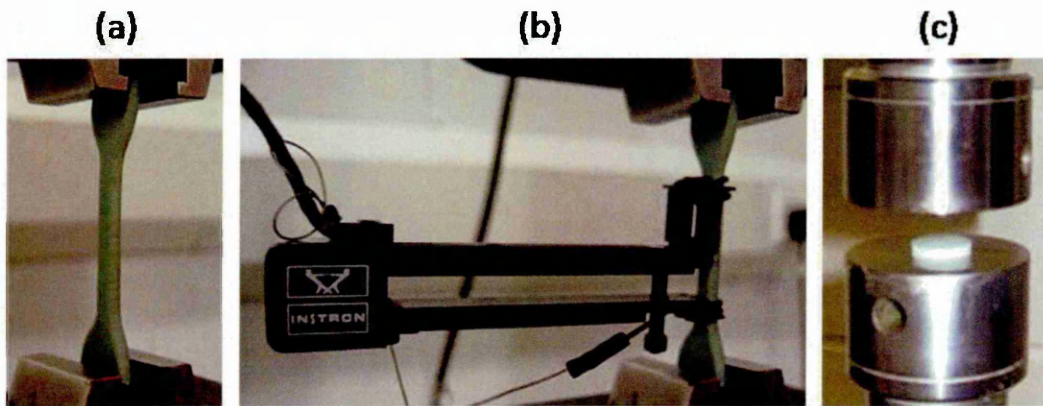
Figure 3.2 (a) Tensile test piece (b) Extensometer (c) Positioning of compression test piece.

All the test pieces were displaced at a rate of 8.33×10^{-4} m·s^{-1}, with an initial preload of 5 N and 20 N for tensile and compression, respectively. The relatively large preload of 20 N was required to remove the "slack" from the compression samples, as a result of them being cut from curved cores. Ensuring the samples were completely flat was necessary to prevent errors when measuring their displacement. The alternative would have to been to manufacture cylindrical samples specifically for the compression tests. It is predicted that using a different manufacturing process would result in larger errors than those which may be caused by using a 20 N preload. The tensile and compression test pieces were each cyclically loaded four times to stabilise the material, with the results obtained from a 5th cycle (Mullins, 1969). There was no measurable change in any of the tensile dog-bones or compression button dimensions after the 4th cycle, so the initial values were kept for the 5th

cycle. All of the test pieces settled into a relatively consistent stress-strain curve after the first two loadings (Figure 3.3), in accordance with Mullins (1969).
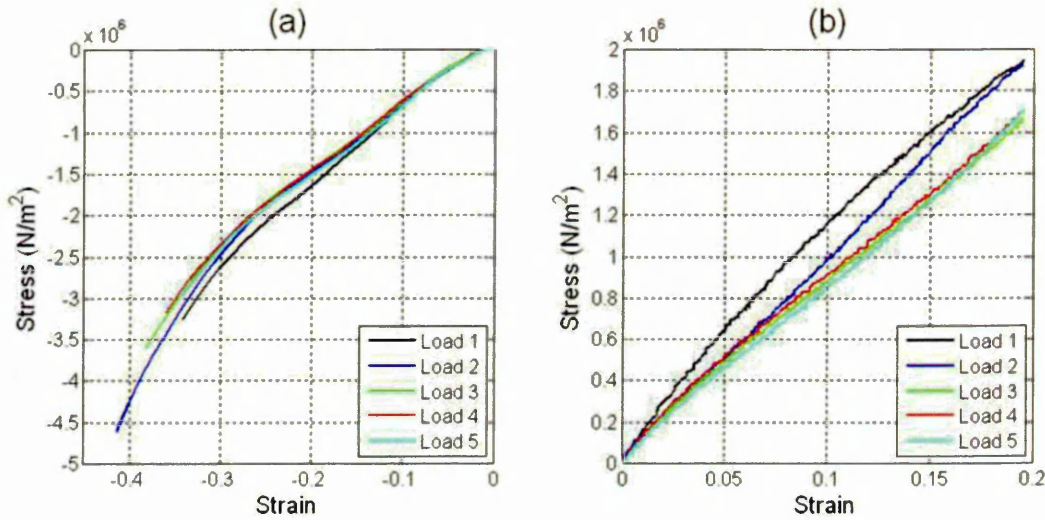
Figure 3.3 Example of cyclic loading of rubber taken from cores used in the construction of tennis balls a) compression, b) tension

The 5th and final loading of each sample is shown in Figure 3.4. Test B was identified as the median for compression and test 4 was selected for tension. Although there is strong agreement between the results for the individual tests, there may still be errors related to the experimental procedure. The main sources of error within both the tension and compression tests will most likely have arisen from measuring the sample dimensions. However, these errors should still be relatively low, as mean dimensions were calculated by undertaking all measurements three times. The most evident issue for the compression tests is the use of a relatively large preload of 20 N. It should also be noted that this preload only represents approximately 3% of the total applied load. The other, major source of error in the compression tests is the inevitable shear forces in the buttons as a result of friction from the compression plates. However, this was kept to a minimum, for this type of test, by using lubricant. There will also be errors in the tensile results due to the use of the clip-on extensometer. Any variation between tests may also be due to slight differences in the materials between the individual cores.
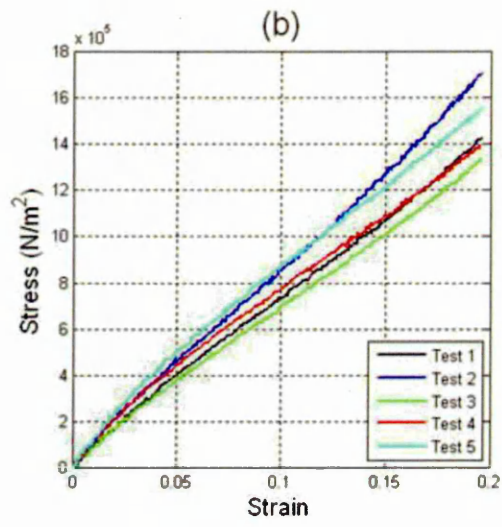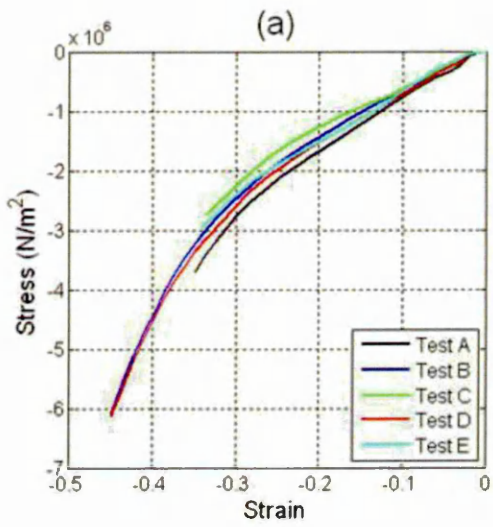
Figure 3.4 Results of tennis ball rubber material testing a) 5th cycle from each compression test, b) 5th cycle from each tensile test.

The results for tension and compression were combined and the number of data points reduced to simplify material model construction in Anys/LS-DYNA 10.0 (Figure 3.5). The shear modulus of the rubber was calculated as 2.39×10^6 N·m^{-2}, using the Young's modulus and Poisson's ratio. As the tensile stress-strain curve is relatively linear (Figure 3.5) the Young's modulus of 7.13×10^6 N·m^{-2} was calculated from the maximum strain. A Poisson's ratio of 0.49 was assumed, as this value is recommended for use in the MAT_OGDEN_RUBBER material model (LSTC, 2003).
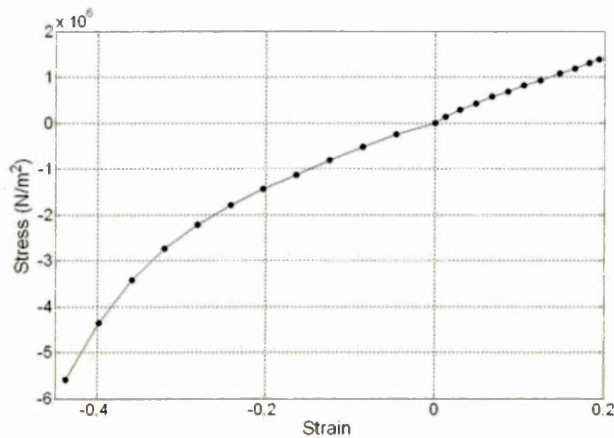
Figure 3.5 Combined tension and compression results for the tennis ball rubber material testing.

In order to model the time dependent nature of rubber the MAT_OGDEN_RUBBER material model requires stress relaxation data (LSTC,

63

2003). Stress relaxation data is obtained by holding a material sample at a constant strain, whilst measuring the time-dependent stress in the test piece, following rapid loading (Menard, 2008). Specialist equipment, which was not available for this project, is required to undertake this type of testing. Therefore, the estimated stress relaxation curve used by Goodwill *et al.* (2005) will be used in the material model.

3.2.3.   Felt cover properties

The felt material properties are difficult to measure using tensile and compressive testing. Ideally, they should be obtained using a biaxial tester, but there was not one available for this project. Therefore, the MAT_LOW-DENSITY_FOAM material model, which will be used for the felt cover, will be identical to the one in Goodwill *et al.* (2005).

3.2.4.   Summary

In this section the majority of the properties of tennis balls which are required to produce an FE model were measured. Material testing was undertaken for tennis ball rubber taken from sample cores, to measure the density, stress-strain properties and enable the shear modulus to be calculated. It was not possible to experimentally measure the stress relaxation properties of the rubber because of the unavailability of specialist test facilities. The density and shear modulus were measured as 1254 $kg{\cdot}m^{-3}$ and 2.39 × 10^6 $N{\cdot}m^{-2}$, respectively. Due to slight errors in the test procedures the material properties may need to be slightly adjusted to provide an optimum fit with the experimental data which will be used to validate the model. The stress relaxation curve which will be used in the MAT_OGDEN_RUBBER material model will be identical to the one used by Goodwill *et al.* (2005). It was also not possible to experimentally obtain the material properties of the felt. The material model used to simulate the felt will be identical to the one in Goodwill *et al.* (2005).

3.3. Finite element model of a pressurised tennis ball

3.3.1.   Details of the FE model

An FE model of a pressurised tennis ball consisting of two parts, a rubber core and felt cover, was produced in Ansys/LS-DYNA 10.0 (Figure 3.6). The internal

and external diameters of the core were 0.05254 m and 0.05942 m and the felt was given a uniform thickness of 0.003 m. The rubber core and felt cover were both made up of 21600 3D solid elements, with four elements through the thickness. This mesh density was selected following a convergence study (Appendix A.1, page 242).
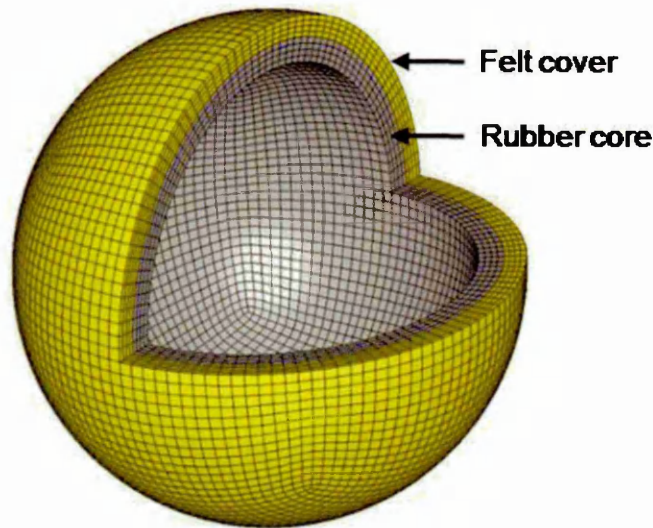
Figure 3.6 Ball model with a quarter section removed.

The internal pressure of the ball was simulated in the model as an airbag, by creating a node set from the elements on the interior surface of the rubber core and assigning an AIRBAG_SIMPLE_PRESSURE_VOLUME command to it (Goodwill *et al.,* 2005). The internal pressure (P) and volume (V) relationship is assumed to be adiabatic during impact and defined by $PV^{1.4}$ equal to a constant (Figure 3.7). The relative volume of the ball is defined as the actual volume divided by the original volume (Figure 3.7). The adiabatic assumption, of no heat transfer between the enclosed volume and its surroundings is based on the short time frame of the impact (~5 ms) and the insulating properties of the rubber core and felt cover. The internal pressure of the balls which was measured experimentally was the gauge pressure (Figure 3.8); the atmospheric pressure of 101.325×10^3 N·m^{-2} was added to this value to give the absolute pressure. The absolute pressure was then calculated for the required range of volumes. As there is no atmospheric pressure in the FE model (Figure 3.8) the absolute pressure at each volume was converted back into the gauge pressure. Hence, the curve in Figure 3.7 is the gauge pressure versus relative volume.

The internal pressure was applied in both the dynamic relaxation and transient phases of the simulations, and the convergence tolerance was 1×10^{-6}. The initial pressure of 85×10^3 N·m^{-2} was found to increase the initial volume of the ball by approximately 5% during the dynamic relaxation phase. Therefore, the initial pressure of 85×10^3 N·m^{-2} was assigned to a relative volume of 1.05 (Goodwill *et al.*, 2005). The external diameter of the ball at the start of the transient phase of the analysis was 0.066 m, which is within the limits of 0.06541 to 0.06858 m set by the International Tennis Federation (ITF).
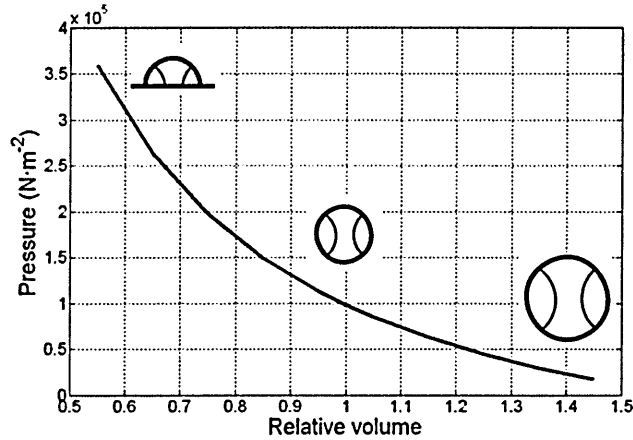
Figure 3.7 Pressure-volume curve used to simulate the internal pressure of the ball.
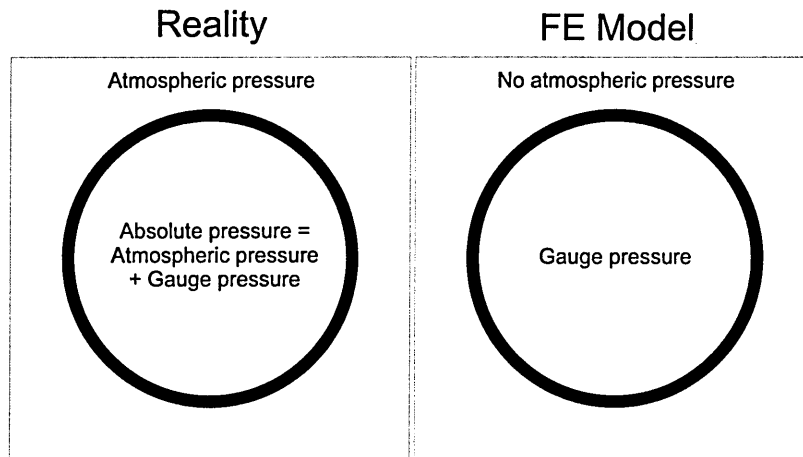
Figure 3.8 Pressure in reality and in the FE model.

MAT_OGDEN_RUBBER was the material model used for the rubber core, as used by Goodwill *et al.* (2005). The density of 1254 kg·m^{-3} resulted in the rubber core having a mass 0.0427 kg. Inspection of the stress-strain curve shows that the highest tensile strain reached during testing was approximately 0.2

(Figure 3.5, page 63), as this was the maximum achievable using the clip-on extensometer. Preliminary investigations, using the material properties from Goodwill *et al.* (2005), have highlighted that the maximum strain in the tennis ball rubber core is around 0.3, when impacted at 30 m·s^{-1} (Figure 3.9). Hence, if the current data was used to construct the material model simulations at high impact speeds would rely on values predicted by Ansys/LS-DYNA 10.0. It is predicted that a more accurate and reliable alternative is to manually estimate the shape of the tensile stress-strain curve beyond the current maximum strain, before it is input into Ansys/LS-DYNA 10.0. This hypothesis will be analysed when the model is experimentally validated.
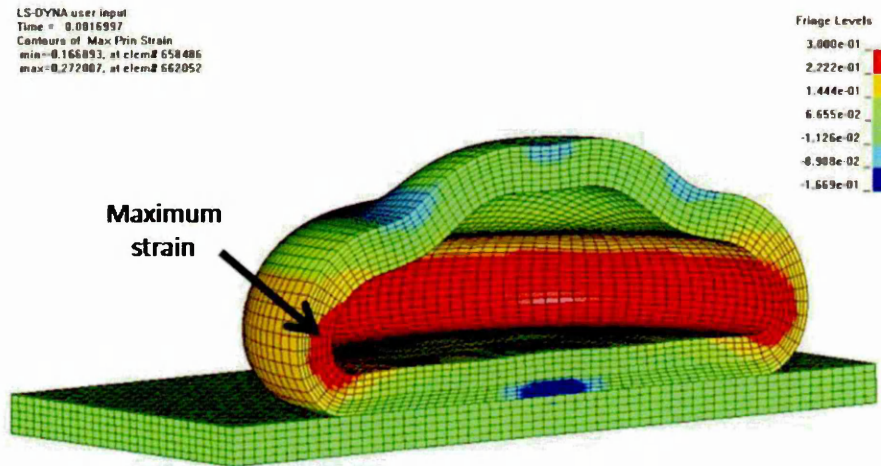
Figure 3.9 State of maximum strain *(red region)* in the rubber core for a perpendicular tennis ball impact at 30 m·s^{-1} on a rigid surface.

It is assumed that the Young's modulus of the rubber will remain relatively constant between a strain of approximately 0.2 and 0.4 (Goodwill *et al.*, 2005; Smith, 1993) (Figure 3.10). The material curve in Figure 3.10 was input into a MAT_OGDEN_RUBBER material model to produce Ogden shear modulus coefficients of -0.01487, 1.552 and 2.149 and alpha constant coefficients of -7.424,-1.664 and 3.280.
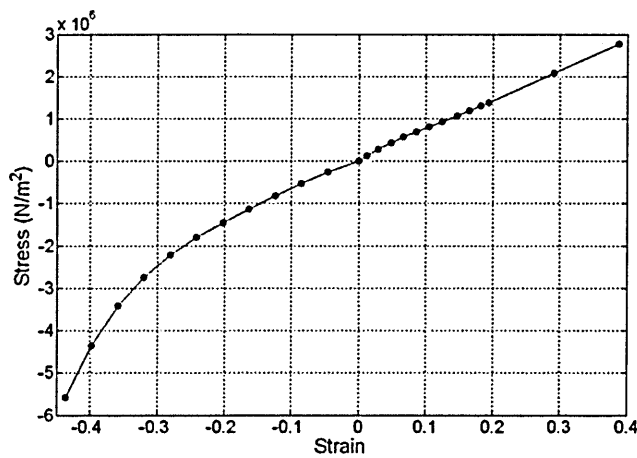
Figure 3.10 Modified quasistatic stress-strain curve for the tennis ball rubber.

As mentioned in the previous section, the estimated relaxation data used by Goodwill *et al.* (2005) was used in the model (Figure 3.11). The relaxation modulus is defined as stress at a set time divided by the applied strain. The relaxation curve in Figure 3.11 resulted in Maxwell shear modulus coefficients of 1.9750×10^{-4}, 1.4491×10^{-1}, 2.0240 and 8.2093×10^{-1} and decay constant coefficients of 2.5675×10^{1}, 2.5957×10^{2}, 2.6242×10^{3} and 2.6531×10^{4}.
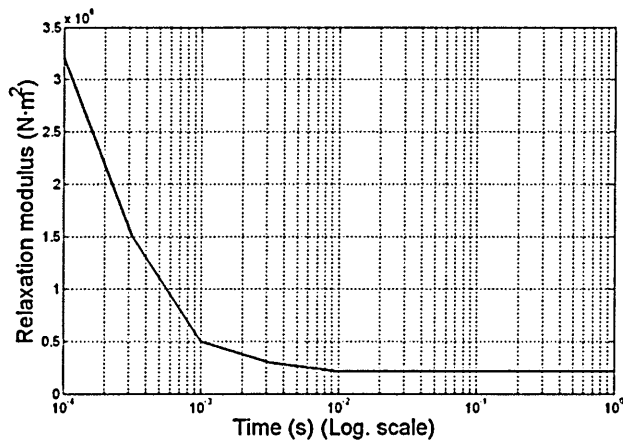
Figure 3.11 Estimated stress relaxation curve for tennis ball rubber.

As described in the previous section, the felt cover was simulated using the MAT_LOW-DENSITY_FOAM material model from Goodwill *et al.* (2005). The mass of the felt cover was 1.67×10^{-2} kg. This resulted in a total mass for the ball of 5.92×10^{-2} kg, which is within the limits of 5.60×10^{-2} to 5.94×10^{-2} kg set by the ITF.

In order to validate the FE model, an impact between the ball and a rigid surface was to be simulated. The material model used for the rigid surface was MAT_RIGID. The rigid surface had 18000 brick elements; this mesh density was selected to produce elements of a similar size to those in the ball and eliminate contact instabilities. CONTACT_AUTOMATIC_SURFACE_TO_SURFACE was used to define contact between the ball and rigid surface. As the rigid surface is considerably stiffer than the felt, the contact option SOFT = 1 was used (LSTC, 2003; Goodwill *et al.*, 2005) and the time step scale factor was changed from the default of 0.9 to 0.5 in order to improve contact behaviour. CONTROL_HOURGLASS, with an hourglass coefficient of 0.15, was also used to prevent zero-energy modes of deformation occurring in the model. The coefficient of friction between the ball and rigid surface was 0.62; this value corresponds to a smooth rebound ace court (*hard court*) (Brody *et al.*, 2002). The initial velocity of the ball was applied using INITIAL_VELOCITY_GENERATION.

3.3.2.   Summary

In the above section, an FE model of a pressurised tennis ball was constructed in Ansys/LS-DYNA 10.0. The model consisted of a felt cover and rubber core, with an airbag replicating the internal pressure. MAT_OGDEN_RUBBER was the material model used for the rubber core, whilst MAT_LOW-DENSITY_FOAM was used for the felt cover. The internal pressure was applied to the interior surface of the core using an AIRBAG_SIMPLE_PRESSURE_VO-LUME command. The next section describes the validation of the model against experimental data.

3.4. Validation of the pressurised tennis ball model

3.4.1.   Experimental methods

The dynamic properties of punctured and pressurised balls and cores were obtained for inbound velocities in the range from approximately 5 to 30 $m \cdot s^{-1}$, using an impact rig (Figure 3.12). Punctured and pressurised balls and cores were used to independently validate the three separate parts of the model, which are the internal pressure, rubber core and felt cover. The punctured core was used to validate the rubber core, whilst the punctured ball was used for the

felt cover. The results for the pressurised cores and balls were used to provide an indication of the accuracy of the internal pressure, which was used in the model. The balls and cores were punctured using a pressure gauge and it was assumed that the small hole which was created would 'reseal', preventing air from leaving the balls during the impacts. The impact rig was used to experimentally obtain the dynamic properties of the tennis balls and cores (Figure 3.12), as it is more efficient than manually tracking images from a high-speed video camera. The rig consisted of an air-cannon for projecting the balls, a set of light gates for measuring inbound and rebound velocities and a force plate for obtaining contact times and force plots. The experimental validation of the impact rig can be found in Appendix A.2 (Page 244).
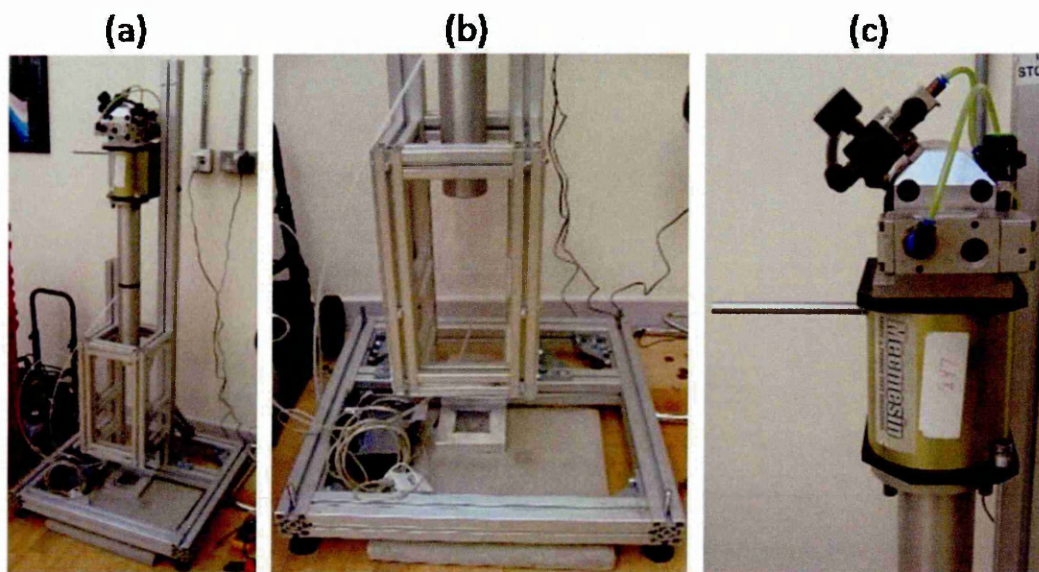
Figure 3.12 Tennis ball impact rig a) Complete rig, b) Light gates and force plate c) Air-cannon

In order to obtain the deformation of the balls/cores, impacts at approximately 5, 15 and 25 m·s^{-1} were recorded separately using a *Phantom v4.2* high-speed video camera, recording at 6000 fps (Figure 3.13a). The camera was positioned parallel to the force plate, as this allowed the maximum deformation of the balls/cores to be calculated by comparing them against an image of a non-deformed ball/core (Figure 3.13b). The inbound velocity and deformation measurements were undertaken manually using *Richimas*. A repeatability study was undertaken for the pressurised and punctured, balls and cores to assess the magnitude of the manual sampling method using *Richimas*. A single impact

for each type of ball was selected at low, medium and high inbound velocity. The inbound velocity and deformation of each of these impacts was measured ten times using *Richimas* and is shown in Table 3.1. The SD obtained for deformation are similar to those measured by Goodwill (2002).

(a) **(b)**

Air-cannon

Light gates

Camera

Force plate
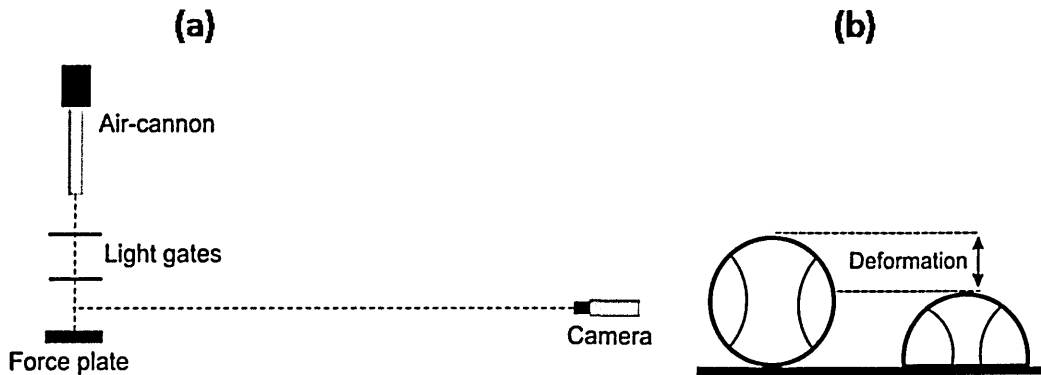
Deformation

Figure 3.13 a) Set up for impact rig validation and measuring ball/core deformation and b) Method for calculating maximum ball/core deformation.

Table 3.1 *Richimas* tracking repeatability for ball and core impacts on a rigid surface. ($value_1$/ $value_2$) = SD / SD as a percentage of the mean.

		Low inbound Velocity (m·s⁻¹)	Medium inbound Velocity (m·s⁻¹)	High inbound Velocity (m·s⁻¹)
Ball	Mean inbound velocity (m·s⁻¹)	6.7 (0.4 / 5.8%)	9.7 (0.4 / 4.1%)	26.1 (0.5 / 1.9%)
	Mean deformation (mm)	11.5 (0.4 / 3.6%)	15.3 (0.2 / 1.4%)	31.9 (0.2 / 0.6%)
Punctured Ball	Mean inbound velocity (m·s⁻¹)	5.4 (0.2 / 3.9%)	15.6 (0.4 / 2.6%)	23.3 (0.5 / 2.3%)
	Mean deformation (mm)	9.8 (0.2 / 1.6%)	23.9 (0.3 / 1.4%)	29.1 (0.2 / 0.7%)
Core	Mean inbound velocity (m·s⁻¹)	6.7 (0.4 / 5.7%)	15.1 (0.6 / 4.1%)	25.1 (0.4 / 1.7%)
	Mean deformation (mm)	15.4 (0.5 / 3.3%)	25.5 (0.3 / 1.3%)	33.0 (0.4 / 1.2%)
Punctured Core	Mean inbound velocity (m·s⁻¹)	4.8 (0.9 / 18.4%)	13.5 (0.9 / 6.6%)	-
	Mean deformation (mm)	9.3 (0.9 / 9.1%)	20.5 (0.3 / 1.5%)	-

The laboratory investigation was replicated in the FE model by simulating impacts of punctured and pressurised cores and balls on a rigid surface with inbound velocities from 5 to 30 m·s⁻¹, at 5 m·s⁻¹ increments. The rubber core model was produced by removing the felt cover from the ball. Although not initially pressurised, the punctured core and ball were assigned airbags, with an initial pressure of 0 at a relative volume of 1, as it was assumed that no air will enter or exit during the collision (Figure 3.14). The pressure volume curve

shown in Figure 3.14 was calculated in the same way as for the pressurised ball model (Page 66).
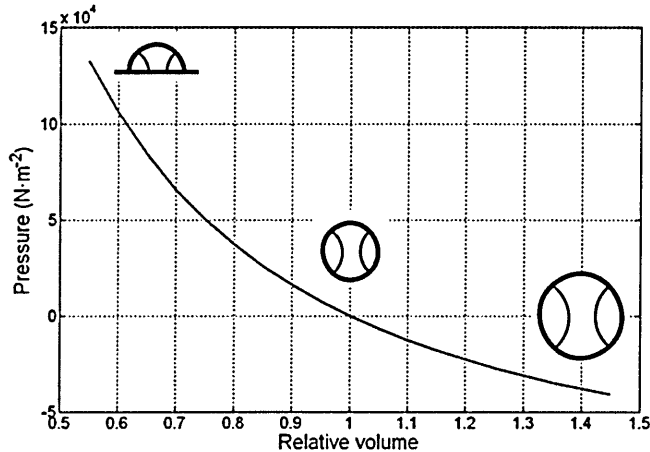
Figure 3.14 Pressure volume curve for the punctured balls and cores.

The MAT_OGDEN-RUBBER model used for the rubber core is based on *extended* tensile material data (Figure 3.10, page 68), due to limitations with the available equipment. In order to ensure the highest possible accuracy a ball model was constructed using the *measured* rubber material properties (Figure 3.5, page 63) and analysed against the model based on the *extended* material data. The shear modulus coefficients from the *measured* model are -1.375, 5.646 and 7.75 and the alpha constant coefficients are -2.624, -1.424 and 3.28. The ball models based on the *measured* and *extended* tensile rubber properties were analysed for rebound velocity.

3.4.2.   Results

Figure 3.15 shows that the rebound speeds of the punctured and pressurised core models are in good agreement with the experiment for inbound velocities above approximately 15 and 20 $m \cdot s^{-1}$, respectively. For lower inbound speeds both models slightly under-calculate the rebound velocity of the cores. The punctured and pressurised ball models show very strong agreement with the experimental data at low speeds, only marginally underestimating the rebound velocity (Figure 3.15). At velocities above 15 $m \cdot s^{-1}$ for the punctured ball and 25 $m \cdot s^{-1}$ for the pressurised ball, the rebound speed was marginally overestimated.
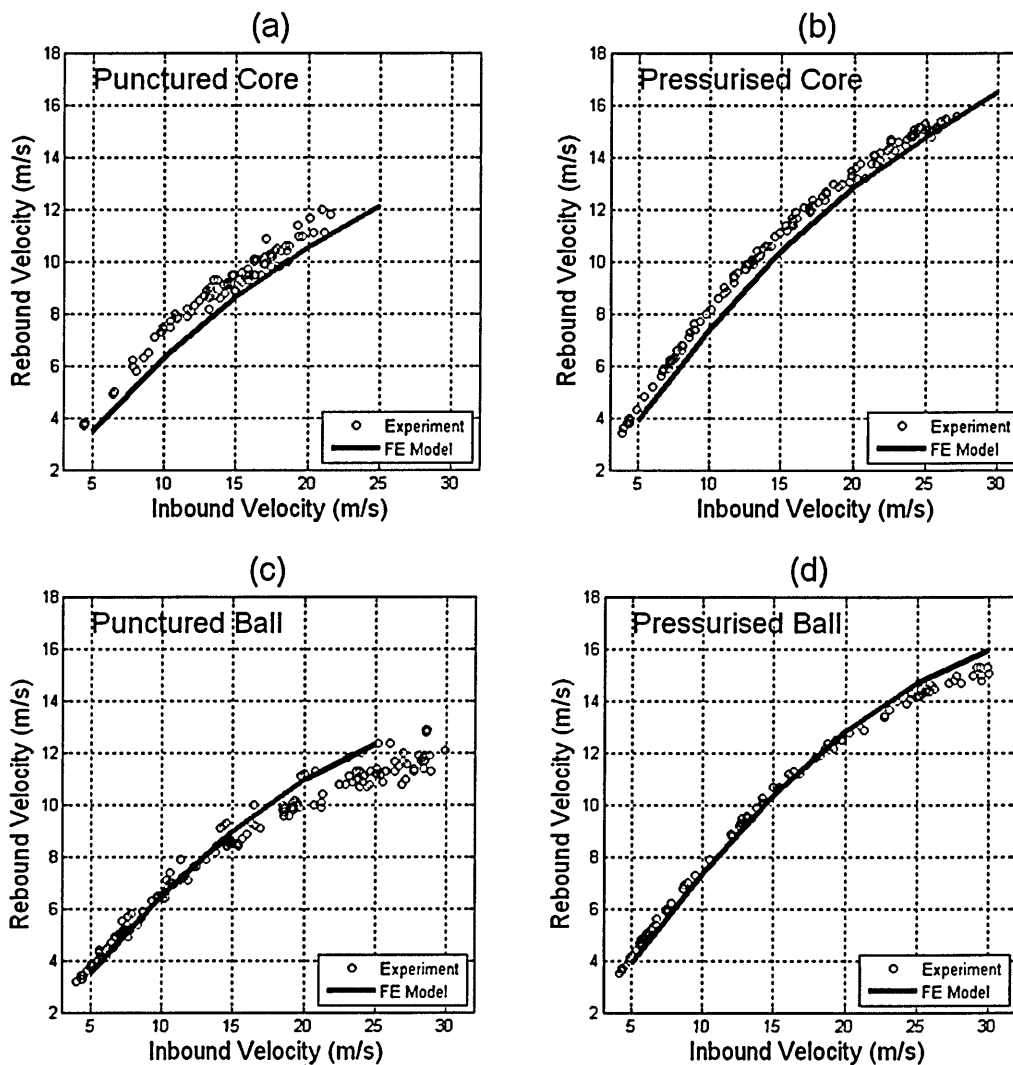
Figure 3.15 Rebound velocity against inbound velocity for perpendicular impacts on a rigid surface a) Punctured core, b) Core, c) Punctured ball, d) Ball (Experimental results obtained using light gates).

A 2nd order polynomial trend line was fitted to each set of results from the four FE models. The equation of this line was used to compare the FE model results with the experimental data, for each calculated inbound velocity. Table 3.2 shows the root mean squared error (RMSE) between the FE models and experimental data was less than 0.8 m·s^{-1} for all four sets of impacts. The same method was used to statistically compare maximum deformations and contact times.

Table 3.2 RMSE between the model and experiment for rebound velocity

	Punctured core	Core	Punctured Ball	Ball
RMSE for rebound velocity (m·s^{-1})	0.79	0.62	0.70	0.39

Table 3.3 shows a comparison between the results obtained for rebound velocities of the pressurised ball models based on the *measured* (Figure 3.5, page 63) and *extended* (Figure 3.1, page 68) rubber material properties. The RMSE between the rebound velocities obtained from the two models is less than 0.05 m·s^{-1}. However, it is predicted that the model based on the *extended* material data will be more reliable for simulating impacts with additional complexity. If the *measured* material data was used, the FE model would have to predict the characteristics of the rubber if the maximum strain was greater than 0.2. Therefore, using the *extended* material data should result in a more stable model.

Table 3.3 Rebound velocity comparison for the pressurised ball models based on the measured and extended tensile rubber material data.

Inbound velocity (m·s^{-1})	*Extended* tension rebound velocity (m·s^{-1})	*Measured* tension rebound velocity (m·s^{-1})	Difference (m·s^{-1})
5	3.87	3.87	-1.3×10^{-3}
10	7.33	7.33	-2.2×10^{-4}
15	10.35	10.36	-4.6×10^{-3}
20	12.86	12.88	-2.0×10^{-2}
25	14.69	14.74	-5.7×10^{-2}
30	15.99	16.07	-8.4×10^{-2}
		RMSE	4.2×10^{-2}

Figure 3.16 shows that the core models both show strong agreement with the experimental data for maximum deformation for the full range of velocities under investigation. It should be noted that the model does tend to appear to slightly under-calculate the deformation of the pressurised core, indicating that the structural stiffness is too high. The pressurised ball model is in excellent agreement with the experiment, as with the results for rebound velocity. However, the punctured ball model slightly over calculates the deformation, suggesting that the structural stiffness is too low. The RMSE for maximum deformation, between the FE models and experimental data, is less than 3 mm for all four sets of impacts (Table 3.4).
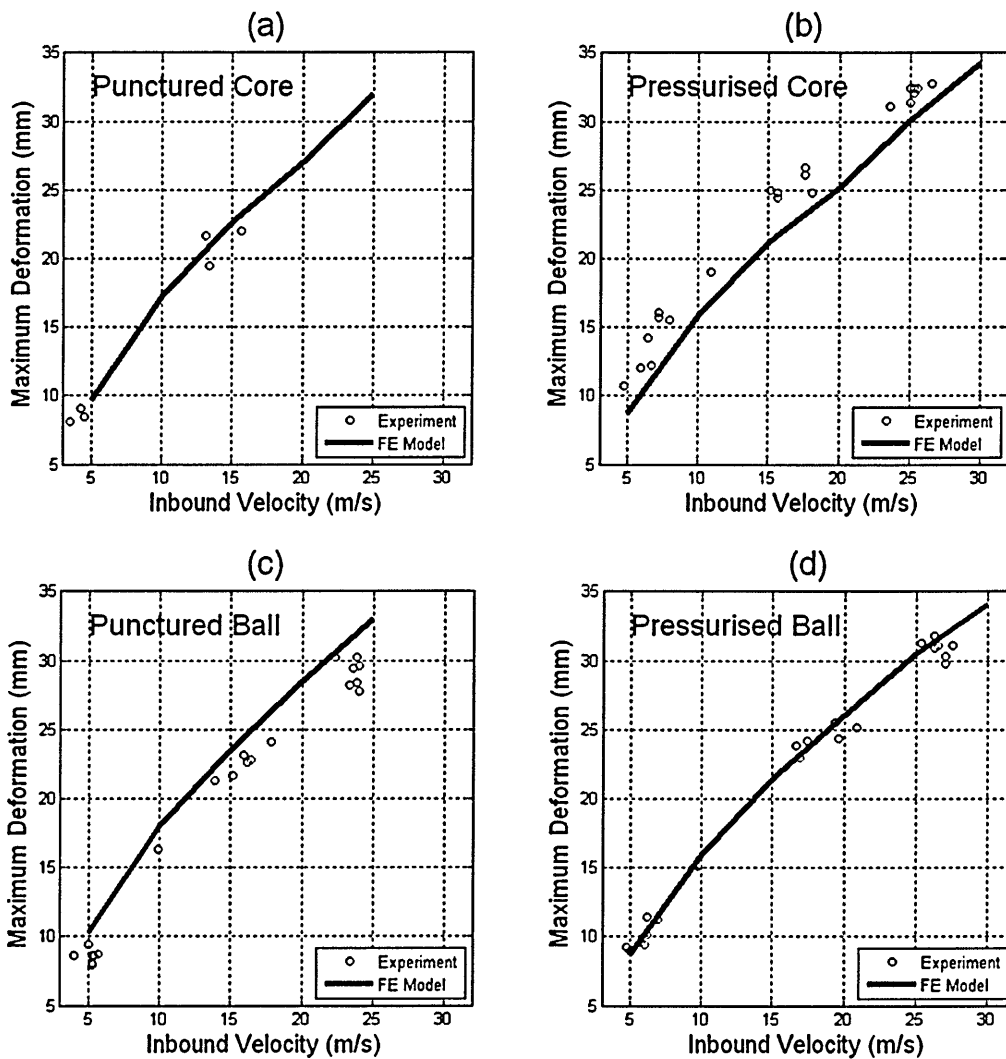
Figure 3.16 Deformation against inbound velocity for a perpendicular impact on a rigid surface a) Punctured core, b) Core, c) Punctured ball, d) Ball (Experimental results obtained a high speed video camera (Figure 3.13, page 71).

Table 3.4 RMSE between the model and experimental data for maximum deformation.

	Punctured core	Core	Punctured Ball	Ball
RMSE for maximum deformation (mm)	1.07	2.60	2.42	0.99

Figure 3.17 shows that the core models have good agreement with the experimental data for contact duration at high impact speeds. At lower velocities, below approximately 7 and 15 m·s^{-1} for the punctured and pressurised model, the contact time is marginally overestimated. Both ball models show excellent agreement with the experiment, except for a slight overestimation of contact duration at slower velocities. This implies that the ball models dissipate too much energy during low speed collisions, which is in

agreement with the results for deformation and rebound velocity. Table 3.5 shows the RMSE between the FE models and experimental data was less than 0.4 ms for all four sets of impacts.
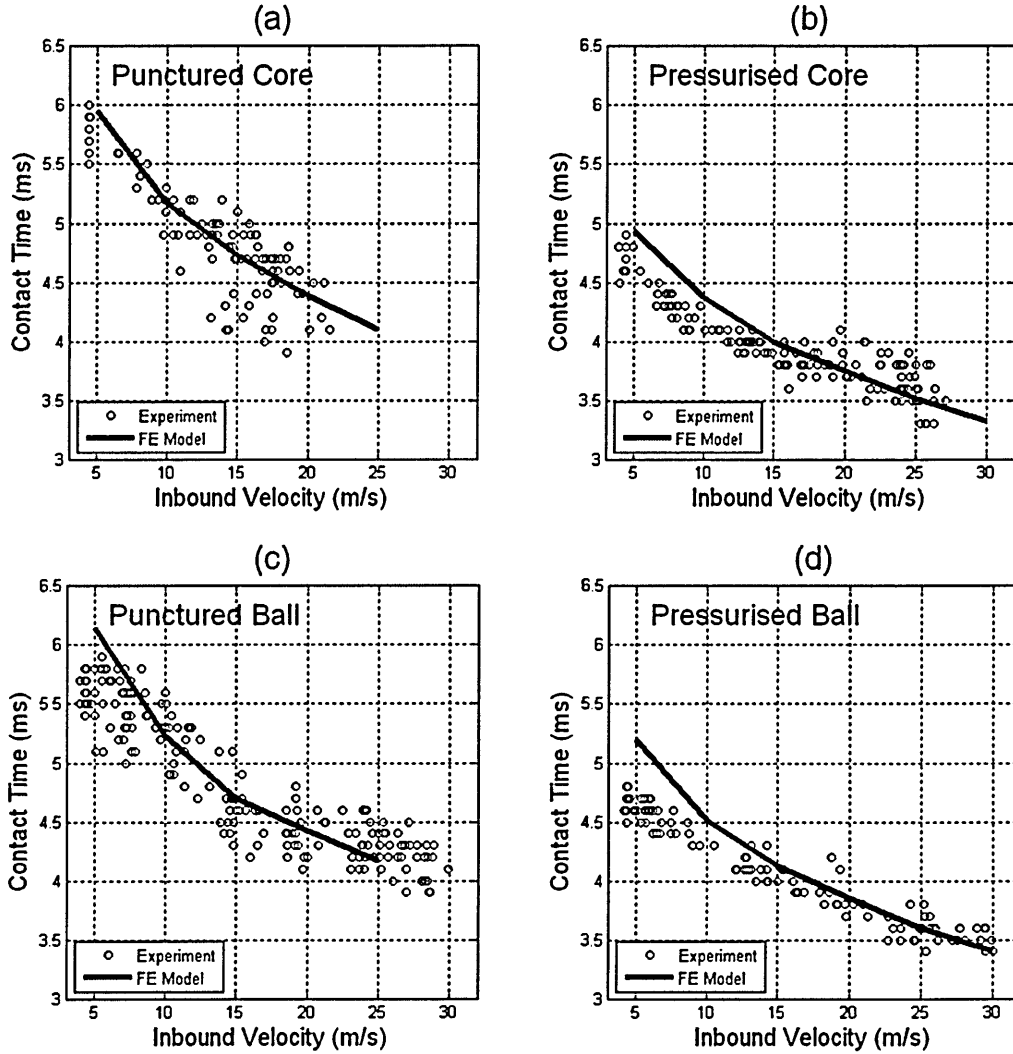
Figure 3.17 Contact time against inbound velocity for perpendicular impacts on a rigid surface a) Punctured core, b) Core, c) Punctured ball, d) Ball (Experimental results obtained a force plate).

Table 3.5 RMSE between the model and experimental data for contact time.

	Punctured core	Core	Punctured Ball	Ball
RMSE for contact time (ms)	0.27	0.23	0.35	0.36

Figure 3.18 shows a comparison of force plots from the FE with force plots obtained experimentally, using a force plate. As vibrations were observed on all of the experimental force plots they were analysed to determine the fundamental frequency. The data was analysed by converting it into the frequency domain in Matlab using a Fast Fourier transform (FFT). The

fundamental frequency was calculated as approximately 8,500 Hz (Appendix A.3, page 244). This high frequency is unlikely to be a mode of the ball, and more likely to be a mode of vibration of the force plate.

Figure 3.18 shows that the force plots for the 5 m·s^{-1} (*experiment correct to 0.6 m·s^{-1}*) impacts are all in good agreement with the experimental results. This is particularly true for the peak force and the drop in force near the start of the impact, due to the wall buckling. However, the model predicts that the buckling occurs approximately 0.15 ms later than the experiment and the overall contact time is over calculated by around 0.5 ms.
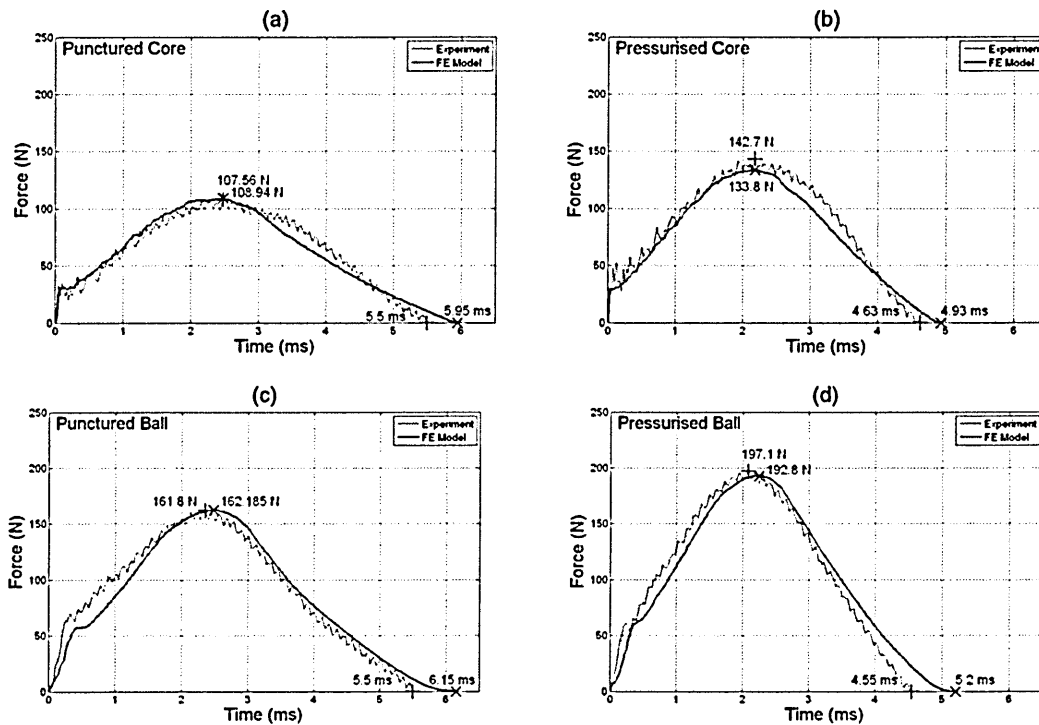
Figure 3.18 Force plot of a 5 m·s^{-1} perpendicular impact for a a) Punctured core, b) Core, c) Punctured ball. d) Ball (Experimental results obtained using a force plate).

Figure 3.19 shows that at an inbound velocity of 15 m·s^{-1} (*experiment correct to 0.1 m·s^{-1}*) all the models, except the punctured core, have relatively good agreement with the experimental data for both the peak force and curve shape. The accurate estimates of contact time, for all the models, indicate that they have the correct structural stiffness (Brody *et al.*, 2002).
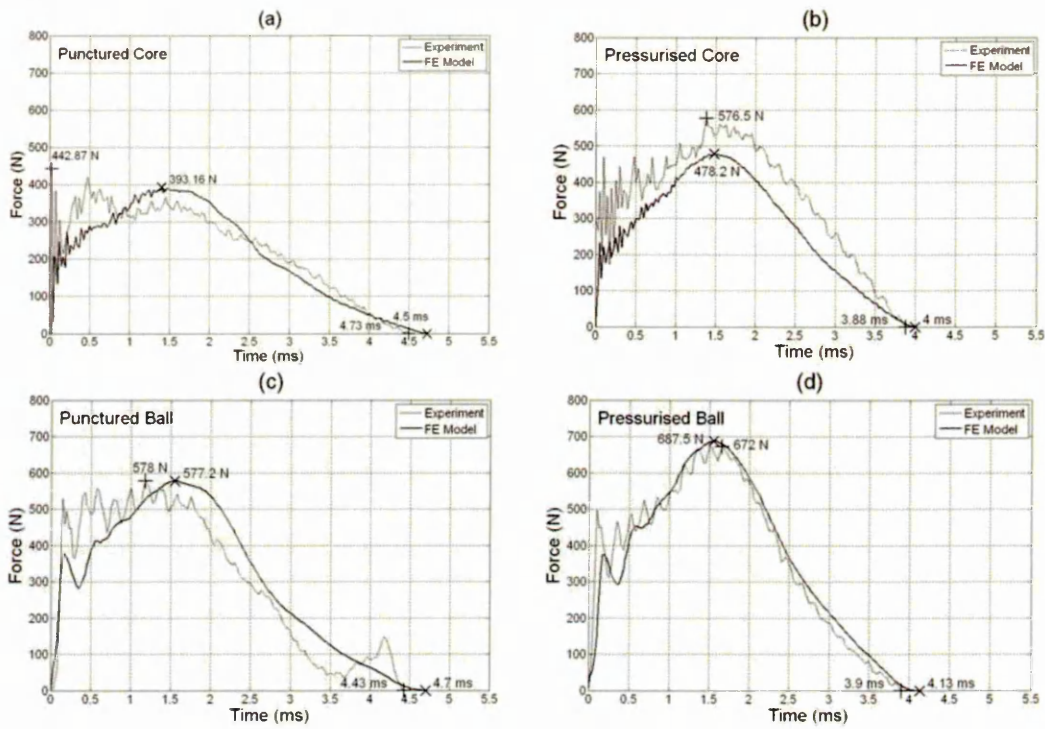
Figure 3.19 Force plot of a 15 m·s^{-1} perpendicular impact for a a) Punctured core, b) Core, c) Punctured ball and d) Ball.

Figure 3.20 shows that at an inbound velocity of 25 m·s^{-1} (*experiment correct to 0.1 m·s^{-1}*) there is a very strong agreement with contact times between the core and punctured and pressurised ball models and the experimental data. There is also good agreement, between model and experimental data, for the time at which buckling of the walls initiates. However, the models under-predict the buckling force, indicating their structural stiffness is too low. No experimental force plots were obtained for the punctured core at 25 m·s^{-1}.
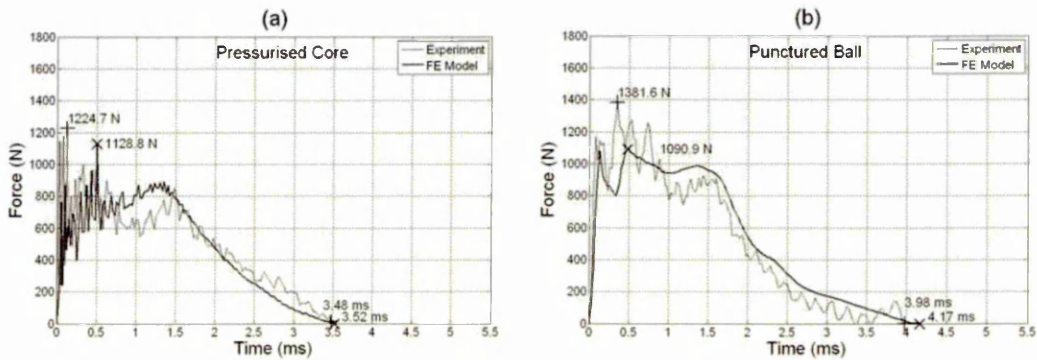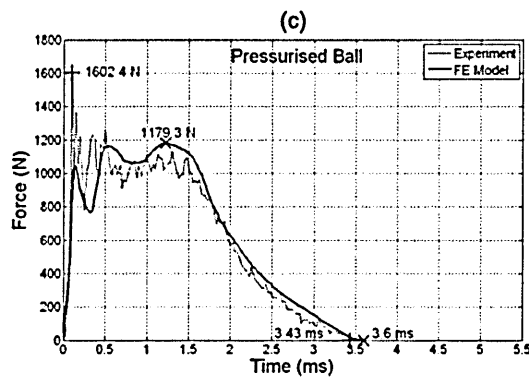
Figure 3.20 Force plot of a 25 m·s⁻¹ perpendicular impact for a a) Core, b) Punctured ball, c) Ball.

3.4.3.   Discussion

An FE model of a pressurised tennis ball has been validated for perpendicular impacts ranging from 5 to 30 m·s⁻¹, on a rigid surface. These impacts give typical ball deformations which are encountered during play. The results show that the punctured core model marginally over predicts the rebound velocity, indicating that the energy losses are insufficient. Any errors within the rubber material model are likely to be as a result of the method used for obtaining the compression data, which does have the ability to produce shear stresses within the test piece. A more accurate method would be to use a biaxial tester as this creates a condition of simple compression.

The purpose of the pressurised core simulations was to test the airbag model. As the punctured and pressurised core models have a very similar agreement with the experimental data it is concluded that the current airbag can be considered to be an accurate representation of the internal pressure within a tennis ball. The punctured ball model is used to assess the accuracy of the felt cover and the results show strong agreement with the experimental data for velocities below approximately 20 m·s⁻¹. The models overestimation of rebound velocity, above 20 m·s⁻¹, is believed to be as a result of the high impact that forces air to escape from the punctured balls during the experiment. The stronger agreement with the experimental results for the pressurised ball model at high impact velocities provided evidence for this prediction. However, the pressurised ball model over predicts the rebound velocity at high impact speeds indicating that the energy losses are insufficient. This is likely to be due to errors within the felt model, as found by Goodwill *et al.* (2005). The felt material model

could be improved by replacing the input properties with those obtained from a biaxial test machine.

3.4.4.   Summary

An FE model of a normal impact between a pressurised tennis ball and a rigid surface has been produced and validated at room temperature. Analysis against experimental data has been undertaken on the complete pressurised ball model, along with separate investigations of its individual components. The model has been validated for impact speeds between 5 and 30 m·s^{-1} and can be used to obtain a range of results including rebound velocities, contact times, impact forces and deformations. This will aid in furthering the understanding of the ball impact and the model can now be extended to simulate the full range of collisions that are encountered during a game of tennis.

3.5. Validation of the tennis ball model for different temperatures

3.5.1.   Modifications to the FE model

In this section the FE model of a tennis ball is modified to simulate temperatures of 283.15 and 313.15 K. The temperature, at which the original FE model's material testing or validation was undertaken, was not recorded. For the purpose of this investigation both of these temperatures were considered to have been 295.15 K (22°C); assuming this to be a realistic estimation of room temperature. Figure 3.21 shows the relationship between the internal pressure and relative volume of the ball, for temperatures of 283.15, 295.15 and 313.15 K. For simplicity the initial volume was assumed to remain constant between temperatures.
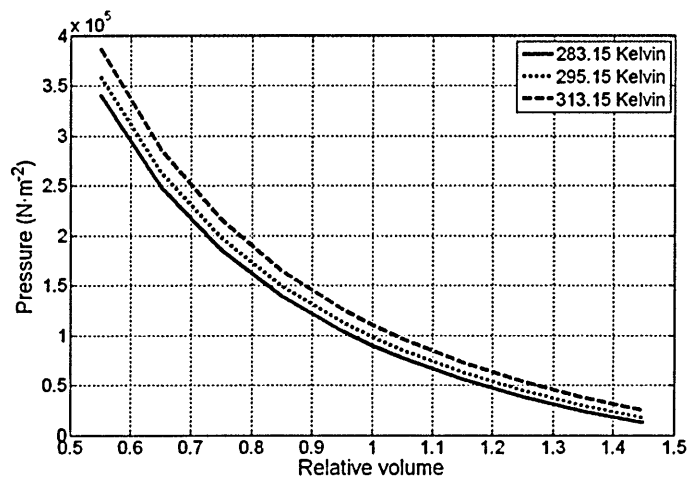
Figure 3.21 Tennis ball internal pressure against relative volume, for temperatures in the range from 283.15 to 313.15 K.

The mechanical properties of the rubber core of a tennis ball also change with temperature. The effect of altering the static stiffness of the rubber core was achieved by adjusting the stress-strain data in the MAT_OGDEN_RUBBER material model (Figure 3.22a). To produce models, which simulated the full effects of adjusting temperature, both the internal pressure (Figure 3.21) and static and dynamic material properties of the rubber were modified. The static modulus of the rubber was increased by 10% for the model at 283.15 and decreased by 10% for the model at 313.15 K (Figure 3.22a). The stress relaxation modulus of the rubber in the model was increased by 75% to simulate a temperature of 283.15 K and it was decreased by 20% for 313.15 K (Figure 3.22b). The results of the fit to the material model and relaxation curve are shown in Table 3.6. The material properties of the felt were not modified with temperature, as any changes were assumed to have an insignificant effect on the rebound characteristics of the ball. The apparatus required to obtain the material properties of the rubber at different temperatures was not available for this project. Therefore, the material properties of the rubber were changed in an iterative process until the models were in good agreement with the experimental data, in terms of both COR and contact time.
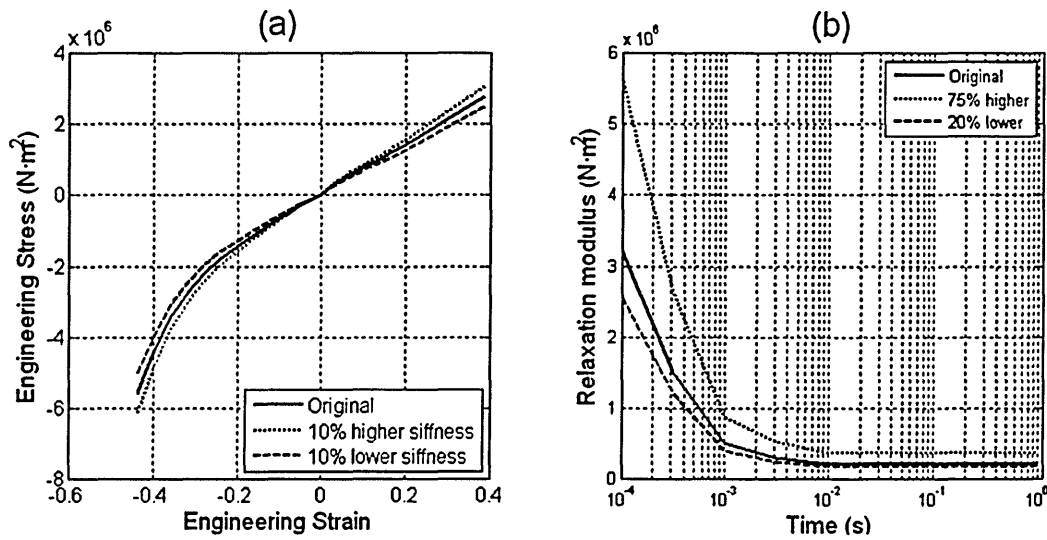
Figure 3.22 a) Static rubber core material properties, a) Dynamic rubber core material properties

Table 3.6 Fit to MAT_OGDEN_RUBBER for temperatures of 283.15 and 313.15 K.

Temperature (K)	283.15	313.15
Ogden shear modulus coefficients	$-0.1636 \times 10^{-1}, 0.1707 \times 10^{1}$ 0.2363×10^{1}	$-0.1338 \times 10^{-1}, 0.139 \times 10^{1}$ 0.1934×10^{1}
Ogden alpha constant coefficients	$-0.7424 \times 10^{1}, -0.1664 \times 10^{1}$ 0.3280×10^{1}	$-0.7424 \times 10^{1}, -0.1664 \times 10^{1}$ 0.3280×10^{1}
Maxwell shear modulus coefficients	$-3.4562 \times 10^{-4}, -2.5360 \times 10^{-1}$ $3.5419, 1.4366$	$1.5800 \times 10^{-4}, 1.1593 \times 10^{-1}$ $1.6192, 6.5675 \times 10^{-1}$
Decay constant coefficients	$2.5675 \times 10^{1}, -2.5957 \times 10^{2}$ $2.6242 \times 10^{3}, 2.6531 \times 10^{4}$	$2.5675 \times 10^{1}, 2.5957 \times 10^{2}$ $2.6242 \times 10^{3}, 2.6531 \times 10^{4}$

The FE models were validated by comparing COR and contact times, for perpendicular impacts with a rigid surface, with the experimental results published by Downing (2007a). Details of the experimental procedures can be found in Downing (2007a). The first stage of this investigation was to analyse the effect of only adjusting the internal pressure of the model for temperatures of 283.15 and 313.15 K. Following this, an analysis was undertaken to identify the effect of increasing and decreasing the static stiffness of the rubber by 10%, whilst keeping the original internal pressure. Finally, the internal pressure and static and dynamic material properties of the rubber were all updated to simulate the two temperatures under investigation.

3.5.2.   *Results*

The results from Downing (2007a) at 298.15 K were initially compared to the FE model and experimental data from the previous section. This was necessary due to different balls being used in each experiment, in addition to discrepancies in the test temperatures. Figure 3.23 shows that COR and contact times were found to be in good agreement between the two sets of experimental data and the original FE model. However, contact times were marginally higher at inbound velocities below 20 m·s^{-1} for the validation data and the FE model in comparison to Downing (2007a).
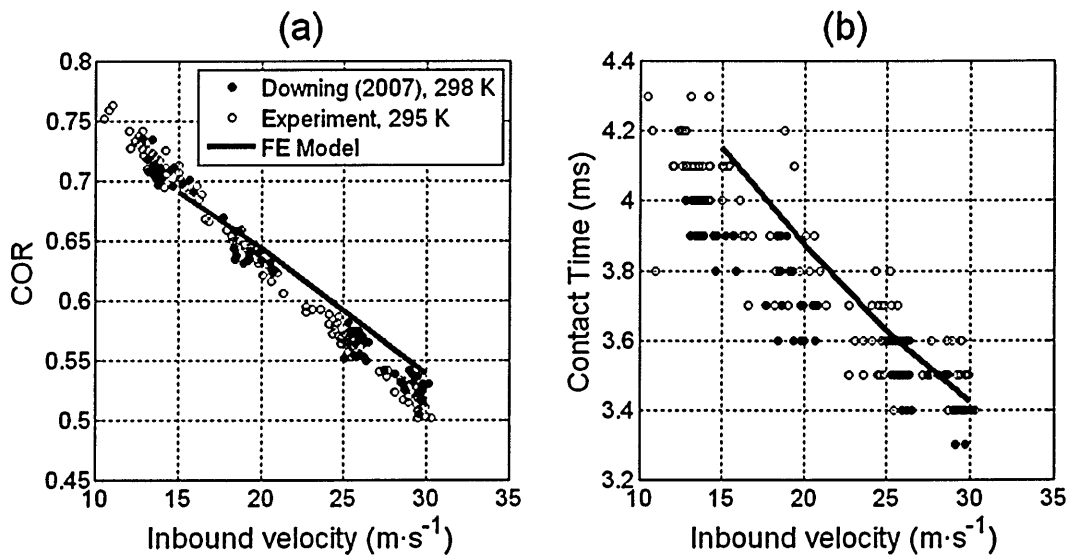
Figure 3.23 a) COR and b) contact time, comparison between the experimental data from the original validation data (295.15 K) and Downing (2007a) (298.15 K) and the original FE model.

Figure 3.24 shows that when only the internal pressure was adjusted, the model over-predicted COR when the temperature was 283.15 K. At 313.15 K the model is in good agreement with the experimental data, although it marginally under-predicted COR for inbound velocities below 20 m·s^{-1}. The FE model and experimental data both show increasing COR with temperature.
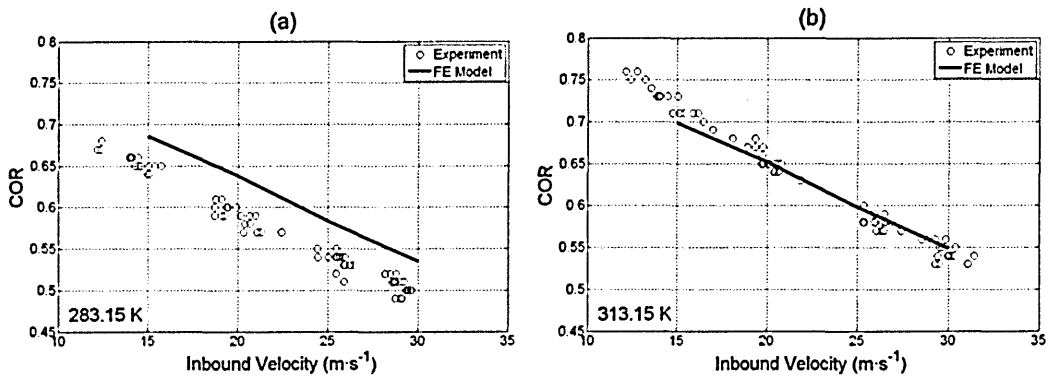
Figure 3.24 COR for adjusted internal pressure at temperatures of a) 283.15 K and b) 313.15 K.

Figure 3.25 shows that that when only the internal pressure was adjusted, the FE model was in relatively good agreement with the experimental data at both temperatures, for contact time. However, the experimental data shows increasing contact time with temperature, whilst the FE model has the opposite trend.
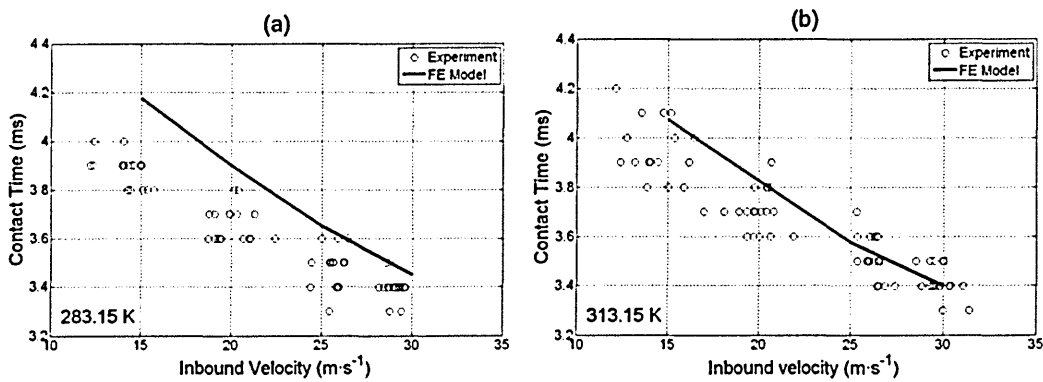
Figure 3.25 Contact time for adjusted internal pressure at temperatures of a) 283.15 K and b) 313.15 K. Experimental data from Downing (2007a).

Figure 3.26a shows that increasing the static stiffness of the rubber in the FE model by 10% results in a marginal increase in the COR (dynamic stiffness kept constant). The opposite was the case for a 10% reduction in static stiffness. Figure 3.26b shows that reducing the static material stiffness by 10% results in a significant increase in contact time. Again, the opposite was the case for a 10% increase in stiffness. The range in both COR and contact time between both FE models (20% change in rubber material stiffness) is approximately equal to the range of scatter in the experimental data, for a specific inbound velocity.
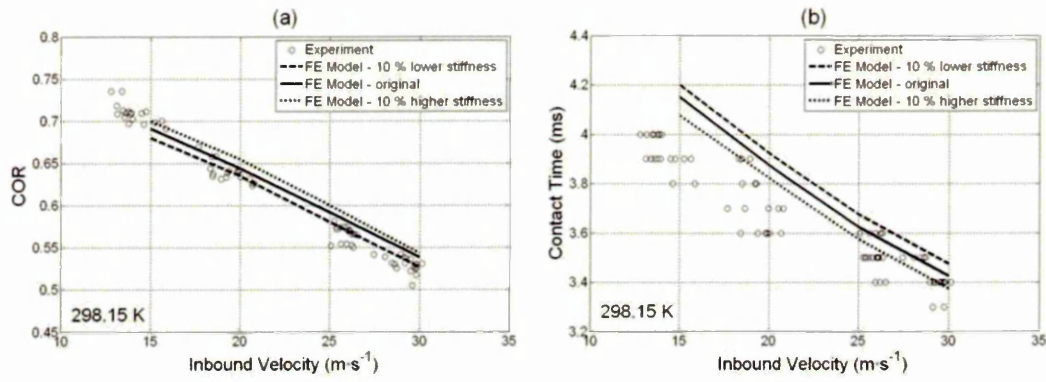
Figure 3.26 Effect of the quasistatic rubber material stiffness on a) COR and b) contact time. Experimental data from Downing (2007a).

Figure 3.27 shows that the FE model, with the updated internal pressure and static and dynamic rubber material properties, is in good agreement with the experiment for COR at 283.15 K (static and dynamic rubber modulus 10 and 75% higher respectively) and 313.15 K (static and dynamic rubber modulus 10 and 20% lower respectively). The model and experiment both show increasing COR with temperature.
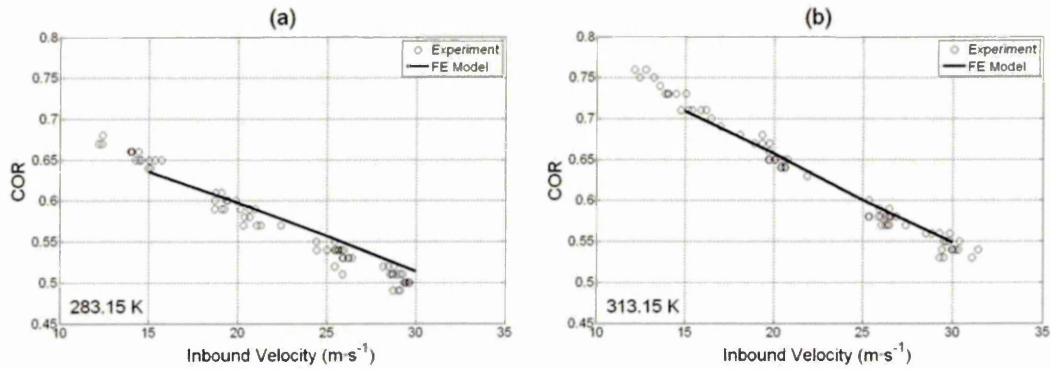
Figure 3.27 COR results for the complete ball model updated to simulate temperatures of a) 283.15 K and b) 313.15 K. Experimental data from Downing (2007a).

Figure 3.28 shows that the complete model is also in good agreement with the experimental data for contact time at both temperatures. Both the model and experiment show increasing contact times with temperature.
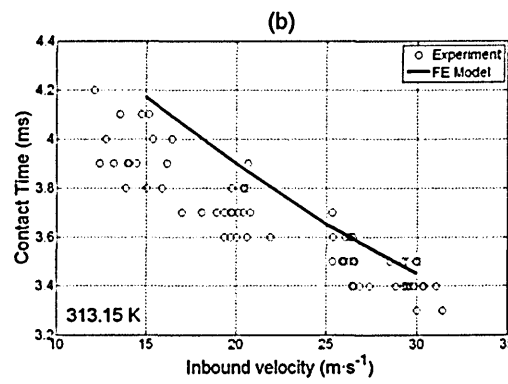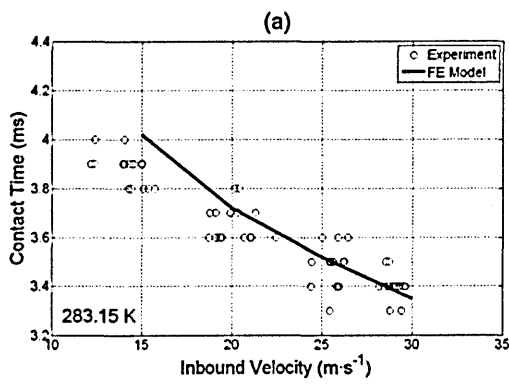
Figure 3.28 Contact time results for the complete ball model updated to simulate temperatures of a) 283.15 K and b) 313.15 K. Experimental data from Downing (2007a).

Figure 3.29 shows that the maximum impact force is marginally higher at 283.15 K in comparison to 313.15 K for all the inbound velocities under investigation. It can also be observed that the maximum force occurs earlier into the impact for the model at 283.15 K for inbound velocities of 15 and 20 m·s^{-1}. At inbound velocities of 25 and 30 m·s^{-1} the maximum impact force at 283.15 K lags that of the model at 313.15 K.
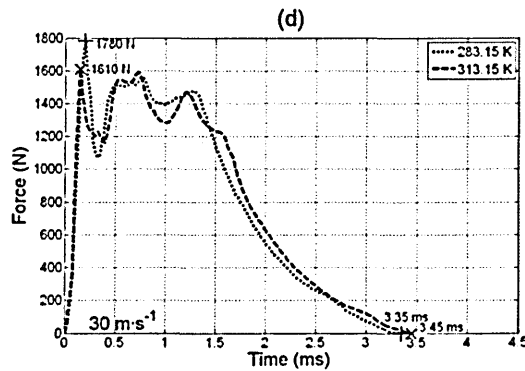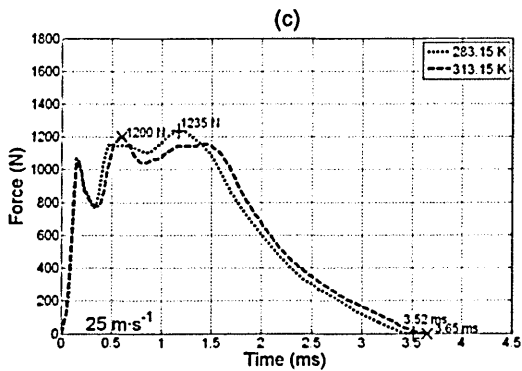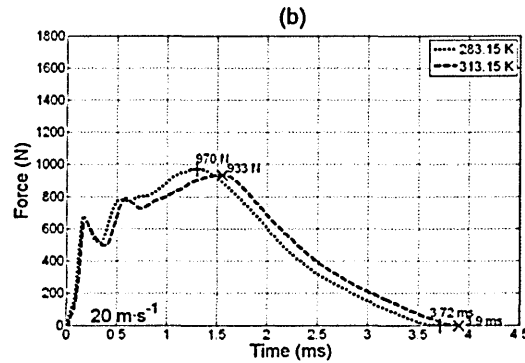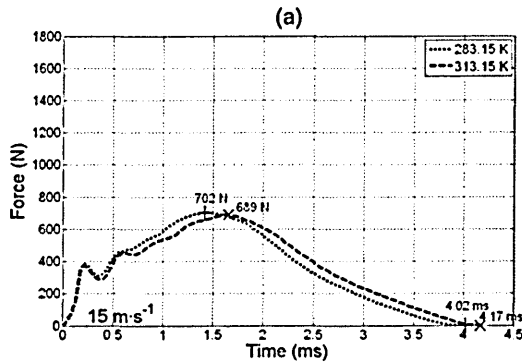
Figure 3.29 Force plots for the complete ball models a) 15 m·s^{-1}, b) 20 m·s^{-1}, c) 25 m·s^{-1}, b) 30 m·s^{-1}.

3.5.3.   Discussion

Increasing the internal pressure of a tennis ball, in isolation, raises its structural stiffness, thus reducing its contact time. Hence, when only the internal pressure of the tennis ball was adjusted, contact times were found to decrease with temperature. This was in contradiction to the experimental data, where contact times increased with temperature. When the effect of changing the material properties with temperature is added into the model, contact time and COR are in good agreement with the experimental data. Therefore, in accord with Downing (2007a), it is concluded that the change in a ball's material properties with temperature, have a greater influence on its rebound characteristics than the alteration in internal pressure. In this paper it was found that a greater change in the dynamic material properties of the rubber was required to simulate a temperature of 283.15 K (75% increase), in comparison to 313.15 K (20% decrease). This was also found by Downing (2007a), who demonstrated that for normal impacts there is a greater difference in both COR and contact times between 298.15 and 283.15 K, in comparison to 298.15 and 313.15 K.

Independently adjusting the static material properties of the rubber resulted in an increase in COR and a reduction in contact time, with increasing stiffness. A tennis ball's static structural stiffness is predicted to be affected by temperature in two ways; 1) the material and hence structural stiffness of the ball is reduced with increasing temperature and 2) the lower static stiffness of the rubber at higher temperatures results in the ball expanding more from the applied internal pressure, which in turn increases its volume lowering its initial internal pressure. The diameter of the ball in the FE model was found to increase from 0.066004 to 0.066204 m when the simulated temperature was increased from 283.15 to 313.15 K. This equated to a 0.62% increase in the frontal area or drag force acting on the ball during flight. Further research is required to determine whether temperature has a significant effect on a tennis ball's cross sectional area and hence flight characteristics.

The results show that when just the internal pressure of the ball was updated to simulate a temperature of 283.15 K, the model over-predicted COR. It was also found that increasing the static stiffness of the rubber, to simulate a drop in temperature, resulted in an increase in the COR, making the model over-predict the COR even more. Therefore, if only the internal pressure and static stiffness

of the rubber were adjusted the model would over-predict COR at 283.15 K, whilst the opposite would be the case at 313.15 K. An increase in damping results in a decrease in COR (Dignall and Haake, 2000); hence including the change in the dynamic material properties of the rubber resulted in strong agreement with the experimental data.

This investigation has provided an indication as to how the static and dynamic material properties of a tennis ball rubber core change with temperature. However, the intention of this study was only to provide a gauge of the extent to which the material properties of a tennis ball change with temperature. In this investigation the static material properties were assumed to adjust with temperature, whilst following the trend of the original data. In reality it is very unlikely that this would be the case, especially in the range from 298.15-283.15 K, which experienced the largest change in rebound characteristics. In addition, more precise material testing would be required to determine how the static properties of rubber cores change with temperature. Relaxation testing at a range of temperatures could be used to determine the stress relaxation properties of the rubber.

The change in felt material properties with temperature may also have an influence on the rebound characteristics of a tennis ball. If the stiffness of the felt were to decrease with increasing temperature, then the ball would stretch more from the internal pressure. This would in turn increase the initial volume of the ball, reducing its internal pressure and hence structural stiffness. However, it is predicted that the stiffness of the felt would change by a very marginal amount within the temperature range used in this investigation. In-depth material testing would be required to quantify how the felt properties change with temperature.

3.5.4.   Summary

An FE model of a tennis ball, validated at room temperature, has been updated to simulate temperatures of 283.15 and 313.15 K for inbound velocities in the range from 15 to 30 m·s^{-1}. This was achieved by modifying the internal pressure in accordance with the laws of thermodynamics, whilst simultaneously estimating the change in the rubber core material properties. The model was found to be in good agreement with the experimental data for the entire range of

velocities under investigation, at both temperatures. Overall, the change in rubber properties with temperature was found to have a more significant effect on the rebound characteristics of a tennis ball than the change in internal pressure (Downing, 2007a). In-depth material testing would be required to determine precisely how the rubber core and felt cover properties change with temperature.

3.6. Chapter summary

In this chapter the properties of tennis balls were obtained and used to produce an FE model in Ansys/LS-DYNA 10.0. The rubber core was simulated with a MAT_OGDEN_RUBBER material model, whilst MAT_LOW-DENSITY_FOAM was used for the felt cover. An AIRBAG_SIMPLE_PRESSURE_VOLUME command was used to replicate the internal pressure of the ball. The complete model and the separate parts were all validated against experimental data obtained at room temperature for perpendicular impacts. There was good agreement between the model and experimental data for the full range of impact velocities (5-30 $m·s^{-1}$) under investigation. The model was subsequently updated to simulate temperatures of 283.15 and 313.15 K for inbound velocities in the range from 15 to 30 $m·s^{-1}$. This was achieved by modifying the internal pressure in accordance with laws of thermodynamics, whilst simultaneously estimating the change in the rubber core material properties. The model was found to be in good agreement with the experimental data for the entire range of velocities under investigation, at both temperatures. The next stage of the project is to build and validate an FE model of a head-clamped tennis racket.

3.7. Practical applications

Tennis balls rebound slower from a rigid surface when they are punctured. The internal pressure of a tennis ball will decrease over time, once it has been removed from its pressurised container. Therefore, it is predicted that using old tennis balls will decrease the speed of the game.

Tennis balls rebound slower from a rigid surface when the temperature is 10°C in comparison to 40°C. Therefore, it is predicted that the speed of the game will be increased when played at 40°C in comparison to 10°C.

4. Head-clamped racket model

4.1. Introduction

Following the work detailed in Chapter 3, the next logical step was to obtain the required properties of tennis strings and construct an FE model of a string-bed. It would be very difficult and computationally inefficient to simulate the entire process of stringing a tennis racket in an FE model. Therefore, the string-bed geometry will be constructed as an interwoven lattice of individual main and cross strings prior to any loads, which represent string tension being applied. The string-bed model will be validated against experimental data, obtained by projecting balls onto a head-clamped racket. To provide a rigorous validation a range of inbound velocities, angles and spin rates will be used. Following this, a model of a head-clamped tennis racket will be constructed and validated against experimental data. This model will be validated for four different impact locations on the string-bed. This will enable a large area of the string-bed to be validated, as opposed to just a single location. The results obtained from the head-clamped racket model will also be analysed against those from the string-bed model. The main objectives of this chapter are;

1. To obtain the required properties of tennis strings.

2. To build an FE model of a tennis racket string-bed.

3. To validate an FE model of a tennis racket string-bed against experimental data.

4. To build an FE model of a head-clamped tennis racket.

5. To validate an FE model of a head-clamped tennis racket against experimental data.

The strings simulated in the model are Prince Premier Softflex 16 (nylon) and the dimensions of the string-bed are based on those of a Prince TX151 racket.

4.2. String properties

4.2.1. Introduction

Tennis strings with a diameter of $1.32 \times 10^{-3} \pm 0.02 \times 10^{-3}$ m and a density of 1100 kg·m^{-3} were provided by the manufacturer for testing. The diameter and density of the strings were also provided by the manufacturer. As previously mentioned the string-bed geometry is to be constructed as an interwoven lattice, prior to any loads which represent string tension being applied. This means the geometry of the non-tensioned string-bed in the model will be representative of the geometry of an actual tensioned string-bed. Therefore, only the string properties above the stringing tension are required. MAT_ELASTIC was the linear material model selected for the strings. This material model was selected as it has low computational requirements and tennis strings are believed to have relatively linear properties in their operational range (Calder *et al.*, 1987), as detailed in the literature review (Section 2.3.3, Page 15). Cross (2001a) proposed two methods for determining the dynamic stiffness of tennis strings in their operational range. In method 1, the *Instron* method, the change in length between 311 and 222 N (70 and 50 lbs) is obtained from the unloading curve of a specific Instron test. Method 2, the *Hammer* method, involves striking a string tensioned to 275 N with a hammer and measuring the change in tension and perpendicular displacement. The change in length of the string is calculated from its perpendicular displacement. In both methods the dynamic stiffness is defined as the ratio of the change in force to change in length. The Young's modulus of the string can be calculated by multiplying the dynamic stiffness by the length and dividing by the cross sectional area. In this section the two methods of obtaining dynamic stiffness will be used to calculate the Young's modulus of the string. The two methods for obtaining the dynamic stiffness of tennis strings are detailed in full in the literature review (Section 2.3.3, Page 15).

4.2.2.   Results

The *Instron* method was used to obtain tensile force-displacement curves for the string (Figure 4.1). The test was repeated ten times (Figure 4.2) and the mean dynamic stiffness was calculated as 33.3 kN·m^{-1}, with a SD of 0.46 kN·m^{-1}. The stiffness obtained from the Instron machine is considered to be dynamic because it is obtained from an unloading curve of a specific test, as detailed in the literature review (Section 2.3.3, Page 15). The slight variation, which can be observed between the repeats, could be due to marginal material or geometric variations between the individual lengths of string tested. Material variations could be a result of the manufacturing process, whilst geometric variations could be due to slight differences in the cross sectional area or gauge length.

Two separate values of dynamic stiffness were used to calculate a Young's modulus for the strings using the *Hammer* method. A value of 26.1 kN·m^{-1}, with a standard deviation of 0.11 kN·m^{-1} was provided by the manufacturer and a value of 30.8 kN·m^{-1} was taken from Lindsey (2006). The marginal discrepancy in the values of dynamic modulus obtained from the two sources is expected due to experimental inconsistency between the different operators.
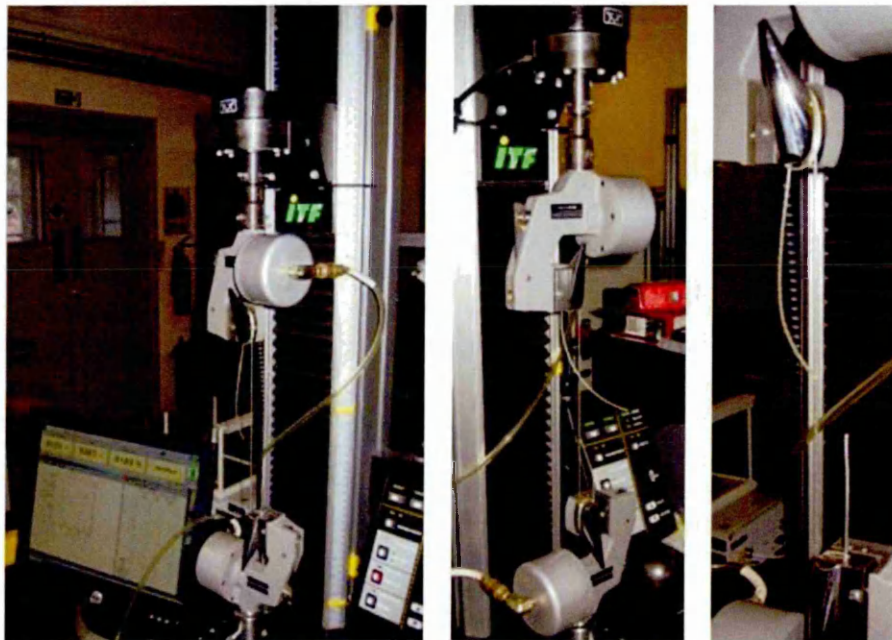
Figure 4.1 Setup for tennis string materials testing using the Instron method.
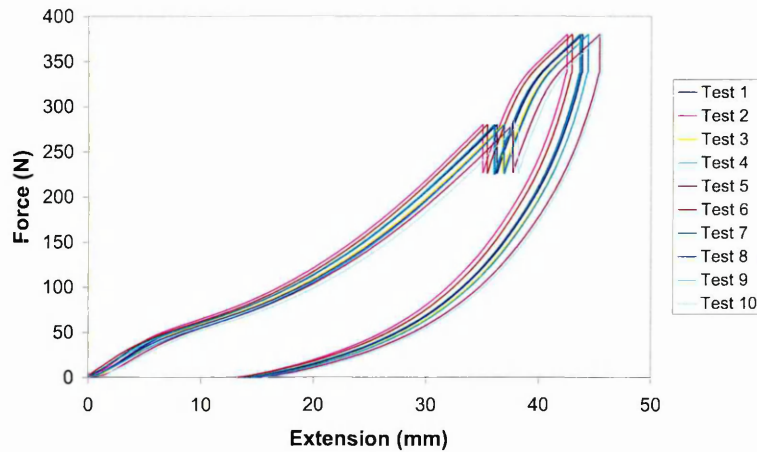
Figure 4.2 Instron force extension plots for tennis strings.

The calculated values of Young's modulus for the different tests are shown in Table 4.1. The values of Young's modulus obtained from the *Hammer* strike method are 17% (manufacturer) and 23% (Lindsey, 2007) higher than the value obtained from the *Instron* method.

Table 4.1 Young's modulus values obtained for the tennis string.

Method	Young's Modulus (GN·m^{-2})
Instron	5.85 ± 0.09
Hammer - Dynamic modulus from manufacturer	6.8
Hammer - Dynamic modulus from Lindsey (2006)	7.2

4.2.3.   Summary

The dynamic properties of Prince Softflex strings have been obtained using the *Instron* and *Hammer* method. There was a relatively large difference in the values of Young's modulus obtained using the two experimental methods. The material properties, from both methods, will now be incorporated into separate FE models of tennis racket string-beds. Further work will be undertaken to determine which method of dynamic string testing results in the optimum value of Young's modulus.

4.3. Finite element model of a tennis racket string-bed

4.3.1.   FE model of a tennis racket string-bed

An explicit FE model of a tennis racket string-bed, consisting of 16 main and 19 cross strings, was created in Ansys/LS-Dyna 10.0 (Figure 4.3). The overall dimensions of the string-bed were 0.331 × 0.253 m, with the strings having a diameter of 1.32 × 10^{-3} m. The string-bed pattern was based on dimensions provided by the racket manufacturer. As explained in the previous section two different methods were used for measuring the Young's modulus of the strings within their operational range, the *Instron* (5.85 GN·m^{-2}) and the *Hammer* (7.2 GN·m^{-2}) method (Section 4.2, page 9190). The operational range of strings is defined as the region between the stringing tension and the maximum load applied during a tennis shot. As the two methods produced different values of Young's modulus two separate MAT_ELASTIC material models were constructed for the strings and independently validated. The density was 1100 kg·m^{-3} and the Poisson's ratio was assumed to be 0.3. SOLID164 3-D 8 node bricks (*identical to the ball*), with single point integration or constant stress, were used to mesh the main and cross strings, which consisted of 19,624 and 17,712 elements, respectively. This mesh density was selected as it produced elements of a similar size to those in the ball and hence prevented contact instabilities.

(a)   **(b)**
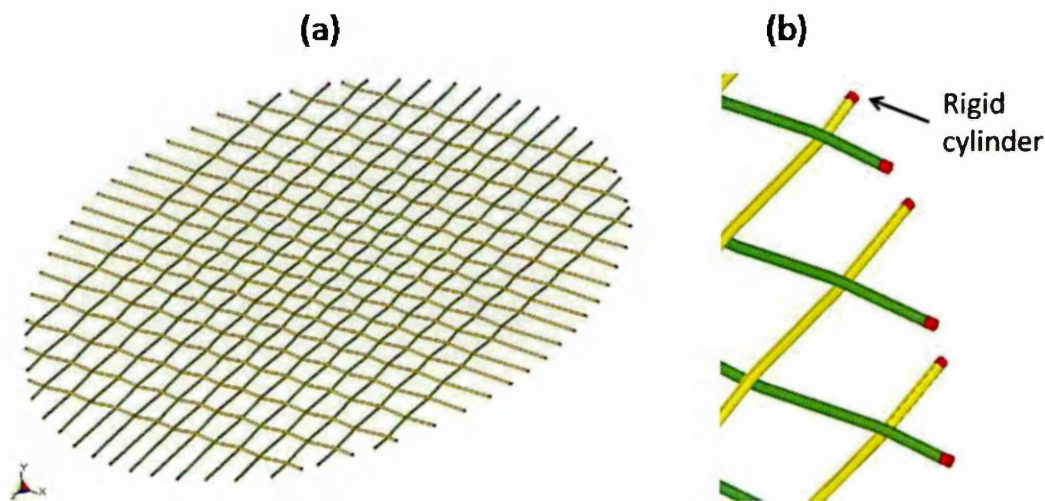
Figure 4.3 a) String-bed model and b) Close-up of string-bed model showing the rigid cylinders on the ends of every string.

Contact between the ball and string-bed was defined as CONTACT_AUTOMATIC_SURFACE_TO_SURFACE with a COF of 0.4 (Cross, 2000b). The same procedure was used for string to string contact, except the COF was set to 0.1. As with the ball to rigid surface model the contact option SOFT = 1 was used for the ball to string-bed contact. When the option SOFT = 1 is used, the contact stiffness is based on the nodal mass and global time step size. This option was used by Goodwill *et al.,* (2005) when simulating an impact between a ball and a rigid surface and is generally better when modelling contact between materials with a large difference in stiffness (LSTC, 2003) i.e. the strings and felt. The hourglass coefficient was set to 0.15, as in the ball model (Section 3.3, Page 64), to prevent zero-energy modes of deformation. Unlike the ball model the time step scale factor was set at the default of 0.9. Reducing the time step scale factor to improve contact behaviour was not required as the strings had a significantly lower stiffness that the rigid surface, which was used in the ball model validation (Section 3.3, page 64). A rigid cylinder 1×10^{-3} m in length and 1.32×10^{-3} m in diameter was attached to both ends of every string (Figure 4.3b). A load of 150 N was applied to each of these rigid volumes, in the required direction during the dynamic relaxation phase, to produce a total tension on every string of 150 N. These rigid volumes were then fully constrained during the transient phase of the simulation, effectively resulting in the string-bed of a head-clamped racket. Applying constraints to rigid cylinders as opposed to directly to the ends of the nylon strings, prevented element distortion, hence resulting in a more stable model. The convergence tolerance for dynamic relaxation was 0.01 (Figure 4.4). This increase in convergence tolerance, in comparison to the ball model (Chapter 3), was required to reduce the elevated convergence time as a result of the extra complexities of the string-bed model. The stated tolerance was necessary to ensure that the simulations would actually converge within a realistic time frame.
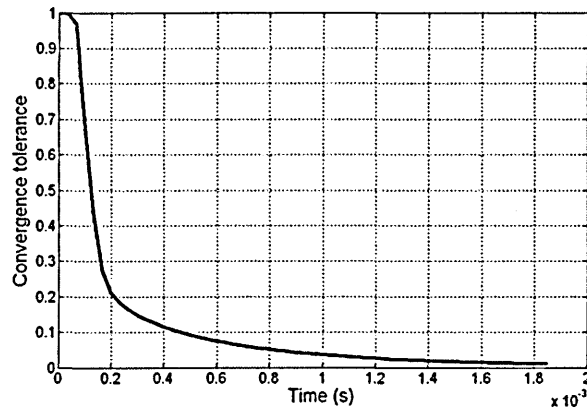
Figure 4.4 Convergence of string-bed model.

The string-bed model was validated by simulating an impact with the tennis ball model (Chapter 3, Page 59). The ball's initial velocity and spin were assigned using INITIAL_VELOCITY_GENERATION. In order to ensure the impact occurred at the correct location, the string-bed's position in the horizontal plane was adjusted according to the distance the ball would travel up to the point of contact. This was achieved using a piece of bespoke software, developed in MS Visual Basic 2005, which modifies the LS-DYNA .k text file by selecting the nodes corresponding to the string-bed and updating their locations. This programme, *Tennis Design Tool* (TDT), is the basis of a tennis racket design tool. The TDT is described in detail in Chapter 6 (Page 159). The initial position of the geometric centre of the ball remained at the origin of the world coordinate system as this allows the simplest application of spin.

4.3.2.   Summary

A string-bed model consisting of 16 main and 19 cross strings was constructed in Ansys/LS-Dyna 10.0. Solid elements were used to mesh the strings and contact between them was defined using CONTACT_AUTOMATIC_SURFACE-_TO_SURFACE. String-bed tension was replicated by applying a load of 150 N to a rigid cylinder on both ends of every string in the dynamic relaxation phase. The model will now be validated against experimental data.

96

4.4. Validation of the string-bed model

4.4.1. Experimental methods

Tennis balls were projected against a head-clamped racket using a modified BOLA device (Figure 4.5). An aluminium tube was fitted to the BOLA to provide greater consistency for the balls inbound angle. An International Tennis Federation (ITF) *Carbon Fibre* tennis racket with a head size of 0.063 m^2 (98 in^2) was used for all tests. Two groups of four rackets were used in the investigation, strung at 200 and 289 N (45 & 65 lbs), respectively. To ensure consistent and accurate results the string-bed deflection of the rackets was measured directly before and after testing using a Babolat RDC machine (Section 2.3.4, Page 19), the mean of these two values are quoted in this section as opposed to the stringing tension. Ball inbound angles and velocities in the range from 20 to 60° and 20 to 30 $m \cdot s^{-1}$ were analysed. A range of velocities and angles were used to provide a rigorous validation of the string-bed. This will ensure that the final user will have confidence in the ability of the complete racket model to accurately simulate a wide range of different tennis shots. The inbound angle was adjusted by tilting the racket as opposed to adjusting the cannon and flight path of the ball. To account for the horizontal distance travelled by the ball whilst in contact with the string-bed the impacts were offset from the long axis of the racket. Changing the frame of reference from the court to the laboratory, where the racket is initially stationary, means that the ball should have backspin prior to impact to represent a topspin shot (Goodwill *et al.*, 2004a). Around twenty impacts were undertaken for every racket at each angle; the inbound backspin was varied from 0 to 600 $rad \cdot s^{-1}$. This range of inbound spin was considered to be representative of the majority of groundstrokes during match play. Two rackets were used for each string tension at 40° and the mean RDC values are quoted in the results section.

Figure 4.5 Experimental setup for the head-clamped racket testing.

The flight of the balls was recorded as a series of bitmap files, using a *Phantom* v4.1 high-speed video camera, positioned 8 m from the racket in the direction of its longitudinal axis and recording at 1000 fps (Figure 4.6). The string-bed axis definitions shown in Figure 4.6 will be used throughout this thesis. Inbound and rebound velocities, angles and spins were measured from the recorded images using *Richimas v3*. Details of the use of *Richimas* can be found in Goodwill and Haake (2004a).
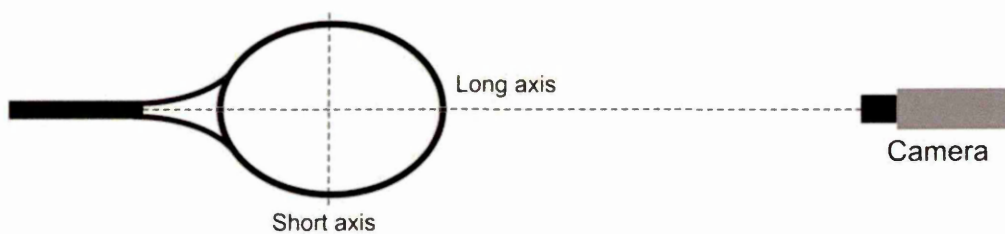
Figure 4.6 Camera position for recording the head-clamped racket impacts.

The mean inbound angles were found to be different from those predicted from the experimental set-up; the calculated values are shown in Table 4.2. For simplicity the inbound conditions will be referred to by their nominal values. The impact locations had to be calculated as they were offset from the centre of the string-bed. The mean horizontal distances from the ball impact location to the geometric string-bed centre (GSC), were calculated for each set of impacts. This was achieved by estimating each ball's impact position relative to the string-bed centre, from its initial location upon exiting the tube fitted to the BOLA

98

and the calculated mean angle corresponding to the experimental set-up. Figure 4.7 shows how the impact locations were calculated when the nominal inbound angle was 40°. The initial location of the ball was used to obtain its horizontal and vertical distance from the centre of the string-bed, labelled X_1 and Y in Figure 4.7, respectively. The distance Y and the inbound angle (θ) where then used to calculate the horizontal displacement of the ball up until the point of impact (X_2). The impact distance from the centre of the string-bed (X_3) was obtained by subtracting X_2 from X_1. Full details of how the impact locations were calculated for the other inbound angles can be found in (Appendix B.1, Page 247). The calculated impact locations are shown in Table 4.2. FE simulations were undertaken with inbound velocities, angles and impact locations identical to those in the laboratory experiment. For each angle and velocity pair, simulations were undertaken with backspin ranging from 0 to 600 rad·s^{-1}, at 200 rad·s^{-1} increments.
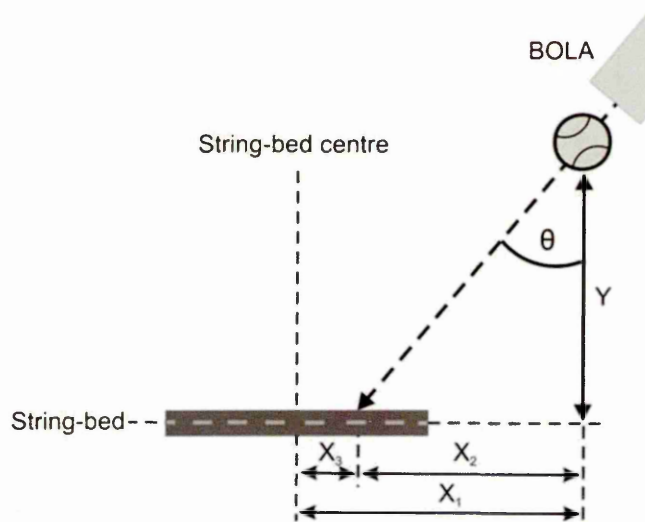
Figure 4.7 Obtaining impact position on the string-bed for a nominal inbound angle of 40°.

Table 4.2 Inbound angles, velocities and impact locations relative to the centre of the string-bed (*mean ± SD*)

Nominal inbound angle (°)	60	60	40	40	20	20
Nominal inbound velocity (m·s⁻¹)	30	20	30	20	25	20
Calculated inbound angle (°)	57.4 ± 1.1	57.6 ± 0.9	37.7 ± 0.8	37.7 ± 1.2	17.9 ± 1	18.3 ± 0.9
Calculated inbound velocity (m·s⁻¹)	29.7 ± 0.9	20.4 ± 0.5	29.9 ± 0.7	20.4 ± 0.5	24.9 ± 0.5	20.4 ± 0.4
Mean horizontal impact distance from the string-bed centre (m)	0.070 ± 0.007	0.069 ± 0.004	0.055 ± 0.007	0.052 ± 0.010	0.045 ± 0.007	0.042 ± 0.010

A repeatability study was undertaken to assess the level of human error in the *Richimas* method. An impact at low, medium and high inbound spin was selected and analysed ten times (Table 4.3). The SD are similar to those found by Goodwill and Haake (2004a). All of the other impacts were analysed once and are assumed to have SD similar to those in Table 4.3.

Table 4.3 Standard deviations for the manual tracking method for ball impacts on a head-clamped racket. (*value*) = SD as a percentage of the mean.

	Low inbound spin (-6 rad·s⁻¹)	Medium inbound spin (331 rad·s⁻¹)	High inbound spin (610 rad·s⁻¹)
Inbound velocity (m·s⁻¹)	0.2 (0.5%)	0.1 (0.4%)	0.2 (0.7%)
Rebound velocity (m·s⁻¹)	0.1 (0.4%)	0.1 (0.6%)	0.1 (0.6%)
Inbound angles (°)	0.3 (0.8%)	0.4 (0.9%)	0.5 (1.2%)
Rebound angles (°)	0.3 (1.0%)	0.4 (2.0%)	0.2 (2.8%)
Inbound spin (rad·s⁻¹)	6.3 (819.5%)	12.2 (3.7%)	10.0 (1.6%)
Rebound spin (rad·s⁻¹)	12.5 (5.1%)	7.2 (3.8%)	3.8 (2.4%)
Impact distance from long axis (m)	0.001 (1.8%)	0.001 (2.1%)	0.001 (2.3%)

4.4.2. Results

Figure 4.8a-f shows that the model results for rebound velocity are in good agreement with the experimental data. Although the model marginally under-estimated the rebound velocity of the ball at 20° and 20 m·s⁻¹, for a backspin of 200 rad·s⁻¹ (Figure 4.8a). The model also appears to slightly over-calculate rebound velocity at 60° and 30 m·s⁻¹ (Figure 4.8f). Overall, the results from both the model and experiment show that rebound velocity decreases as the inbound angle, relative to the racket normal, increases. Rebound velocity can also be seen to decrease with increasing inbound backspin; with the decrease becoming more pronounced as the inbound angle increases. Although, at an

angle of 60° the rate of decrease in rebound velocity drops significantly for inbound backspins greater than around 400 rad·s^{-1} (Figure 4.8e & f). This non-linear relationship of the data appears to be evident in both the model and experiment. The rebound velocities are higher for the rackets strung at lower tension. The rebound velocities are also very slightly higher for the model in which the strings had a Young's modulus of 5.85 GN·m^{-2} (*Instron*), in comparison to the model were the Young's modulus was 7.2 GN·m^{-2} (*Hammer*). The discrepancy between the rackets strung at different tensions and the FE models with different materials properties becomes less pronounced as the inbound angle relative to the normal increases. It should be noted that the difference in the results obtained from the two FE models is less than the scatter in the experimental data.
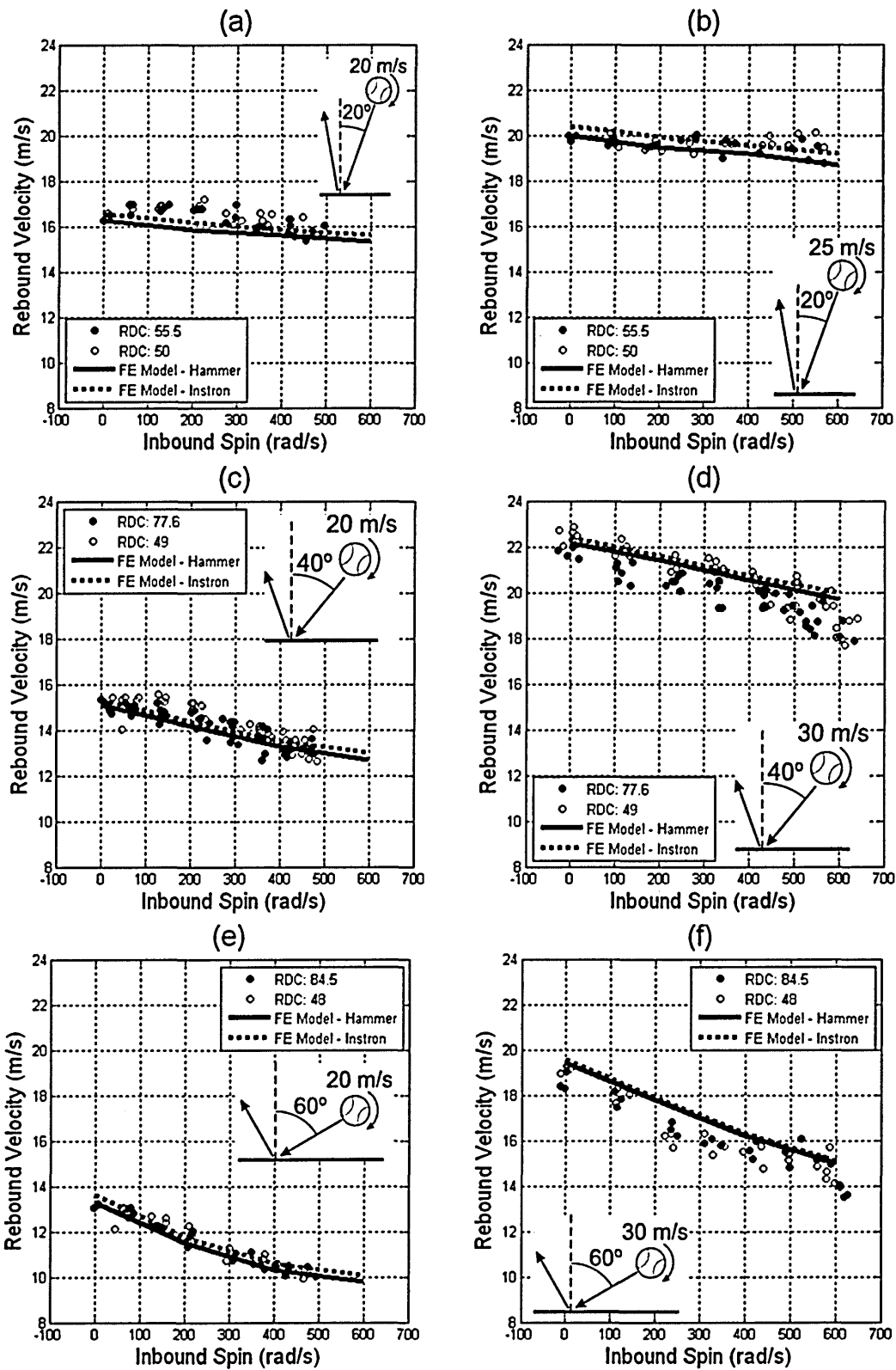
Figure 4.8 Rebound velocity against inbound backspin for ball impacts on a head-clamped racket at a) 20°, 20 m·s⁻¹, b) 20°, 25 m·s⁻¹, c) 40°, 20 m·s⁻¹, d) 40°, 30 m·s⁻¹, e) 60°, 20 m·s⁻¹, f) 60°, 30 m·s⁻¹.

Figure 4.9 shows that the model results for rebound angle are in good agreement with the experimental data. However, the rebound angles for the 20° simulations are slightly higher than the experimental values (Figure 4.9a and b). The general trend is that the rebound angle of the ball increases with the inbound angle. The results also show that rebound angle decreases as inbound backspin increases. However, Figure 4.9e and f show that the reduction in rebound angle with increasing inbound backspin appears to become less pronounced in the experimental data, for backspins greater than approximately 350 rad·s^{-1}. This non-linearity, which is in agreement with the results for rebound velocity, can be observed in the FE model with a nominal inbound angle of 60° at 20 m·s^{-1} but not at 30 m·s^{-1}. The difference in the rebound angle between the two FE models is very small and less than the scatter within the experimental results. Rebound angle doesn't appear to be affected by string-bed stiffness in either the experimental data or FE model. In the experiment string-bed stiffness was determined by string tension, while in the FE model it was determined by the Young's modulus of the strings.
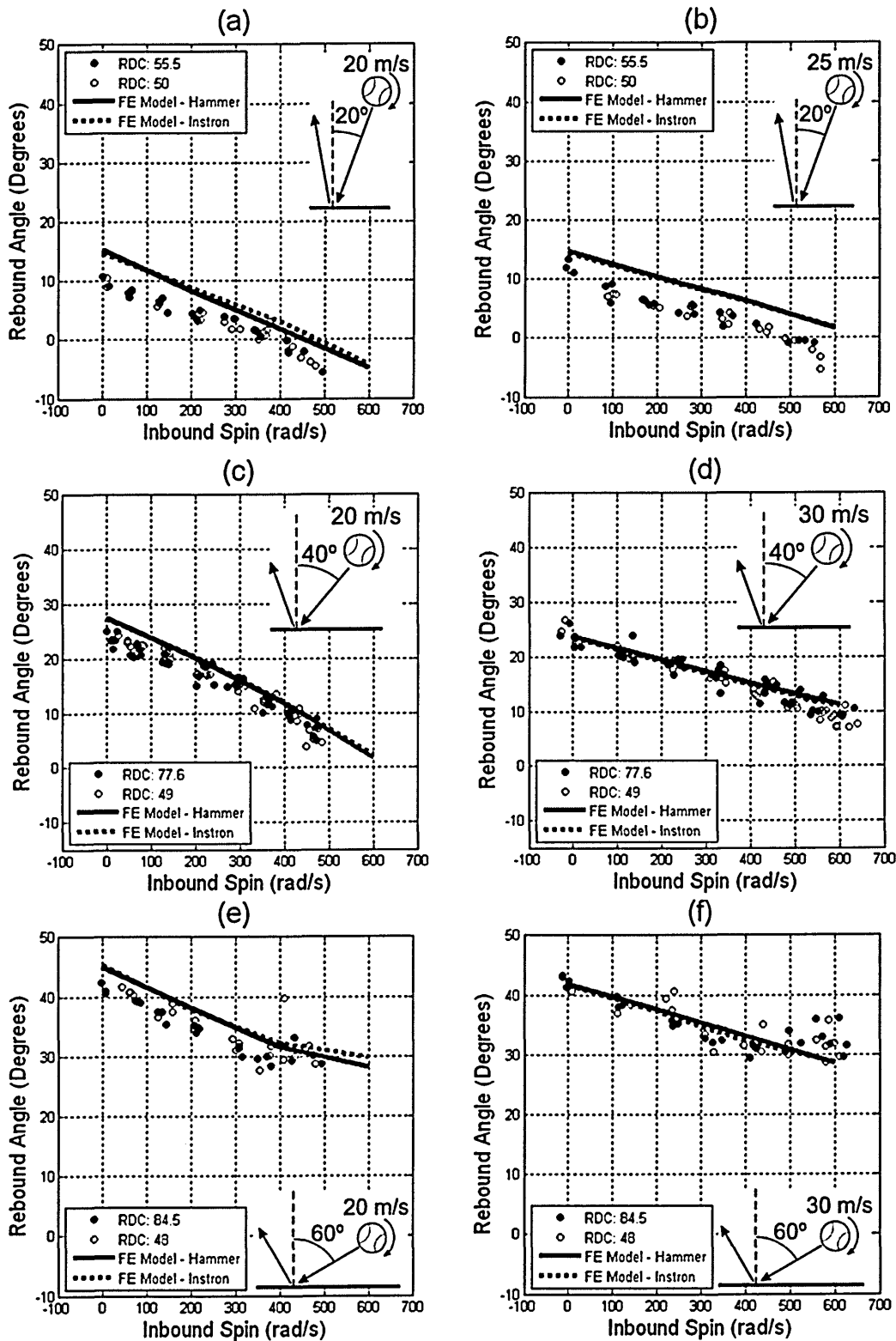
Figure 4.9 : Rebound angle against inbound spin for ball impacts on a head-clamped racket at a) 20°, 20 m·s⁻¹, b) 20°, 25 m·s⁻¹, c) 40°, 20 m·s⁻¹, d) 40°, 30 m·s⁻¹, e) 60 °, 20 m·s⁻¹, f) 60°, 30 m·s⁻¹.

Figure 4.10 shows that all the model results for rebound spin are in good agreement with the experimental data. The results show that rebound spin

decreases with increasing backspin, whilst it increases with the inbound angle. Again, a non-linearity can be observed, for both model and experiment, in the rebound characteristics of the ball for inbound backspins above approximately 350 rad·s^{-1} at a nominal inbound angle of 60° (Figure 4.10e and f). As with the results for rebound velocity and angle, the difference between the two FE models is very small. String-bed stiffness does not appear to have an influence on rebound spin.
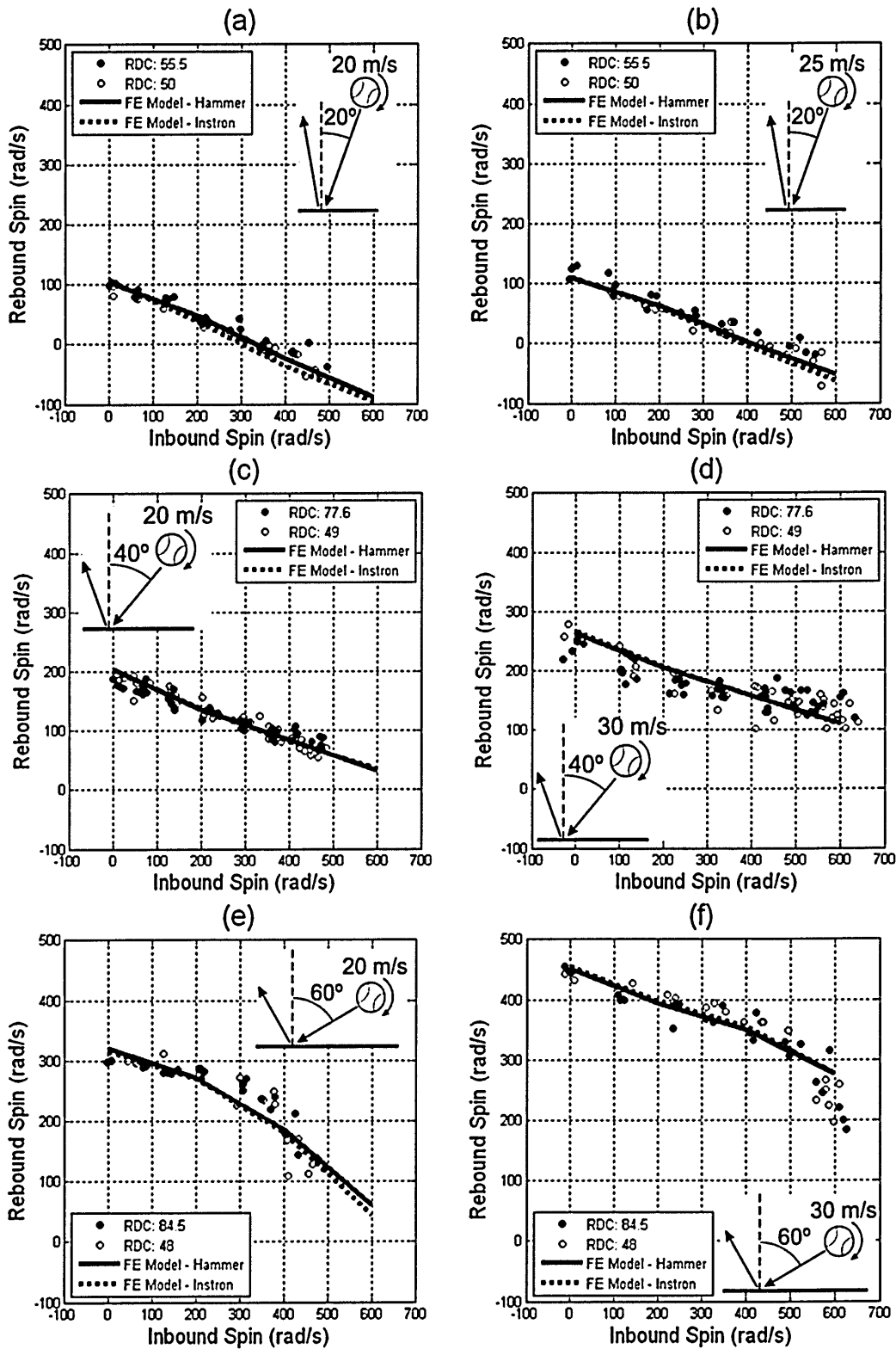
Figure 4.10 : Rebound spin against inbound spin for ball impacts on a head-clamped racket at a) 20°, 20 m·s⁻¹, b) 20°, 25 m·s⁻¹, c) 40°, 20 m·s⁻¹, d) 40°, 30 m·s⁻¹, e) 60 °, 20 m·s⁻¹, f) 60°, 30 m·s⁻¹.

Two different FE models were used in this investigation. One had a material model for the strings based on properties obtained using the *Hammer* method

106

with a string stiffness of 7.2 GN·m^2; whilst the other was based on properties obtained using the *Instron* method with a string stiffness of 5.85 GN·m^2 (Section 4.2, page 91). There is very little difference between the ball rebound results obtained from the different FE models. The Young's modulus of 7.2 GN·m^{-2} obtained using the *Hammer* method will be used for the remainder of the project, as the *Hammer* method is used by the manufacturer.

The FE model was used to analyse the horizontal velocity and spin of the ball throughout an impact. The impact selected for analysis had an inbound velocity of 30 m·s^{-1}, an angle of 40° and a backspin of 200 rad·s^{-1}. Figure 4.11a shows that the horizontal force acting on the ball, comprising of friction and a string-bed horizontal reaction force, switches direction just after the midpoint (2.85 ms) of the impact. The initial horizontal force is negative which means that the force is acting in the opposite direction to the ball motion. At a time of approximately 2.85 ms the horizontal force becomes positive, implying that it is in the same direction as the ball motion. This causes an increase in the horizontal velocity and a decrease in the angular velocity (*spin*) of the ball (Fig.6b and c). The horizontal force switches direction again at around 4.2 ms, resulting in a very slight decrease in the horizontal velocity and an increase in spin. As the horizontal force acting on the ball switches direction during impact there will be an instance at which the ratio of the vertical to horizontal loads will equal zero. This illustrates that any analytical model that assumes a simple, linear relationship between a friction and vertical reaction force is invalid.
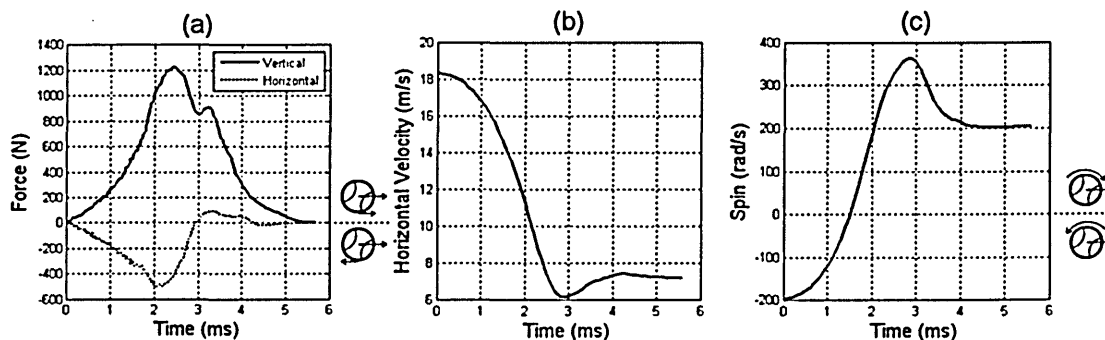
Figure 4.11 Results obtained from an FE model of a string-bed for an impact with an inbound velocity of 30 m·s^{-1}, angle of 40° and backspin of 200 m·s^{-1} a) Vertical and horizontal force, b) Horizontal velocity and c) Spin (E = 7.2 GN·m^2 obtained using the *Hammer* method).

Figure 4.12 shows the results obtained when the COF between the ball and string-bed was adjusted for the FE model with the material properties obtained using the *Hammer* method (E = 7.2 GN·m^2). It can be observed that increasing the COF from 0.4 to 0.6 has only a minor effect on the rebound properties of the ball, with both models in good agreement with the experimental data. Reducing the COF from 0.4 to 0.2 has a more pronounced effect on the rebound characteristics of the ball. The model with the COF of 0.2 over-predicts the rebound spin of the ball (Figure 4.12).
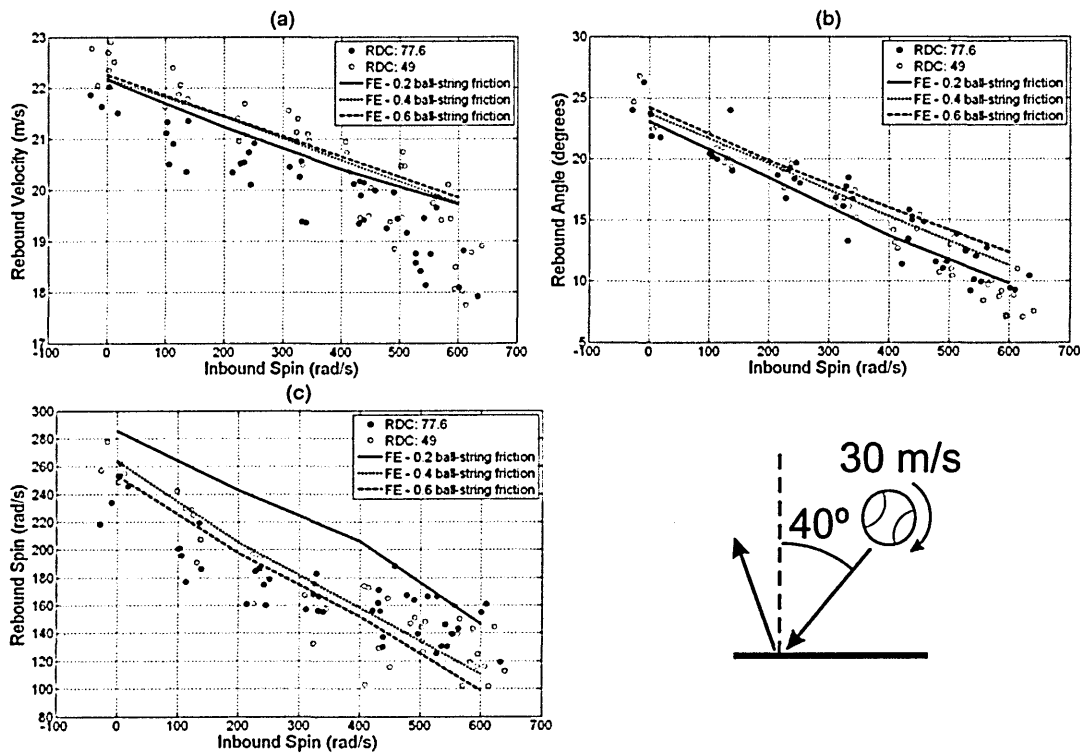
Figure 4.12 Effect of ball to string friction in the string-bed model for an impact with an inbound velocity of 30 m·s^{-1} and an angle of 40° a) velocity, b) angle and c) spin (E = 7.2 GN·m^2 obtained using the *Hammer* method).

The FE model was used to determine why reducing the COF between the ball and string-bed resulted in an increase in rebound spin. The impact selected for analysis had an inbound velocity of 30 m·s^{-1}, an angle of 40° and a backspin of 200 rad·s^{-1}. Figure 4.13a shows that the horizontal force acting between the ball and string-bed was larger for the model with the higher COF. The larger horizontal force acting on the ball, in the model with the higher COF, caused its spin to increase at a faster rate *(decrease in backspin)* (Figure 4.13b). This

108

resulted in the ball in this model having a higher spin rate for the first half of the impact. However, the horizontal force acting on the ball changed direction at around the midpoint of the impact, as previously determined (Figure 4.13a). When the horizontal force changed direction it caused the spin of the ball to decrease (Figure 4.13b). As the horizontal force acting on the ball was larger for the model with the higher COF, the decrease in spin was greater. This resulted in the spin of the ball in this model dropping below that of the other ball at around 3.5 ms and leaving the string-bed with a lower spin rate. Hence, it is the over-spinning of the ball in the FE model that causes the higher COF to result in a lower rebound spin rate. These results indicate that there is an optimum value of ball to string friction for obtaining maximum rebound spin.
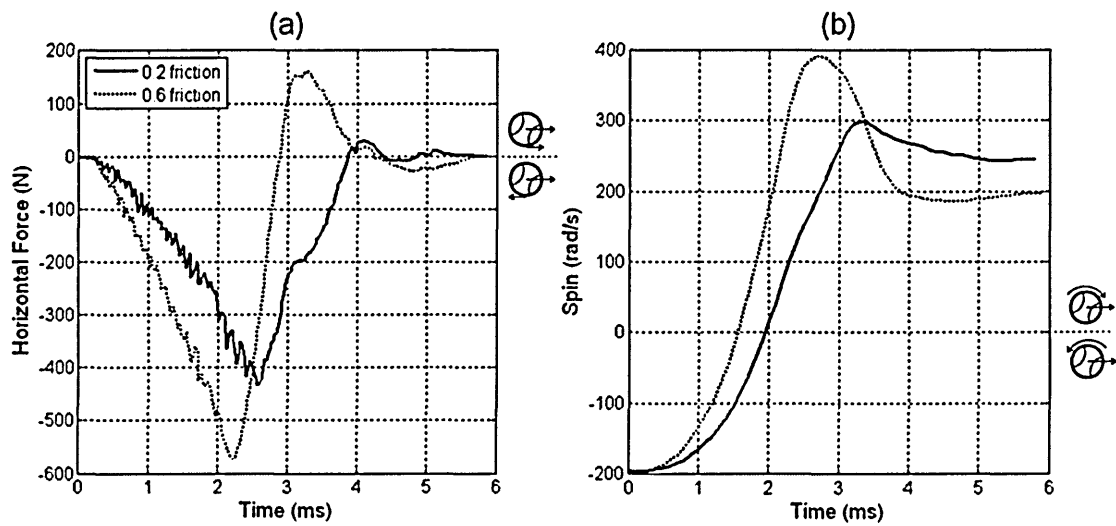
Figure 4.13 Effect of ball to string coefficient of friction for an impact on the FE model of a string-bed with an inbound velocity of 30 m·s^{-1}, angle of 40° and backspin of 200 rad·s^{-1} a) the horizontal force acting between the ball and string-bed and b) the spin of the ball throughout the impact.

A separate investigation was also undertaken to determine the effect of string to string friction. Impacts at the GSC, with an inbound velocity of 30 m·s^{-1} and an inbound angle of 40° were simulated using the string-bed model. The inbound backspin was in the range from 0 to 600 rad·s^{-1}. Adjusting the string to string friction in the range of 0.01-0.3 had no significant effect on the rebound characteristics of the ball (Figure 4.14). Therefore, the string to string COF used in the model will remain at 0.1.

(a)

Rebound Velocity (m/s)

23
22.5
22
21.5
21
20.5
20
19.5
19

COF = 0.01
COF = 0.1
COF = 0.3

0   200   400   600
Inbound Spin (rad/s)

(b)

Rebound Angle (degrees)

20

15

10

5

COF = 0.01
COF = 0.1
COF = 0.3

0   200   400   600
Inbound Spin (rad/s)

(c)

Rebound Spin (rad/s)

300

250

200

150

100

COF = 0.01
COF = 0.1
COF = 0.3

0   200   400   600
Inbound Spin (rad/s)
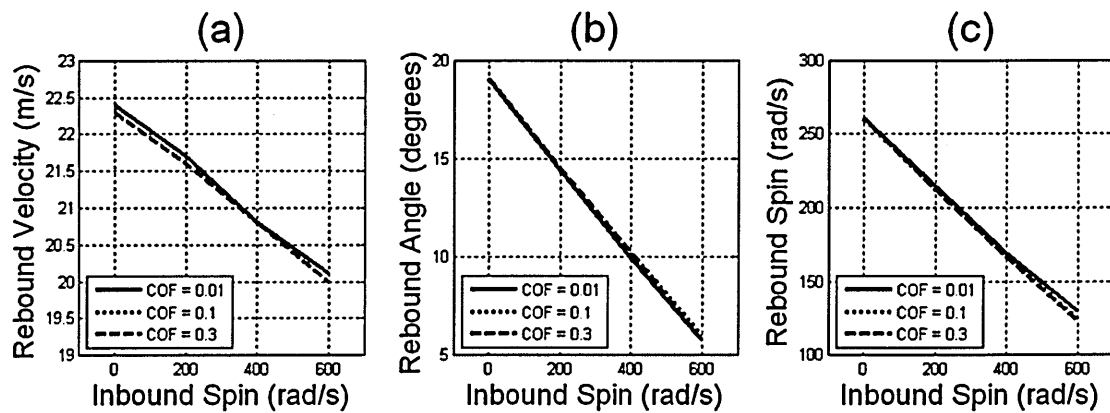
Figure 4.14 Effect of string to string friction for an impact on the FE model of a string-bed with an inbound velocity of 30 m·s⁻¹ and angle 40° a) velocity, b) angle and c) spin.

4.4.3.   Discussion

The FE model has been found to be in good agreement with the experimental data for rebound velocity, angle and spin, albeit with a few small discrepancies. It was found that the horizontal force acting on the ball, switches direction at approximately the mid-point of the impact when the inbound velocity, angle and backspin were 30 m·s⁻¹, 40° and 200 rad·s⁻¹, respectively. This implies that the ball spin rate has exceeded that associated with rolling and is hence over-spinning, as found by Goodwill and Haake (2004a). The fact that the friction force becomes negative again indicates that a tennis ball impacting obliquely to a string-bed converges towards a rolling state. Further research would be required to quantify this hypothesis.

The results indicate that reducing the COF between the ball and string-bed below 0.4 decreases the accuracy of the FE model, whilst increasing the COF has little effect on the rebound properties of the ball. Therefore, the COF between the ball and string-bed will remain at 0.4. A COF of 0.4 is within the range of 0.27 - 0.42 found by Cross (2000b). String to string friction in the range from 0.01 to 0.3 was found to have only a very small effect on the rebound characteristics of the ball. However, further research should be undertaken in order to determine a more precise value for both ball to string and string to string friction.

This investigation has shown that the current FE model is capable of replicating a single impact location on a string-bed for different inbound velocities, angles and spins. In reality, a ball will impact at a variety of locations on a string-bed

during play (Choppin *et al.,* 2007). Therefore, to ensure that the model accurately represents reality it must be validated for different impact positions on the string-bed. These impact positions should be extremes in the longitudinal and lateral directions, to allow the largest possible area of the string-bed to be validated.

4.4.4.   Summary

An FE model of a tennis racket string-bed has been produced and successfully validated against experimental data for different impacts. These impacts had inbound backspins in the range from 0-600 rad·s^{-1}, with nominal velocities from 20-30 m·s^{-1} and angles from 20-60°. The experimental validation was undertaken using a BOLA to project balls onto a head-clamped tennis racket. It was found that a ball will enter into an over-spinning stage during the impact, except when there is a combination of a high inbound angle (60°) and backspin (>400 rad·s^{-1}). Extending the validation to include different impact positions on the string-bed would increase its applicability.

4.5. Head-clamped racket model

4.5.1.   FE model of a head-clamped racket

An FE model of a head-clamped tennis racket was constructed using Ansys/LS-DYNA 10.0. The string-bed was based on the model described previously (Section 4.3, Page 94) with slight modifications to the geometry to encompass the racket frame. The geometry for the strings, in conjunction with the racket, was constructed in Pro Engineer Wildfire 2.0. The Pro Engineer parts representing the strings and racket were brought together as an assembly and imported directly into Ansys/LS-DYNA 10.0 using the ANSYS Connection for Pro Engineer. This is a feature which allows a Pro Engineer part or assembly to be launched into ANSYS directly from Pro Engineer. The modified main and cross strings consisted of 27,395 and 24,960 SOLID164 3-D 8 node brick elements *(same as previously validated string-bed model),* respectively. The racket geometry had an overall length of 0.68 m and a head size of 0.35 × 0.27 m, respectively (Figure 4.15). These dimensions are representative of a modern tennis racket (Haake *et al.,* 2007).

111
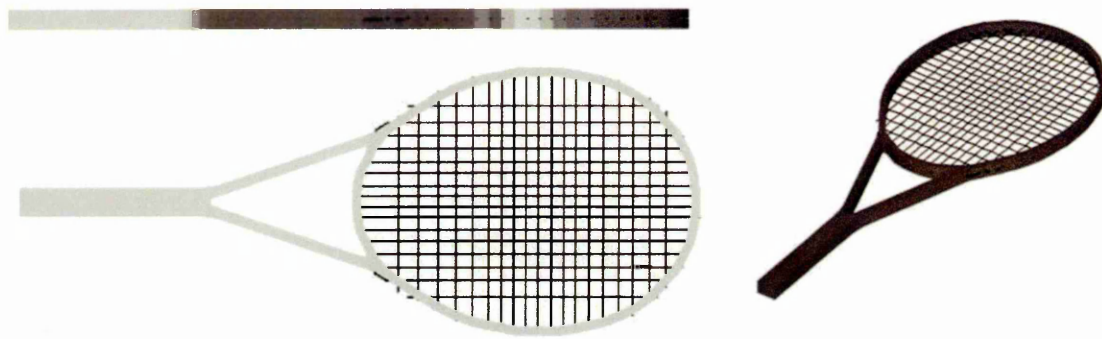
Figure 4.15 Racket geometry used in the FE model.

The racket was assigned a fully constrained MAT_RIGID material model (Table 4.4) consisting of 27,410 SHELL163 elements, 2×10^{-3} m in thickness. Shell elements were used as they are designed for modelling thin walled structures, such as the frame of a composite tennis racket. Shell elements are also computationally more efficient that solid elements. As with the string-bed model, a load of 150 N was applied to a small rigid cylinder attached to both ends of each string in the dynamic relaxation phase of the analysis, to represent the tension applied during stringing (Section 4.3.1, page 94). However, unlike the string-bed model these rigid cylinders were only fully constrained in the transient phase until a simulation time of 0.0013 s; at which point the ends of the strings were tied to the racket using CONTACT_TIED_SURFACE_TO_SURFACE. The simulations were set up so that the ball would contact with the string-bed at a simulation time of 0.0015 s; 0.0002 s after the strings had been tied to the racket frame. The birth time for the ball to string-bed contact was also set to 0.0013 s to reduce the computational requirements of the model. As CONTACT_TIED cannot be used for MAT_RIGID elements (LSTC, 2003) the sections of the frame tied to the ends of the strings were meshed with a MAT_ELASTIC material model. This separate part referred to as 'Racket holes' in Table 4.4 consisted of 4,477 elements. When defining contact with shell elements, it is possible to specify a contact thickness which overrides the geometric thickness. The contact thickness of the shell elements in this part was set to 0.5 mm to prevent distortion of the strings due to overlapping geometry.

Contact between the strings and racket was defined as CONTACT_AUTOMATIC_SURFACE_TO_SURFACE with a COF of 0. A COF of 0 was used to allow the most even possible distribution of stress throughout the strings during the dynamic relaxation phase of the simulations. The contact thickness of the shell elements in the racket was set to 0.2 mm.

Table 4.4 Part material properties for the head-clamped racket model.

Part	Material model	Young's Modulus (GN·m^{-2})	Density (kg·m^{-3})	Poisson's ratio
Strings	MAT_ELASTIC	7.2	1100	0.3
Racket	MAT_RIGID	2000	1600	0.3
Racket holes	MAT_ELASTIC	70	1600	0.3

INITIAL_VELOCITY_GENERATION was used to apply the required initial velocity and spin to the ball. The TDT (*Visual Basic programme,* Chapter 6 Page 159), was used to set the impact location on the string-bed. However, the programme was updated for the head-clamped racket model to ensure the ball impacted at a time of 0.0015 s. The convergence tolerance for dynamic relaxation was 0.1 (Figure 4.16). This increase in convergence tolerance, in comparison to the string-bed model (Section 4.3.1, page 94), was required to reduce the elevated convergence time. The stated tolerance was necessary to ensure that the simulations would actually converge within a realistic time frame.
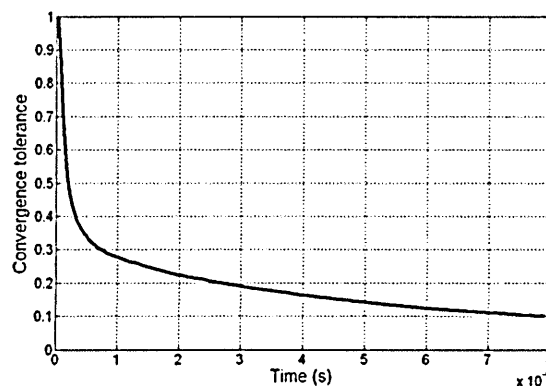
Figure 4.16 Convergence of head-clamped racket model.

4.5.2.   Summary

An FE model of a head-clamped racket was constructed in Ansys/LS-DYNA 10.0. The racket frame was meshed with shell elements and the material model

was MAT_RIGID. The strings were tied to the racket frame using CONTACT_TIED_SURFACE_TO_SURFACE. The model will be validated against experimental data for a range of impact locations on the string-bed.

4.6. Validation of the head-clamped racket model

4.6.1.   Experimental methods

In the laboratory experiment tennis balls were projected from a modified BOLA onto a head-clamped ITF *carbon fibre* test racket (Figure 4.5, page 98). The balls were projected with backspin in the range from 0 to 600 rad·s^{-1} at a nominal inbound velocity and angle (*relative to the racket normal*) of 20 m·s^{-1} and 40°, respectively. A pair of rackets both strung at 289 N (65 lbs) were used for testing and each were impacted at two locations on the string-bed. This resulted in a total of four separate impact locations labelled; centre, off-centre, throat and tip. The reason for using four different impact locations was to validate a large area of the string-bed, as opposed to just a single position. This is the main difference between the experimental work undertaken in this subsection and the validation of the string-bed model (Section 4.4, page 97). The centre, throat and tip impacts were all slightly offset (~0.03 m) from the long axis of the racket towards the BOLA, to account for the horizontal displacement of the ball whilst it remained in contact with the string-bed during impact. The experimental method used previously was developed to enable the impact location on the string-bed to be measured more accurately. The flights of the balls were recorded as a series of bitmap images using two synchronised *Phantom v4.2* high-speed video cameras, recording at 1000 fps (Figure 4.17a). A still bitmap image of a ball resting on the string-bed was also captured from camera 1. This image was used as a reference of the vertical location of the ball upon impact with the string-bed. Four sphere shaped markers were attached to the frame along the two axes of the string-bed (Figure 4.17b). This allowed the horizontal location of the ball to be calculated upon impact with the string-bed, relative to the frame markers. Camera 1 was used to obtain the ball's velocity, angle, spin and the impact distance from the long axis of the string-bed. The impact distance from the short axis of the string-bed was measured using Camera 2.
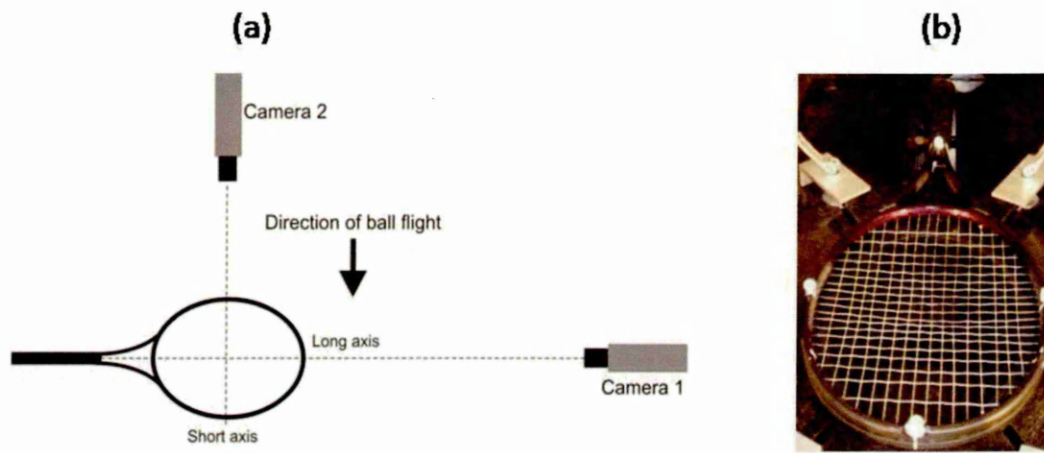
Figure 4.17 a) Camera set up for the head-clamped racket model, b) Racket markers used as a reference for obtaining the impact location on the string-bed.

The bitmap images obtained from the two cameras were manually analysed using *Richimas v3*. Two methods were used to obtain the impact distance from the long axis of the string-bed; the *Angle* method and the *Vertical location* method. The *Angle* method involved estimating the impact location of the ball from its initial position on exiting the tube attached to the BOLA and its calculated inbound angle (Figure 4.18a). This was the same as the method used for the validation of the string-bed model, except frame markers were used to increase accuracy (Figure 4.7, page 99).

For the *Vertical location* method the position of the centre of the ball was measured for the frames around the point of impact with the string-bed. The start of contact was assumed to be when the measured vertical location was closest to the centre of the ball resting on the string-bed. The RMSE between the vertical locations of the impacting and resting ball was 5 mm. The RMSE between the horizontal distances obtained from the two methods of measuring impact location was 4 mm. The impact distance from the short axis of the string-bed was obtained by measuring the location of the ball, in the images from camera 2, just before impact (Figure 4.18b).
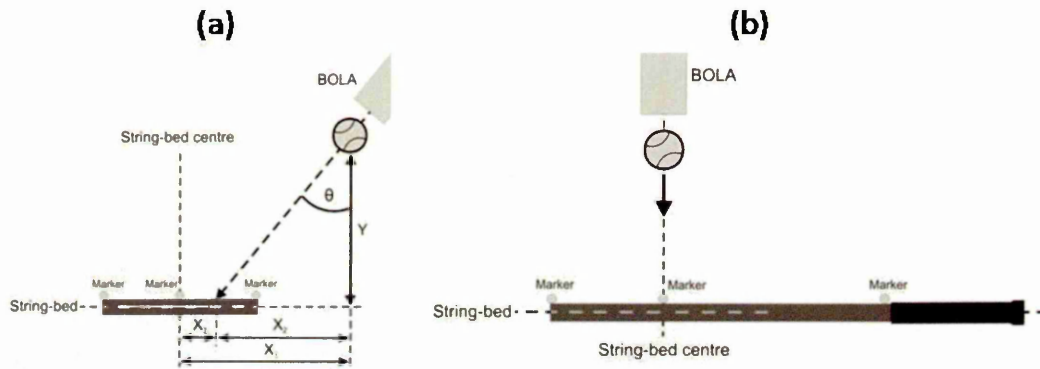
Figure 4.18 Calculating the impact distance from a) the long axis of the string-bed (view from camera 1) and b) the short axis of the string-bed (view from camera 2)

Table 4.5 shows the calculated inbound velocities, angles and impact positions. The relatively large SD for both inbound angle and impact distance from the long axis of the string-bed are predicted to be due to the varying lift force acting on the ball due to the applied backspin. The effect of inbound spin on inbound velocity, angle and impact position is shown in Figure 4.19. A separate investigation indicated that accounting for the difference in inbound properties with increasing backspin, in the FE simulations, had little effect on the rebound properties of the ball (~0.05 m·s^{-1}, $\sim0.6°$, ~5 rad·s^{-1}) (Appendix 0, Page 253). Therefore, FE simulations were undertaken using the average inbound velocities and angles from the laboratory experiment (Table 4.5).

Table 4.5 Actual experimental inbound velocities and angles *(mean ± SD)*

Impact	Inbound Velocity (m·s^{-1})	Inbound Angle (°)	Impact distance from long axis (m) (+ = towards BOLA)	Impact distance from short axis (m) (+ = towards tip)
Centre	21.0 ± 0.3	38.0 ± 1.0	0.029 ± 0.009	-0.017 ± 0.005
Off-centre	21.4 ± 0.4	37.4 ± 0.6	0.058 ± 0.007	-0.025 ± 0.004
Throat	21.3 ± 0.4	37.4 ± 0.5	0.033 ± 0.005	-0.070 ± 0.003
Tip	21.5 ± 0.4	37.3 ± 0.5	0.035 ± 0.005	0.007 ± 0.004

117
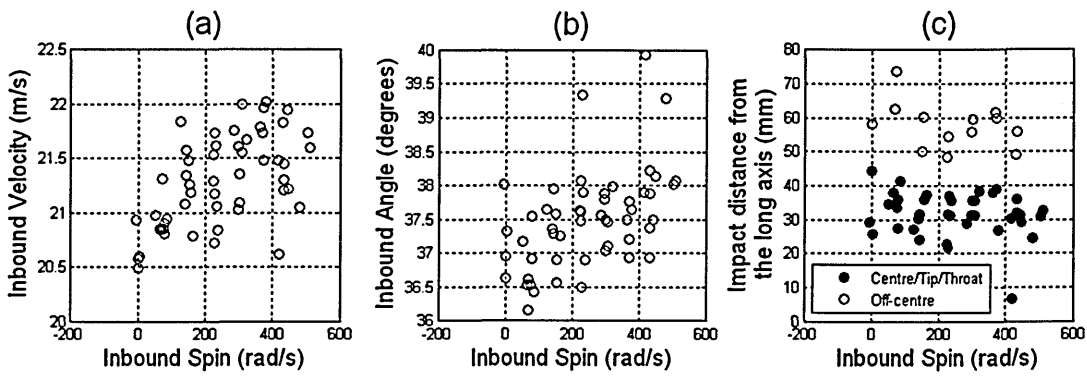
Figure 4.19 Effect of inbound spin on the experimental data for the head-clamped racket model a) inbound velocity, b) inbound angle and c) impact distance from the long axis of the racket.

As the images were manually analysed they were subject to human error, thus three of the centre impacts, with distinctly different inbound backspin, were analysed 10 times to quantify this error. Table 4.6 shows the obtained SD for the inbound and rebound properties of the ball and the impact positions. The SD for velocity, angle and spin are similar to those measured by Goodwill and Haake (2004a). All the other impacts in this section were analysed once and are assumed to have a SD similar to those in Table 4.6.

Table 4.6 Standard deviations for the manual tracking method for the head-clamped racket, $(value)$ = SD as a percentage of the mean.

	Low inbound spin (-3 rad·s⁻¹)	Medium inbound spin (235 rad·s⁻¹)	High inbound spin (472 rad·s⁻¹)
Inbound velocity (m·s⁻¹)	0.1 (0.4%)	0.1 (0.5%)	0.2 (0.9%)
Rebound velocity (m·s⁻¹)	0.2 (0.9%)	0.1 (0.7%)	0.1 (0.6%)
Inbound angle (°)	0.3 (0.9%)	0.4 (1.1%)	0.3 (0.9%)
Rebound angle (°)	0.4 (1.6%)	0.3 (2.1%)	0.3 (3.8%)
Inbound Spin (rad·s⁻¹)	4.3 (136.0%)	4.6 (1.9%)	5.7 (1.2%)
Rebound spin (rad·s⁻¹)	4.7 (2.5%)	2.9 (2.1%)	2.9 (2.7%)
Impact distance from long axis (m)	0.001 (4.0%)	0.002 (5.8%)	0.001 (4.6%)
Impact distance from short axis (m)	0.001 (5.1%)	0.002 (7.2%)	0.001 (18.1%)

Note: table column labels shown with units: Low inbound spin (-3 rad·s⁻¹), Medium inbound spin (235 rad·s⁻¹), High inbound spin (472 rad·s⁻¹)

4.6.2.   Results

Figure 4.20 shows the results obtained for horizontal and vertical coefficient of restitution (COR). In this thesis, horizontal COR is defined as the ratio of the horizontal component of the rebound and inbound velocities (Figure 4.21). The results obtained from the FE model for both horizontal and vertical COR are in good agreement with the experimental data for all four impact positions. The

vertical COR decreased by a very marginal amount with increasing backspin, in agreement with Goodwill and Haake (2004a). The horizontal COR, which is much lower than the vertical COR, decreased considerably with increasing backspin, this was also in agreement with Goodwill and Haake (2004a). A Oneway ANOVA was performed on the experimental data to determine if impact location had a significant effect on either horizontal or vertical COR. There was a significant effect of impact location on vertical COR, $F(3, 48) = 16.356$, $p < 0.05$, $\omega = 0.71$, but not horizontal COR. A Tukey HSD Post Hoc analysis was undertaken to determine which impact locations were significantly different, in terms of vertical COR. The vertical COR for the off-centre impacts was found to be significantly different to the other three locations. The lower vertical COR for the off-centre impacts can be clearly observed in Figure 4.20. It is predicted that the structural stiffness of a tennis racket string-bed will not be constant across the entire area. The structural stiffness is expected to lowest at the GSC and highest in the region close to the racket frame. It is predicted that the off-centre impacts had the lowest vertical COR because the string-bed had the highest structural stiffness in this location. There is very good agreement between the two FE models for vertical COR. The head-clamped racket model has slightly lower horizontal COR than the string-bed model, although the difference is less than the scatter in the experimental data. A separate study was undertaken to determine the cause of the discrepancy between the results obtained from the two models (Appendix B.3, Page 254). The exact reason for the discrepancy was not found. However, it was predicted that the difference is likely to be due to convergence as well as slight differences in the geometry and mesh of the models.
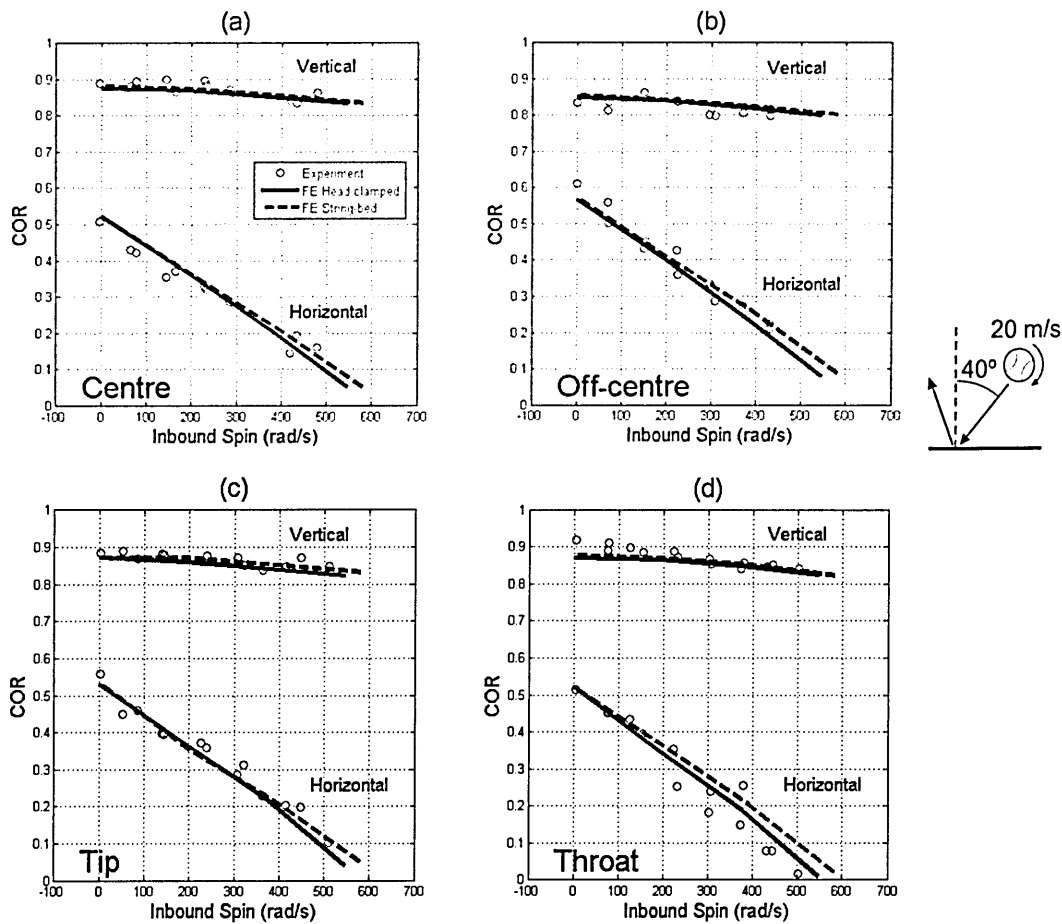
Figure 4.20 Horizontal and vertical COR for oblique spinning impacts on a head-clamped racket a) centre, b) off-centre, c) tip and d) throat.

$$\text{Horizontal COR} = \frac{X\,\text{velocity}_{OUT}}{X\,\text{velocity}_{IN}}$$
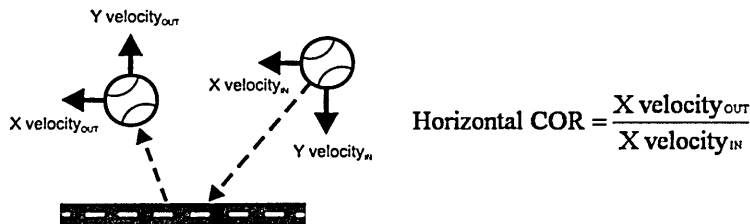
Figure 4.21 Definition of horizontal COR.

Figure 4.22 shows that the FE model results for rebound spin are in relatively good agreement with the experimental data; however, the model does appear to slightly under-estimate the rebound spin of the ball for higher inbound backspins (>300 rad·s^{-1}). A Oneway ANOVA was undertaken using the experimental data to determine if impact location had a significant effect on the rebound spin of the ball. As with horizontal COR, rebound spin does not change significantly with impact location. There is good agreement between the string-

bed and head-clamped racket models. However, the head-clamped racket model has slightly lower rebound spin (~10 rad·s⁻¹) than the string-bed model.
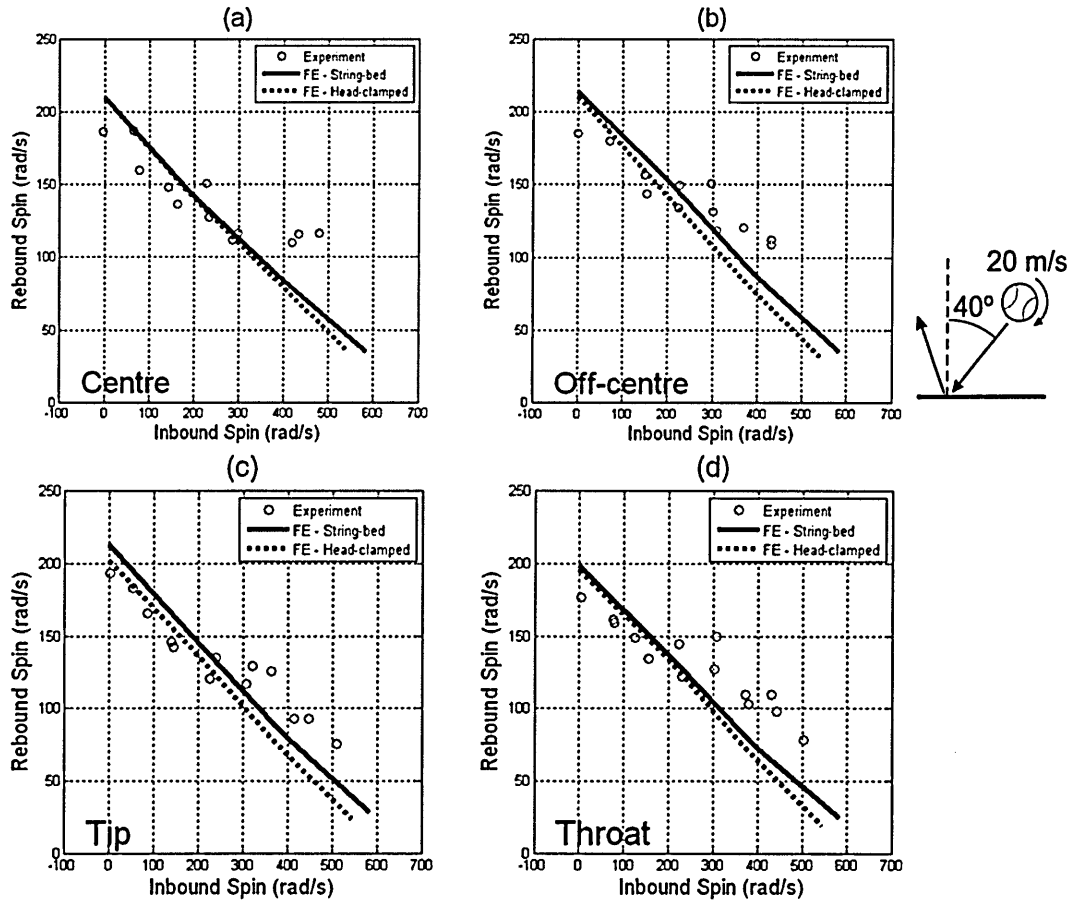
Figure 4.22 Rebound topspin for oblique spinning impacts on a head-clamped racket a) centre, b) off-centre, c) tip and d) throat.

Figure 4.23a shows that for the centre impact with zero inbound spin the horizontal force acting between the ball and string-bed is initially negative. Therefore, the force acts in the opposite direction to which the ball is travelling, resulting in a decrease in its horizontal velocity (Figure 4.23b) and an increase in spin (Figure 4.23c). The horizontal force (Figure 4.23a) becomes positive at approximately the mid-point of the impact, which subsequently increases the balls horizontal velocity (Figure 4.23b), whilst decreasing its spin (Figure 4.23c). The horizontal force then drops to around zero and there appears to be no further change in the horizontal velocity or spin of the ball. Figure 4.23d-i show that similar results are observed as the inbound backspin of the ball is increased. However, the results indicate that the horizontal force acting on the ball, and the time at which it drops to zero at the end of the impact, both

increase with inbound backspin. It is this increase in horizontal force which causes the decrease in horizontal rebound velocity with increasing inbound backspin. The small oscillations in the horizontal force plot are predicted to be due to the movements of strings (Cross, 2003).
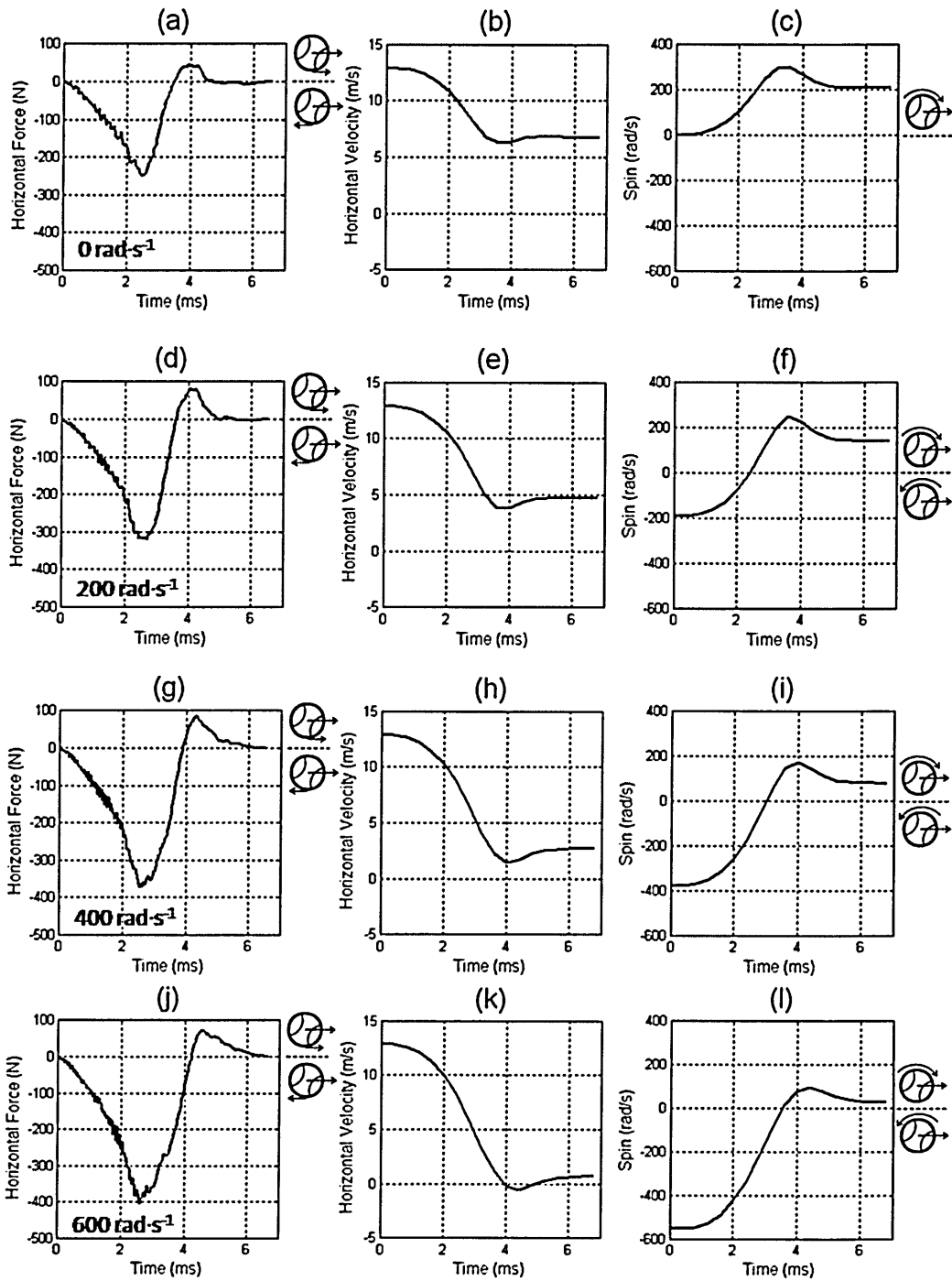
Figure 4.23 Results for a centre impact on the head-clamped racket model at 21 m·s^{-1} and 38° with a-c) no spin, d-f) 200 rad·s^{-1} backspin, g-i) 400 rad·s^{-1} backspin, j-l) 600 rad·s^{-1} backspin.

The FE model was been validated against experimental data for different impact locations. However, unlike the FE model it is not possible to precisely control the impact location when projecting balls onto a head-clamped racket. A separate investigation was undertaken using the string-bed model to determine the effect of impact location on the rebound properties of the ball. The impact locations used in this follow-up investigation are shown in Table 4.7 and Figure 4.24. These impact locations were used as they are within the validated region of the string-bed. The inbound backspin for all of the simulations used in this investigation was 200 rad·s^{-1}. The inbound velocity was 20 m·s^{-1} and the inbound angle was 40°.

Table 4.7 Impact positions for the FE model investigation.

Simulation	Impact distance from the long axis (mm)	Impact distance from the short axis (mm)
1	30	0
2	45	0
3	60	0
4	30	-35
5	45	-35
6	60	-35
7	30	-70
8	45	-70
9	60	-70
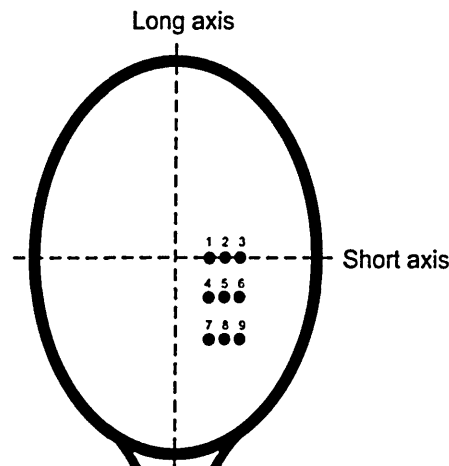
Figure 4.24 Impact positions on the string-bed.

Figure 4.25a shows that the rebound velocity of the ball remains relatively constant across the entire range of impact positions used in this investigation. Although, the rebound velocity of the ball is lowest for the impact at the

maximum offset towards both the throat and away from the long axis of the string-bed (Position 9 in Figure 4.24). This is predicted to be due to the string-bed having a higher structural stiffness in the region close to frame of the racket, as previously mentioned. Figure 4.25b shows that the rebound angle of the ball increases considerably as the impact position moves away from the long axis of string-bed in a direction parallel to the short axis. The larger rebound angle is predicted to be due to the vertical velocity of the ball being lower as a result of higher string-bed stiffness in the region closer to the frame of the racket. The rebound angle remains virtually constant as the impact position moves away from the short axis of the string-bed in a direction parallel to its long axis. Figure 4.25c shows that the rebound spin of the ball remains relatively constant for all the impacts positions used in this investigation. However, the rebound spin is considerably lower for the impact 30 and -70 mm offset from the long and short axis, respectively (Position 7 in Figure 4.24).
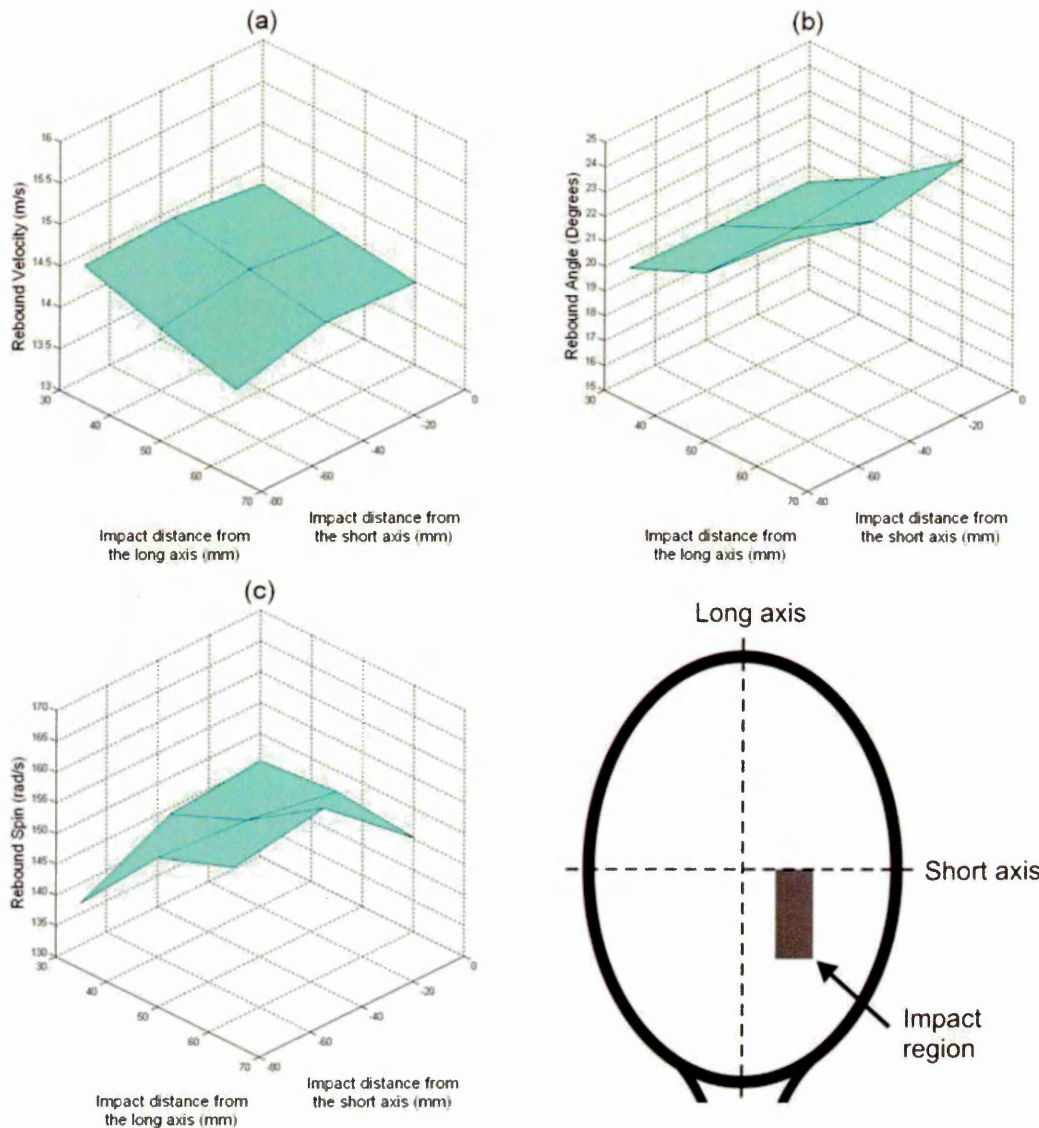
Figure 4.25 Results obtained from the head-clamped racket model for impacts with an inbound velocity of 20 m·s⁻¹, an angle of 40° and backspin of 200 rad·s⁻¹ at a range of locations on the string-bed a) velocity, b) angle, c) spin.

The results suggest that for a head-clamped racket, offsetting the impact position from the short axis of the string-bed has little effect on the rebound characteristics of the ball. Offsetting the impact from the long axis of the string-bed had a larger effect on the rebound characteristics of the ball. This is believed to be due to the more asymmetrical shape of the string-bed (relative to a plane parallel to its short axis) throughout the impact, as shown in Figure 4.26.
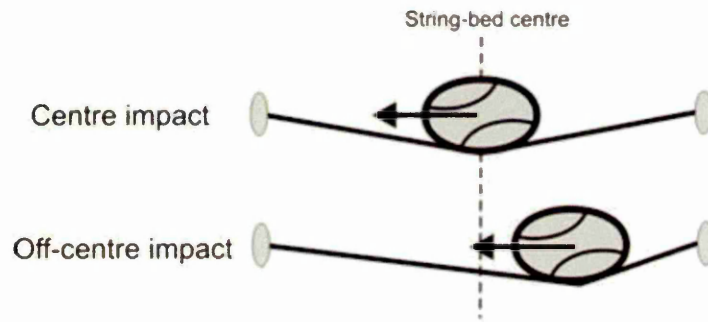
Figure 4.26 Effect of impact position on the deformation of the string-bed of a tennis racket.

4.6.3.   Discussion

In this investigation, an explicit FE model of a head-clamped tennis racket was validated against experimental data for a nominal inbound angle of 40°, relative to the string-bed normal. The results show that the horizontal COR decreases considerably with increasing inbound backspin, whilst the vertical COR decreases by only a very marginal amount, which agrees with Goodwill and Haake (2004a) (Figure 2.7, page 23). Analysis of the horizontal force acting on the ball throughout the impact showed that it increased with inbound backspin. The horizontal force initially acts to decrease the horizontal velocity of the ball; therefore, as the horizontal force increases with inbound backspin the horizontal velocity of the ball decreases by a larger amount and hence causes the reduction in horizontal COR. It was also found that the ball over-spins at around the mid-point of the impact, resulting in a subsequent increase in its horizontal velocity and decrease in spin, in agreement with other studies (Cross, 2003; Goodwill and Haake, 2004a). However, it is not clear from the results as to whether the ball momentarily grips the strings before over-spinning, as found by Cross (2003).

An FE model of a head-clamped racket has been validated for four different impact positions on the string-bed. The good agreement with the experimental data for both horizontal and vertical COR also indicates that the model accurately predicts the rebound angle of the ball. The results show that for a head-clamped racket the rebound characteristics of the ball remain virtually constant as the impact position changes in a direction parallel to the long axis of the string-bed. The rebound characteristics of the ball do change slightly more as the impact position changes in a direction parallel to the short axis. Overall, the effect of changing the impact position is very small compared to varying the

inbound velocity or angle of the ball. Unlike a hand-held racket a head-clamped racket is unable to rotate during impact. The rotations of a hand-held racket are likely to enhance the effect of different impact positions on the string-bed. However, it is difficult to undertake reliable laboratory investigations using a hand-held racket. Brody (1987) concluded that a freely suspended racket is a good laboratory representation of a hand-held racket, as detailed in the literature review (Section 2.4.4, page 28). Goodwill and Haake (2001) experimentally analysed the effect of impact position along the long axis of a freely suspended tennis racket. They projected balls perpendicular to the racket at a range of velocities. It was concluded that the impact location has a large effect on the rebound velocity of both the ball and racket. Future work will involve the validation of an FE model of a freely suspended racket against experimental data. The reasons for using a freely suspended racket are detailed in the literature review (Section 2.4.4, page 28). This model will be used to determine the true effect of different impact positions on the string-bed relative to play. The freely suspended racket model will be created by changing the material model whilst removing the displacement constraints applied to the frame.

4.6.4.   Summary

An explicit FE model of a head-clamped tennis racket has been successfully validated against experimental data. It was found that the impact position on the string-bed does not have a large effect on the rebound properties of the ball. The results from the FE model also indicate that the ball over-spins in the latter part of the impact. It would have been difficult to use the experimental data, in isolation, to determine if the ball was over-spinning during the impacts. Hence, this investigation demonstrates how a validated FE model can be used to enhance academic knowledge. In order to further the scientific understanding of the game of tennis, a freely suspended racket model should be validated against experimental data.

4.7. Chapter summary

In this chapter an FE model of a head-clamped tennis racket was constructed and validated against experimental data. The process of building the model was broken down into three separate stages. The initial stage was to obtain the required properties of the tennis strings. The second stage was to build and validate an FE model of a string-bed. The final stage constructed and validated an FE model of a head-clamped racket. It was found that the inbound velocity and angle had a large effect on the rebound properties of the ball. Impact location was found to have only a minor effect on the rebound properties of the ball.

5. Freely suspended racket model

5.1. Introduction

The aim of this project is to build an accurate FE model for simulating impacts between a tennis ball and racket. In the previous chapter an FE model of a head-clamped tennis racket was validated against experimental data, for a wide range of different impacts (Chapter 1, Page 90). The purpose of this was to validate the string-bed model and in particular, the method used to attach the strings to the racket frame. This chapter will include the creation and experimental validation of an FE model which simulates impacts between a tennis ball and a freely suspended racket. There are two main reasons for using a freely suspended racket;

1) A freely suspended racket will enable the simplest validation of the racket frame, without the additional variable of human grip. This will allow the accurate validation of racket frame parameters, such as stiffness and mass distribution.

2) A freely suspended racket is currently considered to be the best representation of a human grip, as detailed in the literature review (Section 2.4.4, Page 28).

The freely suspended racket model will be created by removing the displacement constraints applied to the frame in the head-clamped racket model. Previous studies have shown that a model which assumes the racket to be rigid is not suitable for predicting the rebound velocity of the ball, for impacts away from the Geometric String-bed Centre (GSC) (Brody, 1997; Goodwill and Haake, 2001 & 2003). Therefore, the MAT_RIGID material model, which was used for the head-clamped racket, will be changed to one which is capable of simulating deformation. The model will be validated against experimental data obtained by projecting balls onto a freely suspended racket. The experimental impacts will be captured using two synchronised high-speed video cameras and reconstructed into 3D for analysis. Only the movements of the ball will be analysed, as it will be too computationally expensive to run FE simulations for

sufficiently long duration to obtain the mean rebound velocity of the racket. Perpendicular impacts will be simulated at different locations on the string-bed to provide a thorough validation of the model. However, in order to develop an effective design tool, which can simulate realistic tennis shots, the model will also be validated for oblique spinning impacts. The mass and balance point of the racket have been found to have a large effect on the rebound velocity of the ball (Haake *et al.*, 2007). Therefore, the mass and balance point of the racket in the FE model must match those of the ITF *Carbon Fibre* racket, which will be used for the laboratory based experiments. The swingweight and twistweight of the racket in the model will also correspond to those of an ITF *Carbon Fibre* racket. The main objectives of this chapter are;

1. To build an FE model of a freely suspended tennis racket.

2. To experimentally validate an FE model of a freely suspended racket, for perpendicular impacts at different locations on the string-bed.

3. To experimentally validate an FE model of a freely suspended racket for oblique spinning impacts, at the centre of the string-bed.

5.2. FE Model of a freely suspended tennis racket

5.2.1.   FE Model of a freely suspended tennis racket

The freely suspended racket model was based on the head-clamped racket model (Section 4.5, Page 111), with a few modifications. The MAT_RIGID material model was changed to MAT_ELASTIC, to provide a better representation of reality and enable racket deformation to be simulated. MAT_ELASTIC was used as a starting point, as it is the simplest material model in Ansys/LS-DYNA 10.0 with the capacity to simulate deformation. A linear material model was considered to be adequate due to the relatively small deformations of a racket during an impact with a ball. The racket geometry was also separated into three parts, i.e. the handle, throat and head (Figure 5.1). The three parts of the frame were assigned separate shell sections to allow them to each have an individual wall thickness. With this model the mass distribution of the racket can be adjusted by changing the shell thickness and density of the handle, throat and head sections.

Handle

| **Throat**   **Head**
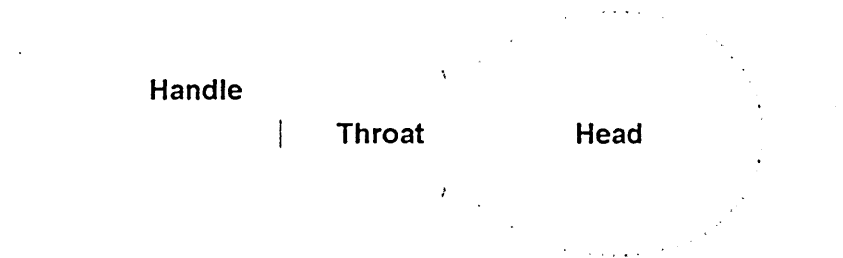
Figure 5.1 FE model racket geometry with three separate sections.

As previously mentioned, ITF *Carbon Fibre* rackets were used for the laboratory experiments. The ITF *Carbon Fibre* racket was selected as it is designed for laboratory testing and hence is likely to have a relatively simple composite lay-up. This should make the racket relatively straightforward to simulate in an FE model. In order to provide an accurate validation, the mass and mass distribution of the racket in the FE model were set to correspond to the ITF *Carbon Fibre* racket. The majority of the properties of the ITF racket were taken from Goodwill (2002) (Table 5.1).

Table 5.1 Properties of the *ITF Carbon Fibre* tennis racket (Goodwill, 2002).

Mass (kg)	Overall length (m)	Width (m)	Handle length (m)	Balance point from butt (m)	Mass moment of inertia from butt (mkg^2)
0.348	0.683	0.265	0.228	0.325	0.05337

The polar moment of inertia (I) *(Twistweight)* of the ITF racket was not measured by Goodwill (2002) and was hence obtained experimentally using Bifilar Suspension theory (Walker, 1991) (Figure 5.2). To do this, the racket was hung vertically from two tennis strings of equal length, as shown in Figure 5.2, and set to oscillate about its central axis. The time for a set number of oscillations was measured using a stopwatch. The experiment was undertaken three times with the period of torsion vibration (T) obtained from 10, 20 and 30 oscillations. For each number of oscillations the experiment was repeated five times.

$$T = 4\pi \sqrt{\frac{Il}{mgd^2}}$$

$$I = \frac{mg}{16l}\left(\frac{Td}{\pi}\right)^2$$
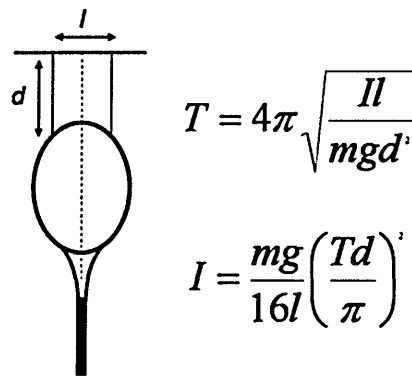
Figure 5.2 Bifilar Suspension used to obtain the polar moment of inertia of a tennis racket.

Table 5.2 shows the mean polar moment of inertia and standard deviation (SD) both decreased with the number of oscillations. The lower SD is predicted to be due to a reduced human error in the timing of the oscillations. In this report the polar moment of inertia of the racket is assumed to be $15.5 \pm 0.5 \times 10^{-4}$ kgm^2.

Table 5.2 Measured polar moment of inertia for the ITF *Carbon Fibre* tennis racket.

Number of oscillations	Mean polar moment of inertia (kgm^2)
10	0.001585 ± 0.000045
20	0.001552 ± 0.000028
30	0.001516 ± 0.000023

The density and shell thickness of the head, handle and throat sections were adjusted until the mass and mass distribution of the racket in the model corresponded to an ITF *Carbon Fibre* racket (Table 5.3). In order to do this successfully the mass of the whole racket in the FE model was firstly set to equal that of the experimental racket. Secondly, the mass of the individual parts of the racket (*handle, throat and head*) were adjusted in order to then fit the balance point, mass moment of inertia and polar moment of inertia of the experimental racket. The mass and polar moment of inertia of the individual parts of the racket were obtained directly from the FE model. The polar moment of inertia of the complete racket was calculated from summing the values for the individual parts. In order to calculate the balance point and mass moment of inertia of the racket about the butt, the distances from the centre of mass (COM) of the three parts to the butt were required. The distance of the COM of the three parts, from the string-bed centre along the length of the racket, was obtained directly from the FE model. The mass moment of inertia of the

individual parts of the racket about an axis through their COM and parallel to the short axis of the string-bed was obtained directly from the FE model. Parallel axis theory was used to obtain the mass moment of inertia about the butt of the racket (Table 5.3).

Table 5.3 Racket mass distribution in the FE model.

Part	Density $(kg \cdot m^{-3})$	Shell thickness (m)	Mass (kg)	Distance to COM from butt (m)	Balance point from butt (m)	Mass moment of inertia about butt (kgm^2)	Polar moment of inertia (kgm^2)
Handle	1900	0.003	0.0980	0.084	0.0082	0.00098	0.000021
Throat	2100	0.002	0.0895	0.257	0.0232	0.00622	0.000125
Head	1350	0.002	0.1618	0.505	0.0813	0.04331	0.001446
Complete racket	-	-	0.3483	-	0.3236	0.05111	0.001592
Required value	-	-	0.3480	-	0.3250	0.05337	0.001550
Difference between FE and reality (%)	-	-	0.1	-	-0.4	-4.4	2.7

The geometry and materials used in the construction of a tennis racket determine its stiffness, which in turn affects the rebound characteristic of the ball (Cross, 2000c; Kanda *et al.*, 2002; Goodwill and Haake 2001 & 2003; Haake *et al.*, 2007). Experimentally obtaining the mechanical properties of composites is difficult, requiring access to both specialist equipment and material samples. Material samples were not available for this project. Therefore, the material properties of the racket were estimated from published data. The material properties of a composite depend on the ratio of the separate components and their individual properties. Jenkins (2003) published tensile modulus values for carbon filaments, as 517 GPa for very high modulus and 350 GPa for high modulus. John (2003) states 4 GPa as a Young's modulus for epoxy resin. Assuming the carbon fibre composite to be around 30 to 50% resin and the Young's modulus to be a third of the maximum in any direction (John, 2003); the Young's modulus of a typical carbon fibre lay-up used in the construction of a modern tennis racket is predicted to fall between 10 and 140 GPa. The natural frequency (f_n) of a 2D beam is determined by its structural stiffness (k) and mass (m) (Equation 1).

$$f_n = \frac{1}{2\Pi}\sqrt{\frac{k}{m}} \qquad (1)$$

As the mass of the racket in the FE model was set to correspond to an ITF *Carbon Fibre* racket, it was possible to obtain the correct natural frequency by adjusting the Young's modulus. The natural frequencies of tennis rackets dating from the 1870's to 2007 are within the range of 70-190 Hz (Haake *et al.,* 2007). The natural frequency of the ITF *Carbon Fibre* racket is 134 Hz (Goodwill, 2002). Modal analysis was undertaken on the racket model using ANSYS Mechanical 10.0, for a range of values of Young's modulus (Figure 5.3). The Young's modulus was set to the same value in the three parts of the racket. An apparent Young's modulus of 20 GN·m^{-2} resulted in a natural frequency of 135 Hz, which is very close to the value of 134 Hz found by Goodwill (2002) for the ITF *Carbon Fibre* racket.
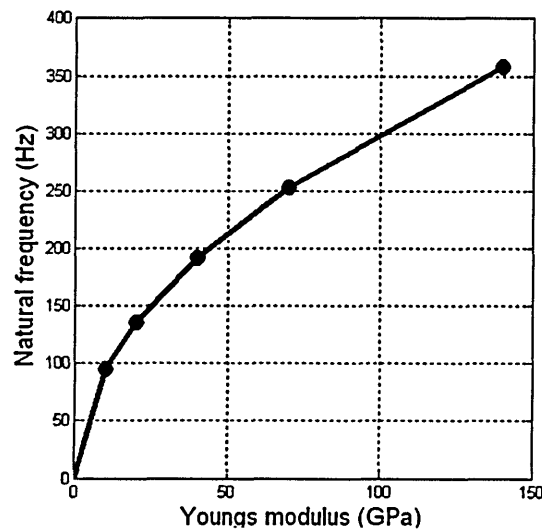
Figure 5.3 The relationship between apparent Young's modulus and natural frequency for the racket in the FE model.

Two FE models were created to encompass the large range of values of racket stiffness typically found (Table 5.4). The model with an apparent Young's modulus of 10 GN·m^{-2} will represent a composite tennis racket with a low structural stiffness. This model should produce lower rebound velocities than obtained from the experimental data, when simulating perpendicular impacts away from the GSC *(node point)* (Kanda *et al.,* 2002; Goodwill and Haake, 2003). The racket with the apparent Young's modulus of 70 GN·m^{-2} is representative of a very stiff racket, this should produce higher rebound velocities than the experimental data, when simulating perpendicular impacts

away from the GSC *(node point)* (Kanda *et al.,* 2002; Goodwill and Haake, 2003). The stiffer racket had a natural frequency of 253 Hz, that was higher than the upper bound of 190 Hz as proposed by Haake *et al.* (2007). However, it is predicted from the trend in Haake *et al.'s* data that rackets will be developed with higher natural frequencies than the maximum values measured in 2007.

Table 5.4 Natural frequencies of the two racket models with different Young's modulus.

Racket	Young's Modulus (GPa)	Natural Frequency (Hz)
Low structural stiffness	10	96
High structural stiffness	70	253

The convergence tolerance for dynamic relaxation was changed from the value of 0.1 used in the head-clamped racket model, to 0.06 and should increase the accuracy of the model (Figure 5.4). This is because the total kinetic energy of the model and string-bed will be lower, causing the stress distribution in the strings to be closer to those which have been subjected to quasistatic loading i.e. a string-bed tensioned using a stringing machine. To account for the slightly longer convergence time, the tied contact between the strings and racket and the contact between the ball and string-bed was set to initiate at a simulation time of 0.00135 s, rather than 0.0013 s in the head-clamped racket model. The rigid cylinders at the ends of the strings were also released from their constraints at 0.00135 s. The use of rigid cylinders to apply tension to the string-bed is described in section 4.3.1, on page 94. When defining contact with shell elements it is possible to override the geometric thickness of the elements with a contact thickness. The contact thickness of the shell elements which were used to tie the strings to the racket frame were set to the actual thickness of the frame (2 mm). The contact thickness of the shell elements used in the contact between the racket and strings was 0.4 mm.
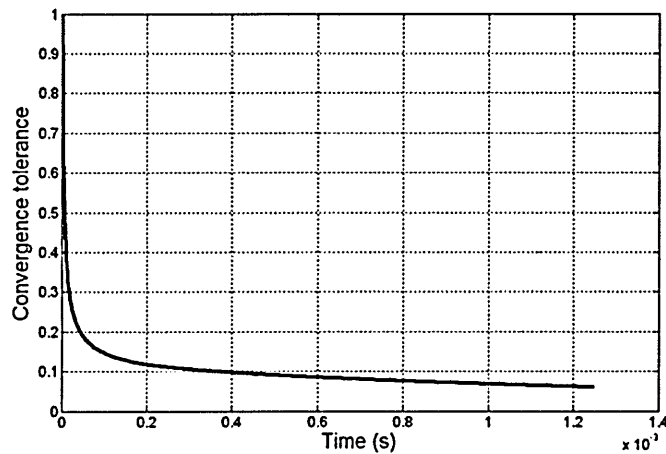
Figure 5.4 Convergence of the freely suspended racket model.

5.2.2.   Summary

An FE model of a freely suspended tennis racket was created in Ansys/LS-DYNA 10.0. The racket frame geometry was separated into three separate parts to allow the mass distribution of the frame to be adjusted. The mass and mass distributions of the racket were set to correspond to that of an ITF *Carbon Fibre* racket. MAT_ELASTIC material models were used for the separate parts of the racket frame as they are capable of simulating deformation. The natural frequencies of racket models with different values of Young's modulus were determined using modal analysis. FE models with natural frequencies of 96 and 253 Hz will now be analysed against the experimental data. The purpose of this is to determine the effect of tennis racket stiffness. The racket was not strung during the frequency analysis, as a method for tensioning the string-bed was not available. Cross *et al.* (2001b) found the fundamental frequency of a tennis racket to drop by 8.5% when strung.

5.3. Validation of the freely suspended racket model

5.3.1.   Experimental methods

Tennis balls were projected from a modified pitching machine (BOLA) onto a freely suspended ITF *Carbon Fibre* racket, using the impact rig detailed in Choppin (2008) (Figure 5.5a). The racket was hung vertically from a pin with its butt at the lower end. The pin was located underneath the tip of the frame between the two central main strings. Using a pin to simulate a freely suspended racket is a technique which had been used by numerous authors (Goodwill and Haake, 2001 & 2003; 2002; Goodwill, 2002; Choppin 2008). The

impacts were captured using two synchronised *Phantom V4.3* high-speed video cameras, recording at 1,900 fps. This frame rate allowed enough images to be obtained to accurately track the ball for the full range of velocities under investigation. The impacts were recorded using two cameras positioned on separate sides of the impact rig to provide 3D coordinates of the ball and racket, as detailed by Choppin (2008) (Figure 5.5b).

Figure 5.5 a) Impact rig used for simulating impacts on a freely suspended tennis racket (Modified from Choppin, 2008) b) Optimum camera positions for measuring the trajectory of a tennis ball in 3D (Modified from Choppin, 2008).

As previously mentioned, the model was validated against experimental data for both perpendicular and oblique impacts. Three rackets were used for the experimental testing, all strung at 289 N (65 lbs). Perpendicular impacts were simulated on two of the rackets at four different impact positions on the string-bed, labelled: centre, off-centre, tip and throat (Figure 5.6). The inbound velocity of the balls in the perpendicular impacts was in the range from 10 to 40 m·s^{-1}.
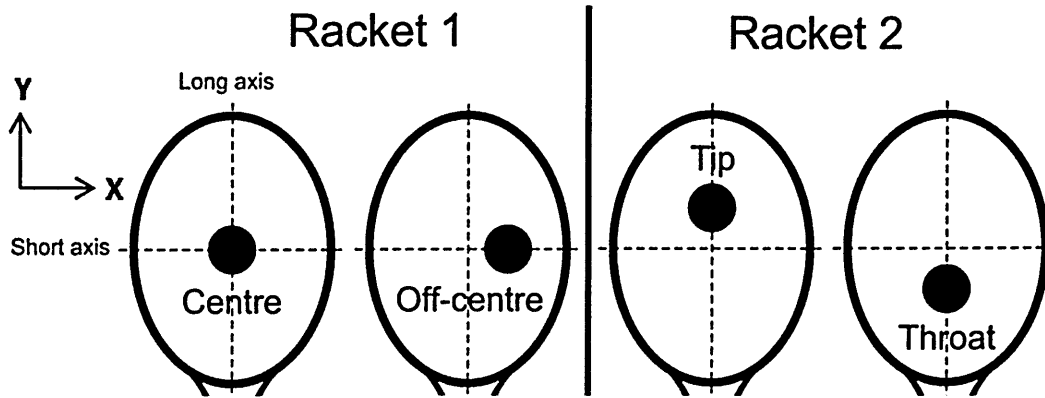
Figure 5.6 Impact positions on the string-bed for the validation of the freely suspended racket model for perpendicular impacts.

Oblique spinning impacts were simulated at nominal inbound velocities of 20 and 30 m·s^{-1} and a nominal angle of 25° to the z axis, on a plane parallel to the x and z axes (*Reference to axes on Figure 5.5*). The inbound backspin of the oblique impacts was in the range from -100 to 500 rad·s^{-1}. Oblique impacts were obtained by tilting the racket about its vertical axis (y) (Figure 5.7). The racket was positioned against a triangular wedge, located beneath the pin, to enable a consistent racket angle of 25° to be obtained for all of the impacts. All three rackets were used for the oblique impacts. The two rackets used previously for the perpendicular impacts were subjected to impacts at a single nominal velocity; the third racket was used for both nominal velocities, effectively acting as a control. Choppin *et al.* (2008) found that male and female players typically impact the ball 0.55 ± 0.032 m and 0.55 ± 0.031 m from the butt of the racket, respectively. Goodwill and Haake (2004b) found that for an oblique impact on a freely suspended racket at 30 m·s^{-1} and 36° *(relative to racket normal)* the ball will travel approximately 0.035 m (±0.005) horizontally *(parallel to short axis)* whilst it remains in contact with the string-bed. The nominal impact location of the oblique impacts was 0.55 m from the butt of the racket (0.0295 m above GSC) and 0.02 m offset from the long axis. The offset from the long axis was to compensate for the horizontal displacement of the ball whilst it remains in contact with the string-bed during the impact.
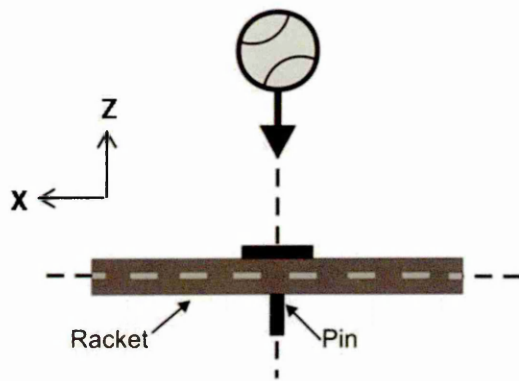
Figure 5.7 Racket positioning for perpendicular and oblique impacts on a freely suspended racket *(View from above).*

The impacts were recorded as bitmap images and analysed using *Richimas v3.* The intrinsic 2D positions of the ball were obtained manually from each camera using *Richimas* image analysis software. The pairs of 2D coordinates obtained using *Richimas* were converted into extrinsic global 3D coordinates *(camera frame of reference)* using a readily available *MATLAB R2006b* Toolbox which was developed by Bouguet (2008). The 3D calibration was undertaken using a checkerboard, as developed by Zhang (1999) and applied to tennis impact testing by Choppin (2008). To ensure high accuracy, over 15 pairs of calibration images were obtained (Zhang, 1999). To measure the impact position on the string-bed, the 3D coordinates of the ball were converted into the racket frame of reference, with the GSC at the origin (Figure 5.8). The GSC was located at the origin by obtaining the global 3D coordinates of three white markers at known locations on the racket frame. A transformation matrix was used to convert the global 3D coordinates of the ball into local 3D coordinates in the racket's frame of reference. To ensure the highest possible accuracy when calculating the velocity of the ball, its position *(x, y and z coordinates)* was obtained at four discrete locations before and after impact. The velocity of the ball was calculated separately in the x, y and z directions using the gradient of the distance-time data. The resultant velocity was resolved from the x, y and z velocities. Assuming the velocity of the ball to be linear in each plane, it was possible to predict the position of the ball at any possible time point *(d = v.t).* The time step *(t₁)* was chosen as 0.13 ms *(0.25 frames)*, in order to be sufficiently small enough to accurately estimate the impact position of the ball

on the string-bed. Impact was assumed to initiate at the first instance when the ball's perpendicular distance (Z) from the string-bed *(XY plane at Z = 0)* was less than its radius *(33 mm)*. The horizontal (x) and vertical (y) impact distances from the GSC were obtained from the position of the ball at the first point of contact with the string-bed. The global 3D coordinates of the racket markers, used in the calculations, were the mean values obtained for each set of impacts. For full details of the method used to validate tennis ball to racket impacts in 3D using two high-speed video cameras, refer to Choppin (2008).
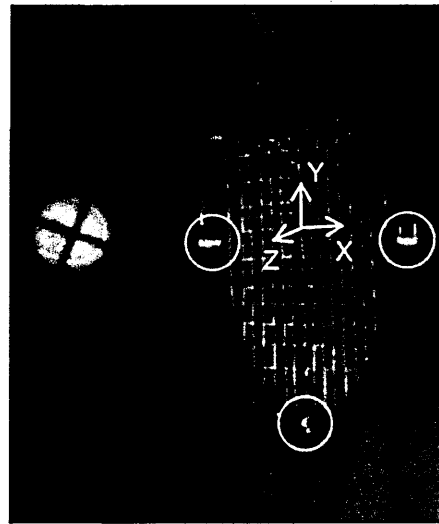
Figure 5.8 Racket position showing throat and side markers and axis coordinate system.

Ball spin from the oblique impacts was calculated using markers, which were drawn on the felt (Figure 5.8). The process involved using *Richimas* to obtain the coordinates of the geometric ball centre (GBC) (A) and a marker *(intercept of lines on the ball)* (B) (Figure 5.9). The radius of the ball and the distance (X) were then used to obtain the angle θ. The process was repeated to obtain four angles before and after impact. The top/back spin about the y axis, relative to the racket, was calculated from the gradient of the angle time data. The sidespin about the x axis was also calculated using this technique.
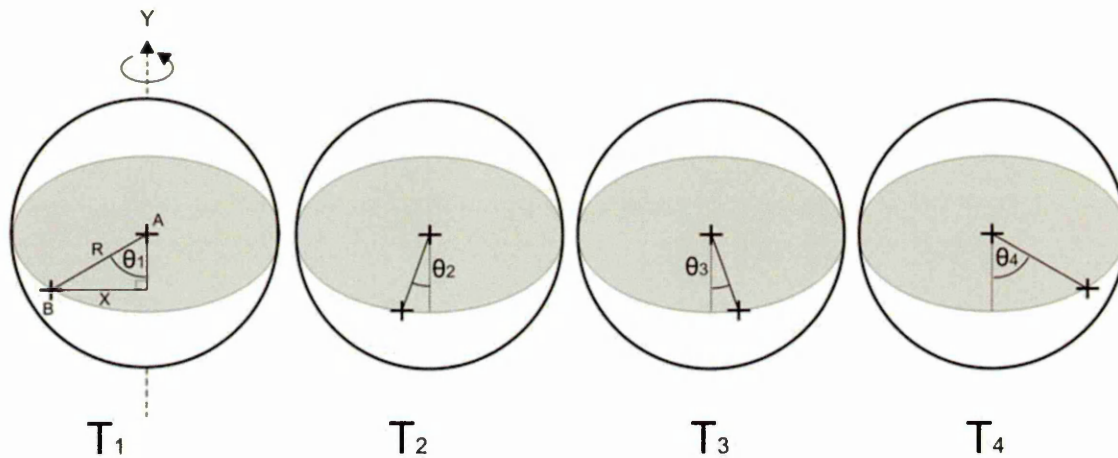
Figure 5.9 Method used for calculating the top/back spin of a tennis ball, by calculating the change in θ over time.

There will be errors in the method used for calculating spin, due to the angle between the flight path of the ball and the cameras, as shown in Figure 5.10. If the ball is incident with no spin, the view from both cameras will perceive it to be spinning in the direction in which it is travelling (Figure 5.10). In this investigation the ball was defined as having positive inbound backspin when it was spinning in the same direction as its flight path, relative to the right camera. Therefore, using this orientation the right and left camera will over and under predict the inbound backspin, respectively. Theoretically, if the angle of the left camera relative to the flight path of the ball is the same as that of the right camera, the error in each camera will be equal and opposite. Hence, the mean of the inbound spin rates obtained from the two cameras should be approximately equal to the correct value. The actual rebound path of the ball is currently unknown, which makes it difficult to predict the error in the spin calculation. To ensure the highest possible accuracy with this method, the spin was calculated independently from both cameras and the mean value was used to validate the model. It may have been possible to calculate the spin of the ball in 3D, by positioning the cameras so they could both track the movement of a single marker. However, this would have meant changing the camera positions from the optimum ones found by Choppin (2008), which would have led to subsequent errors.
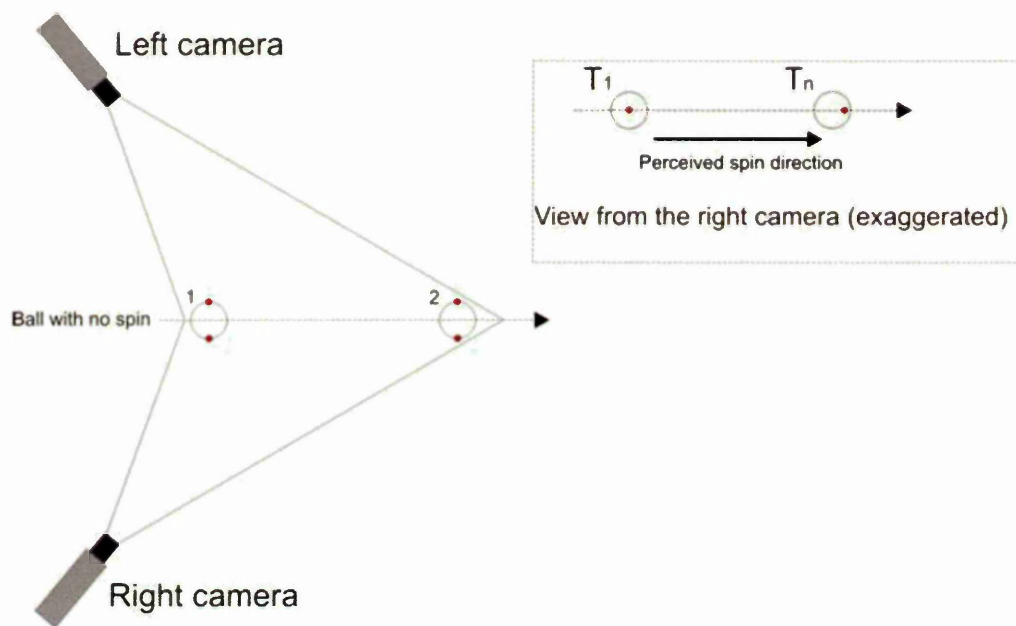
Figure 5.10 Spin error in the experimental data as a result of camera positions.

5.3.2.   Impact parameters - Perpendicular impacts

Table 5.5 and Figure 5.11 show the calculated impact locations for the perpendicular impacts. FE simulations were undertaken with the same mean impact locations as the laboratory experiment. The root mean squared error (RMSE) between the resultant and z velocities *(perpendicular to string-bed)* for all the perpendicular impacts in the experiment was 0.008 m·s^{-1} for inbound and 0.04 m·s^{-1} for rebound. As the RMSE is very low the impacts were considered to be perpendicular to the racket and the resultant velocities were analysed against the FE models. The FE simulations of the perpendicular impacts had inbound velocities of 10, 20, 30 and 40 m·s^{-1}. Two sets of simulations were undertaken with values of Young's modulus of 10 GPa and 70 GPa, whilst the Poisson's ratio remained constant at 0.3.

Table 5.5 Impact locations for the perpendicular impacts on a freely suspended racket *(mean ± SD)*.

Impact location	Horizontal distance from the string-bed centre (mm)	Vertical distance from the string-bed centre (mm) (+ = towards tip)
Centre	13 ± 7	8 ± 7
Off-centre	31 ± 10	4 ± 7
Throat	18 ± 8	-55 ± 16
Tip	13 ± 11	49 ± 7

142
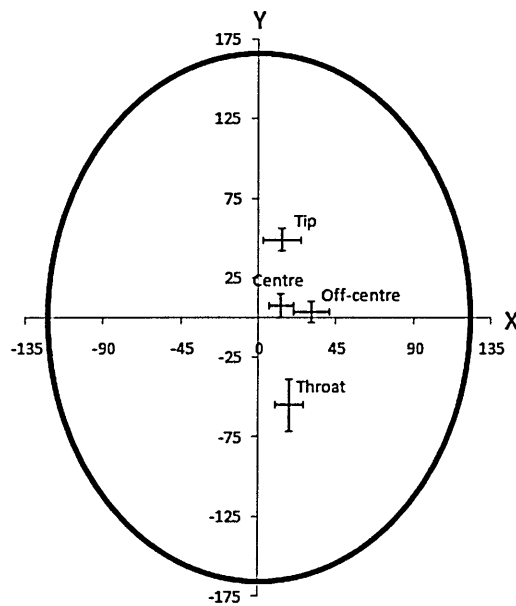
Figure 5.11 Diagram showing the standard deviations in impact locations for the perpendicular impacts on the freely suspended racket.

5.3.3.   Impact parameters - Oblique impacts

Table 5.6 shows the calculated inbound velocities, inbound angles and impact locations on the string-bed for the oblique impacts. The inbound side spin of the balls *(relative to the racket)* was found to be negligible, therefore, only the top/back spin was used to validate the FE models. Figure 5.12 shows the top/back spin measured from the two cameras was in good agreement. The RMSE between the spin measured from the left and right camera was, 20.6 rad·s^{-1} for inbound and 11.1 rad·s^{-1} for rebound. Assuming both cameras were positioned in equal and opposite locations relative to the inbound path of the ball; the error in inbound spin from each camera is predicted to be approximately 10 rad·s^{-1}. The rebound path of the balls was in the direction of the left camera and approximately parallel to the lens of the right camera. This is predicted to be the reason for the lower discrepancies between the two cameras for rebound spin. As a comparison another method was used to measure the spin of the balls (Appendix C).

Table 5.6 Inbound velocities, angles and impact locations for the oblique impacts on a freely suspended racket *(mean ± SD)*.

	20	30
Nominal inbound velocity (m·s⁻¹)	20	30
Nominal inbound angle (°)	25	25
Calculated inbound velocity (m·s⁻¹)	18.0 ± 0.5	28.0 ± 0.4
Calculated inbound angle (°)	23.7 ± 1.3	22.9 ± 0.9
Horizontal distance from the string-bed centre (mm)	9 ± 16	15 ± 10
Vertical distance from the string-bed centre (mm) (+ = towards tip)	9 ± 12	8 ± 11
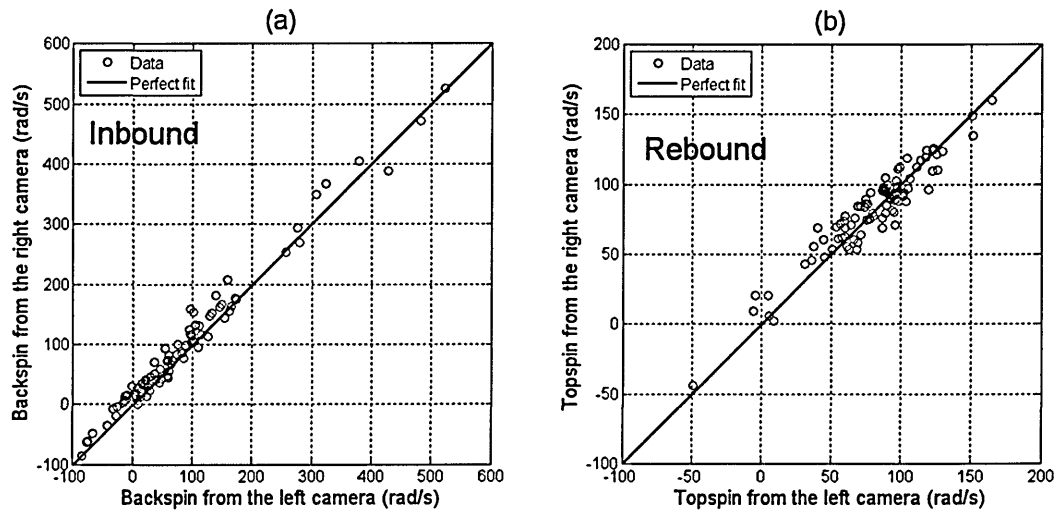
Figure 5.12 Comparison of spin calculated from the left and right camera a) inbound and b) rebound.

A repeatability study was undertaken to assess the level of human error in the manual tracking method. An impact with low, medium and high inbound spin was selected and analysed ten times (Table 5.7). The spin rate was the average obtained from both cameras as described previously. The impacts had a nominal inbound velocity of 20 m·s⁻¹. All of the other impacts in this investigation were analysed once and are assumed to have a SD similar to those in Table 5.7. The uncertainties in the measured values are similar to those reported by Goodwill and Haake (2004b).

144

Table 5.7 Results of a repeatability test for impacts with low medium and high inbound spin. *(value)* = SD as a percentage of the mean.

	Low spin (-4.9 rad·s^{-1})	Medium spin (251.6 rad·s^{-1})	High spin (529.9 rad·s^{-1})
Resultant inbound velocity (m·s^{-1})	0.1 *(0.4%)*	0.1 *(0.6%)*	0.1 *(0.5%)*
Resultant rebound velocity (m·s^{-1})	0.1 *(1.0%)*	0.1 *(0.8%)*	0.1 *(1.5%)*
Inbound angle (degrees)	0.3 *(1.4%)*	0.5 *(2.0%)*	0.4 *(1.4%)*
Rebound angle (degrees)	0.3 *(0.9%)*	0.5 *(3.1%)*	0.9 *(18.1%)*
Inbound spin (rad·s^{-1})	8.6 *(176.3%)*	8.0 *(3.2%)*	20.6 *(3.9%)*
Rebound spin (rad·s^{-1})	9.4 *(9.2%)*	4.4 *(38.5%)*	8.4 *(18.9%)*
Impact distance from long axis (mm)	1 *(56.2%)*	2 *(17.4%)*	2 *(13.0%)*
Impact distance from short axis (mm)	1 *(8.8%)*	1 *(19.8%)*	1 *(2.7%)*

The FE simulations of the oblique impacts had inbound velocities, inbound angles and impact locations, identical to those measured in the laboratory experiment. In the FE simulations, the inbound backspin was in the range of 0 to 400 rad·s^{-1}, at 200 rad·s^{-1} increments. As with the perpendicular impacts, FE models with natural frequencies of 96 and 253 Hz were analysed against the experimental data.

5.3.4.   Summary of experimental conditions

Tennis balls were projected onto a freely suspended tennis racket using a modified BOLA. Perpendicular impacts were simulated at four discrete locations on the string-bed, with inbound velocities in the range from 10 to 40 m·s^{-1}. Oblique spinning impacts were simulated at approximately the centre of the string-bed, with nominal inbound velocities of 20 and 30 m·s^{-1}. The nominal inbound angle was 25° and the backspin was in the range from -100 to 500 rad·s^{-1}. The impacts were captured using two synchronised *Phantom V4.3* high-speed video cameras and analysed in 3D. The uncertainties in the measured values was in the range of 0.1 m·s^{-1} for velocity, 0.9° for angle, 21 rad·s^{-1} for spin and 2 mm for impact position.

FE simulations with the initial conditions shown in Table 5.8 were undertaken to correspond to the experimental data.

Table 5.8 Initial conditions used in the FE model to simulate an impact between a tennis ball and freely suspended racket.

	Inbound velocity (m·s^{-1})	Inbound angle (°)	Inbound backspin (rad·s^{-1})	Number of impact locations
Perpendicular impacts	10, 20, 30 & 40	0	0	4
Low velocity oblique impacts	18	23.7	0, 200 & 400	1
High velocity oblique impacts	28	22.9	0, 200 & 400	1

5.4. Results and discussion of the freely suspended racket model validation

5.4.1.   Results of perpendicular impacts

Figure 5.13 shows a comparison of the FE model with the experimental data in terms of the rebound velocity of the ball, for the perpendicular impacts at the four locations on the string-bed. There are two sets of data from the FE model corresponding to different racket stiffnesses. The rebound velocity of the ball is slightly lower for the off-centre impacts, in comparison to those at the centre. The rebound velocity is lowest for the tip impacts and highest for those at the throat, in agreement with Goodwill and Haake (2001 & 2003) and Kanda *et al.* (2002). Figure 5.13c shows that four of the tip impacts, which had low inbound velocity (<20 m·s^{-1}), had a larger rebound velocity than expected from the trend of the rest of the data (*See highlighted data points*). Three of these four impacts were closer to the GSC in comparison to the mean impact location, in both the vertical and horizontal directions. The remaining impact had an offset distance from the long axis of the string-bed which was less than the mean value.

Raising the Young's modulus of the racket in the FE model, increased the rebound velocity of the ball for the throat impacts whilst having a negligible effect on those at the other locations, in agreement with Goodwill and Haake (2003). The FE model of the racket with the Young's modulus of 10 GPa, was in relatively good agreement with the experimental data for all four of the impact locations on the string-bed. The model with the higher Young's modulus of 70 GPa slightly over-predicted the rebound velocity of the ball for the impacts at the throat. This over-prediction increased with inbound velocity.
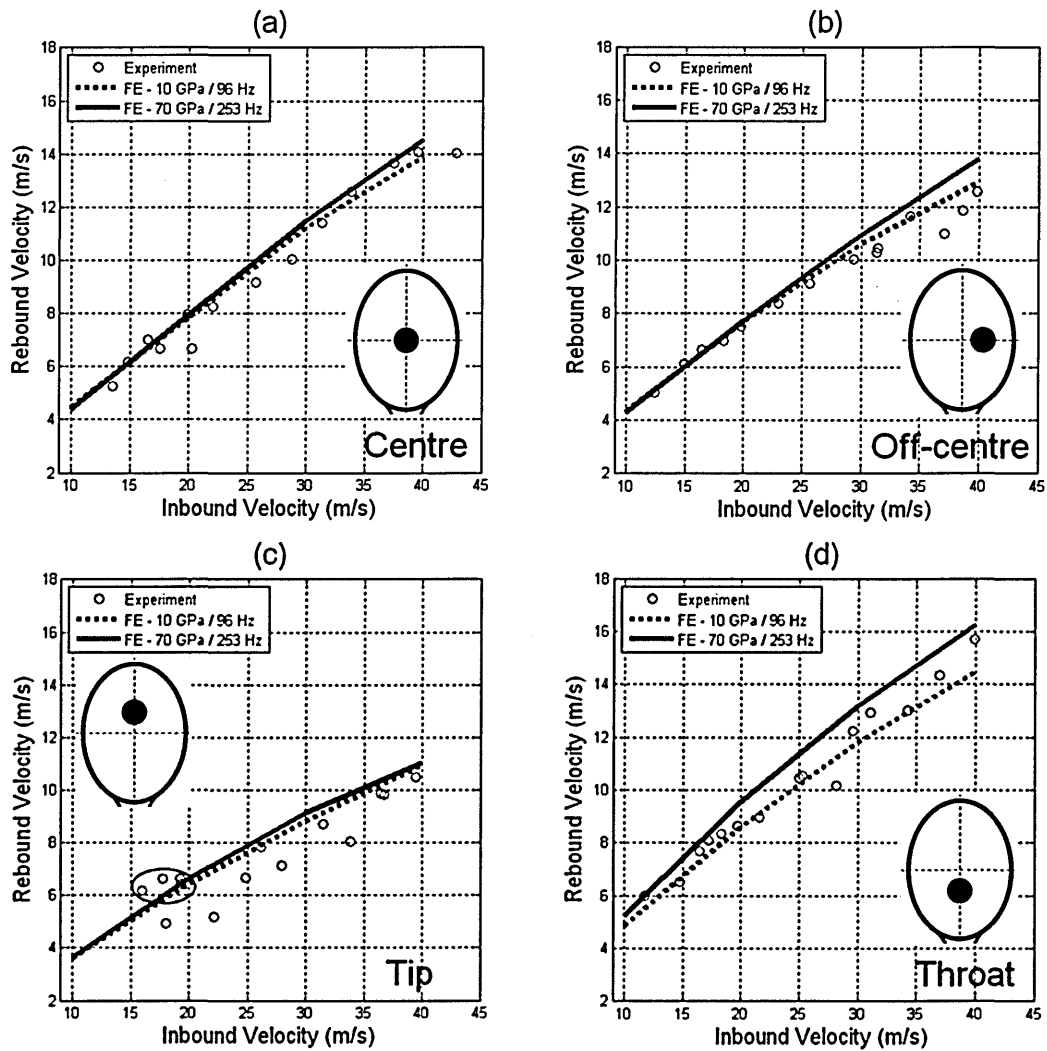
Figure 5.13 Ball rebound velocity for perpendicular impacts on a freely suspended racket a) Centre, b) Off-centre, c) Tip and a) Throat.

Second order polynomial trend lines were fitted to the results obtained from each of the FE models. The equation of each of these lines was used to obtain a rebound velocity for each of the calculated experimental inbound velocities. The RMSE's between both racket models and the experimental data was then obtained for each impact location on the string-bed (Table 5.9). The results show that, overall, the FE model with the Young's modulus of 10 GPa was in better agreement with the experimental data.

Table 5.9 RMSE between the FE models and experimental data for rebound velocity, for perpendicular impacts on a freely suspended racket.

Impact location	Centre	Centre	Off-centre	Off-centre	Tip	Tip	Throat	Throat
Young's modulus (GPa)	10	70	10	70	10	70	10	70
RMSE for rebound velocity (m·s⁻¹)	0.55	0.67	0.48	0.85	0.91	1.04	0.57	1.02

Figure 5.14 shows resultant force plots obtained from the FE model for the perpendicular impacts with an inbound velocity of 40 m·s^{-1}. The results indicate that the structural stiffness of the racket does not have a large effect on the impact force between the ball and string-bed; although the results do indicate that the impact location has a large influence on the contact force throughout the impact. The impacts at the centre had the highest peak forces, whilst the impacts at the tip had the lowest. The difference in the maximum force between the centre and tip impacts was approximately 400 N. The highest impact force was experienced for the centre impacts, as these were closest to one of the rackets two node points. The plots for the off-centre, tip and throat impacts all show a dip in force around the mid-point of the impact. This dip is due to the racket deforming as the ball and string-bed reach the point of maximum displacement during the impact. The impact forces are slightly larger for the stiffer racket because it deformed less during the impacts. There is no dip in the force plot for the centre as this impact location was close to a node point and the racket had very little deformation.
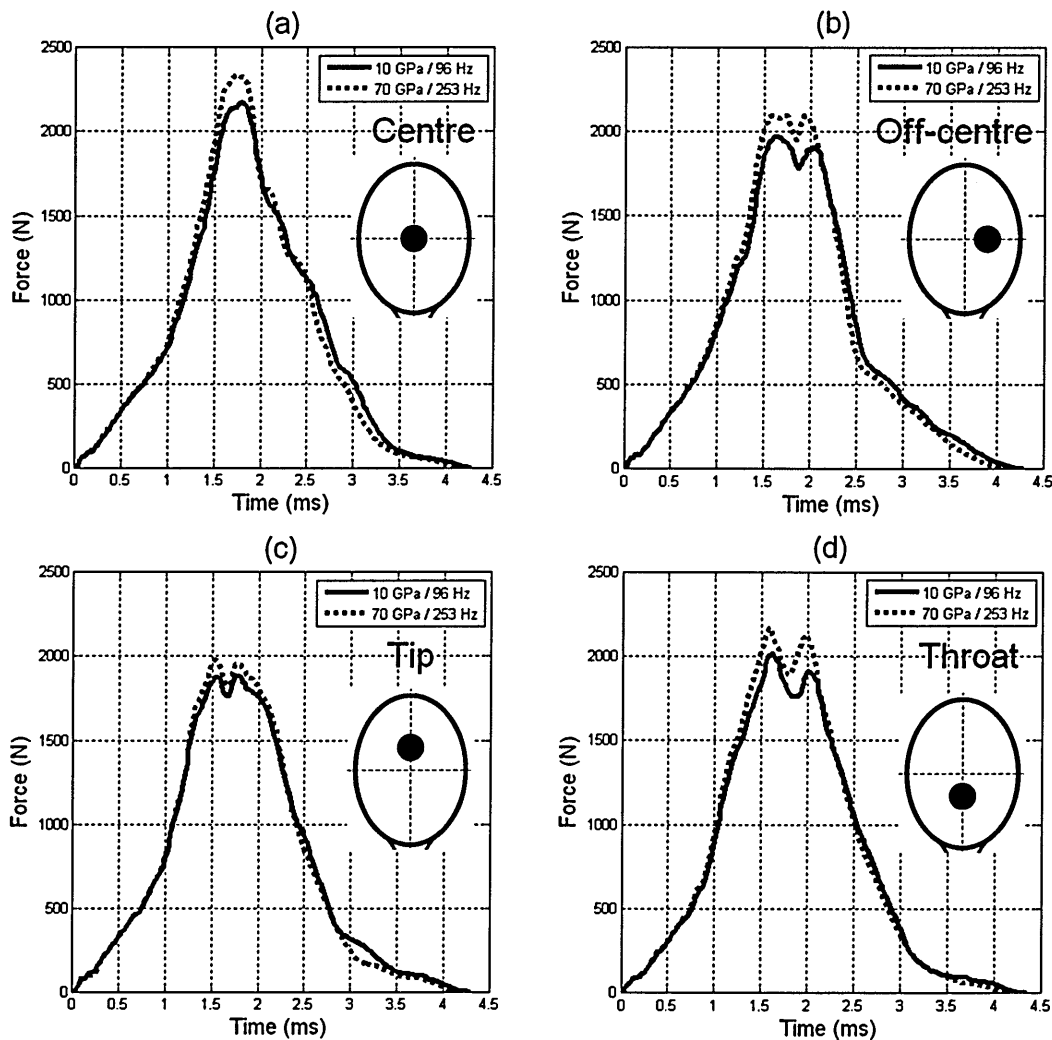
Figure 5.14 Ball to racket resultant force plots for perpendicular impacts at 40 m·s⁻¹, a) Centre, b) Off-centre, c) Tip and d) Throat.

5.4.2. Discussion of perpendicular impacts

The FE model was in relatively good agreement with the experimental data in terms of the rebound velocity of the ball, for all four of the impact locations used in this investigation. However, there was a large amount of scatter in the experimental data. This is predicted to be due to the relatively high variation in the actual impact positions, for each of the four nominal impact locations on the string-bed. The scatter in the experimental data highlights the complexities in accurately validating an FE model, whilst also providing evidence for its requirement. Goodwill and Haake (2004b) also had a large amount of scatter in their experimental data when analysing oblique impacts on a freely suspended racket. They stated the scatter in their data to be due to; 1) uncertainty in their experimental measurements and 2) the rebound characteristics of the ball being

highly dependent on the impact position, as a result of the non-uniformity of the string-bed. The FE model was in better agreement with the experimental data when the Young's modulus of the racket was 10 GPa in comparison to 70 GPa. Increasing the stiffness of the racket resulted in an increase in the rebound velocity of the ball for impacts at the throat, in agreement with Goodwill and Haake (2003) and Kanda *et al.* (2002). Modal analysis showed that a Young's modulus of 20 GPa would result in a natural frequency of 135 Hz, which is effectively equal to the natural frequency of the ITF *Carbon Fibre* racket (Goodwill, 2002). Therefore, it is predicted that using a Young's modulus of 20 GPa would result in better agreement with the experimental data for impacts at the throats. Changing the Young's modulus of the racket to 20 GPa would have only a very marginal effect on the rebound velocity of the ball at the other impact locations.

5.4.3.   Results of oblique impacts

Figure 5.15 shows a comparison of the FE model with the experimental data, for the oblique impacts at the two inbound velocities. As with the perpendicular impacts there are two sets of data for the FE model corresponding to different racket stiffnesses. The rebound velocity of the ball decreased with increasing inbound backspin and was lower for the impacts at 18 m·s^{-1} in comparison to those at 28 m·s^{-1}. The resultant rebound velocities obtained from the two FE models were in very good agreement with the experimental data, for both inbound velocities. There was only a very small difference in the rebound velocities obtained from the two FE models of different racket stiffness. This was in agreement with the results obtained for the perpendicular impacts at the centre of the string-bed.
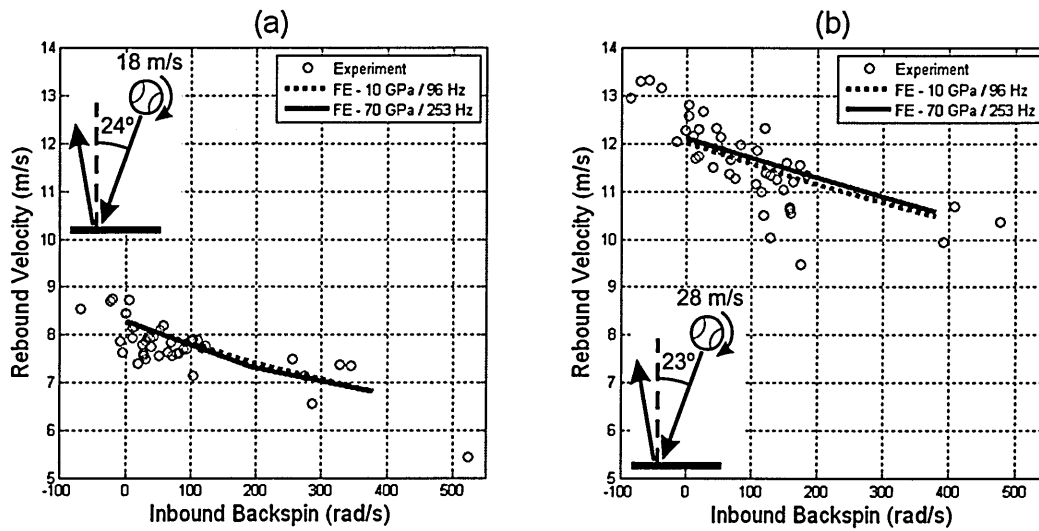
Figure 5.15 Ball rebound velocity for oblique impacts on a freely suspended racket a) 18 m·s⁻¹ and 24° b) 28 m·s⁻¹ and 23°.

Figure 5.16 shows that the rebound angle of the balls *(relative to the racket normal)* decreased with increasing inbound backspin. The rebound angles were virtually identical for both inbound velocities when the balls were incident with a negligible amount of inbound spin. However, the rebound angle decreased more with increasing inbound backspin when the inbound velocity of the balls was 18 m·s⁻¹, in comparison to 28 m·s⁻¹. Therefore, when the balls were incident with high inbound backspin (>100 rad·s⁻¹) the rebound angle of the balls was lower for the inbound velocity of 18 m·s⁻¹.

As with rebound velocity, there was very little difference in the results obtained from the two FE models. The FE models were both in relatively good agreement with the experimental data, although the models slightly under-predicted the rebound angle of the ball by a few degrees, for both inbound velocities.

152
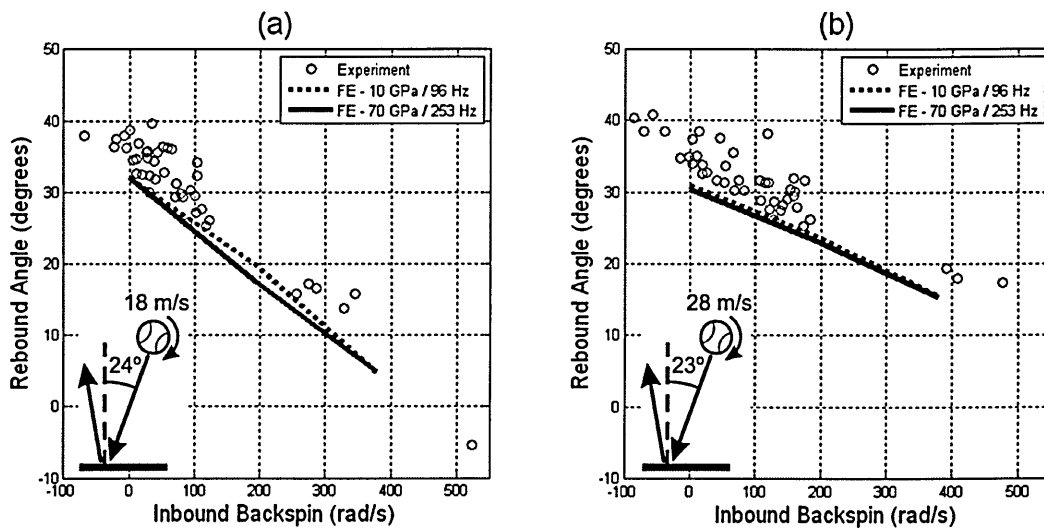
Figure 5.16 Ball rebound angle for oblique impacts on a freely suspended racket a) 18 m·s⁻¹ and 24° b) 28 m·s⁻¹ and 23°.

Figure 5.17 shows that the rebound spin of the balls decreased with increasing inbound backspin. The rebound spin was lower for the inbound velocity of 18 m·s⁻¹ and it decreased more with inbound backspin. As with rebound velocity and angle there was very little difference in the results obtained from the two FE models. The FE models were in good agreement with the experimental data for inbound backspins which were lower than approximately 200 rad·s⁻¹. At higher inbound backspins the models slightly under-predicted the rebound spin of the balls. It is difficult to precisely assess the accuracy of the FE model for high inbound backspins, due to the low number of experimental data points and the relatively large uncertainty in the measurement of inbound and rebound spin *(approx.20 rad·s⁻¹).*
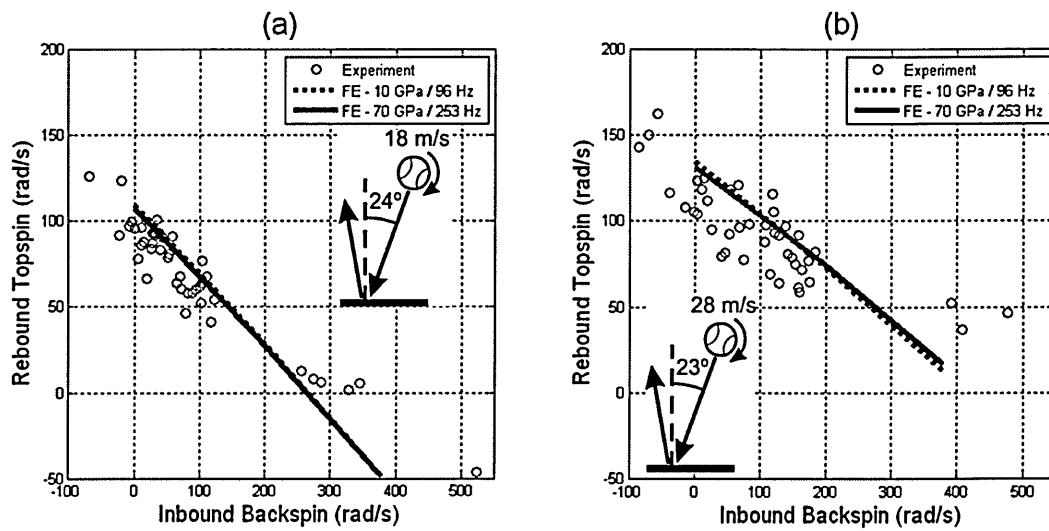
Figure 5.17 Ball rebound spin for oblique impacts on a freely suspended racket a) 18 m·s⁻¹ and 24° b) 28 m·s⁻¹ and 23°.

5.4.4. Explaining the effects of inbound spin on the rebound properties of the ball

An investigation was undertaken to ascertain how and why the rebound properties of the ball changed with inbound spin. An impact at 28 m·s⁻¹ and 23°, with 200 rad·s⁻¹ of backspin was selected for analysis. These values of inbound velocity and backspin were used as they are considered to be representative of those employed in play (Choppin *et al.*, 2008); these impacts were also in good agreement with the experimental data.

Figure 5.18 shows how the horizontal and vertical forces acting on the ball and its horizontal velocity and spin change throughout the impact. The horizontal and vertical planes are defined as being parallel and perpendicular to the string-bed, respectively. The horizontal force acting on the ball was initially negative. This means that the force was initially acting in the opposite direction to the horizontal motion and spin of the ball. This caused a decrease in the horizontal velocity of the ball and an increase in its spin (*decrease in backspin*). At approximately the mid-point of the impact the horizontal force acting on the ball switched direction. This caused an increase in the horizontal velocity of the ball and a decrease in its topspin. The horizontal force acting on the ball then converged towards zero. Once the horizontal force equalled zero, there was no further change in the horizontal velocity or spin of the ball. This implies that the ball was rolling off the string-bed. These results are in agreement with those found for the head-clamped racket model (Figure 4.23, page 122).
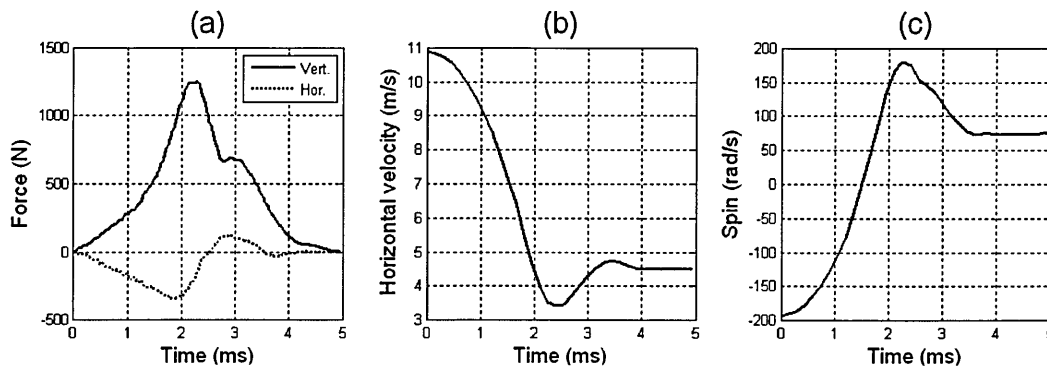
Figure 5.18 a) Force b) Horizontal velocity and c) Spin, throughout an impact at the centre of a freely suspended racket with an inbound velocity of 28 m·s^{-1}, angle of 23° and with 200 rad·s^{-1} of backspin (*70 GPa / 253 Hz*).

5.4.5. Discussion of oblique impacts

In this investigation, racket models with natural frequencies of 96 and 253 Hz were analysed against experimental data, for oblique spinning impacts. As with the perpendicular impacts, there was a large amount of scatter in the experimental data. This was due to slight variations in the inbound properties of the ball and the impact location on the string-bed. The FE models were both in very good agreement with the experimental data, in terms of the rebound velocity of the ball. The models were also in relatively good agreement with the experimental data for rebound angle and spin; although, they did slightly under-predict the rebound angle of the ball for the entire range of inbound backspins. The models also under-predicted the rebound spin of the ball for inbound backspins greater than approximately 200 rad·s^{-1}. However, it was difficult to precisely determine the accuracy of the FE model due to the uncertainty in experimentally measuring both inbound and rebound spin (*~20 rad·s^{-1}*). The stiffness of the racket frame had very little influence on the rebound characteristics of the ball. The difference between the two models was much lower than the scatter in the experimental data. This agreed with the results obtained for perpendicular impacts close to the GSC. The GSC corresponds to a node point of the racket and hence has very low vibrations. It is likely that racket stiffness will have a greater influence on the rebound characteristics of the ball for impacts away from the GSC, particularly in the throat region, as found with the perpendicular impacts. Currently the material model for the racket is MAT_ELASTIC. Changing the material model to

MAT_ORTHOTROPIC_ELASTIC may provide a better representation of a carbon fibre composite tennis racket.

The FE model's under-prediction of rebound angle is not due to the racket being of an incorrect structural stiffness. This is known because a wide range of values of racket stiffness had no notable effect on the rebound characteristics of the ball. The under-prediction of rebound angle is also unlikely to be due to errors in the mass and mass distribution of the racket, as these were set to correspond to the ITF *Carbon Fibre* racket, which was used in the laboratory experiment. However, the model could be improved by splitting the racket geometry into more parts to allow further control over its mass distribution. Therefore, the under-prediction of rebound angle could more likely be due to errors in the structural stiffness of the string-bed. Goodwill and Haake (2004b) found string tension to have no effect on rebound velocity or spin, for an oblique impact with no inbound spin on a freely suspended racket (Section 2.4.5, page 31). However, in Goodwill and Haake's investigation the rebound angle of the balls was approximately 5° larger for the rackets strung at 70 lbs, in comparison to those strung at 40 lbs. This indicates that the FE models under-prediction of rebound angle may have been because the structural stiffness of the string-bed was lower than that of the racket in the experiment. The model is predicted to correspond to that of a racket strung at around 40 lbs, as opposed to 65 lbs in the experiment. Further testing is required to quantify this hypothesis.

The results indicate that the ball was over-spinning at around the mid-point of the impact. This was in agreement with the results obtained for the head-clamped racket model. It would have been very difficult to come to these findings using a conventional laboratory based experiment. However, it is difficult to rely on these results whilst there is still uncertainty in the structural stiffness of the string-bed.

5.4.6.   Summary

An FE model of freely suspended tennis racket was validated against experimental data for both perpendicular and oblique impacts. Two FE models were validated with Young's modulus values for the racket of 10 and 70 GPa (96 and 253 Hz). The reason for this was to determine the effect of racket stiffness on the rebound characteristics of the ball. When simulating

perpendicular impacts, the FE model with the Young's modulus of 10 GPa had the best agreement with the experimental data, and this is a similar stiffness to the ITF *Carbon Fibre* racket used in the laboratory experiment. The results from the FE model showed that the stiffness of the racket had no notable effect on the rebound characteristics of the ball for oblique impacts at the GSC. This is predicted to be because the GSC corresponds to a node point of the racket. There was a large amount of scatter in the experimental data, which was concluded to be due to; 1) uncertainty in measurement and 2) deviation in the inbound properties of the ball and impact location on the string-bed. The FE model was in relatively good agreement with the experimental data for both perpendicular and oblique impacts.

5.5. Chapter summary

An FE model of an impact between a tennis ball and freely suspended racket was constructed in Ansys/LS-DYNA 10.0 and validated against experimental data. A MAT_ELASTIC material model was used to simulate the racket frame. The model was validated against laboratory based experimental data for perpendicular and oblique impacts. There was a large amount of scatter in the experimental data due to slight variations in the inbound characteristics of the ball and the impact location on the string-bed. Two values of Young's modulus were used for the racket when validating the model; 10 and 70 GPa. The model with the value of 10 GPa was in better agreement with the experimental data when simulating perpendicular impacts. There was no notable difference in the results obtained from the two FE models when simulating oblique spinning impacts at the GSC. For the oblique impacts, the model was in very good agreement with the experimental data for rebound velocity and in relatively good agreement for rebound angle and spin. The next stage of the project is to analyse the model against data obtained from match play. The model will also be used to analyze the effect of racket parameters such as structural stiffness and mass, for different impact locations on the string-bed.

The main outcomes of this chapter were;

1. An FE model of a freely suspended tennis racket was constructed in Ansys/LS-DYNA 10.0.

157

2. The FE model was validated against experimental data for perpendicular impacts at four different locations on the string-bed.

3. The FE model was validated against experimental data for oblique spinning impacts at the centre of the string-bed.

5.6. Practical applications

For perpendicular impacts away from the GSC, the rebound velocity of the ball increases with racket stiffness. Perpendicular impacts are considered to be a good representation of a serve. The tip of the racket has the highest velocity during a serve and hence is where players aim to impact the ball. The rebound velocity of the ball also decreases as the impact location moves away from the long axis of the racket. Therefore, a player should do the following to achieve the highest rebound velocity for the ball when performing a serve;

1. Use a racket with a high structural stiffness

2. Impact the ball on the long axis of the racket

For oblique impacts at the centre of the string-bed, the rebound characteristics of the ball are not affected by the stiffness of the racket. Oblique spinning impacts are considered to be representative of a topspin forehand. Players typically impact topspin forehands in a region close to the centre of the string-bed. Therefore, it is predicted that the stiffness of the racket will have only a very small effect on the rebound velocity of the ball when performing a typical topspin forehand.

For oblique impacts rebound topspin decreases with increasing inbound backspin (*racket frame of reference*). Therefore, it will be easier for a player to perform a forehand shot with high topspin, when the ball rebounds from the court with little or no topspin (*court frame of reference*).

158

6. Parametric modelling program

6.1. Introduction

For an FE model of a tennis racket to function as an effective design tool, it must be possible to easily adjust the input parameters. The adjustment of these parameters should be both straightforward and efficient, thus enabling design engineers to concentrate on the meaning of the results, rather than the intricacies of the FE model. A parametric modelling program was produced using Visual Basic 2005. This program serves as a Graphical User Interface (GUI), which can be used to adjust parameters in the FE model and run simulations. The objective of this chapter is to describe this parametric modelling program.

6.2. Description of the parametric modelling program

A program was created, using Visual Basic 2005, to enable properties of the FE models, such as the inbound trajectory of the ball, to be easily and quickly adjusted. The program is called the Tennis Design Tool (TDT). The TDT enables users who are not familiar with Ansys/LS-DYNA 10.0, to run a variety of simulations, including all the models detailed in this thesis. The TDT is structured on a template system; the templates are the Ansys/LS-DYNA 10.0 .k files *(text file containing keyword commands)* and there is a separate template for each of the models detailed in this thesis. The user selects the corresponding template for the type of simulation they require, the TDT thus edits selected values in the template and writes a new .k file to a specified location. The TDT consists of four sections representing individual models of the ball (Rigid Surface), string-bed, head-clamped racket (Clamped Racket) and freely-suspended racket (Racket). Figure 6.1a shows the start up screen for the TDT and the initial step would be to select the type of impact from the drop down list (Figure 6.1b).

159

Figure 6.1 a) Start up screen for the parametric modelling program and b) The four impact types available in the parametric modelling program.

The four impact types will now be explained in detail starting with the 'Rigid Surface' (Figure 6.1b) or 'ball to rigid surface' impact. Figure 6.2 shows the view when Rigid Surface is selected as the impact type. The ball parameters available for editing are the inbound velocity, angle and spin (Figure 6.2a). The simulation controls include the simulation time and dynamic relaxation tolerance, as well as the template and output locations. Once the 'Write file' button has been selected, a .k file with the input parameters will be created in the specified location and the calculated x and y velocities of the ball will be displayed. Once the .k file has been created there are two options; run the simulation, or add it to the scheduler list. The scheduler list can be copied into a batch file, enabling a batch of simulations to be sent to the solver. Following this, there is the option of using the last created file as a template, selecting a new one or keeping the original *(as per the default)*. In addition, there is the option of creating multiple files with different spin rates (Figure 6.2b). Deselecting an adjust box results in the corresponding parameter remaining unchanged from how it appears in the template (Figure 6.2a).

Figure 6.2 a) Ball parameters in the parametric modelling program and b) The display in the parametric modelling program when creating multiple files.

Figure 6.3a shows the view when Stringbed is selected as the impact type. There are the additional options of changing the ball's impact location and the string-bed parameters. The TDT alters the impact location of the ball by editing the coordinates of the nodes, which correspond to the string-bed. By default, the location of the string-bed is adjusted with the inbound angle of the ball to ensure the impact initiates at the Geometric String-bed Centre (GSC). The impact location can be moved from the GSC by inputting x and z offset distances (Figure 6.3a and b). If the location of the string-bed is moved and the template is updated to the last created file, the option to change the impact location will again be removed. This is to ensure that the string-bed is always in the same position before being moved. The adjustable string-bed parameters are the string tension, string-to-string friction and Young's modulus. The Young's modulus is calculated from the strings diameter and dynamic stiffness, using the *Hammer* method (Section 4.2, page 91). There is also the option of selecting preset strings from a drop-down list. When Clamped Racket is selected as the impact type the same options are available as for the Stringbed; however, the distance of the ball from the string-bed is automatically updated to ensure the impact initiates at 0.0015 s (Section 4.5, page 111).

161

(a)
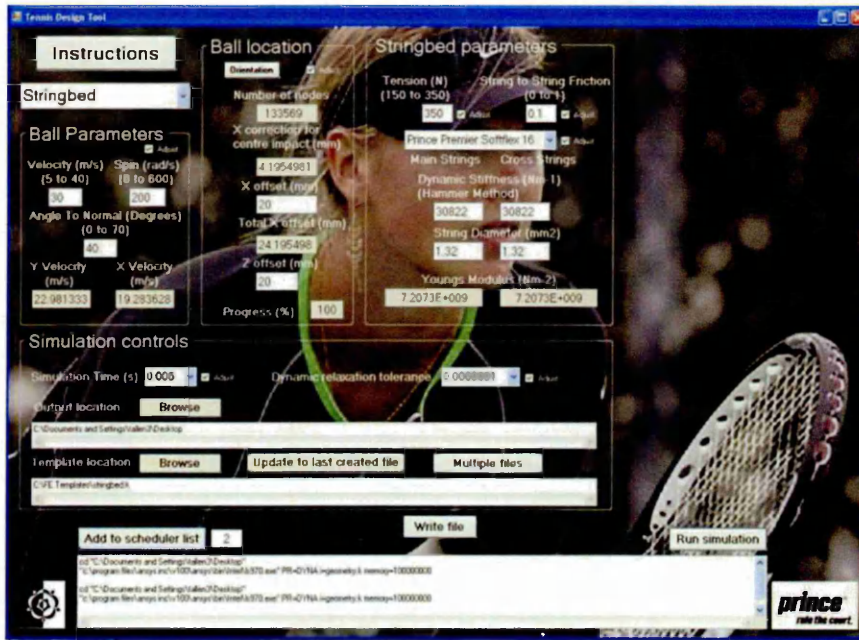
(b)
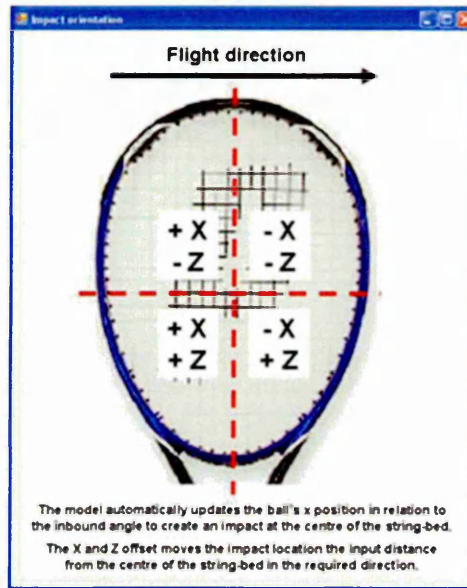
Figure 6.3 a) String-bed parameters in the parametric modelling program and b) Impact orientation in the parametric modelling program.

Figure 6.4 shows the view when Racket is selected as the impact type. The adjustable racket parameters are the density and Young's modulus of the head, throat and handle. When the .k file is created, the racket mass, balance point, twistweight and swingweight are displayed. The balance point is displayed as the distance from the butt in meters and the percentage of the racket length (Figure 6.4).
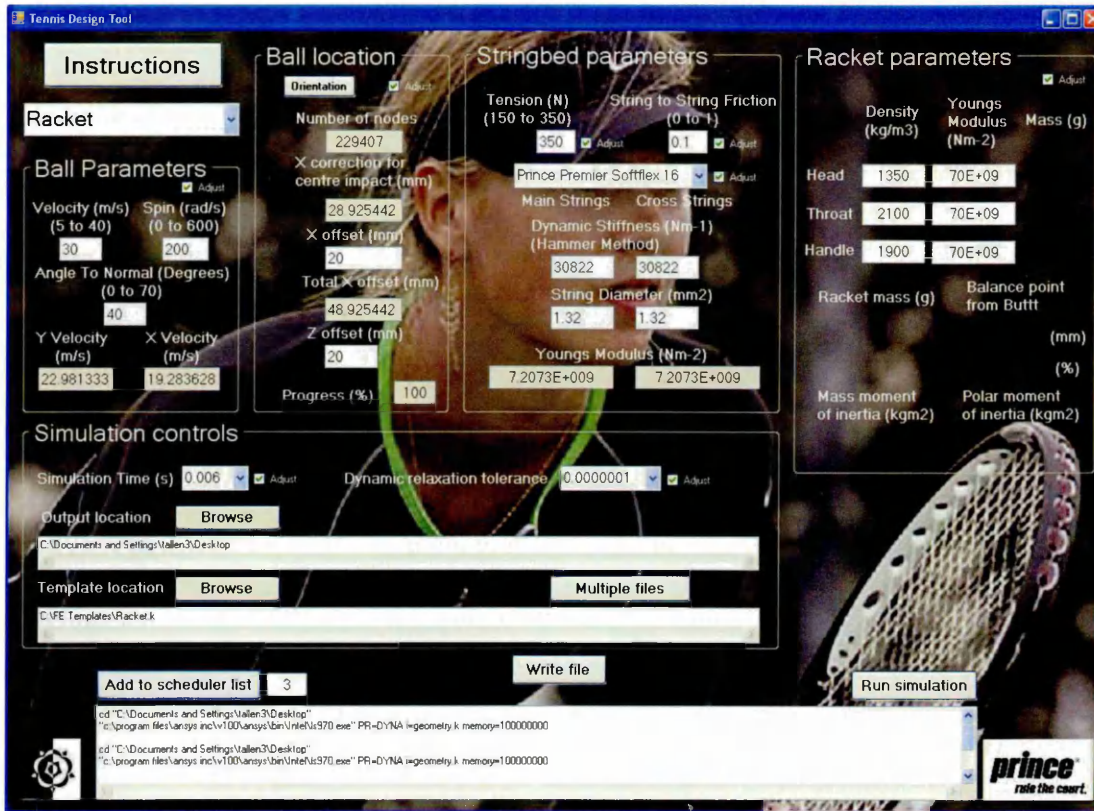
Figure 6.4 Racket parameters in the parametric modelling program.

A separate program was produced to decrease the total time required to analyse the results obtained from the FE simulations (Figure 6.5). This program can be used to obtain contact times, maximum forces and force plots for all impact types detailed within this thesis. In addition, maximum ball deformation and ball deformation plots can be obtained for perpendicular, non-spinning impacts.
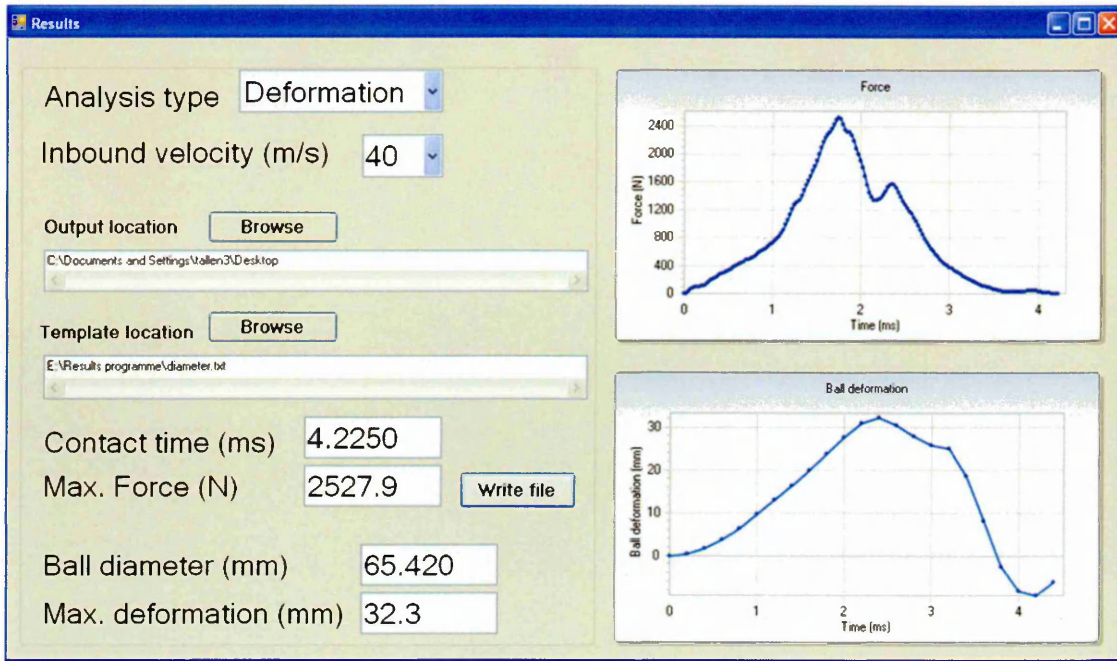
Figure 6.5 Results programme, showing results for a 40 m·s⁻¹ perpendicular impact at the GSC of a freely-suspended racket.

A text file containing the contact force between the ball and rigid surface / string-bed can be obtained from LS-Prepost. However, the ball is not in contact with the rigid surface / string-bed for the entirety of the simulation. Figure 6.6a shows a plot of contact force, for a ball impacting with a freely suspended racket, which was obtained directly from a text file created using LS-Prepost. Figure 6.6b shows a force plot of the same impact, where the text file has been edited using the program. The superfluous contact force has been removed i.e., when it equals to zero before and after impact, and the time data has been changed from seconds to milliseconds. The start of contact is defined as the last instance of when the force is equal to zero, prior to any nonzero force being recorded. The opposite is the case for the end of contact. The updated text file containing the results will be created in the specified location using the 'Write file' button. The modified force-time plot is displayed along with the contact time and maximum force (Figure 6.5).
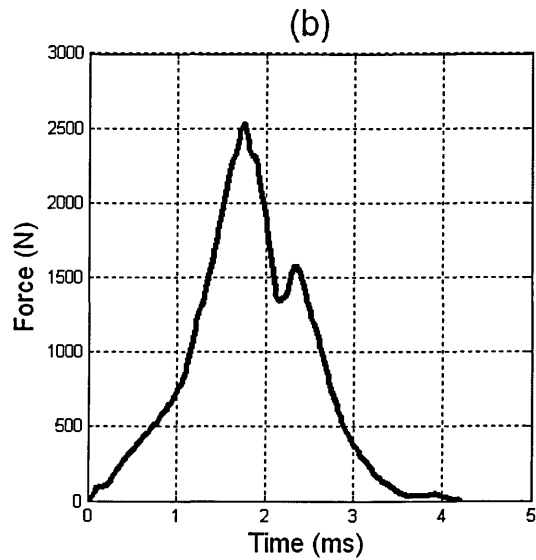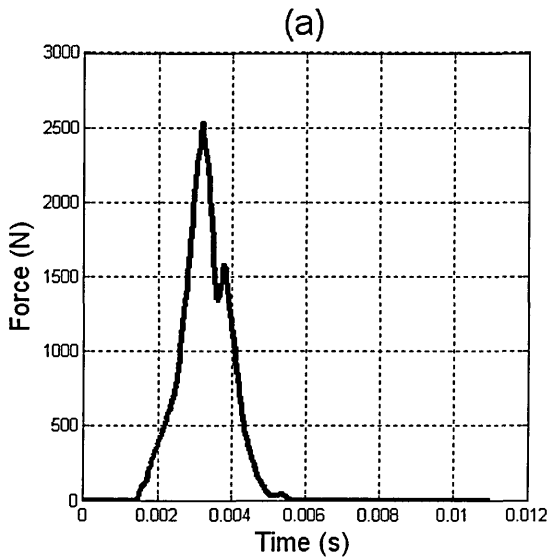
Figure 6.6 Force plot for a 40 m·s⁻¹ perpendicular impact at the GSC of a freely suspended racket a) Original force plot from ANSYS/LS-Dyna and b) Force plot updated in the results program.

The deformation of the ball is obtained by measuring its changing vertical diameter (Figure 6.7a) using LS-Prepost *(perpendicular impact only)*. The definition for the deformation of the ball is shown in Figure 3.13b on page 71. The program edits the text file, corresponding to the plot shown in Figure 6.7a, to obtain the deformation of the ball throughout the impact (Figure 6.7b). The deformation of the ball is obtained automatically by subtracting its diameter at each time step from its original diameter. The start of contact is defined as the last instance of when the current diameter is greater than or equal to the original. The contact time is taken from the previous analysis of the corresponding contact force data. As with the contact force data, the time is converted from seconds to milliseconds and a deformation plot is displayed along with the maximum deformation. The modified text file containing the deformation-time data for the ball will be created in the specified location.
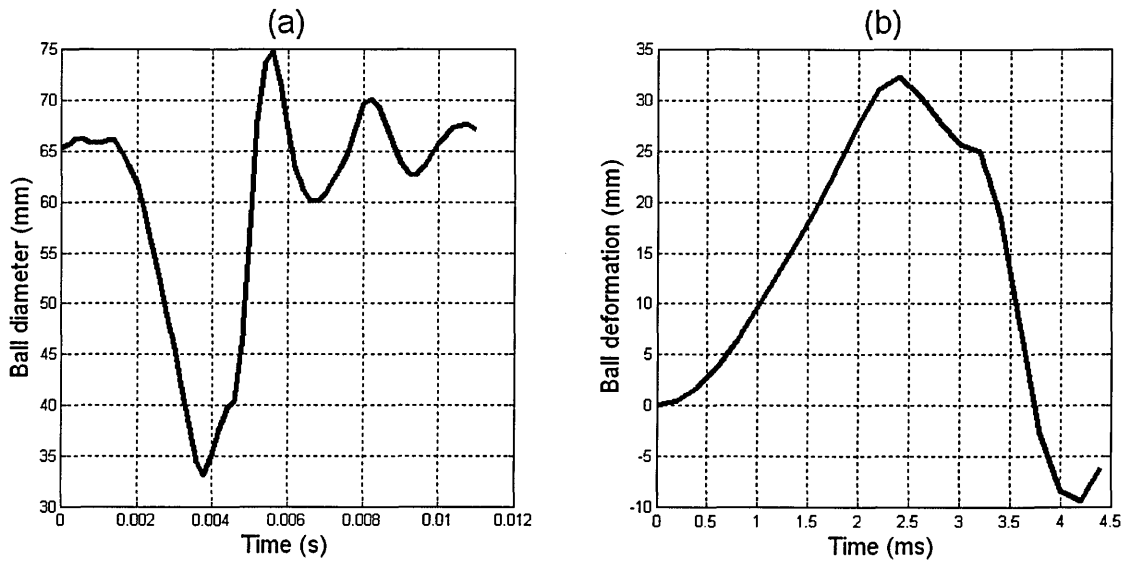
Figure 6.7 Ball diameter for a 40 m·s⁻¹ perpendicular impact at the GSC of a freely suspended racket a) Ball diameter from ANSYS/LS-Dyna and b) Ball deformation calculated in the results program.

6.3. Discussion

The first program described in this chapter, the TDT , has proven efficient for setting up large numbers of different simulations. It has the ability to easily create a model with a specific ball impact location on a string-bed, with the required inbound properties. The alternative, of using the Ansys/LS-DYNA 10.0 interface to change all the required parameters and inherently having to manually undertake the calculations, would be very inefficient. The separate results program has also proven effective for obtaining contact times and forces, as well as ball deformation properties. A robust design tool could potentially be produced, by combing the two programs into a single interface, with the additional ability to automatically read-in and analyse the results. A design engineer would be able to send a batch of simulations to the solver and return to the completed simulations, with the results displayed in a standard format.

The material properties of a large number of strings could be added to the program, allowing their performance with different rackets to be assessed. Using a drop-down list, similar to that of the strings, material properties of various composite lay-ups could also be added to the program. In the current version this would allow different composite lay-ups to be assigned to the head, throat and handle of the racket. However, the geometry could be separated into

a larger number of individual parts, enabling the composite lay-ups to be more realistic. The design engineer could then analyse the effect of adjusting the material properties of the racket.

6.4. Chapter summary

A program has been produced to allow certain parameters of the existing FE models to be easily adjusted. This is more efficient and less prone to human error than using the Ansys/LS-DYNA 10.0 interface. The program has been designed to be developed alongside the FE model. In addition, a separate program has been produced to aid in the analysis of the results obtained from the FE simulations. Combing the two programs into a single interface, with the additional ability to automatically read-in and analyse the results, could potentially result in a very effective design tool.

6.5. Practical applications

A program has been produced which can be used to asses the effect of various racket parameters, such as mass and structural stiffness, on a wide range of different impacts. This has vast practical applications for manufacturers to assess the effect of changing different components of the racket.

7. Comparison of the FE model with simulated play

7.1. Introduction

The preceding chapters of this thesis have been concerned with building an FE model of a freely suspended tennis racket. The model has been extensively validated against laboratory based experimental data. The next logical step is to compare the results obtained using the FE model with tennis ball to racket impact data for actual tennis shots. In this chapter, the ball to racket impact data collected by Choppin *et al.* (2007a & b) at the 2006 Wimbledon Qualifying Tournament will be used. The main objective of this chapter is;

- To compare the FE model of a freely suspended racket with impact data from the 2006 Wimbledon Qualifying Tournament (Choppin *et al.* 2007a & b).

7.2. Method

In this section the FE model of a freely suspended tennis racket will be compared with impact data obtained from players practicing at the 2006 Wimbledon Qualifying Tournament (Choppin *et al.,* 2007a & b).

7.2.1.   *Analysis of ball to racket impact data obtained from testing elite players*

Choppin *et al.* (2007a, 2007b and 2008) undertook testing on nineteen elite players at the 2006 Wimbledon Qualifying Tournament, as detailed in the literature review (Section 2.5, page 34). The raw data from the player testing was obtained from Simon Choppin, with his permission to use in this investigation. The results obtained for each tennis shot were;

1. The inbound and rebound velocity and spin of the ball;

2. The inbound velocity of the racket;

3. The resultant inbound angle *(relative to racket normal)* between the ball and racket;

4. The impact location on the string-bed.

168

5. The length, width, mass and balance point of the racket.

Haake *et al.* (2007) demonstrated that the mass, balance point and structural stiffness of a tennis racket all influence serve velocity. Therefore, ideally, all the different players' rackets should be modelled and compared against the experimental data. For practicality, a threshold for inclusion was used to reduce the required number of simulations. The threshold relative to the ITF *Carbon Fibre* racket was within 0.5% for length, 3.5% for width, 2.5% for balance point and 3% for mass. Cross (2001b) stated that the swingweight of a tennis racket is primarily determined by its length, mass and balance point. The racket used in the FE model and the ITF *Carbon Fibre* racket used to experimentally validate the model, were both compared against each of the 19 player's rackets (Figure 7.1). Rackets 4, 7, 9, 10, 18 and 19 were considered to have similar properties to the racket in the FE model. Therefore, the results from the players who used these rackets were selected for analysis against the FE model. The results from the other players were discarded.

(a)

(b)

(c)

(d)
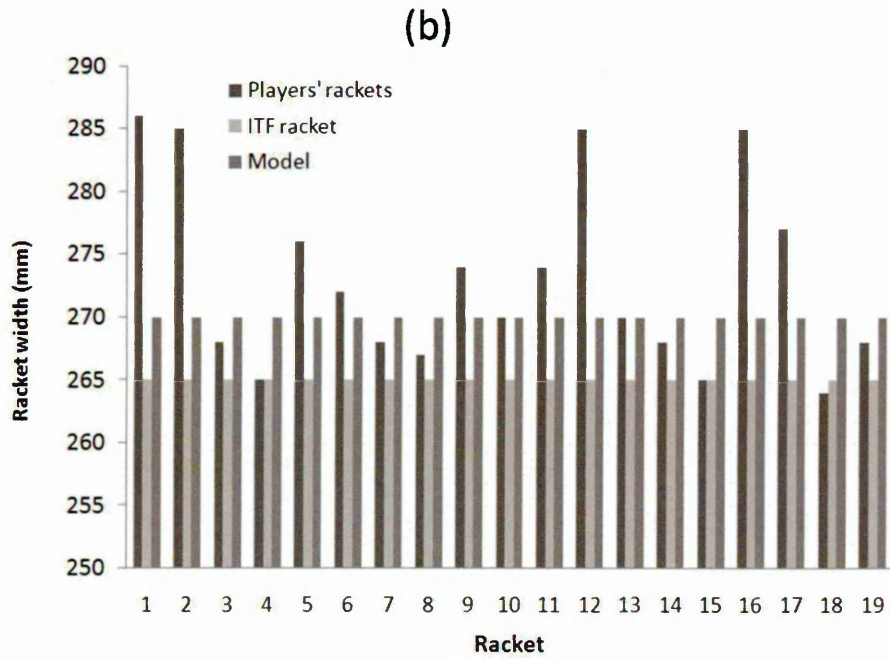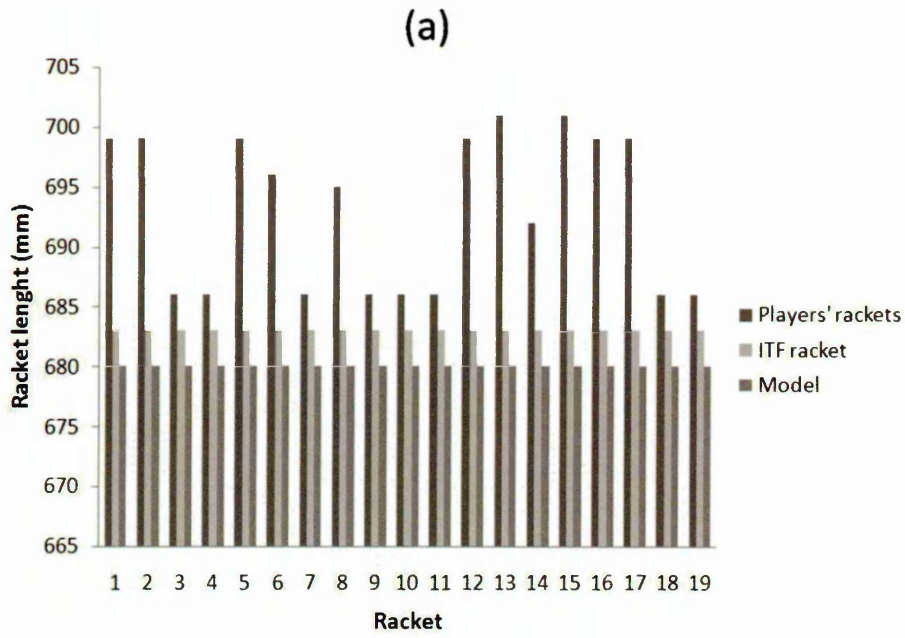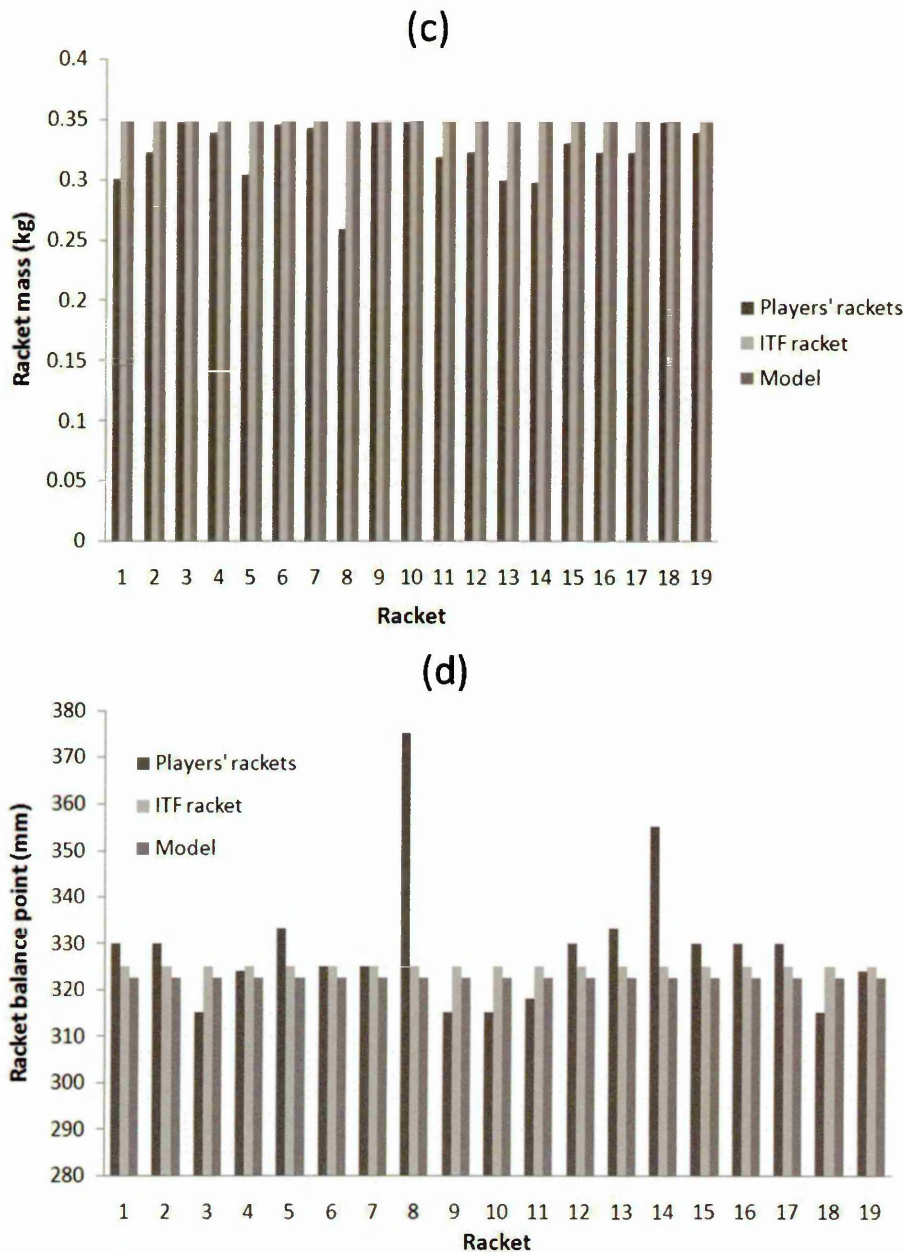
Figure 7.1 Comparison of the racket in the FE model and the ITF *Carbon Fibre* racket with each of the 19 players' rackets, a) length, b) width, c) mass and d) balance point.

Figure 7.2 shows a comparison of the six selected players' rackets, the ITF *Carbon Fibre* racket (*experimental*) and the racket in the FE model. All of the players were right handed except the player using racket 9. Therefore, to ensure consistency these results were discarded. There are small differences between the properties of the selected players' rackets and the racket in the model. However, these differences are unlikely to have a significant effect on the rebound characteristics of the ball.

171

(a)

(b)

(c)

(d)
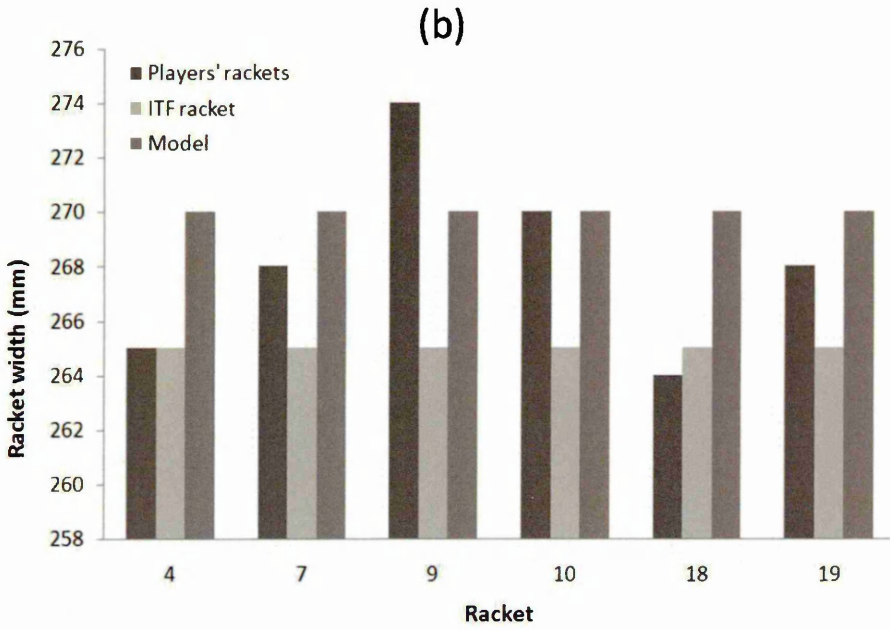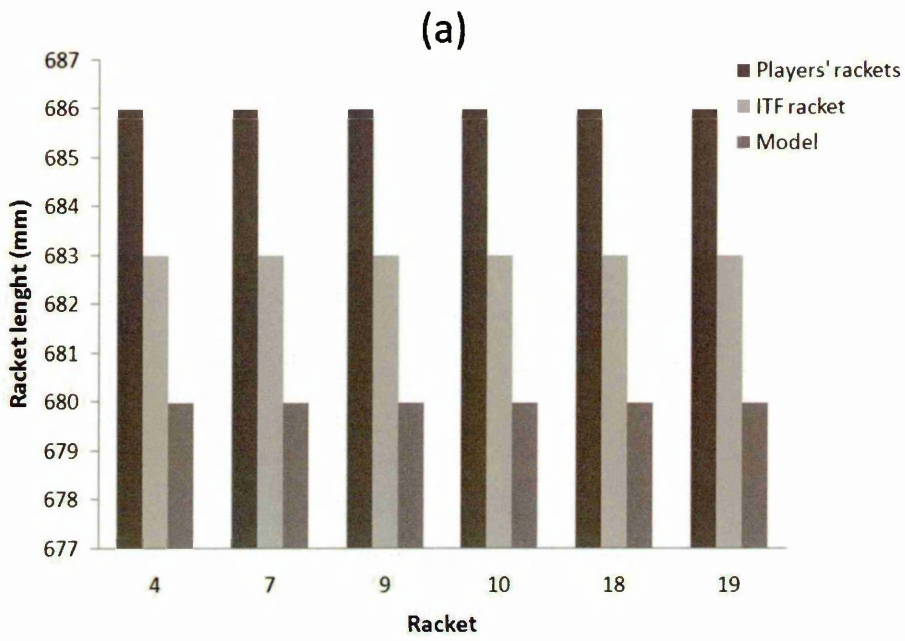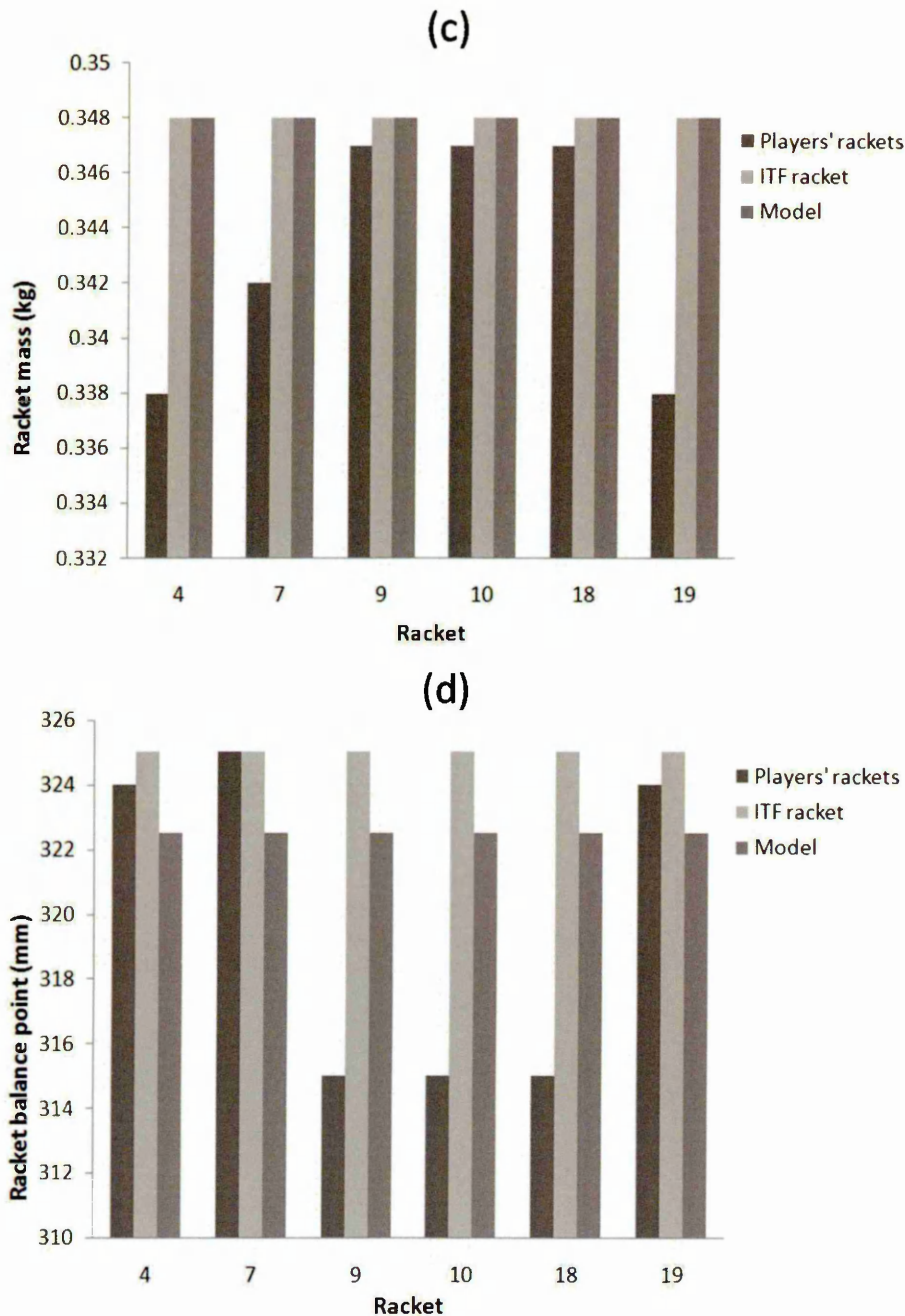
Figure 7.2 Comparison of the racket in the FE model and the ITF test racket with a selection of the players' rackets, a) length, b) width, c) mass and d) balance point.

It is doubtful that the players will have all used a racket with the same structural stiffness. However, the structural stiffness of a tennis racket does not have a significant influence on the rebound characteristics of the ball, for impacts close to the geometric string-bed centre (GSC) (Figure 5.15, Figure 5.16 & Figure 5.17, page 152-154). Therefore, 18 shots with impact positions close to the GSC were selected from the player testing data for analysis against the FE

173

model (Figure 7.3a). The ball in the freely suspended racket model travelled approximately 25 mm horizontally whilst in contact with the string-bed when the inbound velocity was 28 m·s^{-1}, the angle was 23° and the backspin was 400 rad·s^{-1}. This was in agreement with the amount of horizontal displacement of the ball measured by Goodwill and Haake (2004b), for an oblique impact on a freely suspended tennis racket. Choppin *et al.* (2007a) obtained the impact position on the string-bed when the centre of the ball was equal to a plane through markers on the racket frame. In this investigation the position measured by Choppin *et al.* was assumed to be the mid-point of the impact. Therefore, the impacts were all offset horizontally by an additional 12.5 mm, to account for the horizontal displacement of the ball while it remains in contact with the string-bed (Figure 7.3b).
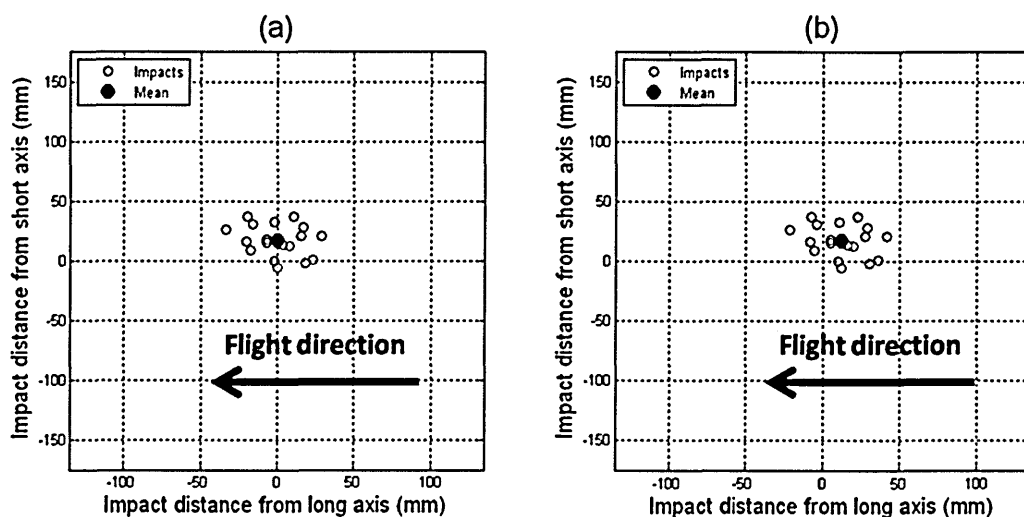
Figure 7.3 Impact positions a) player testing and b) FE simulations.

Table 7.1 shows the pre-impact conditions obtained from the selected ball to racket impact data. The resultant pre-impact velocity between the ball and racket was calculated in 3D. The spin axis of the ball was assumed to be parallel to the long axis of the racket (*top/back spin relative to racket*). The resultant inbound angle between the ball and racket was calculated in 2D, as done by Choppin *et al.* (2007a). However, the inaccuracy as a result of using the 2D angle was expected to be small, as the root mean squared error (RMSE) between the resultant 2D and 3D resultant pre-impact velocities was only 1.53 m·s^{-1}.

Eighteen FE simulations were undertaken, using the freely suspended racket model, with inbound ball velocities, angles, spin rates and impact positions identical to the player testing data shown in Table 7.1. In the FE simulations the adjusted x-offset from the long axis was used (Figure 7.3b). The model was validated against the ball to racket impact data in the racket's frame of reference. This meant that the vertical velocity of the ball was perpendicular to the string-bed, whilst the horizontal velocity was parallel to the string-bed. The comparison was undertaken in the racket's frame of reference to allow an initially stationary racket to be used in the simulations. Cross and Lindsey (2005) provide a detailed description of how to convert the Newtonian frame of reference from the court to the racket.

Table 7.1 Pre-impact conditions from the player testing results (+ x offset = towards inbound path of the ball) (+ y offset = towards tip) (Player data from Choppin *et al.* (2007a & b))

Shot	Racket tilt (°)	Inbound spin (rad·s⁻¹)	Resultant inbound velocity (m·s⁻¹)	Inbound angle (°)	x-offset from long axis (mm)	Adjusted x-offset from long axis (mm)	y-offset from short axis (mm)
1	-0.5	273.3	28.9	18.1	-1.9	10.6	32.9
2	0.0	120.4	30.1	17.8	-16.1	-3.6	31.2
3	0.4	392.7	34.1	16.0	-17.4	-4.9	9.1
4	3.2	31.4	37.0	19.4	-7.0	5.5	15.3
5	8.4	369.7	39.1	20.5	-20.6	-8.1	16.2
6	8.1	392.7	38.6	24.3	10.2	22.7	37.6
7	5.2	90.1	36.2	24.4	18.0	30.5	-2.1
8	3.1	314.2	36.7	23.3	-0.1	12.5	-5.8
9	7.1	314.2	34.0	24.8	-34.0	-21.5	26.4
10	2.4	299.5	35.6	25.5	-19.6	-7.1	36.9
11	0.6	136.1	37.4	23.9	28.9	41.4	21.2
12	5.7	285.9	36.9	22.6	-2.4	10.2	0.5
13	8.7	369.7	39.0	23.5	16.8	29.3	28.2
14	4.9	152.9	37.2	20.9	-7.2	5.3	18.3
15	7.7	314.2	29.7	19.8	23.4	35.9	0.8
16	1.0	299.5	30.9	21.3	3.8	16.3	13.9
17	2.3	299.5	32.4	20.3	7.6	20.1	12.7
18	5.0	330.9	34.0	14.3	15.1	27.6	20.6
Average	*4.1*	*265.3*	*34.9*	*21.1*	*-0.1*	*12.4*	*17.4*
SD	*3.1*	*109.9*	*3.3*	*3.2*	*17.2*	*17.2*	*13.4*

The Young's modulus of the racket in all of the FE simulations was 20 GPa. This Young's modulus was used as it resulted in the racket having a natural

175

frequency of 135 Hz (Figure 5.3, page 134), which is effectively the same as the ITF *Carbon Fibre* racket. However, the structural stiffness of the racket frame was not expected to have a large influence on the rebound trajectory of the ball, as all of the impacts were close to the GSC (*approx. node*).

7.3. Results

Figure 7.4a shows that the FE model was in relatively good agreement with the player testing data for horizontal rebound velocity. The RMSE between the model and player testing data was 1.9 m·s^{-1}. Figure 7.4b shows that the model was in better agreement with the player testing data for vertical rebound velocity. The RMSE between the model and player testing data was 1.0 m·s^{-1}. As both the horizontal and vertical rebound velocities were in good agreement with the player testing data, the model was also in good agreement with the player testing data in terms of the resultant rebound velocity (Figure 7.4c). The RMSE for resultant rebound velocity was 0.9 m·s^{-1}.
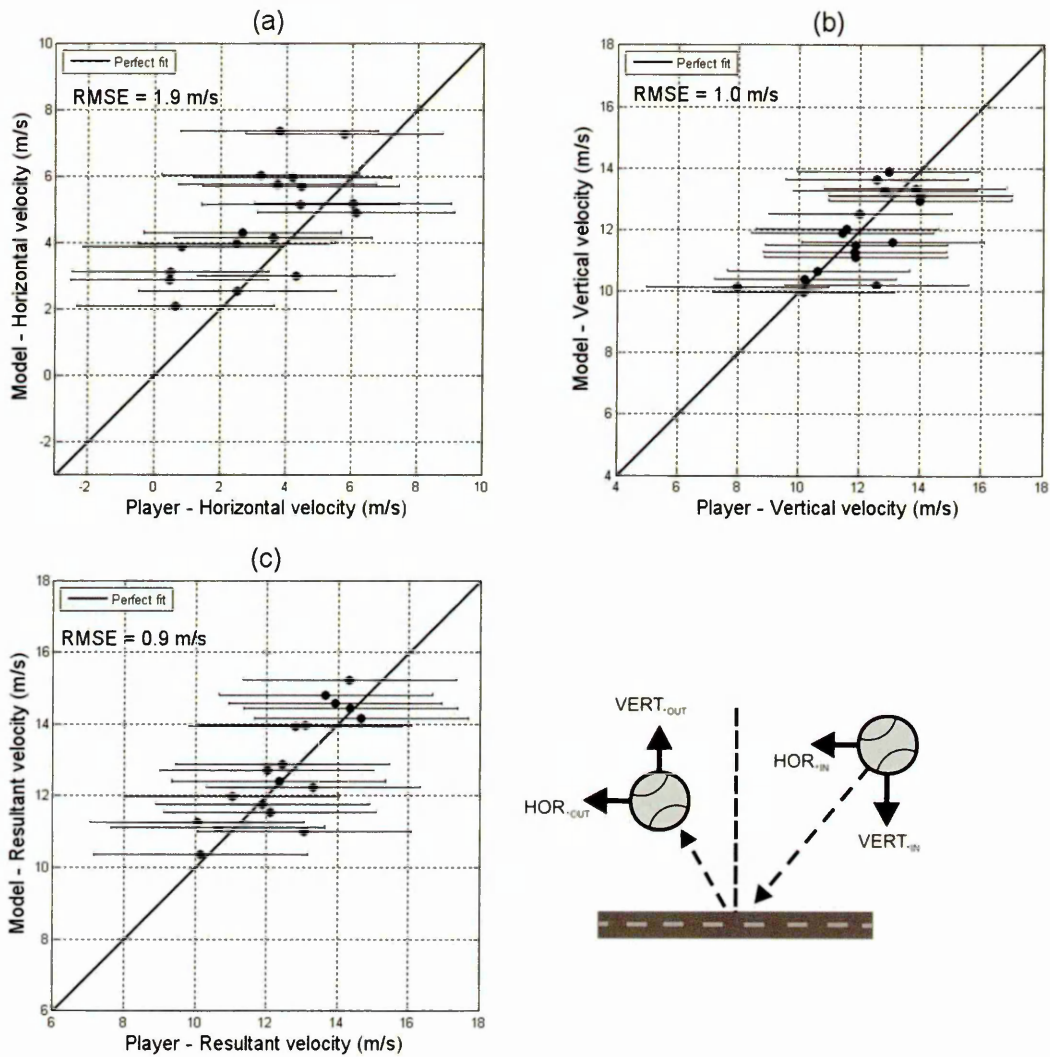
Figure 7.4 Comparison of rebound velocity from the player testing and FE model a) Horizontal, b) Vertical (*perpendicular to string-bed*) and c) Resultant (Player data from Choppin *et al.* (2007a & b)).

Figure 7.5 shows that the FE model was in relatively good agreement with the player testing data for rebound angle, although the RMSE between the two was relatively large at 9.1°. This discrepancy, in the angles, may be as a result of slight errors in both the horizontal and vertical rebound velocity of the ball (Figure 7.4a & b) becoming exaggerated in the rebound angle calculation.
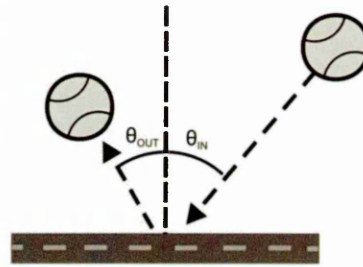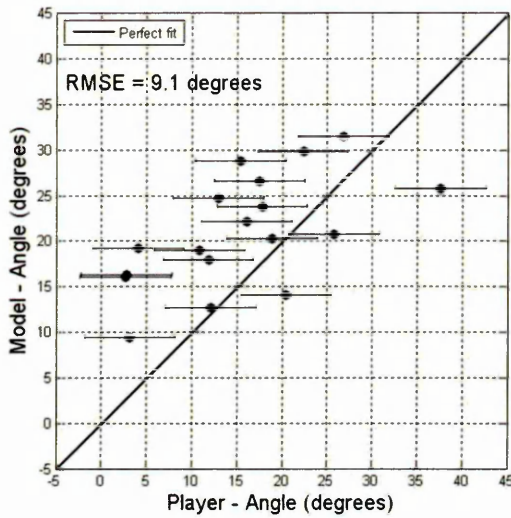
Figure 7.5 Comparison of rebound angle from the player testing and FE model (*relative to racket normal*) (Choppin *et al.,* 2007a & b).

Figure 7.6 shows that the FE model consistently under-estimated the rebound spin of the ball, in comparison to the player testing data. The RMSE between the two sets of data was 61.3 rad·s^{-1}. However, this is approximately equal to the uncertainty in the player testing data.
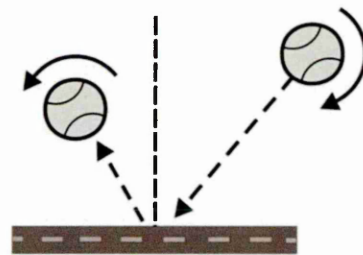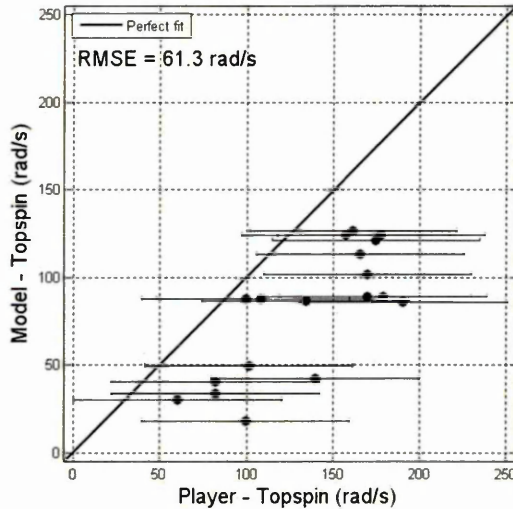
Figure 7.6 Comparison of rebound topspin from the player testing and FE model (Player data from Choppin *et al.,* 2007a & b).

7.4. Discussion of player testing

An FE model of a freely suspended tennis racket has been analysed against experimental data taken from elite players, obtained by Choppin *et al.* (2007a &

b). The model was in very good agreement with the player testing data for rebound velocity and in relatively good agreement for rebound angle. The model consistently under-predicted the rebound spin of the ball, in comparison to the player testing data.

The model was in very good agreement with laboratory based experimental data, for the rebound velocity of the ball (Figure 5.15, page 152). Therefore, the model was expected to be in good agreement with the player testing data in terms of rebound velocity. The main racket parameters which influence the rebound velocity of the ball are mass, mass distribution, structural stiffness (Haake *et al.*, 2007a) and string-bed stiffness (Haake *et al.*, 2003; Goodwill and Haake, 2004b; Cross and Lindsey, 2005; Brody *et al.*, 2002). Only data from players who used rackets with a similar length, width, mass and balance point to the racket simulated in the FE model were selected for analysis. Therefore, the main variables between the FE model and player testing data, were the structural stiffness of the racket and the string-bed. Only impacts close to the GSC were selected for analysis, to limit the influence of the structural stiffness of the racket on the rebound characteristics of the ball. Therefore, the marginal discrepancy between the model and player testing data is likely to be due to differences in string-bed stiffness.

The FE model slightly under-predicted the rebound angle of the ball, in comparison to laboratory obtained experimental data (Figure 5.16, page 153). Therefore, the model was also expected to under-predict the player testing data, in terms of the rebound angle of the ball. The slight discrepancy between the model and player testing data was predicted to be partly due to differences in both string-bed stiffness and ball to string friction. However, the discrepancy could also have been due to differences in the twistweight of the rackets or because the players were applying a torque to the handle. Applying a resistive torque to the handle, in the range of 7-15 Nm, has been found to reduce the rebound angle of the ball by approximately 2°, for perpendicular impacts at 30 $m \cdot s^{-1}$ (Choppin, 2008). Applying a resistive torque to the handle of the racket in the FE model may reduce the rebound angle of the ball and hence increase agreement with the player testing data.

The FE model consistently under-predicted the rebound spin of the ball in comparison to the player testing data. However, the model was in relatively good agreement with experimental data obtained by projecting balls onto a freely suspended tennis racket (Figure 5.17, page 154). This also indicates that the player's grip may be influencing the impact. The players could have been applying a torque to the handle, causing the ball to rebound with a higher spin rate than an identical impact on a freely suspended racket. It is likely that a racket with a resistive torque applied to the handle would produce higher rebound spin than a freely suspended racket. This has implications for experimentalists using the freely suspended racket as an approximation of a hand-held racket.

Discrepancies between the FE model and player testing data could be due to the impact location on the string-bed. In the FE simulations the impacts were offset horizontally by an additional 12.5 mm to account for the horizontal displacement of the ball, whilst it remains in contact with the string-bed. This was based on the assumption that the location obtained from the player testing data corresponded to the mid-point of the impact. In the next section the FE model will be used to determine the effect of changing the impact location on the string-bed, for oblique spinning impacts.

The discrepancies between the two sets of data could also be due to the uncertainty in measured velocities, spin rates and impact positions, during the player testing. The inbound velocities and spin rates and the impact locations on the string-bed were based on the values obtained from the player testing data. Therefore, errors in the inbound conditions could have resulted in incorrect ball rebound properties.

7.5. Summary of player testing analysis

The model was in relatively good agreement with elite player testing data obtained in 3D, in terms of the rebound characteristics of the ball. The results indicate that the model can predict rebound velocities to within 1 m·s^{-1}, angles to within 10° and spin rates to within 65 rad·s^{-1}. These values are for an impact close to the GSC of a racket, which is similar in size and mass to the one in the FE model. Discrepancies between the model and player testing data are

predicted to be due to differences in the structural stiffness of the string-bed, torque applied to the handle of the racket and uncertainty in the player testing data. Validating the model against data obtained from players using a ball (*Prince Tour*), strings (*Prince Premier Softflex 16*) and racket (*ITF Carbon Fibre*) identical to those in the model would provide a better indication of its accuracy. Reducing the uncertainty in the player testing data would also provide a better indication of the accuracy of the model.

7.6. Chapter summary

In this chapter an FE model of a freely suspended tennis racket was analysed against data obtained from elite players, at the 2006 Wimbledon Qualifying Tournament. The model was in very good agreement with the player testing data for the rebound velocity of the ball and in relatively good agreement for rebound angle. The discrepancy for angle was considered to be partly due to the combination of errors in the vertical and horizontal rebound velocity of the ball. The model consistently underestimated the rebound spin of the ball. This was concluded to be because the player was applying a torque to the handle of the racket, which was not accounted for by the model.

8. Applications of the model

8.1. Introduction

The FE model will be used to determine the effect of the structural stiffness, mass and balance point of a tennis racket, for an oblique spinning impact at a variety of locations on the string-bed. The results will then be analysed to determine the influence that each of the individual racket parameters may have on a typical forehand shot. Finally, the implications to tennis racket design will be discussed. The main objectives of this chapter are;

1. To determine the influence of racket stiffness, mass and balance point on a typical forehand tennis shot.

2. To determine how this would be perceived by players on the court.

3. To outline guidelines for tennis racket design.

8.2. Method

An investigation was undertaken using the freely suspended racket model to determine the effect of racket structural stiffness, mass and balance point on a forehand shot. In order to determine the overall effect of each of the racket parameters, impacts were simulated at six locations on the string-bed (Table 8.1, Figure 8.1). The FE simulations had an inbound velocity of 35 m·s^{-1}, an angle of 20° (*relative to racket normal*) and a backspin of 300 rad·s^{-1}. These inbound conditions were found to be representative of a tennis shot for an elite player, in the previous section (Table 7.1, page 175). Two sets of simulations were undertaken for each of the three racket parameters under investigation (*Stiffness, mass and balance point*). This gave six different impact locations and six different racket parameter configurations, which required 36 simulations.

182

Table 8.1 Impact locations on the string-bed used to determine the effect of different racket parameters.

Simulation	Impact distance from the long axis (mm)	Impact distance from the short axis (mm)
1	0	60
2	0	0
3	0	-60
4	60	60
5	60	0
6	60	-60
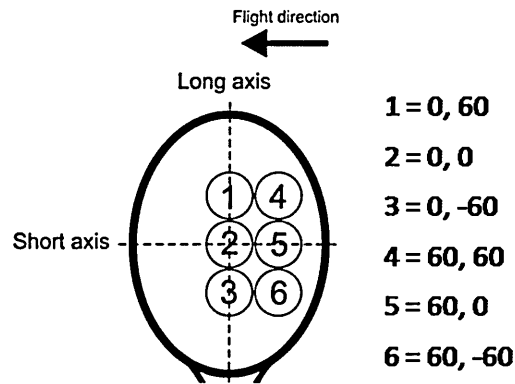
Figure 8.1 Impact locations on the string-bed used to determine the effect of different racket parameters.

The structural stiffness of the racket was adjusted by changing the Young's modulus. The first set of six simulations had an apparent Young's modulus of 10 GPa and a natural frequency of 96 Hz. The second set of simulations had an apparent Young's modulus of 70 GPa and a natural frequency of 253 Hz. Refer to Figure 5.3, on page 134, for the relationship between Young's modulus and natural frequency of the racket. The mass and balance point of the racket remained identical to the original model (Table 5.1, page 131).

Table 8.2 Two sets of FE simulations used to determine the effect of racket structural stiffness.

Simulation set	Young's Modulus (GPa)	Natural frequency (Hz)
1	10	96
2	70	253

The mass of the racket was adjusted by changing the density. The densities of the three parts were all changed by the same percentage to ensure the balance point of the racket remained constant. Haake *et al.* (2007) found the mass of 150 tennis rackets, from the 1870's to 2007, to be in a range of 0.24-0.44 kg (Figure 2.9, page 26). The mass of the racket in the FE model was increased

183

and decreased by 20% (0.07 kg) (Table 8.3). Table 8.4 shows the density and mass of the separate parts of the racket. Changing the mass of the racket also alters the natural frequency, swingweight and twistweight, as shown in Table 8.3 and Figure 8.2. Natural frequency would increase as the mass of the racket decreased (Figure 8.2a). The swingweight and twistweight of the racket would both increase with racket mass (Figure 8.2b).

Table 8.3 Two sets of FE simulations used to determine the effect of racket mass. The mass moment of inertia, the polar moment of inertia and natural frequency of the racket in the FE model are also displayed.

Simulation set	Racket mass (kg)	Mass moment of inertia (*swingweight*) (kgm²)	Polar moment of inertia (*twistweight*) (kgm²)	Natural frequency (Hz)
1	0.279	0.0406	0.0013	151
2	0.418	0.0605	0.0019	123

Table 8.4 Density and mass of the separate parts of the racket in the two FE models used to determine the effect of racket mass.

Simulation set	Handle density (kg·m⁻³)	Handle mass (kg)	Throat density (kg·m⁻³)	Throat mass (kg)	Head density (kg·m⁻³)	Head mass (kg)	Racket mass (kg)
1	1520	0.078	1680	0.072	1080	0.127	0.279
2	2280	0.118	2520	0.107	1620	0.190	0.418
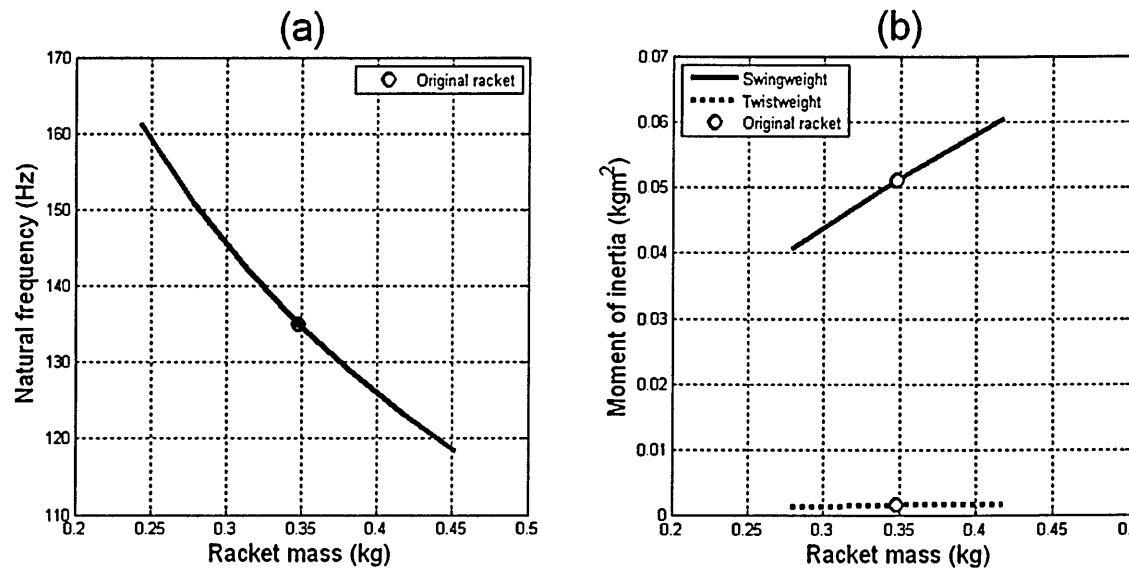
Figure 8.2 Relationship between the mass of the racket in the FE model and a) its natural frequency, b) its moment of inertia.

The balance point of the racket was adjusted by changing the density of the handle and head. Haake *et al.* (2007) found the balance point of 150 rackets,

from the 1870's to 2007, to be between 0.30 and 0.39 m from the butt of the racket. The balance point was set to 0.299 m from the butt by adding 0.02 kg to the handle and removing 0.02 kg from the head (Table 8.5). The balance point was set to 0.396 m from the butt by removing 0.06 kg from the handle and adding 0.06 kg to the head (Table 8.5). The density and mass of the handle and head of both rackets are shown in Table 8.6. Changing the balance point of the racket also alters the natural frequency, swingweight and twistweight, as shown in Table 8.5 and Figure 8.3. In relation to the racket in the original model, the natural frequency increased when the balance point was moved closer to both the butt and the tip (Figure 8.3a). The swingweight and twistweight of the racket both increased as the balance point moved closer to the tip of the racket (Figure 8.3b). The twistweight increased because, in the model, mass is added to the entire racket head. In reality, mass could be added at the tip of a racket to increase its swing weight, whilst keeping the twistweight virtually constant.

Table 8.5 Two sets of FE simulations used to determine the effect of the balance point of the racket. The mass moment of inertia, the polar moment of inertia and natural frequency of the racket in the FE model are also displayed.

Simulation set	Balance point from Butt (m)	Mass moment of inertia (*swingweight*) (kgm²)	Polar moment of inertia (*twistweight*) (kgm²)	Natural frequency (Hz)
1	0.299	0.0454	0.0014	137
2	0.396	0.066	0.0021	143

Table 8.6 Density and mass of the separate parts of the racket in the two FE models used to determine the effect of the position of the balance point.

Simulation set	Handle density (kg·m⁻³)	Handle mass (kg)	Head density (kg·m⁻³)	Head mass (kg)	Balance point from Butt (m)
1	2288	0.118	1180	0.139	0.299
2	737	0.038	1859	0.218	0.396
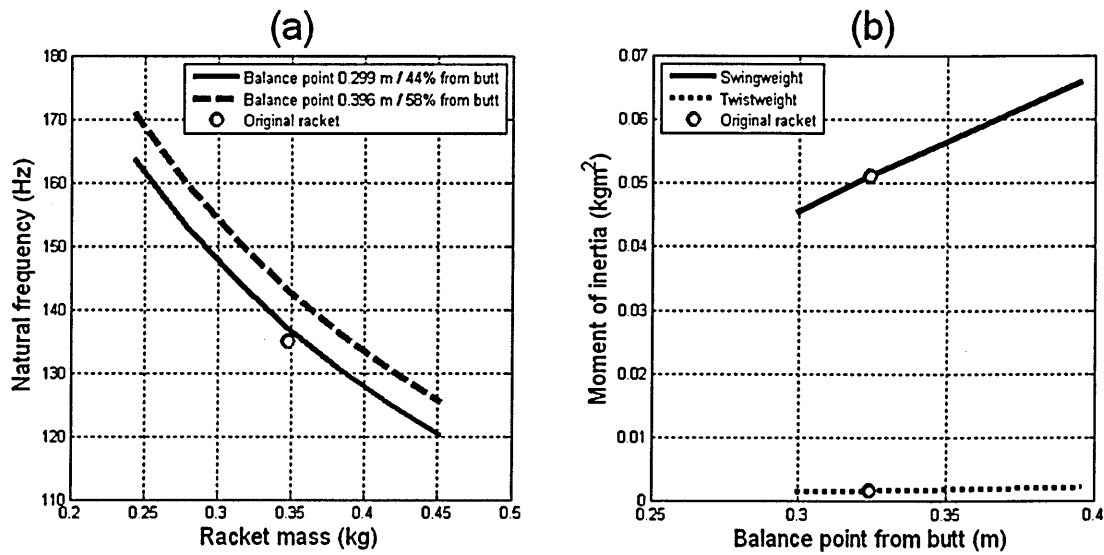
Figure 8.3 Relationship between the position of the balance point of the racket in the FE model and a) natural frequency, b) moment of inertia.

8.3. Results

8.3.1.   Racket structural stiffness

Figure 8.4 shows that the rebound velocity increased with the structural stiffness of the racket, for all six impact positions. Rebound velocity decreased as the impact position moved closer to the tip (0, 60) of the racket, along the long axis. Rebound velocity also decreased as the impact position moved away from the long axis. The structural stiffness of the racket had the largest effect on rebound velocity for the impacts in the throat region (0, -60 & 60, -60).

Figure 8.4 Effect of the structural stiffness of a tennis racket on the rebound velocity of the ball, for an impact at 35 m·s^{-1} and 20° with 300 rad·s^{-1} of backspin.

The longitudinal rebound angle was very small for the impacts in the central region of the string-bed (0, 0 & 60, 0) (Figure 8.5). The two rackets also had relatively similar rebound angles for the impacts at the throat and tip which were offset from the long axis (60, -60 & 60, 60). However, the rebound angles were approximately 9-12° larger than at the GSC. The structural stiffness of the racket had a larger influence on the longitudinal rebound angle of the ball for the impact at the throat and tip on the long axis (0, -60 & 0, 60). At these locations the longitudinal angle was larger for the racket with low structural stiffness. This is likely to be due to the racket with low structural stiffness deforming more throughout the impact. A large longitudinal angle may cause the ball to deviate horizontally from its intended path and hence reduce 'control'.
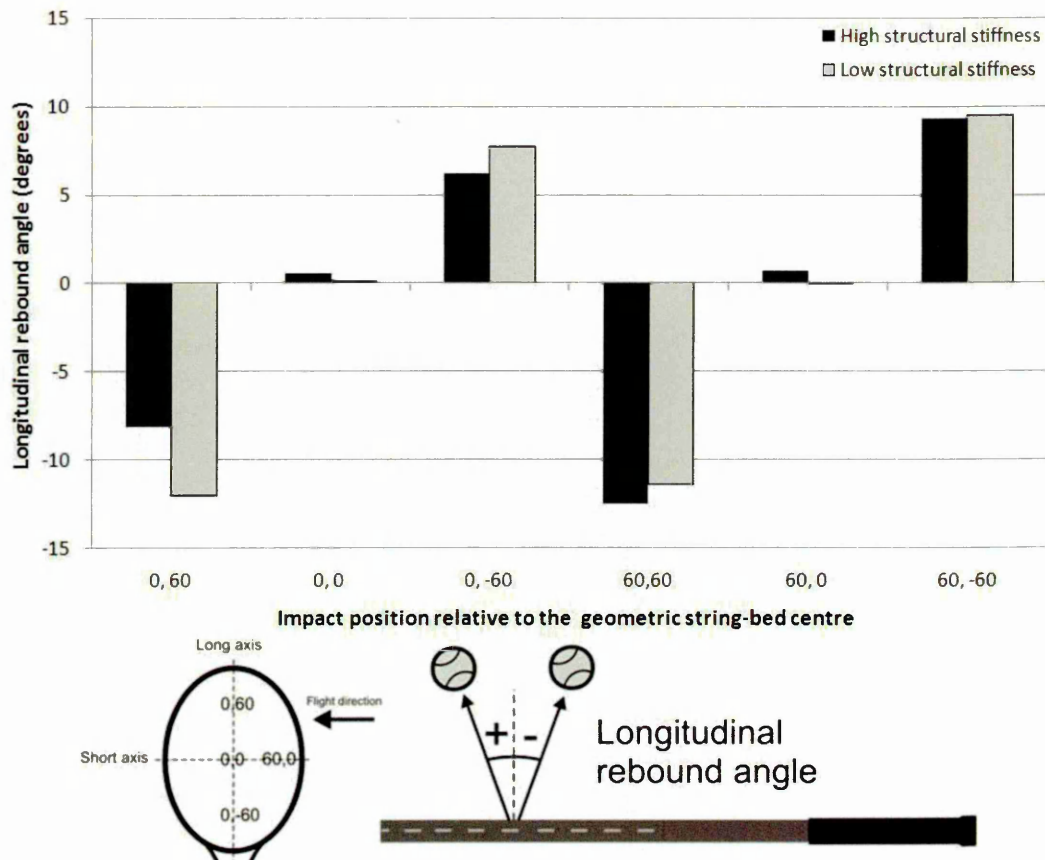
Figure 8.5 Effect of the structural stiffness of a tennis racket on the longitudinal rebound angle of the ball, for an impact at 35 m·s^{-1} and 20° with 300 rad·s^{-1} of backspin.

Figure 8.6 shows that the horizontal rebound angle increased for all three impact locations on the long axis (0, -60, 0 & 0, 0, 60), when the structural stiffness of the racket was decreased. For both rackets, the rebound angle increased as the impact position moved from the throat (0, -60) to the tip (0, 60) along the long axis. The rebound angles also increased as the impact positions moved away from the long axis of the racket. This is likely to be due to a decrease in the vertical rebound velocity of the ball, as a result of the racket rotating about its long axis. The largest rebound angle for both rackets was at the tip location offset from the long axis of the string-bed (60, 60). At this location and the throat impact offset from the long axis (60, -60) the rebound velocity of the ball was effectively independent of the structural stiffness of the racket. A larger rebound angle could be regarded as being equivalent to the ball rebounding closer to the racket normal in the court's frame of reference. This may give the impression of reduced 'power' (Bower and Cross, 2005).
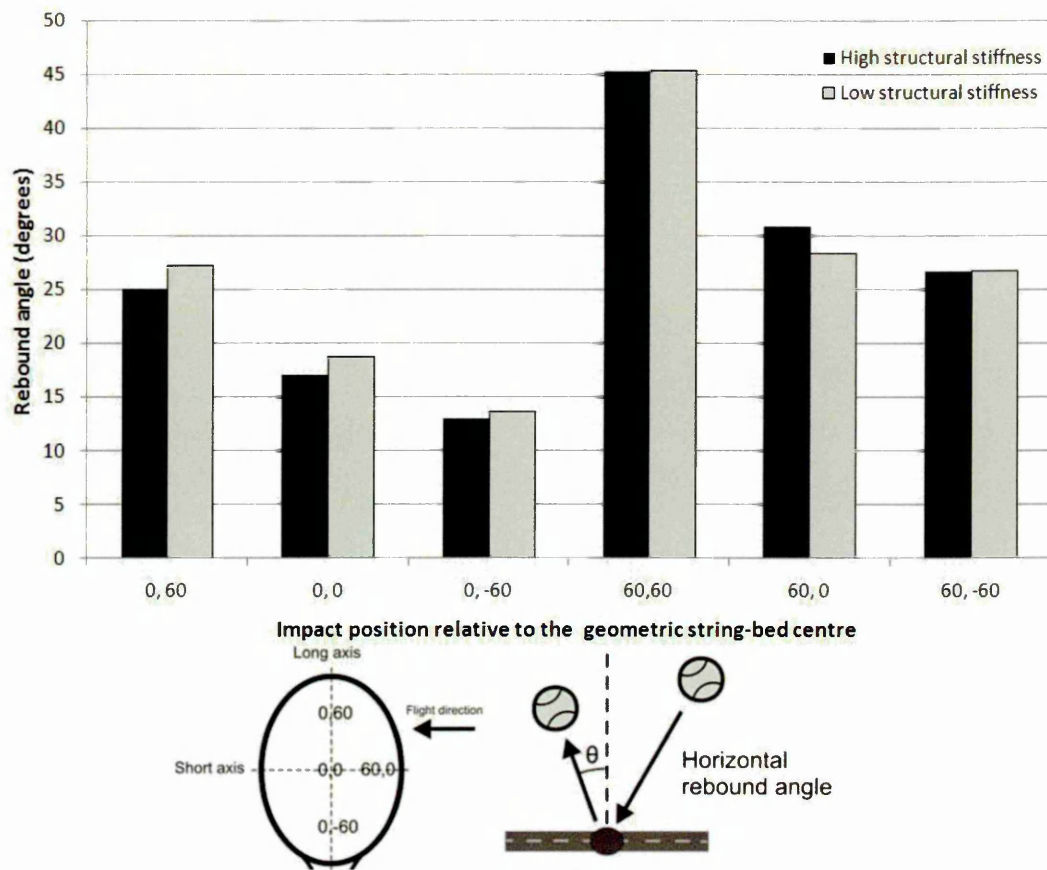
Figure 8.6 Effect of the structural stiffness of a tennis racket on the horizontal rebound angle of the ball, for an impact at 35 m·s^{-1} and 20° with 300 rad·s^{-1} of backspin.

Figure 8.7 shows that the sidespin was slightly higher for the structurally stiff racket at the GSC (0, 0) and throat (0, 60), in comparison to the racket with low structural stiffness. However, the sidespin was over 20 rad·s^{-1} larger at the tip of the racket (0, 60) with low structural stiffness. For the structurally stiff racket the highest sidespin was for the impact at the throat (0, -60). Sidespin will result in a horizontal force acting on the ball during flight. If large enough, this horizontal force could potentially cause the ball to deviate from its intended trajectory.
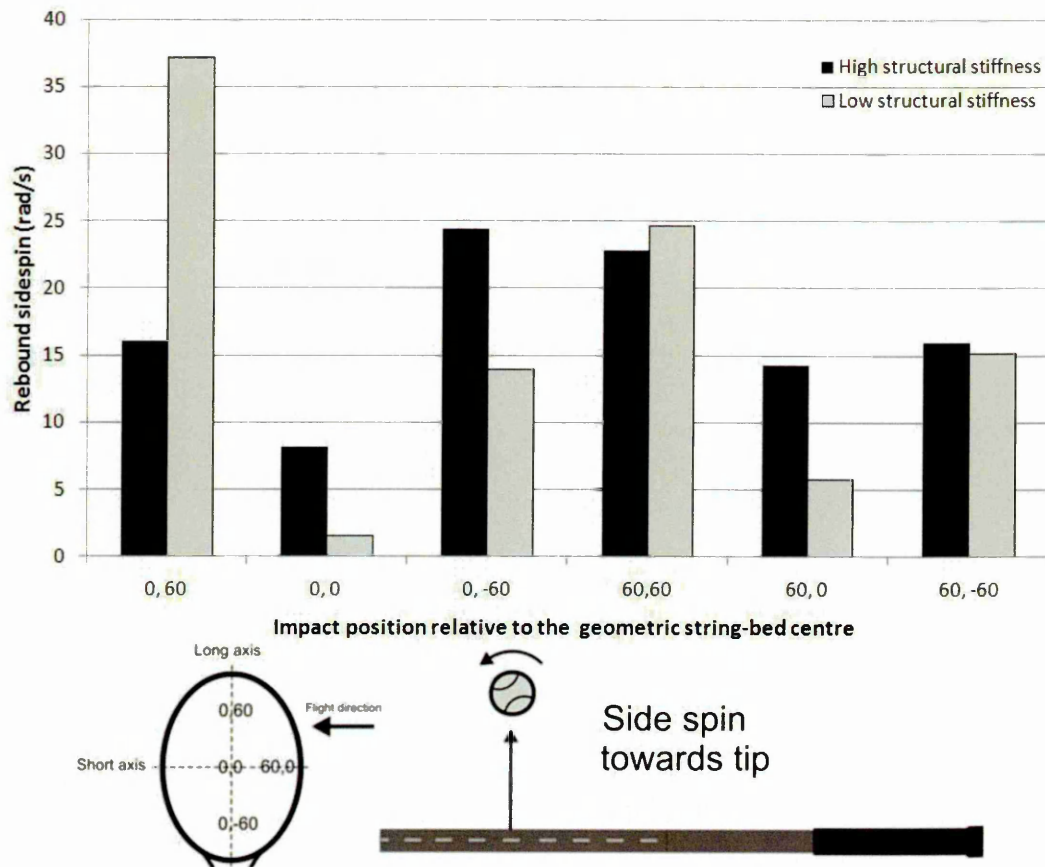
Figure 8.7 Effect of the structural stiffness of a tennis racket on the rebound sidespin of the ball, for an impact at 35 m·s^{-1} and 20° with 300 rad·s^{-1} of backspin.

Increasing the structural stiffness of the racket resulted in a very slight increase in topspin for impacts at the GSC (0, 0) (Figure 8.8). For both rackets, the rebound topspin of the ball increased as the impact position moved away from the GSC (0, 0), along the long axis of the string-bed towards both the tip (0, 60) and throat (0, -60). The rebound topspin was approximately 11 rad·s^{-1} higher at the throat (0, -60) for the racket with low structural stiffness. The rebound topspin at the tip (0, 60) was virtually identical for both rackets. Offsetting the impact from the long axis of the string-bed resulted in a considerable decrease in rebound topspin for both rackets. The decrease in topspin was slightly less pronounced for both rackets in the impact offset from the GSC (60, 0).
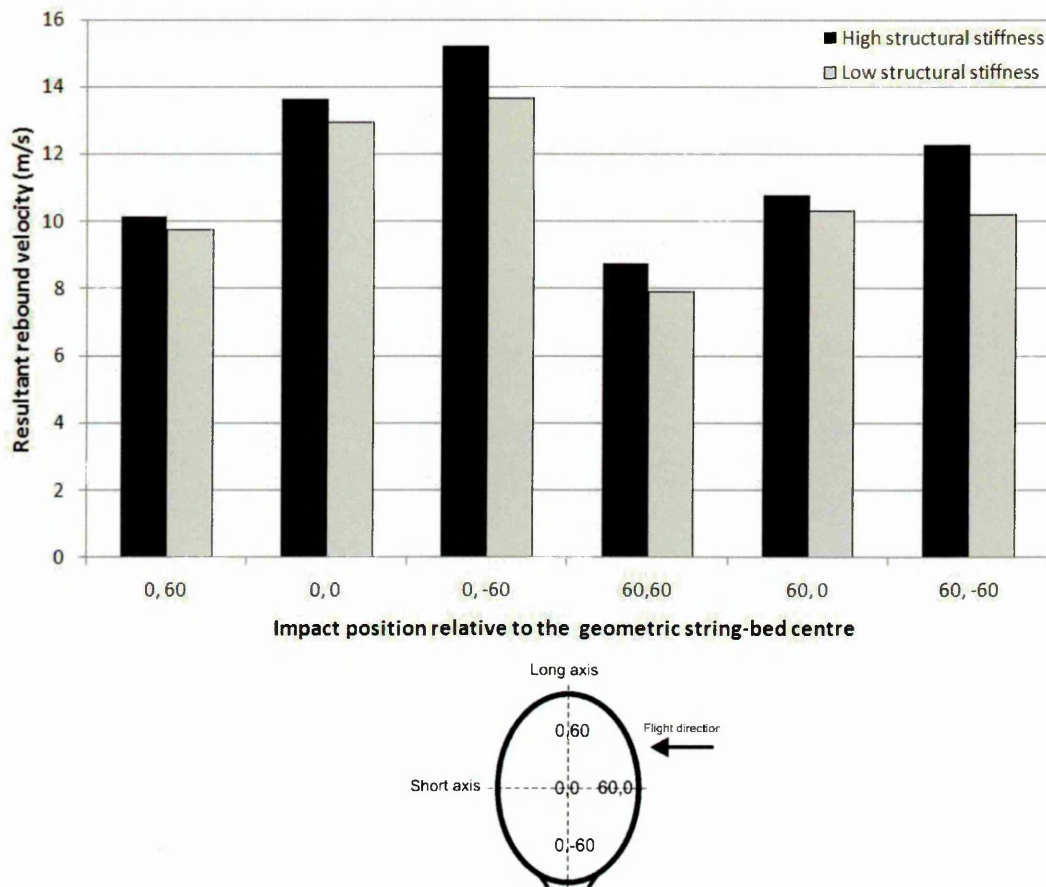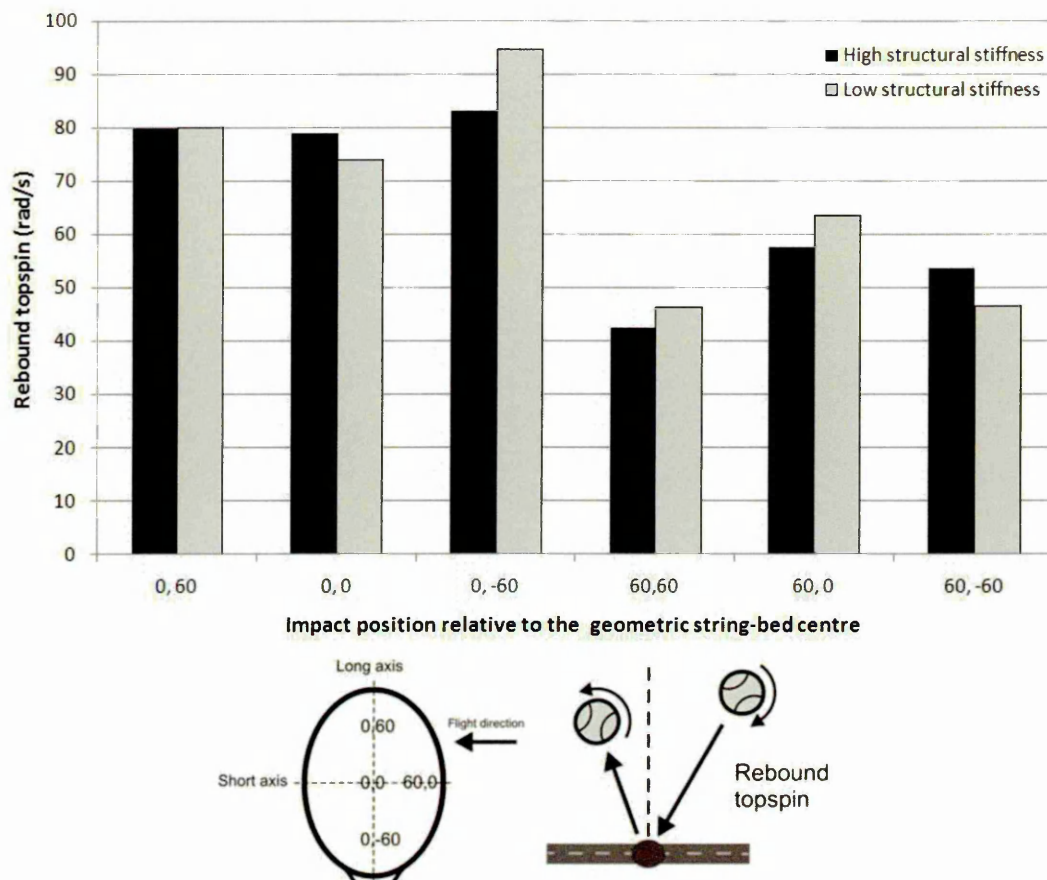
Figure 8.8 Effect of the structural stiffness of a tennis racket on the rebound topspin of the ball, for an impact at 35 m·s^{-1} and 20° with 300 rad·s^{-1} of backspin.

8.3.2.   *Summary of racket structural stiffness*

The results indicate that the structural stiffness of a tennis racket influences the rebound velocity, angle and spin of the ball. A stiffer racket will cause the ball to rebound slightly faster and with a larger angle in the court frame of reference, as shown in Figure 8.9. This indicates that a stiffer racket will provide a player with more 'power'. A racket with low structural stiffness will cause the ball to rebound at a larger longitudinal angle and with considerably more sidespin, for impacts in the tip region. A large longitudinal angle and high sidespin may cause the ball to deviate horizontally from its intended trajectory and hence reduce 'control'. The magnitude of topspin for a ball rebounding off a racket with high structural stiffness is much less dependent on the impact location. This also indicates that a stiffer racket may increase 'control' and improve consistency. Elite players typically impact the ball close to the GSC, when performing a topspin forehand (Choppin *et al.,* 2008). A ball impacting at the

GSC of a racket with high structural stiffness, will rebound very slightly faster and higher (*court frame of reference*) and with a little more topspin and sidespin.
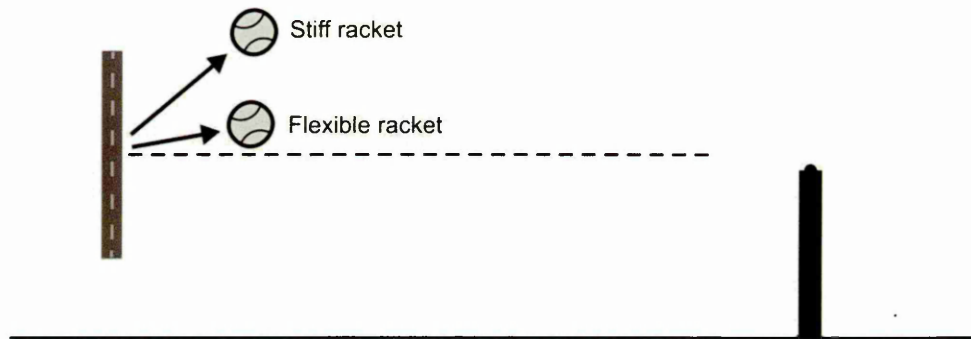
Figure 8.9 Diagram to illustrate the difference between using a stiff and flexible racket when performing a forehand shot.

8.3.3.   Racket mass

Figure 8.10 shows that rebound velocity increased considerably with the mass of the racket, for all six impact positions. For both rackets, rebound velocity decreased as the impact position moved closer to the tip of the racket (0, 60), along the long axis. Rebound velocity also decreased as the impact position moved away from the long axis. The difference in rebound velocity for the two rackets was approximately 3.5 $m·s^{-1}$, for all the impact positions on the string-bed.
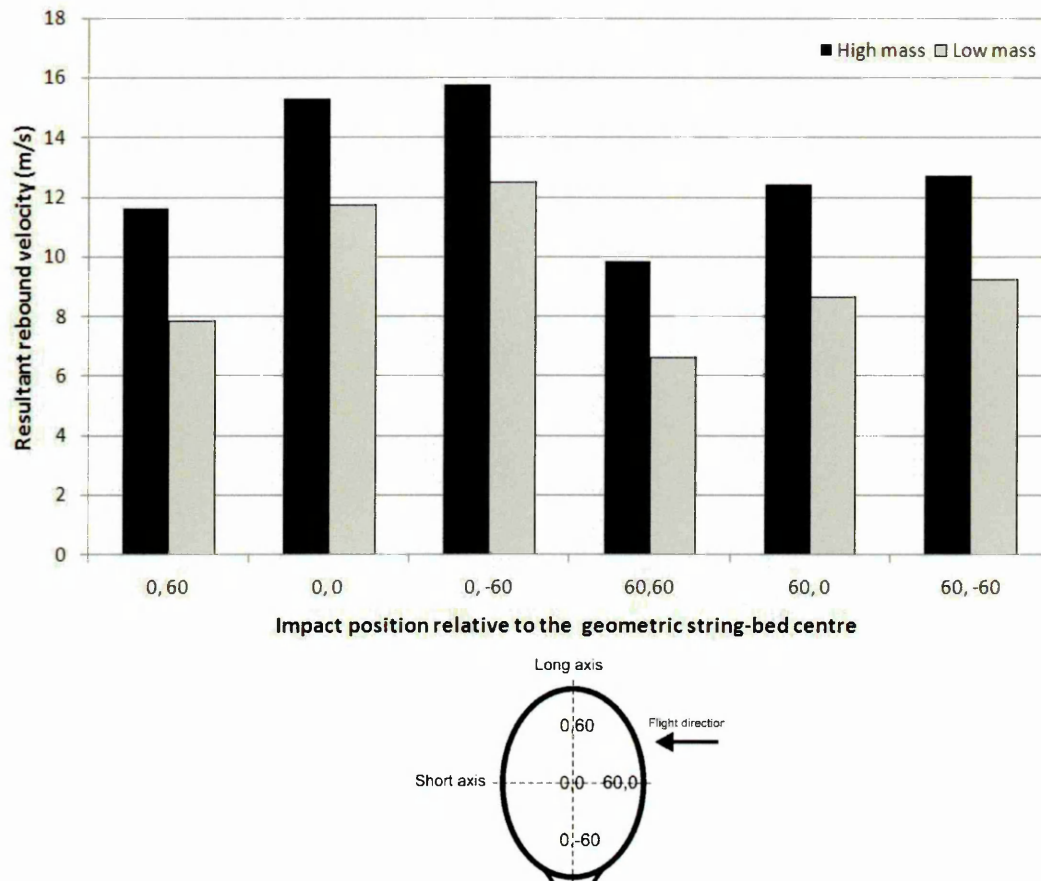
Figure 8.10 Effect of the mass of a tennis racket on the rebound velocity of the ball, for an impact at 35 m·s^{-1} and 20° with 300 rad·s^{-1} of backspin.

Figure 8.11 shows that the longitudinal rebound angle was approximately zero in both rackets for the impacts in the central region of the string-bed (0, 0 & 60, 0). The impacts with the lighter racket produced larger longitudinal rebound angles for all of the other positions on the string-bed. The largest rebound angle for both rackets was for the impact at the tip offset from the long axis (60, 60). The discrepancy between the rebound angles of the two rackets was also largest at this location, with a difference of approximately 10°. As mentioned previously, a large longitudinal angle may cause the ball to deviate horizontally from its intended path, thus reducing 'control'.
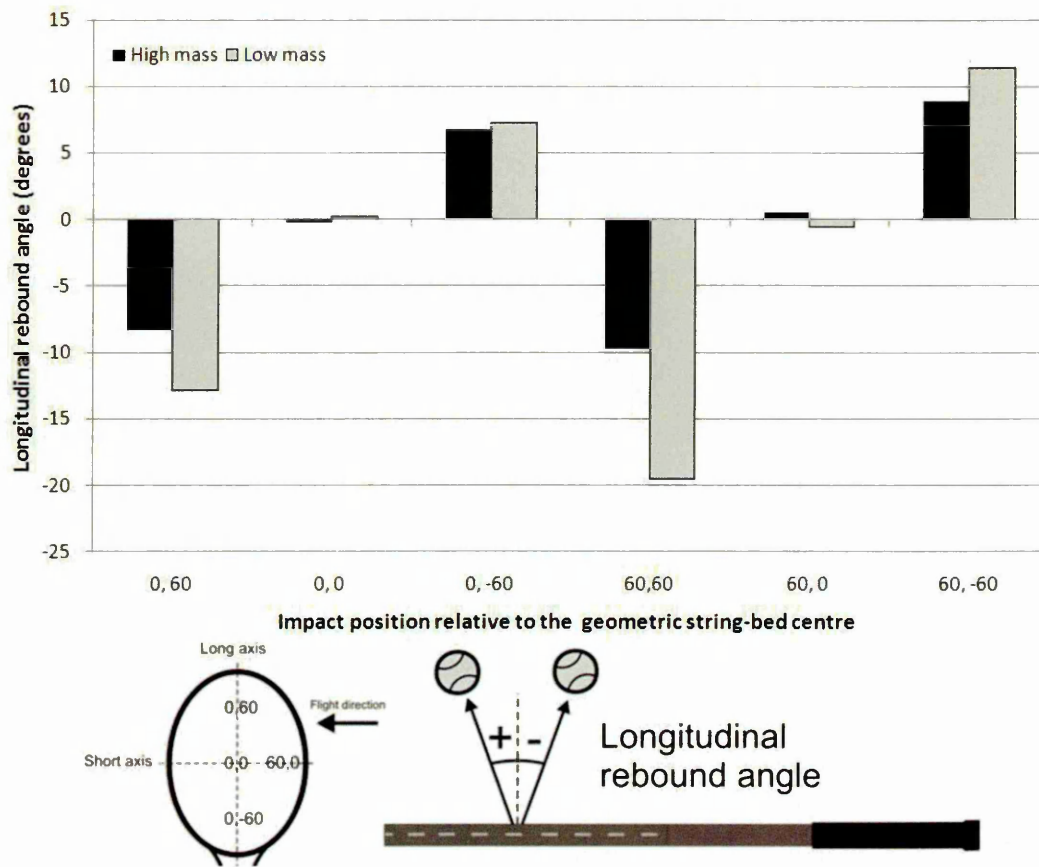
Figure 8.11 Effect of the mass of a tennis racket on the longitudinal rebound angle of the ball, for an impact at 35 m·s^{-1} and 20° with 300 rad·s^{-1} of backspin.

Figure 8.12 shows that the horizontal rebound angle increased for all six impact locations, when the mass of the racket was decreased. For both rackets, the rebound angle increased as the impact position moved from the throat (0, -60) to the tip (0, 60) along the long axis. The rebound angles also increased as the impact positions moved away from the long axis of the racket. This is likely to be due to the racket rotating about its long axis. The largest rebound angle for both rackets was at the tip location offset from the long axis of the string-bed (60, 60). This was also the location where the discrepancy between the two rackets was largest at approximately 25°. As previously mentioned, a larger rebound angle equates to the ball rebounding closer to the racket normal in the court frame of reference, which may give the impression of reduced 'power' (Bower and Cross, 2005).

194
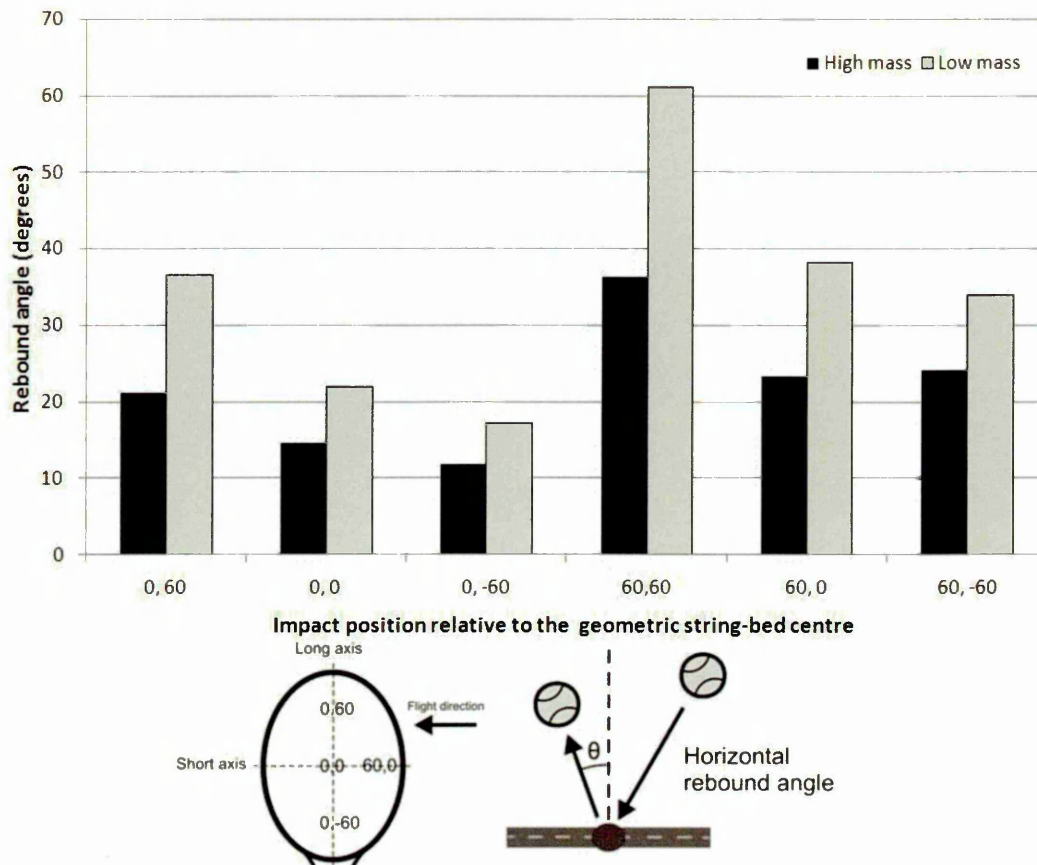
Figure 8.12 Effect of the mass of a tennis racket on the horizontal rebound angle of the ball, for an impact at 35 m·s^{-1} and 20° with 300 rad·s^{-1} of backspin.

Figure 8.13 shows that the sidespin of the ball was lower for all the impact locations on the heavy racket. The largest discrepancy in the sidespin in the two rackets was for the impacts at the tip (0, 60). As previously mentioned, sidespin could potentially cause the ball to deviate horizontally from its intended course.
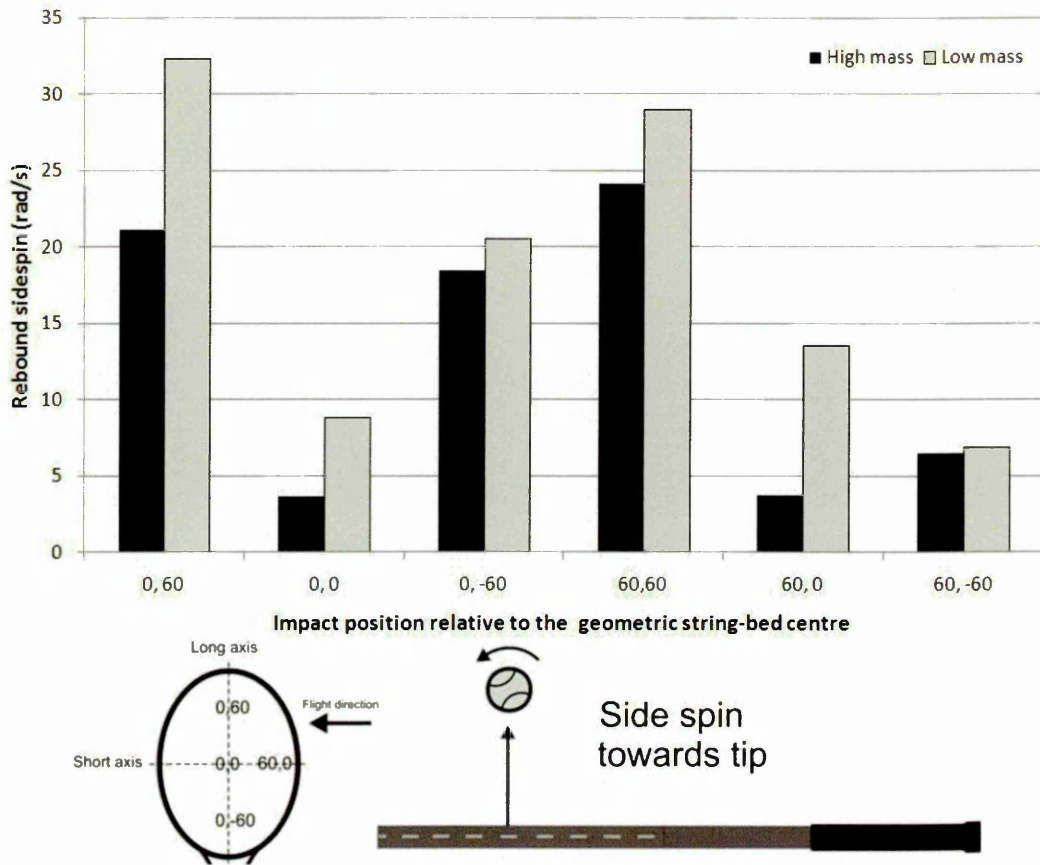
Figure 8.13 Effect of the mass of a tennis racket on the rebound sidespin of the ball, for an impact at 35 m·s^{-1} and 20° with 300 rad·s^{-1} of backspin.

Figure 8.14 shows that increasing the mass of the racket resulted in an increase in topspin, for all six impact locations. For both rackets, the rebound topspin of the ball increased as the impact position moved away from the GSC (0, 0), along the long axis of the string-bed towards both the tip (0, 60) and throat (0, -60). Offsetting the impact from the long axis of the string-bed resulted in a considerable decrease in rebound topspin for both rackets. The decrease in topspin was much less pronounced for the impact on the heavy racket offset from the GSC (60, 0).

Figure 8.14 Effect of the mass of a tennis racket on the rebound topspin of the ball, for an impact at 35 m·s^{-1} and 20° with 300 rad·s^{-1} of backspin.

8.3.4.   Summary of racket mass

The results indicate that the mass of a racket has a relatively large influence on the rebound characteristics of the ball. Assuming racket mass is independent of swing speed for a forehand shot, the ball will rebound both faster and higher from a heavy racket (*court frame of reference*). Coupled with an increase in topspin, this is likely to give the impression of more 'power'. Reducing the mass of the racket caused the ball to rebound with a larger longitudinal angle and more sidespin, particularly for impacts near the tip. This may cause the ball to deviate from its intended path and reduce 'control'. A heavier racket is likely to increase rebound velocity, angle and spin for forehand shots at the GSC, which is where elite players typically impact the ball (Choppin *et al.*, 2008). The effect of racket mass on serve velocity will be discussed at the end of the chapter.

8.3.5.   Balance point

Figure 8.15 shows that the rebound velocity of the ball was considerably higher for the head-heavy racket, at all six impact positions on the string-bed. For both rackets, rebound velocity decreased as the impact position moved to the tip region of the racket (0, 60, 60, 60). The position of the balance point had the largest influence on the impacts in the tip region (0, 60 & 60, 60), with a difference of approximately 4 $m·s^{-1}$ between the two rackets.
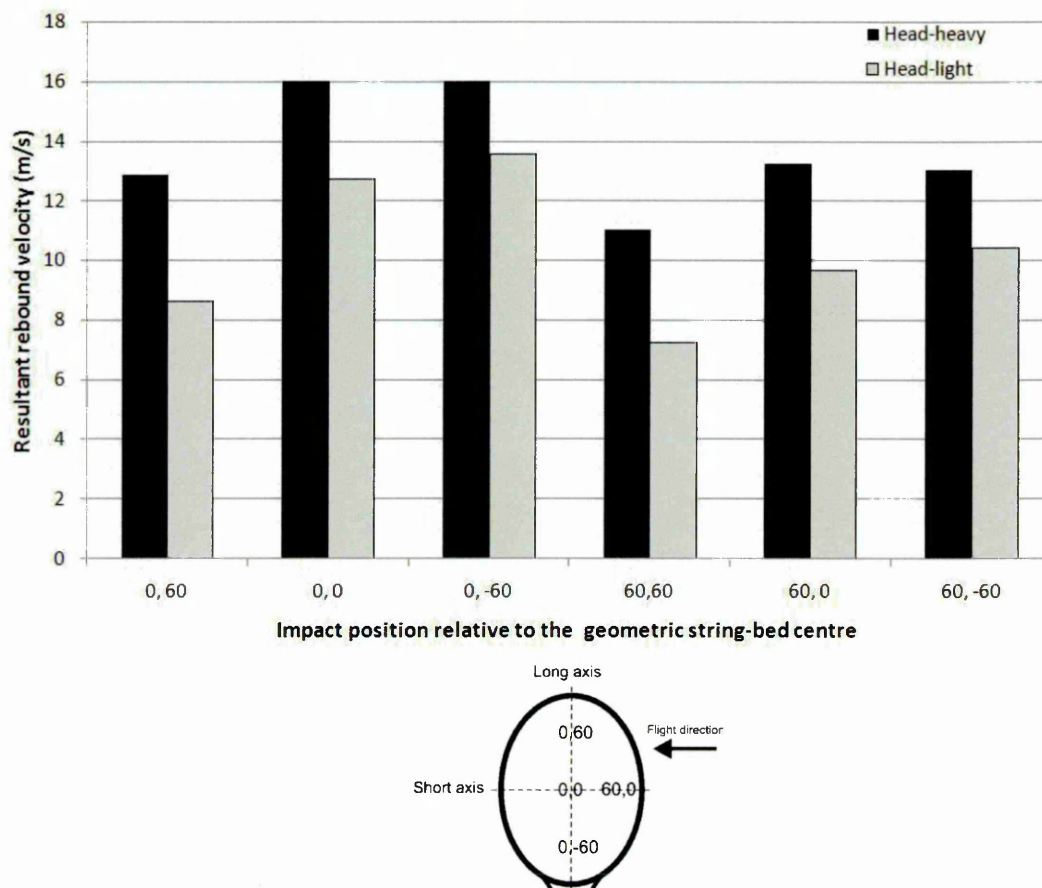
Figure 8.15 Effect of the position of the balance point of a tennis racket on the rebound velocity of the ball, for an impact at 35 $m·s^{-1}$ and 20° with 300 $rad·s^{-1}$ of backspin.

Figure 8.16 shows that the longitudinal rebound angle was negligible for both rackets for the impacts at the centre of the string-bed (0, 0, 60, 0). The rebound angles were larger for the head-light racket in comparison to the head-heavy racket, at all the other impact locations on the string-bed. The largest discrepancy between the head-light and head-heavy rackets was for the

impacts in the tip region (0, 60 & 60, 60). A large longitudinal angle could potentially result in a reduction in 'control'.
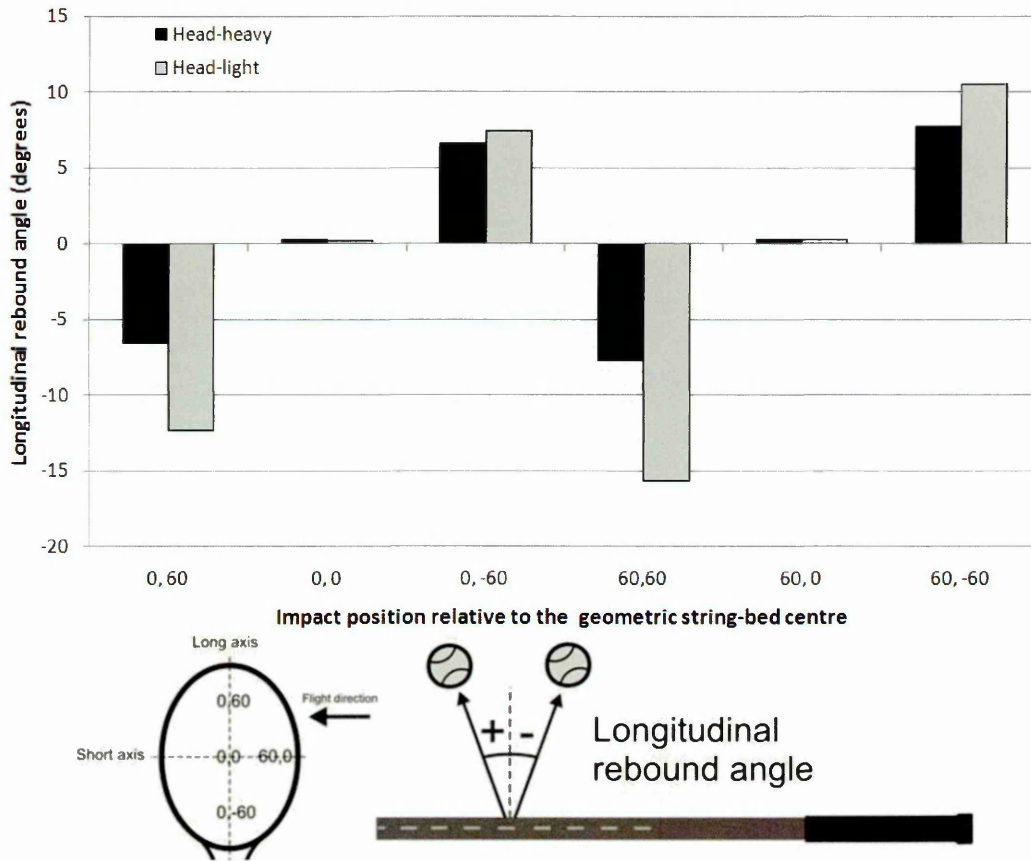
Figure 8.16 Effect of the position of the balance point of a tennis racket on the longitudinal rebound angle of the ball, for an impact at 35 m·s^{-1} and 20° with 300 rad·s^{-1} of backspin.

Figure 8.17 shows that the horizontal rebound angle was lower for the head-heavy racket, in all six impact positions. The rebound angles increased as the impact positions moved away from the long axis of the racket. For both rackets, the rebound angle increased as the impact position moved from the throat region (0, -60 & 60, -60) to the tip region (0, 60 & 60, 60). The increase in rebound angle was much more pronounced for the head-light racket. A larger rebound angle could potentially give the impression of reduced 'power' (Bower and Cross, 2005).
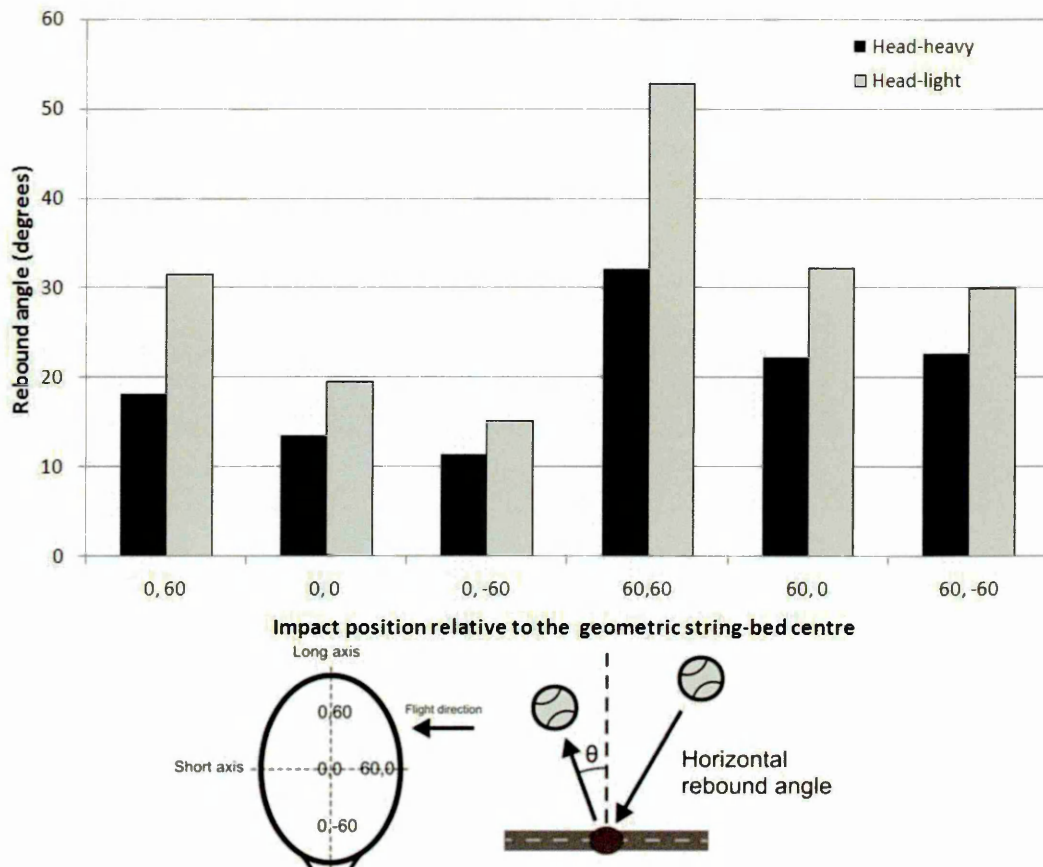
Figure 8.17 Effect of the position of the balance point of a tennis racket on the horizontal rebound angle of the ball, for an impact at 35 m·s^{-1} and 20° with 300 rad·s^{-1} of backspin.

Figure 8.18 shows that the sidespin of the ball was higher for all the impact positions on the head-light racket, except the off-centre impact at the throat (60, -60). The largest difference in sidespin between the two rackets was for the impacts in the tip region (0, 60 & 60, 60). The sidespin of the ball was approximately 20 rad·s^{-1} higher for the impact at the tip (0, 60) of the head-light racket, in comparison to the head-heavy racket.
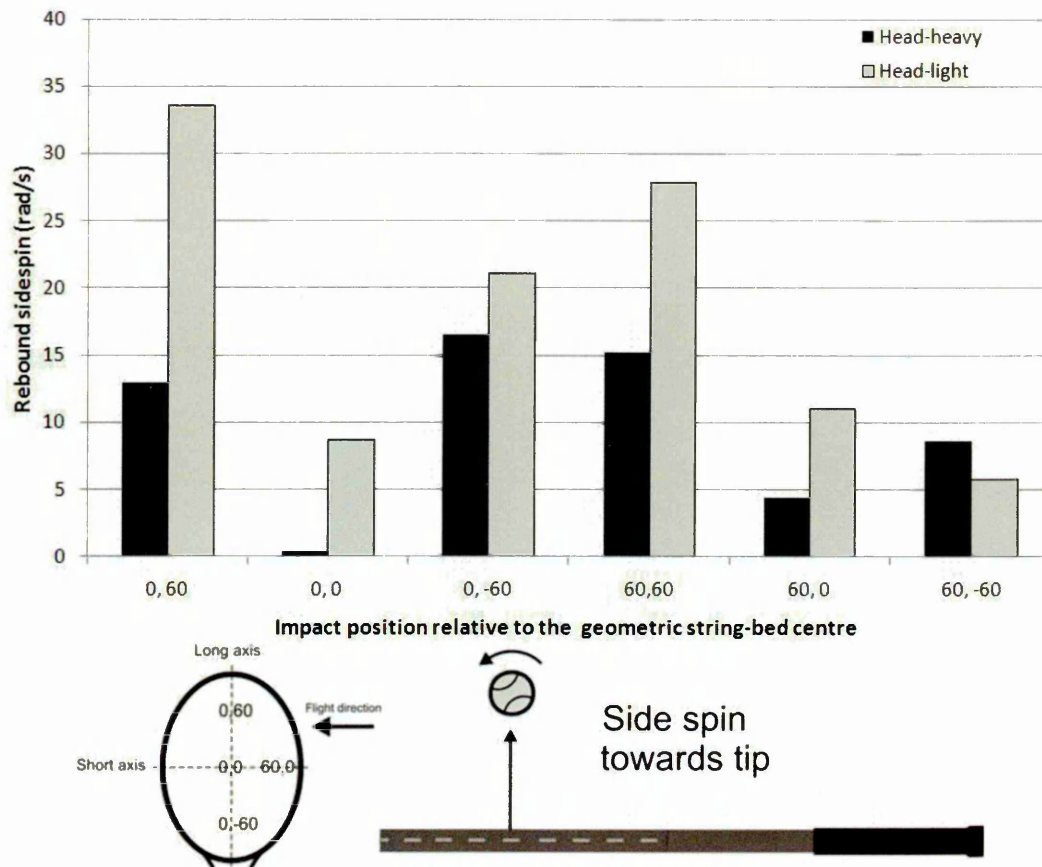
Figure 8.18 Effect of the position of the balance point of a tennis racket on the rebound sidespin of the ball, for an impact at 35 m·s^{-1} and 20° with 300 rad·s^{-1} of backspin.

Figure 8.19 shows that moving the balance point closer to the tip resulted in an increase in topspin, for all six impact locations. For both rackets, the rebound topspin of the ball increased as the impact position moved away from the GSC (0, 0), along the long axis of the string-bed towards both the tip (0, 60) and throat (0, -60). Offsetting the impact from the long axis of the string-bed resulted in a considerable decrease in rebound topspin for both rackets. The decrease in topspin was slightly less pronounced for the impact that was offset from the GSC (60, 0) in the head-heavy racket.
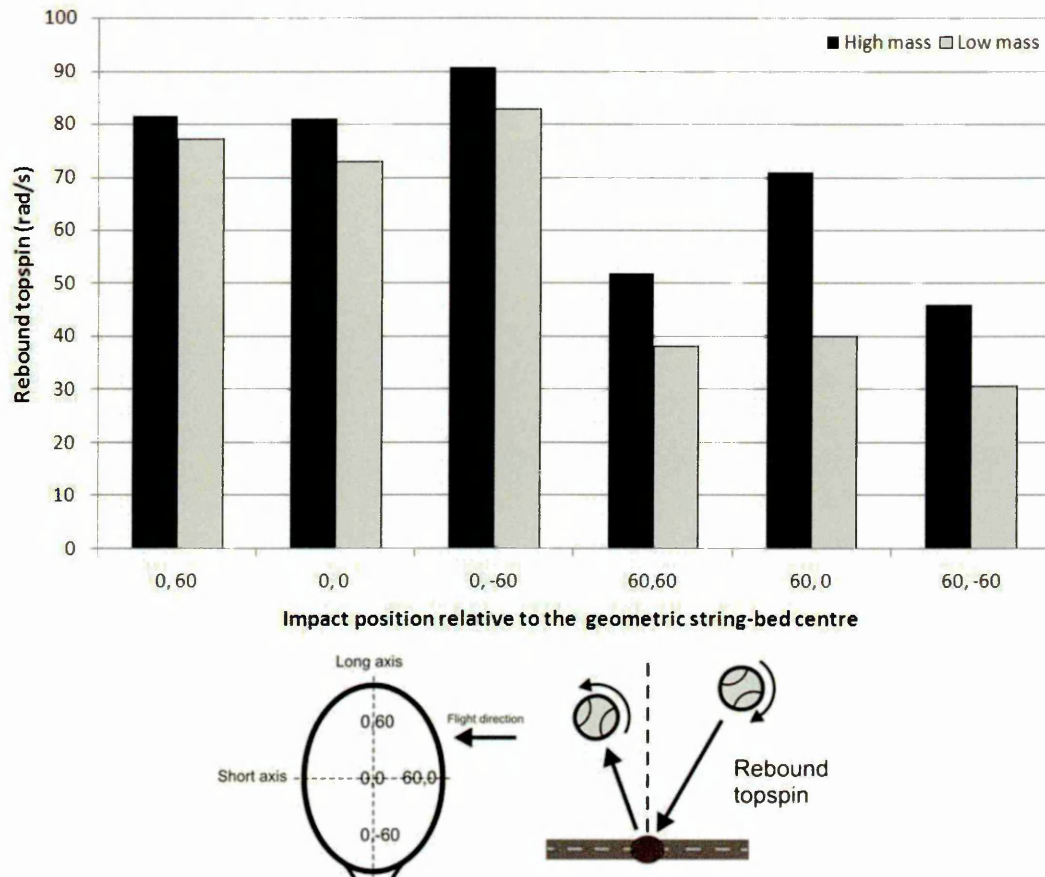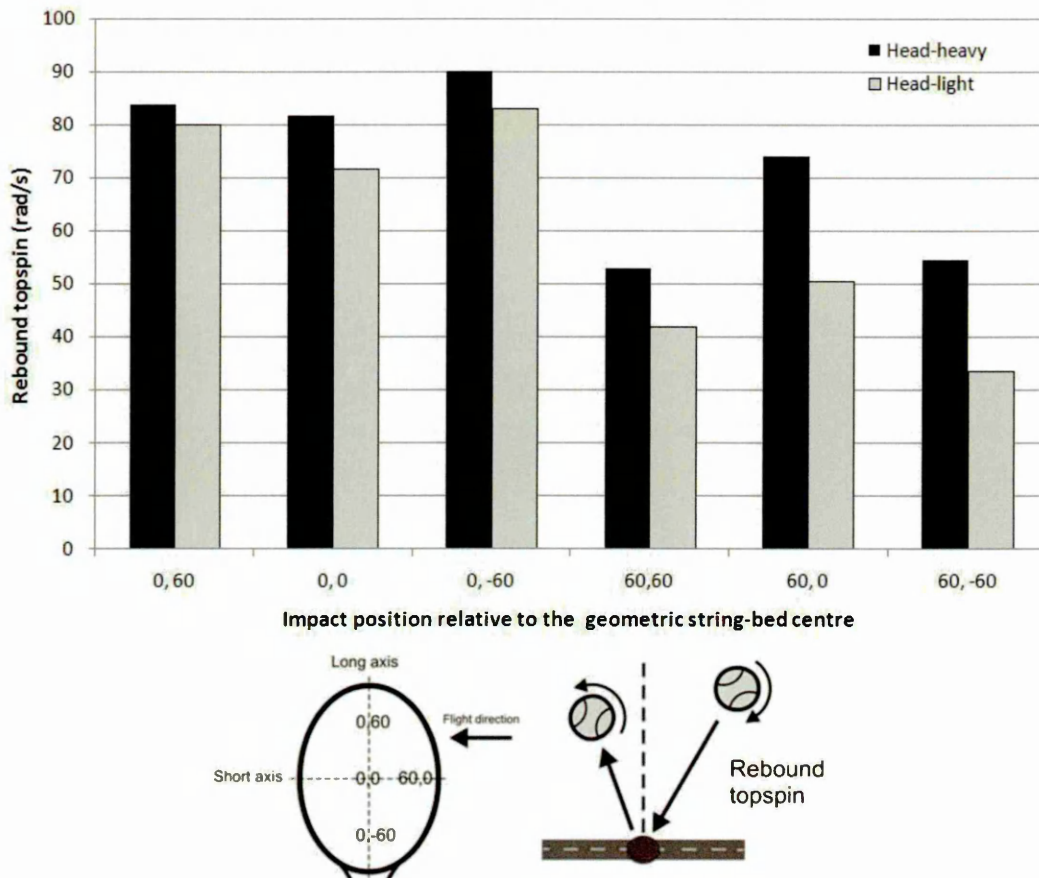
Figure 8.19 Effect of the position of the balance point of a tennis racket on the rebound topspin of the ball, for an impact at 35 m·s^{-1} and 20° with 300 rad·s^{-1} of backspin.

8.3.6.   Summary of racket balance point

The results indicate that the ball will rebound faster, higher and with more topspin, if a player uses a head-heavy racket to perform a forehand shot. This is based on the assumption that the angular velocity of the racket is independent of its swingweight. The results also indicate that more 'control' can be obtained from a head-heavy racket. This is partly due to better consistency in the rebound properties of the ball, for different impact locations on the string-bed. It is also due to the ball rebounding with a smaller longitudinal angle and less sidespin. For forehand shots with the impact at the GSC, a head-heavy racket is likely to result in the ball rebounding faster and with more topspin, in comparison to a head-light racket with the same mass.

8.4. Explanation of results

The results were analysed to determine how the individual racket parameters affect the rebound characteristics of the ball. Separate explanations are given

for the vertical and horizontal directions, as defined in Figure 8.20. Only the impacts on the long axis of the string-bed were analysed. This was because there was uncertainty as to whether players might apply a torque to the handle of the racket, which is likely to have a significant affect on impacts offset from the long axis.
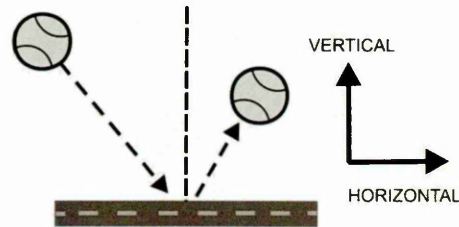
Figure 8.20 Definition of vertical and horizontal velocity for an impact between a tennis ball and freely suspended racket.

8.4.1.   *Vertical rebound velocity*

Figure 8.21 shows the effect of racket structural stiffness on the vertical force, ball velocity, racket tip and COM displacement throughout an oblique impact at the tip. The maximum vertical impact force (Figure 8.21a) and vertical ball velocity (Figure 8.21b) were both marginally lower for the racket with low structural stiffness. The vertical displacement at the tip was slightly larger for the racket with low structural stiffness (Figure 8.21c), while the vertical centre of mass (COM) displacement was virtually identical between both rackets (Figure 8.21d). This indicates that more of the energy from the impact was converted into deforming the racket with low structural stiffness, as shown in Figure 8.22, resulting in a slight reduction in the vertical rebound velocity of the ball.
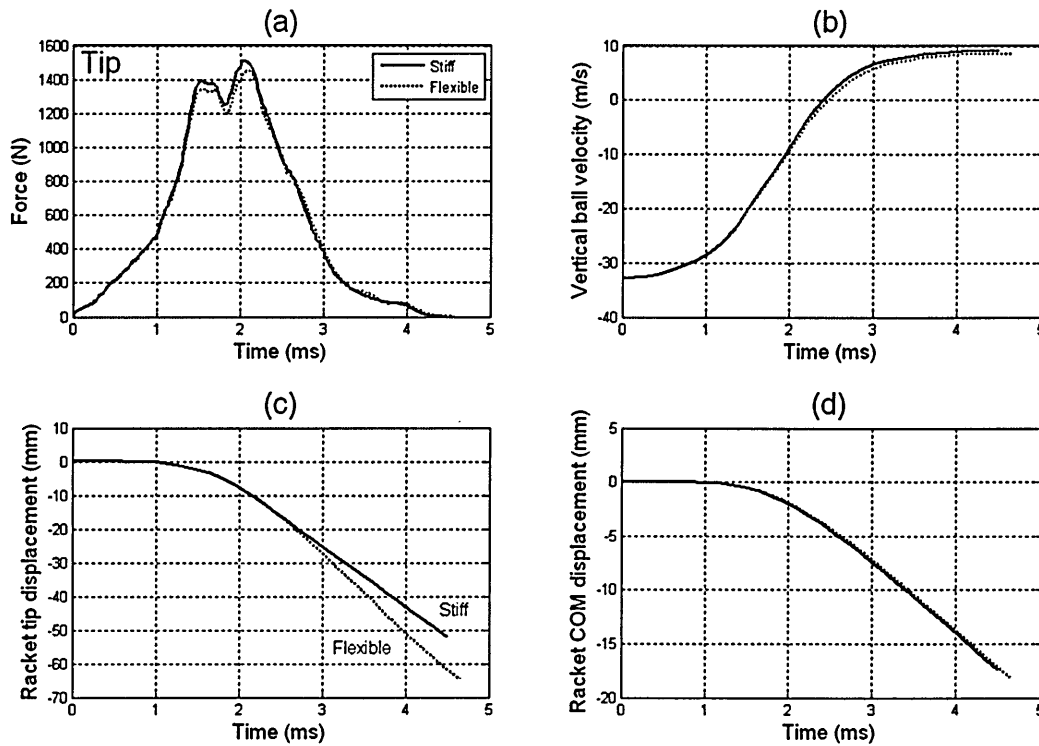
Figure 8.21 Effect of racket structural stiffness on the vertical velocity of an impact at the tip at 35 m·s^{-1} and 20° with 300 rad·s^{-1} of backspin a) Vertical force, b) Vertical ball velocity, c) Vertical racket tip displacement and d) Vertical racket COM displacement.
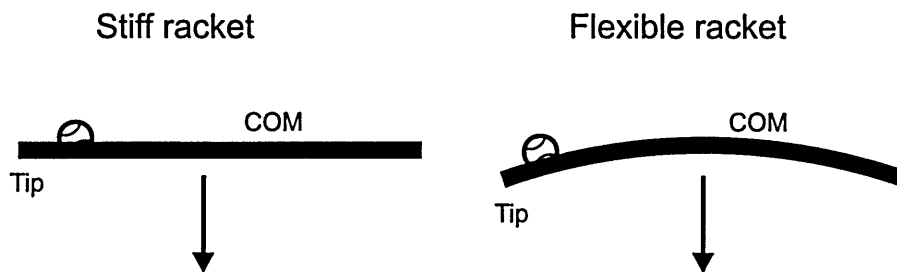
Figure 8.22 The vertical deformation of a stiff and flexible freely suspended tennis racket for an impact at the tip.

Figure 8.23d shows that the COM displacement was very similar for the racket with high structrual stiffness and the racket with low structrual stiffness, for the impact at the throat. The maximum vertical force (Figure 8.23a) and tip displacement (Figure 8.23c) were both slightly larger for the racket with high structural stiffness. As the COM of both rackets was translating vertically at the same rate (Figure 8.23d), a larger tip displacement indicates less deformation of the racket, as shown in Figure 8.24. This resulted in less 'wasted' energy and a

slightly higher vertical rebound velocity for the ball impacting the racket with high structural stiffness (Figure 8.23b).
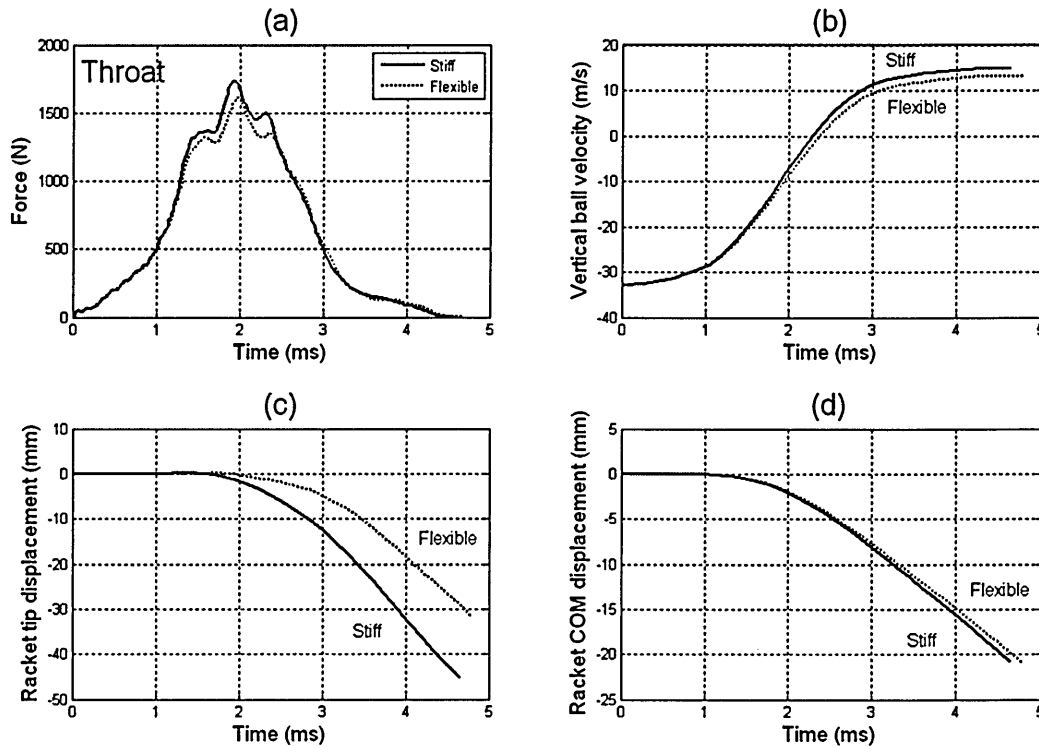
Figure 8.23 Effect of racket structural stiffness on the vertical velocity of an impact at the throat at 35 m·s^{-1} and 20° with 300 rad·s^{-1} of backspin a) vertical force, b) vertical ball velocity, c) racket tip displacement and d) racket COM displacement.
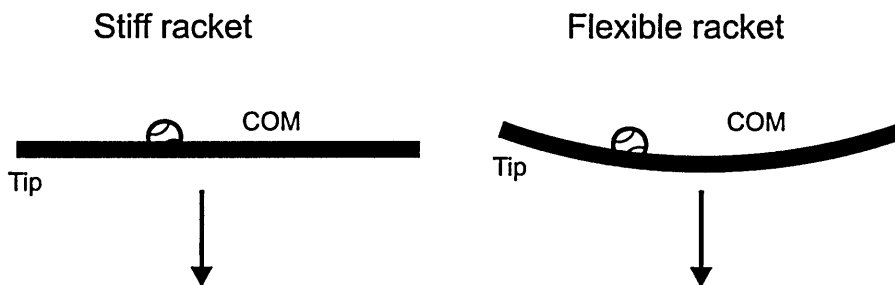
Figure 8.24 The vertical deformation of a stiff and flexible freely suspended tennis racket for an impact at the throat.

For the impact at the tip, the vertical impact force was considerably larger for the heavy racket, from approximately 1.5 ms into the impact (Figure 8.25a). The vertical displacement of the tip (Figure 8.25c) and COM (Figure 8.25d) were also smaller from approximately 1.5 ms into the impact, for this racket. This

indicates that the heavier racket was translating less and rotating less about its COM. As less energy went into translating and rotating the heavier racket, the vertical rebound velocity of the ball was significantly larger (Figure 8.25b).
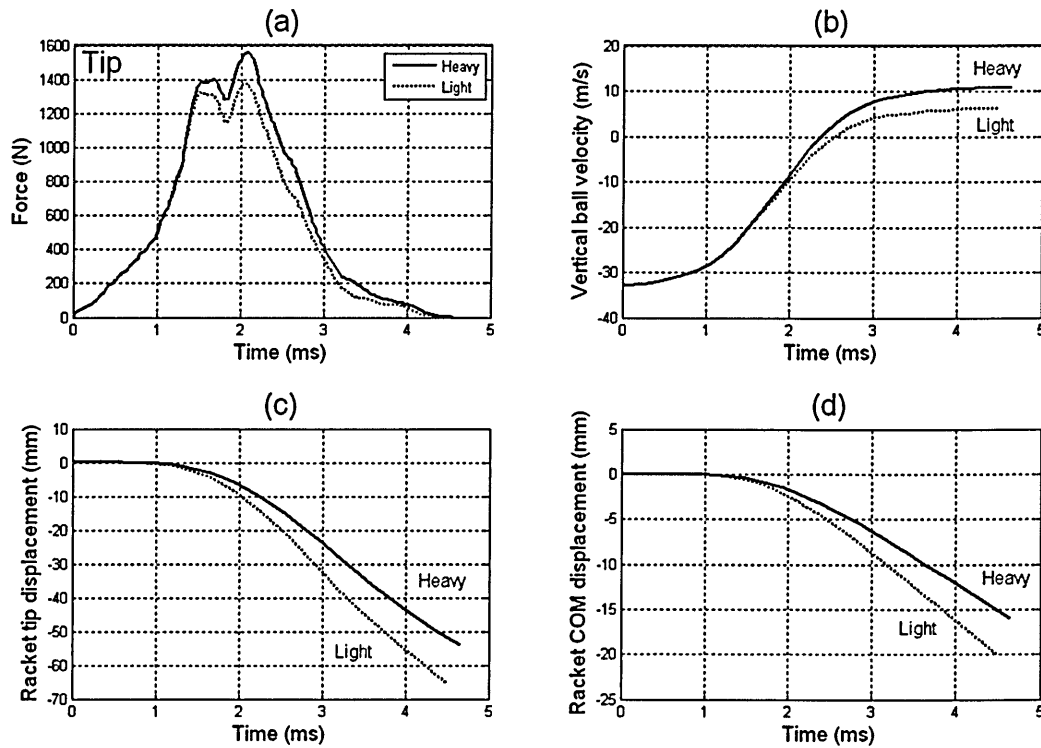
Figure 8.25 Effect of racket mass on the vertical velocity of an impact at the tip at 35 m·s⁻¹ and 20° with 300 rad·s⁻¹ of backspin a) vertical force, b) vertical ball velocity, c) racket tip displacement and d) racket COM displacement.

The results in Figure 8.26a, c and d indicate that the heavier racket was also translating and rotating less for the impact at the throat. As with the impact at the tip, the vertical rebound velocity of the ball was larger for the heavier racket, as less energy went into displacing it.

206
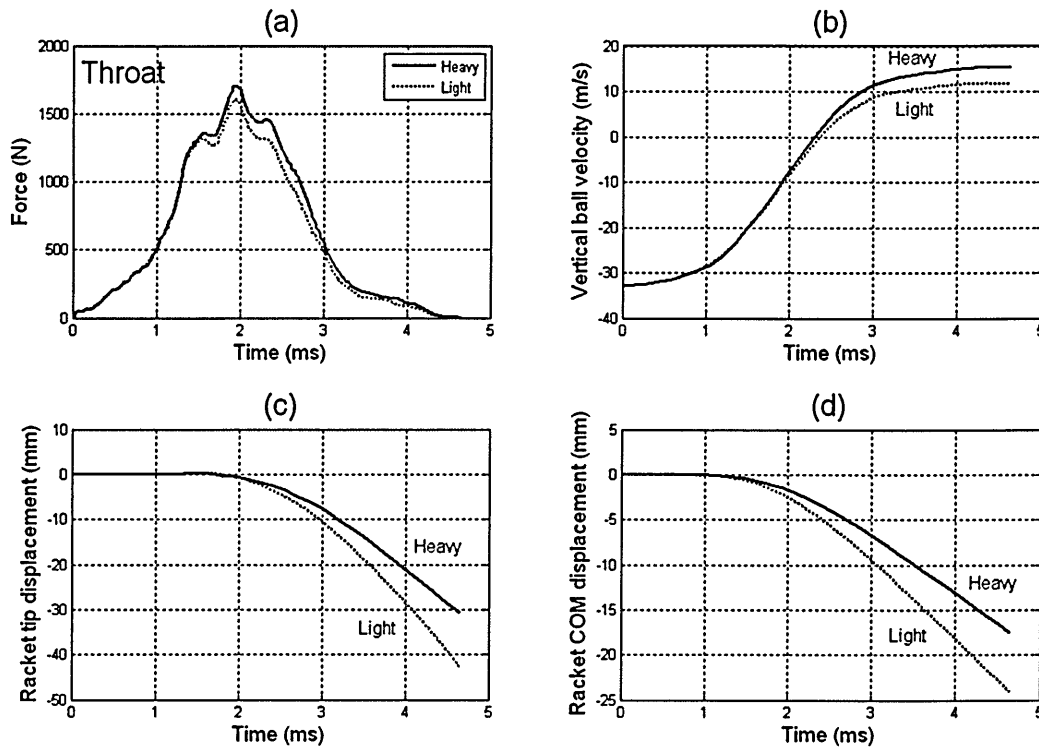
Figure 8.26 Effect of racket mass on the vertical velocity of an impact at the throat at 35 m·s⁻¹ and 20° with 300 rad·s⁻¹ of backspin a) vertical force, b) vertical ball velocity, c) racket tip displacement and d) racket COM displacement.

For an impact at the tip, the vertical COM displacement (Figure 8.27d) of the head-light racket was slightly lower, while the displacement at the tip was larger (Figure 8.27c). This indicates that the head-light racket was rotating more about its COM, in comparison to the head-heavy racket. The head-light racket may also have been deforming more as a result of the increased distance from the impact point to the pivot (COM). The higher proportion of the energy from the impact, which went into rotating and deforming the head-light racket, resulted in the ball rebounding at a lower velocity (Figure 8.27b).
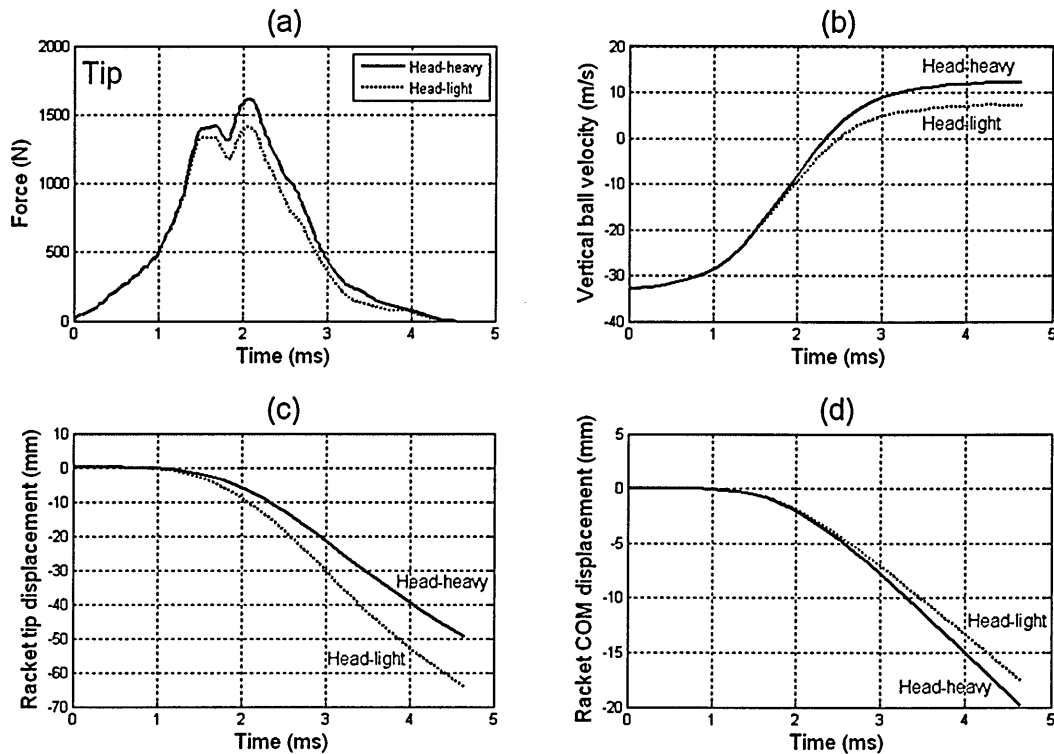
Figure 8.27 Effect of balance point on the vertical velocity of an impact at the tip at 35 m·s⁻¹ and 20° with 300 rad·s⁻¹ of backspin a) vertical force, b) vertical ball velocity, c) racket tip displacement and d) racket COM displacement.

Figure 8.28c and d show that the COM displacement was smaller and the tip displacement was larger, for the impact at the throat of the head-light racket. This indicates that the head-light racket was rotating and deforming more, throughout the impact. As more energy was used to rotate and deform the head-light racket, the rebound velocity of the ball was lower (Figure 8.28b).

208
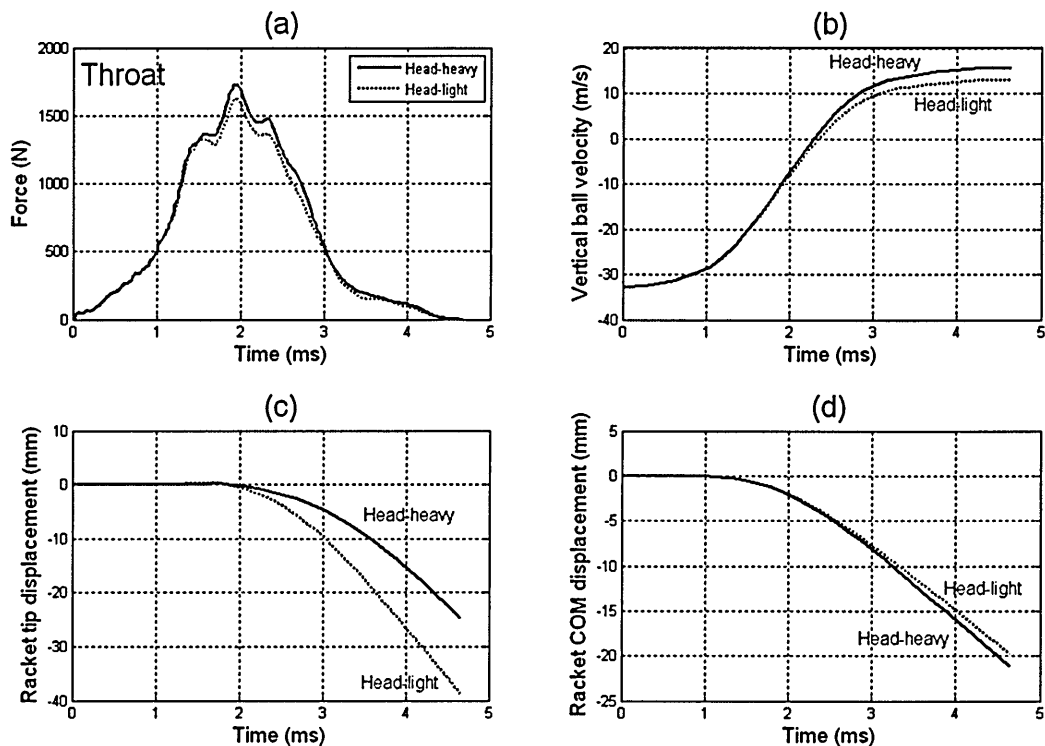
Figure 8.28 Effect of balance point on the vertical velocity of an impact at the throat at 35 m·s⁻¹ and 20° with 300 rad·s⁻¹ of backspin a) vertical force, b) vertical ball velocity, c) racket tip displacement and d) racket COM displacement.

8.4.2.   Horizontal rebound velocity and spin

In order to determine how the individual racket parameters affect rebound spin, it is imperative to understand how spin is generated. Therefore, the FE model was used to determine how spin is generated during an oblique impact. An impact close to the GSC with an inbound velocity of 28 ms, angle of 23° and no initial spin, was selected for analysis (Figure 5.17, page 154). An impact with no initial spin was selected to allow the velocity of a node (*point*) at the top and bottom of the ball to be traced throughout the impact (Figure 8.29b). Prior to impact, the velocity at the two points was equal to the COM velocity of the ball. From the start of contact to approximately 2 ms into the impact, the top of the ball accelerated, whilst the bottom decelerated. During this period the topspin of the ball increased from 0 to a maximum of approximately 250 rad·s⁻¹ (Figure 8.29c). The horizontal velocity of the bottom of the ball then remained at approximately 1 m·s⁻¹, until around 3.5 ms into the impact. This indicates that the ball was 'gripping' the string-bed, as suggested by Cross (2003) (Figure 2.6, page 22). During the period from 2-3.5 ms, the top of the ball decelerated, but

was travelling faster than the bottom. This indicates that the ball was deforming forwards and storing energy, which was also in agreement with Cross (2003). The peak in the horizontal force and velocity of the top of the ball at approximately 3.7 ms indicates the release of the stored energy. Once the ball lost its 'grip' with the string-bed there was no further change in the horizontal force, COM velocity or spin. This indicates that the ball was rolling off the string-bed.

| T = 0 ms | T = 0.9 ms | T = 1.8 ms | T = 2.7 ms | T = 3.6 ms | T = 4.5 ms |
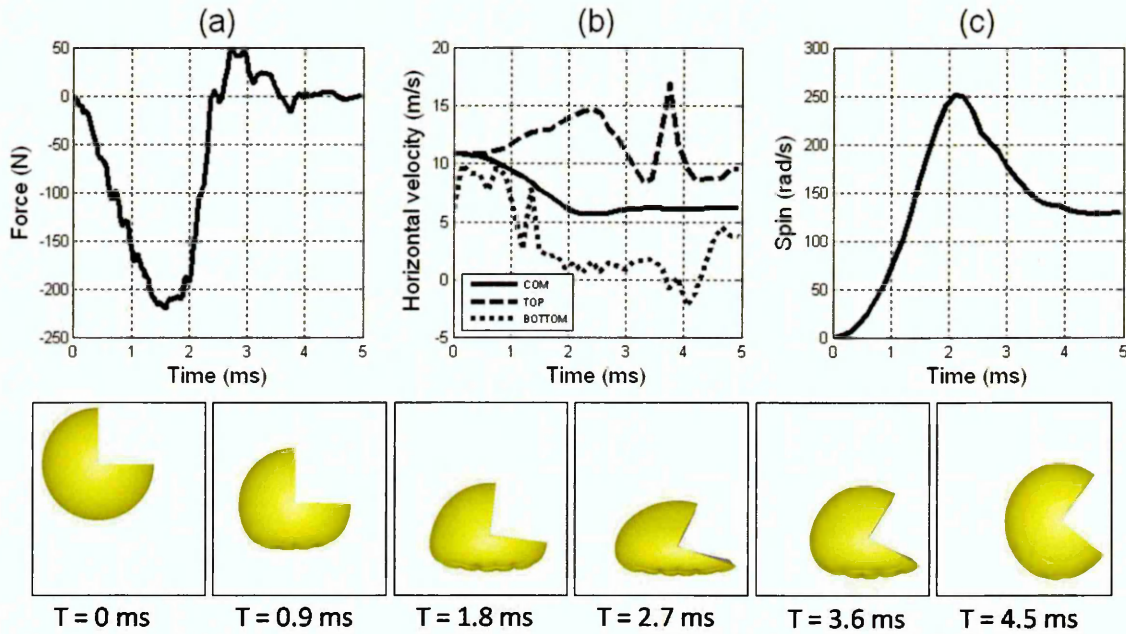
Figure 8.29 Spin generation for an impact close the GSC of a freely suspended racket, with an inbound velocity of 28 m·s⁻¹, angle of 23° and zero spin.

Figure 8.30 shows the horizontal force, horizontal velocity, topspin and the horizontal displacement of the racket tip and COM throughout the impact at the tip of the stiff and flexible racket. The horizontal contact force was very similar for both rackets, although it was slightly larger at approximately 2.5 ms for the flexible racket (Figure 8.30a). The horizontal velocity of the ball was also slightly higher for the flexible racket from approximately 2.5 ms (Figure 8.30b), while the topspin throughout the impact was essentially the same for both rackets (Figure 8.30c). The horizontal displacement of the tip of both rackets was also very similar, up until approximately 2 ms into the impact (Figure 8.30d). The horizontal COM displacement was virtually identical between the racket with

high structural stiffness and the racket with low structural stiffness (Figure 8.30e). This implies that both rackets were translating horizontally at the same speed throughout the impact. This means that the impacts on both rackets were effectively identical up until approximately 2 ms, hence the balls had the same horizontal velocity and topspin. The horizontal displacement of the tip of the racket with low structural stiffness was larger in the latter half of the impact. This indicates that after 2 ms, the racket with low structural stiffness had a slightly larger deformation in the horizontal direction, as shown in Figure 8.31, resulting in a slight reduction in the resultant horizontal velocity between the ball and racket. This increased the horizontal contact force between the ball and string-bed (Figure 8.30a), as the ball was 'overspinning' in the second half of the impact. Overspinning is defined as occurring when the ball has a faster rotation than that associated with rolling. The additional force was large enough to provide a very slight increase in the horizontal velocity of the ball, whilst having no notable effect on its topspin. The larger rebound angle of the ball impacting the racket with low structural stiffness (Figure 8.6, page189) was a result of marginally increased horizontal velocity, in combination with a slightly decreased vertical velocity (Figure 8.21b, page 204).
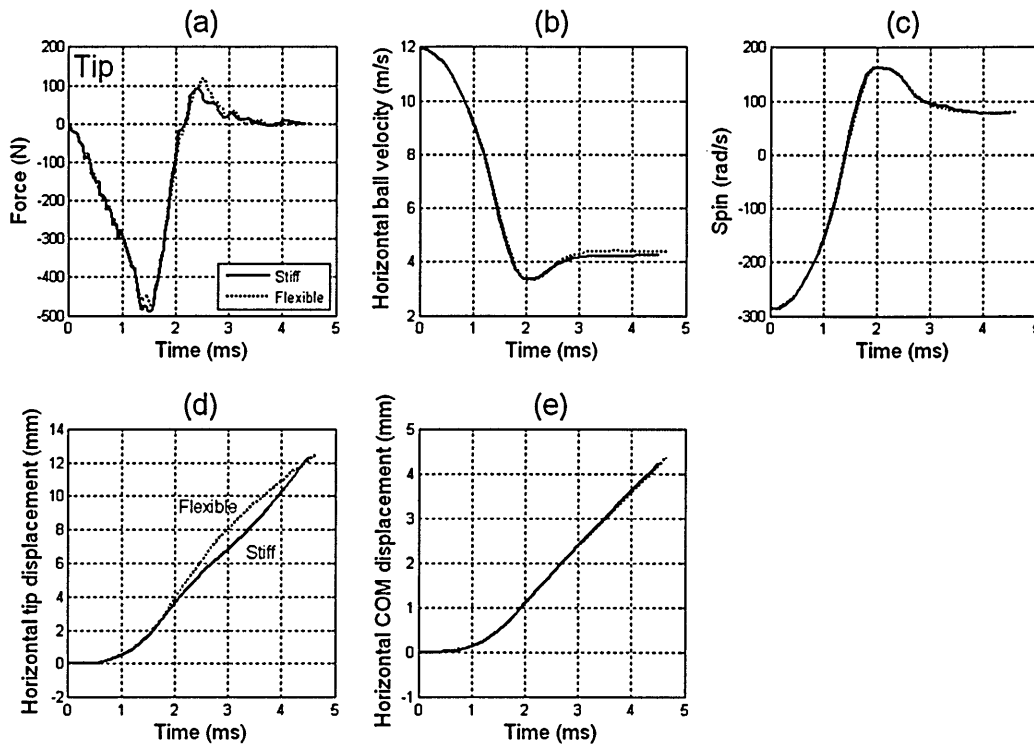
Figure 8.30 Effect of racket stiffness on an impact at the tip at 35 m·s⁻¹ and 20° with 300 rad·s⁻¹ of backspin a) Horizontal force, b) Horizontal ball velocity, c) Topspin, d) Horizontal tip displacement and e) Horizontal COM displacement.
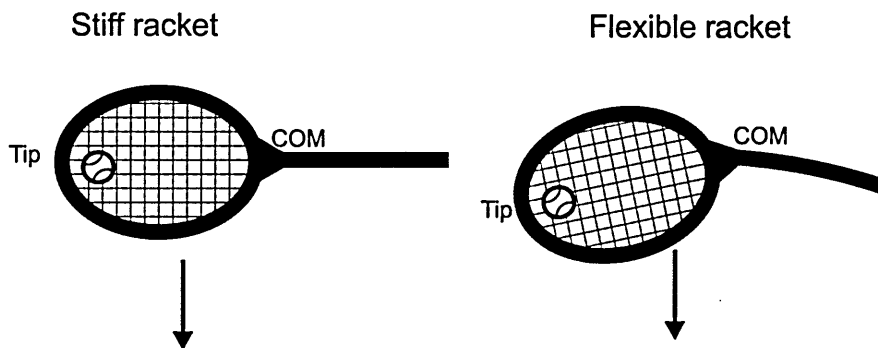
Figure 8.31 The horizontal deformation of a stiff and flexible freely suspended tennis racket for an oblique impact at the tip.

Figure 8.32 shows the affect of stiffness of the racket for an impact at the throat. As with the tip impact, the horizontal COM displacement was effectively the same for both rackets (Figure 8.32e). However, the horizontal displacement of the tip was larger for the stiffer racket from approximately 1 ms into the impact (Figure 8.32e). This indicates the stiffer racket was deforming less in the horizontal direction after 1 ms, as shown in Figure 8.33. It also suggests that the

discrepancy in the deformation of the two rackets initiated earlier, in comparison to the impact at the tip. The increased horizontal deformation of the racket with low structural stiffness reduced the resultant horizontal velocity between the ball and racket. This caused a slightly lower horizontal force in the first half of the impact, which resulted in the ball having a lower horizontal velocity (Figure 8.32b) and topspin (Figure 8.32c) at approximately 2.2 ms, when it started to overspin. The reduced horizontal force acting on the ball resulted in a less pronounced increase in horizontal velocity (Figure 8.32b) and decrease in topspin (Figure 8.32b) during the overspinning stage. As the ball was closer to rolling it started underspinning, causing it to rebound at a lower horizontal velocity and with more topspin, in comparison to the racket with high structural stiffness.
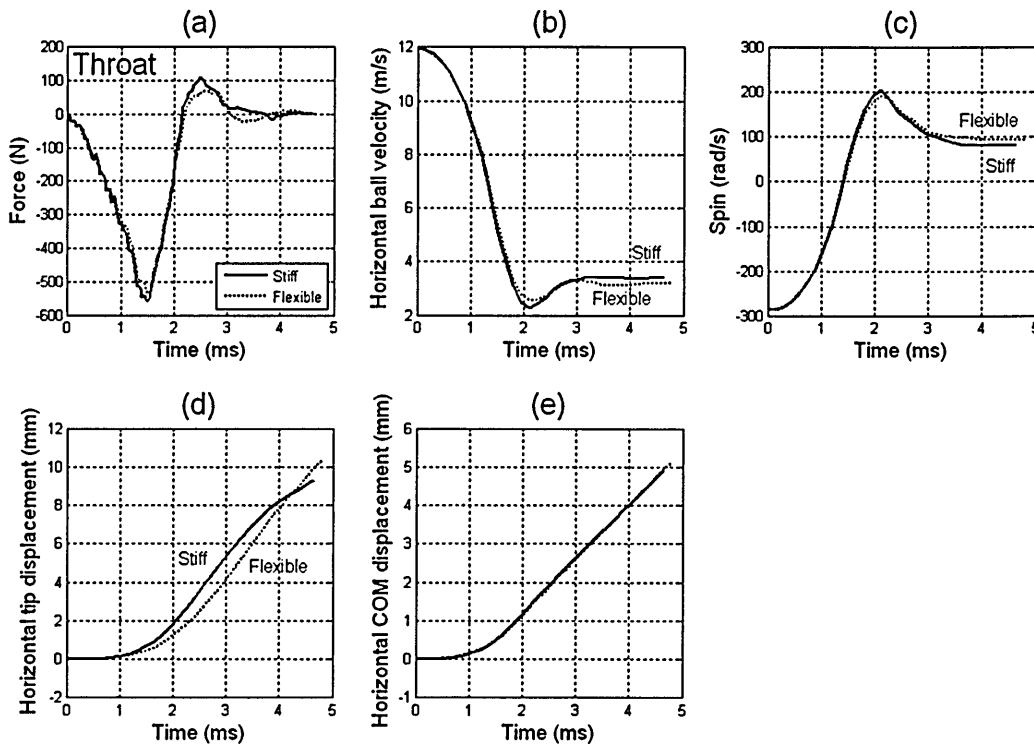
Figure 8.32 Effect of racket stiffness on an impact at the throat at 35 $m \cdot s^{-1}$ and 20° with 300 $rad \cdot s^{-1}$ of backspin a) Horizontal force, b) Horizontal ball velocity, c) Topspin, d) Horizontal tip displacement and e) Horizontal COM displacement.
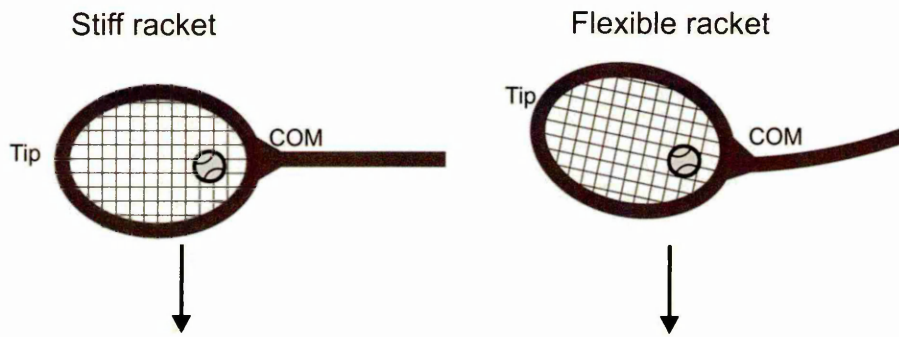
Figure 8.33 The horizontal deformation of a stiff and flexible freely suspended tennis racket for an oblique impact at the throat.

Figure 8.34 shows the effect of racket mass on the horizontal rebound velocity and topspin of the ball, for an impact at the tip. The COM (Figure 8.34e) and tip (Figure 8.34d) displacement was larger for the lighter racket, from approximately 1 ms to the end of the impact. This indicates that the lighter racket was translating and rotating about its COM. Therefore, the resultant horizontal velocity between the ball and racket was lower for the lighter racket. This caused the ball impacting the lighter racket to start overspinning at a lower velocity (Figure 8.34b) and spin rate (Figure 8.34c). Therefore, the ball rebounded from the lighter racket with slightly less topspin (Figure 8.34c) and slightly more horizontal velocity (Figure 8.34b). The increased horizontal rebound velocity (Figure 8.34b), coupled with the lower vertical rebound velocity (Figure 8.30b, page 212) caused the considerably larger rebound angle for impacts on the light racket (Figure 8.12, page 195).
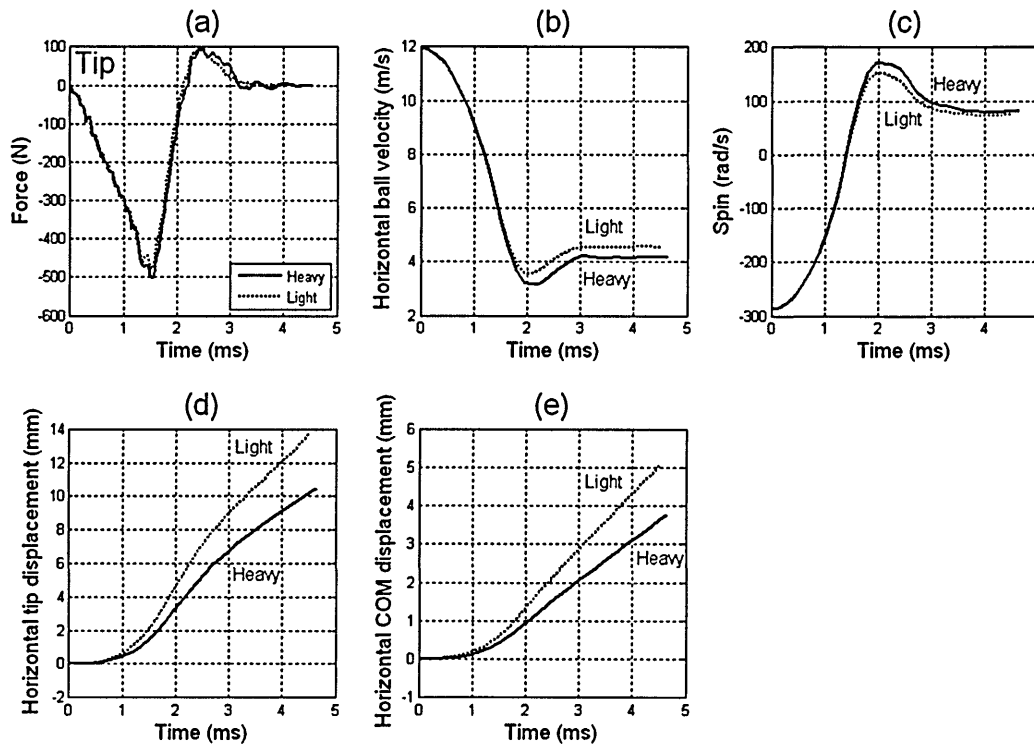
Figure 8.34 Effect of racket mass on an impact at the tip at 35 m·s⁻¹ and 20° with 300 rad·s⁻¹ of backspin a) Horizontal force, b) Horizontal ball velocity, c) Topspin, d) Horizontal tip displacement and e) Horizontal COM displacement.

For the impact at the throat, the horizontal displacement of the COM (Figure 8.35e) and tip (Figure 8.35d) were considrably larger for the lighter racket. This indicates that the lighter racket was displacing and rotating more about its COM. Hence, the ball impacting the lighter racket started overspinning at a lower horizontal velocity (Figure 8.35b) and spin rate (Figure 8.35c). This caused the ball impacting the lighter racket to rebound with slightly less topspin (Figure 8.35c) and more horizontal velocity (Figure 8.35b), as with the impact at the tip. However, the mass of the racket had less influence on the rebound velocity and spin of the ball, in comparison to the impact at the tip. This is because the impact was closer to the COM causing the racket to rotate less.
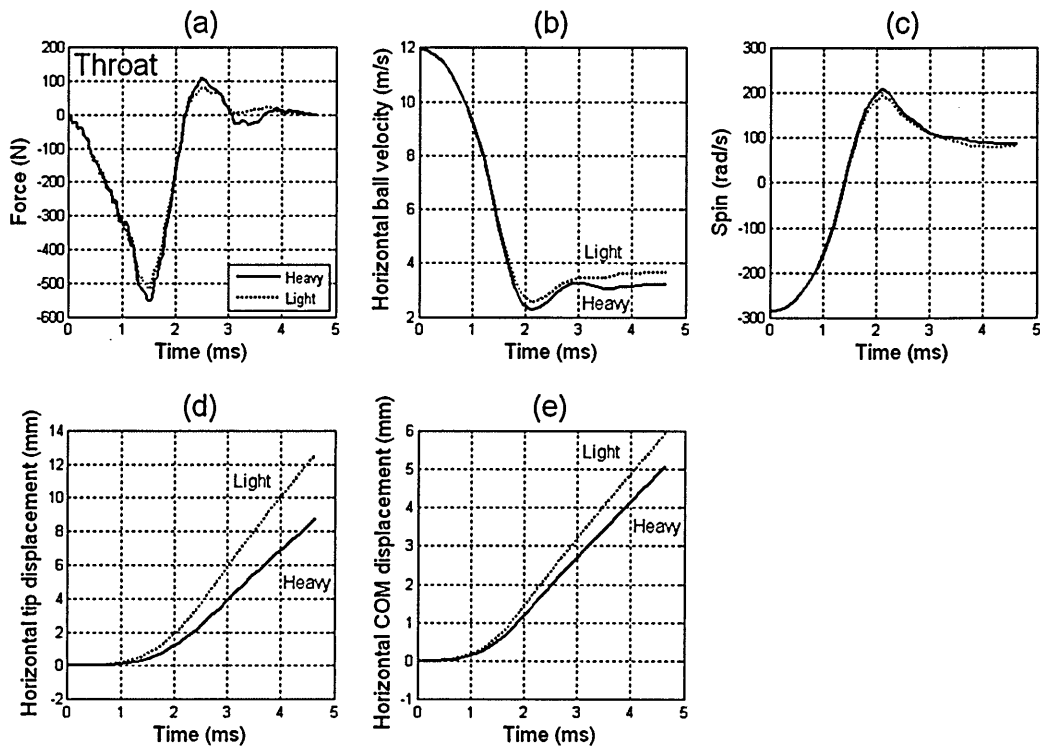
Figure 8.35 Effect of racket mass on an impact at the throat at 35 m·s⁻¹ and 20° with 300 rad·s⁻¹ of backspin a) Horizontal force, b) Horizontal ball velocity, c) Topspin, d) Horizontal tip displacement and e) Horizontal COM displacement.

For the impact at the tip, the horizontal COM displacement was very slightly lower for the head-light racket (Figure 8.36e); whilst the horizontal tip displacement was considerably larger (Figure 8.36d). This indicates that the head-light racket was translating slightly less and rotating more about its COM. The extra rotation decreased the resultant horizontal velocity between the ball and racket. This caused the ball to overspin at a lower horizontal velocity (Figure 8.36b) and spin rate (Figure 8.36c) enabling the ball to rebound with more horizontal velocity (Figure 8.36b) and very slightly less spin (Figure 8.36c). The effect is comparable to increasing the mass of the racket (Figure 8.35, page 216). The combination of increased horizontal velocity (Figure 8.36b) and decreased vertical velocity (Figure 8.27b, page 208) resulted in the ball rebounding at a larger angle (Figure 8.17, page 200).
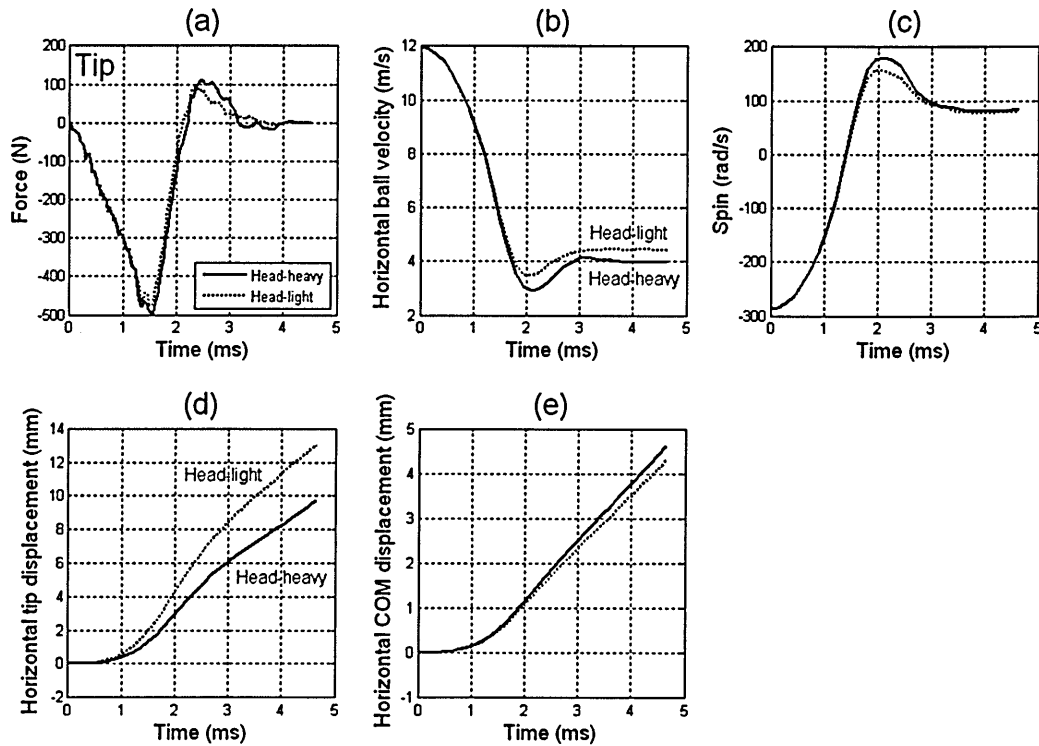
Figure 8.36 Effect of racket balance point on an impact at the tip at 35 m·s⁻¹ and 20° with 300 rad·s⁻¹ of backspin a) Horizontal force, b) Horizontal ball velocity, c) Topspin, d) Horizontal tip displacement and e) Horizontal COM displacement.

For the impact at the throat, the COM displacement (Figure 8.37d) was slightly smaller for the head-light racket, while the tip displacement (Figure 8.37d) was considerably larger. This reduced the resultant horizontal velocity between the ball and racket, causing an increase in horizontal velocity (Figure 8.37b) and topspin (Figure 8.37c). This was comparable to the impact at the tip, but the effect was reduced as the impact was closer to the COM for both rackets.
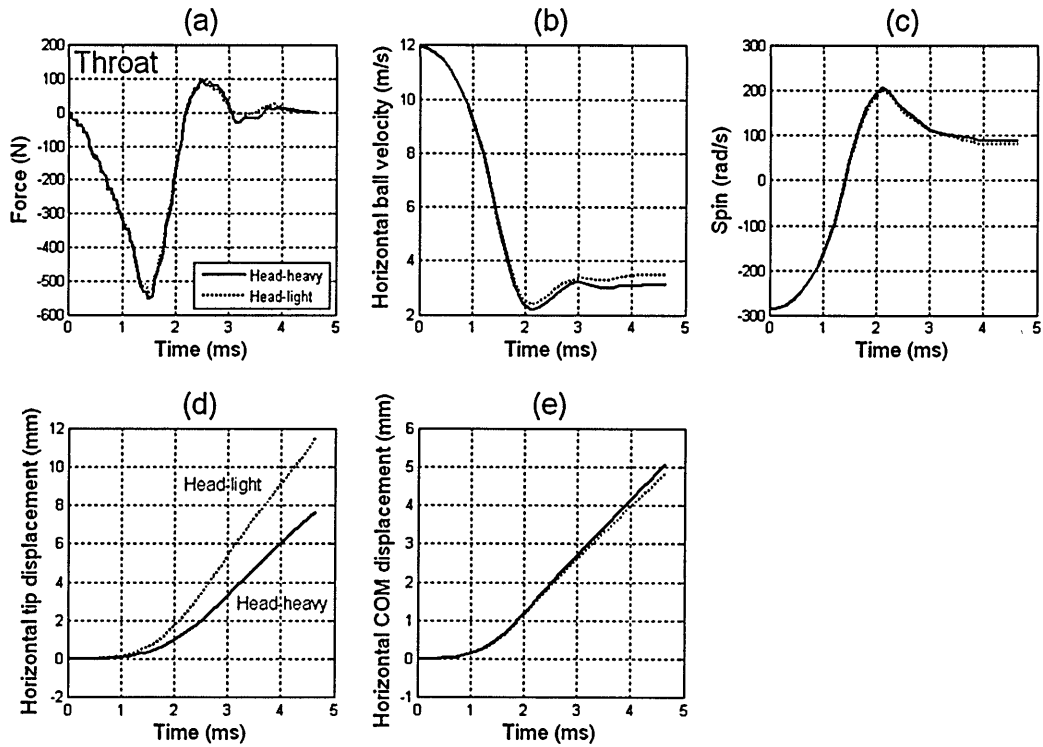
Figure 8.37 Effect of racket balance point on an impact at the throat at 35 m·s⁻¹ and 20° with 300 rad·s⁻¹ of backspin a) Horizontal force, b) Horizontal ball velocity, c) Topspin, d) Horizontal tip displacement and e) Horizontal COM displacement.

As previously mentioned, the impacts offset from the long axis of the string-bed were not analysed in detail. This is because the model consistently under-predicted the rebound spin of the ball, in comparison to player testing data (Figure 7.6, page 178). The reason for the under prediction is likely to be because the players were applying a grip to the handle, and hence reducing the rotation of the racket about its long axis. The effects of racket rotation will now be discussed. The resultant rebound velocity was lower for the impacts offset from the long axis of the string-bed for all the rackets. This is because energy was 'wasted' in rotating the racket about its long axis. The rebound spin was also lower for the off-centre impacts as a result of the rotation of the racket. Figure 8.38 shows a comparison between a centre and off-centre impact. Assuming no or little rotation for a centre impact, the horizontal component of the balls velocity will be parallel to the string-bed. This will maximise the horizontal traction force acting on the bottom of the ball and result in the highest rebound topspin. The off-centre impact caused the racket to rotate, meaning the horizontal velocity of the ball was no longer parallel with the string-bed. This

218

reduced the horizontal force acting on the bottom of the ball and hence the rebound topspin was lower.

Centre impact   Off-centre impact
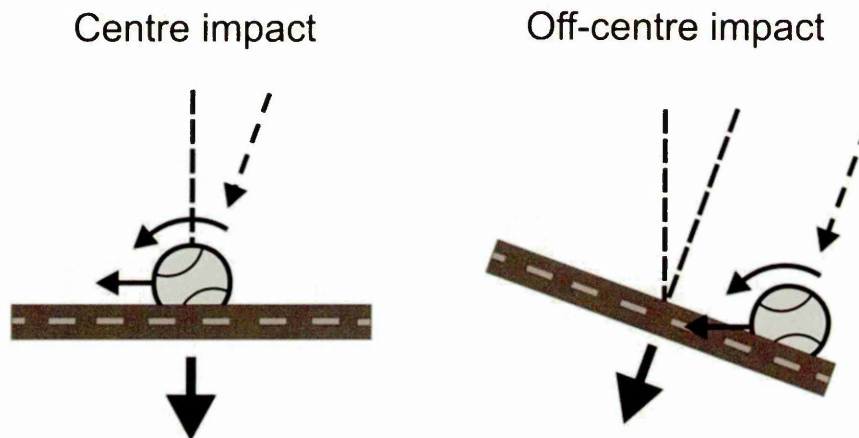
Figure 8.38 Diagram showing a centre and off-centre impact on a freely suspended racket.

8.4.3.   Summary of the effect of racket parameters and implications to design

It is widely accepted that elite tennis players wish to maximise the rebound velocity and topspin of the ball, when performing the majority of shots. Structural stiffness has no influence on swingweight. Increasing the structural stiffness of a racket will always increase the rebound velocity of the ball (Haake *et al.* 2007). However, the influence of the structural stiffness of a racket, on the rebound velocity of the ball is relatively small. The effect of structural stiffness on the rebound topspin of the ball is complex, as it depends on when the racket starts to deform. However, the rebound topspin of the ball was more consistent for the different impact positions on the stiffer racket. As with rebound velocity, the effect of structural stiffness on topspin was also relatively small. Therefore, the structural stiffness of a tennis racket should be maximised to increase the rebound velocity of the ball and provide more consistent topspin for different impact positions on the string-bed.

Assuming swing speed is independent of swingweight, the rebound velocity and topspin of the ball can be maximised by increasing the mass of a tennis racket or by moving its COM closer to the impact position. This assumption can be considered valid, within reason, for a forehand shot, as the player is unlikely to be swinging the racket as fast as physically possible (Cross, 2001b). However,

this assumption is not valid for a serve, where the maximum pre-impact racket velocity is dependent on swingweight (Mitchell *et al.*, 2000). This indicates that it is not possible to design a tennis racket to achieve both maximum serve velocity and maximum forehand velocity and topspin, although, there are a number of different combinations of racket mass and balance point, which provide the optimum swingweight for maximum serve velocities (Haake *et al.* 2007). These range from a light racket with a balance point closer to the tip, to a heavy racket with a balance point closer to the butt (Haake *et al.* 2007). The exact mass and balance point will depend on the relationship between swingwight and pre-impact racket velocity, for each player.

The results indicate a large decrease in the rebound velocity and topspin of the ball, for impacts offset from the long axis of the racket. This is due to the racket rotating about its long axis. The rotation can be reduced by increasing the twistweight of the racket. An increase in twistweight can be achieved by making the racket wider, adding mass offset from the long axis or a combination of both. The most efficient method of increasing twistweight is to position any additional mass as far from the long axis as possible. Increasing the width of a tennis racket will increase its twistweight without significantly altering the mass and swingweight.

A racket optimised for all-round play is shown in Figure 8.39. The racket has low mass (*approx. 0.26 kg*) and a balance point positioned towards the tip (*approx. 0.327 m from the butt*) to provide the correct swingweight for maximum serve velocity (Haake *et al.*, 2007). The racket is also as wide as possible (0.3175 m) to increase its twistweight and hence maximise ball velocity and topspin for impacts offset from the long axis. The twistweight is maximised without compromising swingweight by making the racket light and adding mass at the widest points, as shown in Figure 8.39. This would also have the benefit of locating the COM closer to the GSC, where elite players typically impact the ball when performing a forehand shot (Choppin *et al.*, 2008). The racket is also as stiff as possible to maximise ball velocity and increase consistency for different impact positions on the string-bed. Figure 8.40 shows that the sections of the racket frame assigned high mass in Figure 8.39 experience relatively large Von Mises stresses, throughout an oblique impact at the GSC. Using

additional material in these regions to increase mass would also have the advantage of increasing stiffness and reducing stress. The current FE model could be modified to allow the adjustment of twistweight and then be used to determine the optimum mass distribution for the racket.
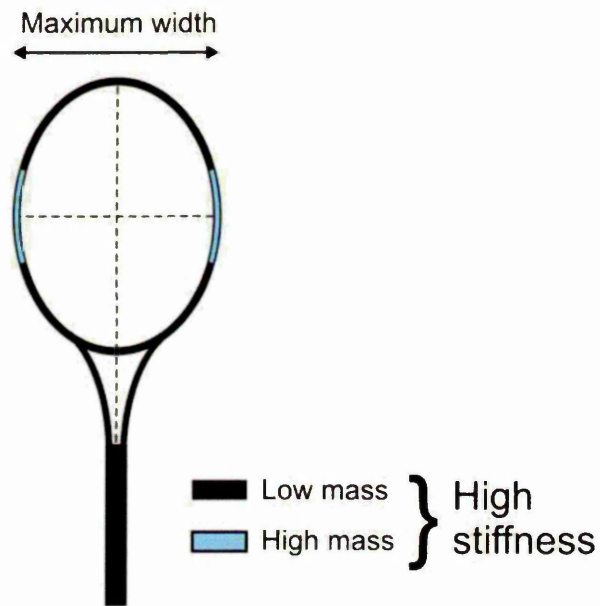
Figure 8.39 Predicted optimised tennis racket design for all round performance
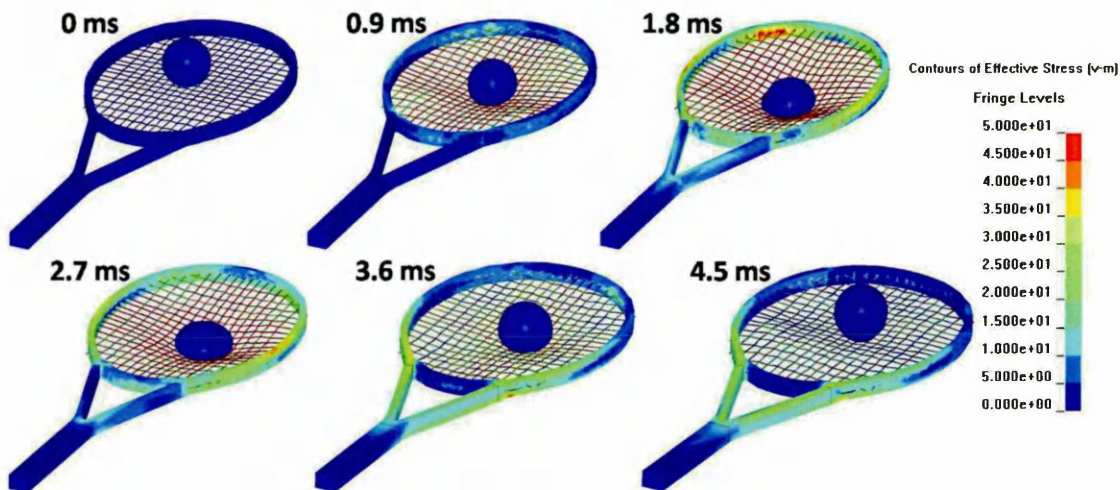
Figure 8.40 Von Mises stress for an impact between a ball and freely suspended racket with an inbound velocity of 35 m·s^{-1}, an angle of 20° and a backspin of 300 rad·s^{-1}. The racket has a mass of 0.348 kg, a natural frequency of 143 Hz and a balance point 0.396 m from the butt.

The following points should be taken into account when designing a tennis racket;

1. The structural stiffness of a tennis racket should be maximised to increase rebound velocity.

2. The pre-impact swing speed of a tennis racket is dependent on its swingweight when undertaking a serve (Mitchell *et al.,* 2000).

3. There are a range of different combinations of racket mass and balance point, which can be utilised to achieve maximum serve speed (Haake *et al.,* 2007).

4. A heavy racket with a balance point as close as possible to the impact point will provide maximum rebound velocity and topspin for a forehand shot.

5. Increasing the twistweight of a tennis racket will provide higher rebound velocity and topspin for impacts offset from the long axis.

8.5. Chapter summary

The FE model was used to determine the influence of racket structural stiffness, mass and balance point on a typical forehand shot. Making the racket stiffer slightly increased the rebound velocity of the ball, although the effect was marginal. Increasing the mass of the racket and moving the balance point closer to the tip both increased the rebound velocity and topspin of the ball.

9. Conclusions

9.1. Introduction

This final chapter summarises all the research that has been undertaken in this project. The chapter includes a summary of the validation of the ball, string-bed and freely suspended racket models. The applications of the complete model as a tool which can be used for both racket design and analysing the influence of technology on the game of tennis, are also discussed. Finally, there is a section on areas of possible future research.

9.2. Summary of research

9.2.1.   Ball model

An FE model of a pressurised tennis ball, consisting of an airbag, rubber core and felt cover, was produced in Ansys/LS-DYNA 10.0. The model was validated by comparing FE simulations of rubber cores and tennis balls, impacting normal to a rigid surface with experimental data. The laboratory investigation was undertaken by firing balls and cores from an air cannon onto a force plate, at a range of velocities between 5 and 30 m·s^{-1}. Force plots and contact times were obtained from a force plate, whilst the inbound and rebound velocities were recorded using a set of light gates. A *Phantom v4.2* high-speed video camera was used to measure the maximum deformation of the balls and cores. The FE model was in very good agreement with the experimental data, for the entire range of impacts. This model supersedes previous FE models as the separate parts were independently validated against experimental data. The FE model of a tennis ball was updated to simulate the extreme playing temperatures of 10 and 40°C and validated against experimental data obtained inside a climate chamber. The rebound velocity of a pressurised tennis ball was found to increase with temperature. Furthermore, the density of the air will decrease with increasing temperature causing a reduction in the drag force acting on the ball during flight. Therefore, the speed of the game is likely to be higher when the temperature is 40°C, in comparison to 10°C. Further research would need to be undertaken to provide more evidence for this hypothesis.

9.2.2.   Head-clamped racket model

An FE model of a string-bed was produced and validated against experimental data. The experiment was undertaken by firing balls from a modified BOLA onto a head-clamped racket. Impacts were undertaken at inbound angles in the range from 20-60° with inbound velocities in the range of 20-30 m·s^{-1}, whilst backspin was increased from 0-600 rad·s^{-1}. The impacts were recorded using a *Phantom v4.2* high-speed camera and the footage was used to calculate inbound and rebound velocities, angles and spin rates. The FE model was in good agreement with the experimental data for the entire range of impacts. The model was then developed to include a racket frame. The main difference between the validation of the head-clamped racket model and the string-bed model was that impacts were simulated at four nominal locations on the string-bed. The head-clamped racket model was in good agreement with the experimental data and the string-bed model. It was concluded that the ball over-spins at around the mid-point of an impact with a head-clamped racket when incident obliquely with backspin. This was in agreement with previous authors (Cross, 2003; Goodwill and Haake, 2004a). Reducing ball to string friction in the FE model had no notable effect on rebound velocity or angle but it increased topspin considerably. Increasing the string-bed stiffness of the head-clamped racket model, slightly reduced rebound velocity while having no notable effect on angle or spin. This model is more advanced that previous FE models as the individual strings are allowed to move independently. However, the results obtained cannot be related directly to play as the method used to clamp the racket is not representative of a player's grip.

9.2.3.   Freely suspended racket model

An FE model of a freely suspended tennis racket was constructed and validated against experimental data. The experimental data was obtained by projecting balls from a BOLA onto a freely suspended tennis racket. The impacts were recorded using two synchronised *Phantom v4.2* high-speed video cameras and reconstructed in 3D for analysis. Perpendicular impacts were simulated with inbound velocities in the range from 10-40 m·s^{-1} at four nominal impact locations on the string-bed. The model was in good agreement with the experimental data. The rebound velocity of the ball was highest at the throat

and lowest at the tip as found by previous authors (Brody, 1997a; Goodwill and Haake, 2001 & 2003). Increasing the structural stiffness of the racket raised the rebound velocity of the ball for impacts at throat, while having little effect at other locations on the string-bed, in agreement with Goodwill and Haake (2003). However, it was concluded that using a stiffer racket will slightly increase serve velocity. Oblique spinning impacts were simulated with nominal inbound velocities of 20 and 30 m·s^{-1}, a nominal angle of 25° and backspin in the range from -100 to 500 rad·s^{-1}. The model was in relatively good agreement with the experimental data and it was found that the structural stiffness of the racket had no effect on the rebound characteristics of the ball for impacts close to the geometric string-bed centre (GSC). As with the head-clamped racket model, the ball was found to be over-spinning during the oblique impacts. This is the first model with the capability of accurately simulating oblique spinning impacts, at different locations on the string-bed of a freely suspended tennis racket.

9.2.4.   Parametric modelling program

A parametric modelling program was produced to allow FE simulations with different parameters to be set-up efficiently. Parameters which can be adjusted include the inbound trajectory of the ball, impact location on the string-bed, string tension and the material properties of the strings and racket. The parametric modelling program has been designed so it can be used without an in-depth knowledge of the FE models. This was one of the main objectives of the project.

9.2.5.   Applications of the model

The FE model was found to be in relatively good agreement with ball to racket impact data obtained from testing elite players, which had been analysed in 3D. This indicates that the model can be used to determine the effect of altering different racket parameters, in relation to a typical tennis shot. Following the comparisons between the model and realistic data, the model was used to determine the effect of racket structural stiffness, mass and the position of the balance point, for an impact which was considered to be representative of a typical forehand shot. The investigation was undertaken for a range of impact positions on the string-bed. The structural stiffness of the racket was found to have only a marginal effect on the rebound characteristics of the ball. However,

using a racket with very high structural stiffness is likely to slightly increase the rebound velocity of the ball. Increasing the mass of the racket and moving the balance point closer to the tip both resulted in an increase in the rebound velocity and topspin of the ball. This indicates that a structurally stiff heavy racket, with the centre of mass (COM) at the GSC, will result in the maximum velocity and topspin for a forehand shot. In relation to tennis racket design, a manufacturer should prioritise optimising the mass and mass distribution of the frame well above increasing the structural stiffness. This is the first investigation which has determined the effect of racket structural stiffness, mass and balance point, for oblique spinning impacts at different locations on the string-bed.

9.3. Conclusions

Previous analytical models have been based on experimentally obtained parameters such as, coefficient of restitution (COR) and contact time. The FE models outlined in this thesis are based on parameters which were obtained independently of the validation experiments. The final result was a model, which can be used to accurately predict how individual parameters affect the 3D deformation of the ball, string-bed and racket throughout an impact. As well as adjusting the material properties to determine their influence, it is also possible to model different balls, strings and rackets efficiently by simply obtaining the required data and using it to replace the existing values within the model. For example, a different racket could be simulated using the CAD geometry for the frame and string-bed.

The main conclusions of the study are listed below;

- The rebound velocity of a tennis ball increases with temperature, predominantly because of an increase in the internal pressure of the ball.

- String-bed stiffness slightly affects rebound velocity and hence angle, while having no notable influence on spin. This is because string-bed stiffness determines the velocity of the ball in a direction perpendicular to the string-bed while having little influence on the displacement of the ball across the strings.

- Decreasing ball to string friction increases rebound topspin, because there is a smaller friction force acting to reduce the topspin of the ball when it is 'over-spinning' in the latter half of the impact.

- Increasing the mass of a racket will increase the rebound velocity and topspin of the ball for an oblique impact, because the racket will translate and rotate less during the impact.

- Moving the balance point of a racket as close as possible to the impact point will increase the rebound velocity and spin of the ball for an oblique impact, because the racket will rotate less during the impact.

- Increasing the structural stiffness of a racket will increase the rebound velocity of the ball, because less energy from the collision will go into deforming the racket.

The main advantages of the FE model detailed in this thesis over current published models are;

- The model has been extensively validated against both experimental and elite player testing data.

- The model has the ability to accurately simulate oblique spinning impacts at different locations on the string-bed of a freely suspended racket.

9.4. Future research

This investigation has highlighted a number of possibilities for future research. This final section discusses possible areas of further study.

9.4.1.   Ball model

The ball model used in this investigation was only validated for perpendicular impacts on a rigid surface. The next logical step would be to validate the model for oblique spinning impacts, as these are far more representative of play. This will aid the researcher in understanding the behaviour of a ball throughout an oblique impact; in particular, the 3D deformation of the ball, which has proved difficult to simulate using analytical models. The model could then be used to determine further insight into the influence of different parameters, such as the material properties and internal pressure of the ball. Through experimental testing of the COF and material properties, the model could be extended to include the different surfaces that tennis is played on.

227

The viscoelastic properties of the rubber core were estimated in an iterative process, until the model was in good agreement with experimental data. This makes it difficult to determine precisely how changing the properties of the rubber would influence the characteristics of the ball. Ideally, the rate-dependent properties of the rubber should be obtained through materials testing. The model could then be used more effectively as a design tool. The FE model could potentially be used to aid in the design of a ball with consistent rebound characteristics across the entire range of temperatures at which tennis is played.

9.4.2.   Freely suspended racket model

The freely suspended racket model was only validated for oblique impacts which were close to the GSC. As players do not always contact the ball at the GSC (Choppin et al. 2007a, 2007b & 2008), the next logical step would be to validate the model for oblique impacts at different locations on the string-bed. Further research could also be undertaken to determine a method of restraining the handle, which is more representative of a player's grip.

The FE model slightly underestimated the rebound angle of the ball, in comparison to the experimental data, when simulating oblique impacts. This indicates that the structural stiffness of the string-bed may be too low (Goodwill and Haake, 2004b). Further material testing was undertaken on the tennis strings, using the method developed by Cross *et al.* (2000) (Section 2.3.3, page 15) (Appendix D). It was thought that the frequency response of the s-type load cell may have resulted in an under prediction of the impact force and hence dynamic stiffness. Therefore, the s-type load cell was replaced with a **Kistler** piezoelectric force sensor. The piezoelectric force sensor produced results which were very similar to those obtained using an s-type load cell. However, it was concluded that the strain rate in all of the tests may have been too low, in comparison to an impact between a tennis ball and racket. Further research could involve determining the relationship between dynamic stiffness and strain rate for tennis strings. This could be undertaken using the impact rig (Appendix D) or possibly a dynamic material tester.

The oblique impacts in this thesis were all parallel to a plane, which was normal to the string-bed and passed through its short axis. It is predicted that in match

play, many impacts will not involve the ball travelling parallel to this plane. Therefore, the FE model should be validated for oblique spinning impacts, which are at an angle to a plane through the short axis of the string-bed. This will ensure the model is accurate at simulating a wide range of tennis shots.

In the current model, the racket frame was separated into three parts (*head, handle and throat*), which were each assigned individual material properties. The material model used for the three parts was MAT_ELASTIC. The material model could be updated to one capable of simulating composite lay-ups and the racket could be separated into more parts. This would allow more control over the structural stiffness and mass distribution of the racket. In-depth testing would be required to determine the properties of the composite materials used in a tennis racket.

The FE model used in this investigation was based on an ITF *Carbon Fibre* racket. This racket was designed for laboratory testing and is not used during competitive play. The next logical step would be to simulate a number of different racket geometries. This could include rackets from different eras, in particular the 1870's and 1970's, as well as those currently in production. A methodology for getting the racket geometry into Ansys/LS-DYNA would need to be developed.

The intention of this project was to create a tool for designing and developing the next generation of tennis rackets. The next logical step would be to test and implement the tool into an actual design process. This would require collaboration with a racket manufacturer and would result in a more accurate validation of the model, as well as furthering scientific understanding. The model could be used to predict the performance of a new design of tennis racket. The FE model could then be validated against experimental data obtained from a prototype of the new design, to determine the accuracy of its predictions.

9.4.3.   Analytical modelling

In this project, FE models have been used to enhance the understanding of tennis ball impacts on both a rigid surface and a freely suspended racket. FE models have the disadvantage that it takes a relatively long time to run simulations and obtain results. Analytical models can be solved almost instantly

using software such as Matlab, making them more suitable for use in predictive programs, such as *Tennis GUT* (Haake *et al.* 2007). The results and findings from the FE models could be used to produce analytical models which are more advanced than those which are currently available.

9.4.4.   Parametric program

A parametric program was produced to enable FE simulations to be undertaken with different parameters. The program could be developed alongside the FE models. Currently the inbound characteristics of the ball can be adjusted, as well as various properties of the strings and racket. The current ball model is only relevant for an impact on a rigid surface at room temperature. The program could be updated to include impacts on various court surfaces at different temperatures. As the material properties of different rackets and strings are obtained they could be implemented into the program. The number of templates could also be expanded to include different rackets.

In order to provide an effective design tool, the FE model should be used to analyse player's shots. A methodology could be developed to provide a streamlined process for obtaining player testing data, running FE simulations with the same parameters and analysing the results. This could include determining the effects of undertaking the same shot with a different racket. Ideally, the parametric program should be updated to specifically interpret player testing data. In order for the parametric program to be used as a really effective tool, it should be updated to automatically read in and display the results of FE simulations.

References

Babolat (2009) Babolat *[online]*, last accessed on 01/03 2009 at URL: www.babolat.com/#/tennis/us/products/355

Becker, A. A. (2004). *An introductory guide to finite element analysis.* 1st ed., Proffessional Engineering Publishing.

Beisen, E. & Smith, L. (2007) Describing the plastic deformation of aluminium softball bats. *Sports Engineering,* **10** (4), 185-194.

BOLA (2009) BOLA *[online]*, last accessed on 01/03 2009 at URL: www.bola.co.uk

Bouguet, J. (2008) Camera calibration toolbox for matlab *[online]*, last accessed on 01/03 2008 at URL: www.vision.caltech.edu/bouguetj/calib_doc

Bower, R. and Cross, R. (2005). String tension effects on tennis ball rebound speed and accuracy during playing conditions. *Journal of Sports Sciences,* **23** (7), 765-771.

Bridge, N.J. (1998) The way balls bounce. *Physics Education,* **33,** (3), 174-181.

Brody, H (1979) Physics of the tennis racket, *American Journal of Physics,* **47,** (6), 482-487.

Brody, H. (1997a). The physics of tennis 3: The ball-racket interaction. *American Journal of Physics,* **65** (10), 981-987.

Brody, H. (1997b). The influence of racquet technology on tennis strokes. *Tennis Pro,* **Sept/Oct** (1),1997, 10-11.

Brody, H. (1984). That's how the ball bounces. *The Physics Teacher,* **22,** (8), 494-497.

Brody, H. (1987). Models of tennis racket impacts. / (modeles d' impacts sur raquette de tennis.). *International Journal of Sport Biomechanics (Champaign, Ill.),* **3** (3), 293-296.

Brody, H. (1988). Why slow courts give you more time to get to the ball. *TennisPro,* (1), 8-9.

Brody, H. (1990). Predicting the likelihood of tie-breaks. *Tennis Pro,* **47** (1),March-April, 482-487.

Brody, H., Cross, R. and Lindsey, C. (2002). *The Physics and Technology of Tennis.* 1st ed., Racquet Tech Publishing.

Calder, C A, Holmes, J G and Mastny, L L (1987), Static and Dynamic Characteristics of Tennis String Performance. In: *Progs 1987 Sem Conference on Experimental Mechanics*, Houston, USA, pp 613-616

Calder, C. and Sandmeyer, B. (1997). Modelling the bat-ball impact using finite element analysis. In: *Proceedings of the Society for Experimental Mechanics,* 1997. 158-159.

Capel-Davies, J. (2007) Velocity dependence of the surface pace rating of tennis courts. *Tennis Science and Technology 3,* **1,** International Tennis Federation, London, 65-72.

Chadwick, S.G. & Haake, S. (2000) Methods to determine the aerodynamic forces acting on tennis balls in flight. *Tennis Science and Technology,* **1,** Blackwell Science, London, 127-134.

Choppin, S. (2008) Modelling of tennis racket impacts in 3D using elite players. *The Department of Mechanical Engineering,* The University of Sheffield, Sheffield, pp. 320.

Choppin, S., Goodwill, S., Haake, S. & Miller, S. (2007a) 3D player testing at the Wimbledon Qualifing Tournament. *Tennis Science and Technology 3,* **1,** International Tennis Federation, London, 333-340.

Choppin, S., Goodwill, S., Haake, S. & Miller, S. (2007b) 3D player testing results from the Wimbledon Qualifing Tournament. *Tennis Science and Technology 3,* **1,** International Tennis Federation, London, 341-348.

Choppin, S., Goodwill, S., Haake, S. & Miller, S. (2008) Ball and Racket Movements Recorded at the 2006 Wimbledon Qualifying Tournament. *The Engineering of Sport 7,* **1,** Springer, France, 563-569.

Cross, R (1998) The sweet spots of a tennis racket, *Sports Engineering,* **1,** 63-78.

Cross (1999). Dynamic properties of tennis balls. *Sports Engineering,* **2** (1), 23-33.

Cross, R (2000a), Dynamic Properties of Tennis Strings. In: *Tennis Science and Technology,* Blackwell Science, London, pp 119-126.

Cross, R. (2000b). Effects of friction between the ball and strings in tennis. *Sports Engineering,* **3** (1), 85-97.

Cross, R. (2000c) Dynamics of the collision between a tennis ball and a tennis racket. *Tennis Science and Technology,* **1,** Blackwell Science, London, 67-74.

Cross, R. (2001a) Stretch tests on strings. *Racket Tech,* **September,** 12-19.

Cross, R (2001b) Customising a Tennis Racket By Adding Weights, *Sports Engineering,* **4** (4), 1-14.

Cross, R. (2002). Grip-slip behaviour of a bouncing ball. *American journal of physics,* **70** (11), 1093-1102.

Cross, R. (2003) Oblique impact of a tennis ball on the strings of a tennis racket. *Sports Engineering,* **6** (1), 235-254.

Cross, R. and Lindsey, C. (2005). *Technical Tennis.* 1st ed., Racquet Tech Publishing.

Cross, R., Lindsey, C. and Andruczyk, D. (2000). Laboratory testing of tennis strings. *Sports Engineering,* **3** (4), 219-230.

Dignall, R. J. and S. J. Haake (2000). Analytical modelling of the impact of tennis balls on court surfaces. In: HAAKE, S. j. and COE, A. O. (eds.). *Tennis Science and Technology.* First ed., Blackwell science Ltd, 155-162.

Dignall, R.J., Goodwill, S. & Haake, S. (2004) Tennis GUT - Modelling the game. *The Engineering of Sport 5,* **2,** International Sports Engineering Association, California, 382-388.

Downing, M. (2007a) A comparison of static and dynamic tennis ball stiffness. *Tennis Science and Technology 3,* **1,** International Tennis Federation, London, 31-40.

Downing, M. (2007b) The effects of climate changes on the properties of tennis balls. *Tennis Science and Technology 3,* **1,** 49-55.

Downing, M. (2007c) The effect of temperature on the court pace rating of tennis surfaces. *Tennis Science and Technology 3,* **1,** International Tennis Federation, London, 81-86.

Goodwill, S R (2002) The dynamics of tennis ball impacts on tennis rackets. *The Department of Mechanical Engineering,* The University of Sheffield, Sheffield, pp. 338.

Goodwill, S R and Haake, S J (2002), Why were 'Spaghetti String' Rackets Banned in the Game of Tennis? In: *4th International Conference on Sports Engineering*, Blackwell Science, Kyoto, Japan.

Goodwill, S., Capel-Davies, J., Haake, S. & Miller, S. (2007) Ball spin generation of elite players during match play. *Tennis Science and Technology 3*, **1,** International Tennis Federation, London, 349-356.

Goodwill, S., Haake, S. & Miller, S. (2007) Validation of the ITF racket power machine. *Tennis Science and Technology 3*, **1,** International Tennis Federation, London, 113-120.

Goodwill, S. R. and Haake, S. J. (2001). Spring damper model of an impact between a tennis ball and racket. *Proceedings of the Institution of Mechanical Engineers, part C: Journal of Mechanical Engineering Science,* **215** (11), 1331-1341.

Goodwill, S. & Haake, S. (2003) Modelling of an impact between a tennis ball and racket. *Tennis Science and Technology 2,* **1,** International Tennis Federation, London, 79-86.

Goodwill, S., Haake, S. & Chin, S. (2004) Aerodynamics of spinning and non-spinning tennis balls. *Journal of Wind Engineering and Industrial Aerodynamics,* **92** (11), 935-958.

Goodwill, S. R. and Haake, S. J. (2004a). Ball spin generation for oblique impacts with a tennis racket. *Experimental Mechanics,* **44** (2), 195-206.

Goodwill, S R and Haake, S J (2004b), Effect of String Tension on the Impact between a Tennis Ball and Racket. In: *The Engineering of Sport 5*, International Sports Engineering Association, California, pp 3-9.

Goodwill, S. R., Kirk, R. and Haake, S. J. (2005). Experimental and finite element analysis of a tennis ball impact on a rigid surface. *Sports Engineering,* **8** (3), 145-158.

Gu, Y. & Li, J. (2007) Dynamic simulation of tennis racket and string. *International Journal of Sports Science and Engineering,* **1** (1), Blackwell Science, London, 55-60.

Haake, S., Allen, T., Choppin, S. & Goodwill, S. (2007) The evolution of the tennis racket and its effect on serve speed. *Tennis Science and Technology 3,* **1,** International Tennis Federation, London, 257-271.

Haake, S. J., Carre, M. J. and Goodwill, S. R. (2003a) The dynamic impact characteristics of tennis balls with tennis rackets. *Journal of Sports Sciences,* **21** (10), 839-850.

Haake, S., Carre, M. & Goodwill, S. (2003b) Modelling of oblique impacts of tennis ball impacts on tennis surfaces. *Tennis Science and Technology 2,* **1,** International Tennis Federation, London, 133-137.

Haake, S.J., Chadwick, S.G., Dignall, R.J., Goodwill, S. & Rose, P. (2000) Engineering tennis - slowing the game down. *Sports engineering,* **3** (2), 131-143.

Haake, S.J., Carre, M.J., Kirk, R. & Goodwill, S.R. (2005) Oblique impact of thick walled pressurized spheres as used in tennis. *Proceedings of the Institution of Mechanical Engineers C, Journal of Mechanical Engineering Science,* **219** (11), 1179-1189.

Haines, R (1993) The sporting use of polymers, *Shell petrochemicals,* 22

Haines, R.C., Curtis, M.E., Mullaney, F.M. & Ramsden, G. (1983) The design, development and manufacture of a new and unique tennis racket. *ARCHIVE:*

Proceedings of the Institution of Mechanical Engineers, Part B: Management and Engineering Manufacture 1983-1988 (vols 197-202), **197,** 79.

Head, H (1975) Oversize Tennis Racket, *United States Patent 3,999,756*

Holmes, G. and Bell, M. J. (1986) Playing surface hardness and tennis ball rebound resilience. *J. Sports Turf Res. Inst.,* **62** (1), 207-210.

Hubbard, M. and Stronge, W.,J. (2001). Bounce of hollow balls on flat surfaces. *Sports Engineering,* **4** (2), 49-61.

Ismail, K. & Stronge, B. (2008) Calculated golf ball performance based on measured visco-hyperelastic material properties. *The Engineering of Sport 7,* **1,** Springer, France, 11-18.

ITF TECHNICAL DEPARTMENT, (2009). *International Tennis Federation [online].* Last accessed on 01/03 2009 at URL: www.itftennis.com/technical.

Jenkins, M. (2003). *Materials in Sports Engineering.* 1st ed., Woodhead Publishing Limited.

Jenkins, C. and Calder, C. A. (1990) Transient Analysis of a Tennis Racket Using PC-based Finite Elements and Experimental Techniques, *Experimental Mechanics,* **30** (2), 130-134.

John, V. (2003). *Introduction to engineering materials.* 4th edn. Palgrave Macmillan.

Kanda, Y. Nagao, H. & Naruo T. (2002), Estimation of Tennis Racket Power using Three-Dimensional Finite Element Analysis. In: *The Engineering of Sport 4,* Blackwell Publishing, Kyoto, Japan, pp 207-214.

Kelley, J. Goodwill, S. Capel-Davies, J. & Haake, S. (2008) Ball Spin Generation at the 2007 Wimbledon Qualifying Tournament. *The Engineering of Sport 7,* **1,** Springer, France, 571-578.

Knudson, D.V. & Blackwell, J.R. (2005) Variability of impact kinematics and margin for error in tennis forehand of advanced players. *Sports Engineering,* **8,** 75-80.

Kotze, J. Mitchell, S.R. & Rothberg, S.J. (2000) The role of the racket in high-speed tennis serves. *Sports Engineering,* **3** (2), 67-84.

Kurowski, P. M. (2004). *Finite element analysis for design engineers.* 1st ed., SAE International.

Lindsey C. (2006). String selection map 2006. *Racquet Sports Industry,* **34** (9), September/October, 22-28.

LSTC (2003) LS-DYNA version 970 Keywords users manual.

Mase, T. & Kersten, A.M. (2004) Experimental evaluation of a 3-D hyperelastic, rate-dependent golf ball constitutive model. *The Engineering of Sport 5,* International Sports Engineering Association, California, 238-244.

Menard, K.P. (2008). *Dynamic modulus analysis.* 2nd edn. USA: CRC Press.

Miller, K. (2006) *Axel Products [online],* last accessed on 06/07 2006 at URL: www.axelproducts.com.

Miller, S. (2007) The role of the ITF Science and Technical in evaluating and regulating tennis equipment. *Tennis Science and Technology 3,* **1,** International Tennis Federation, London, 1-19.

Miller, S. & Messner, S. (2003) On the dynamic coefficient of restitution of tennis balls. *Tennis Science and Technology 2, 1,* International Tennis Federation, London, 97-104.

Mitchell, S.,R., Jones, R. & King, M. (2000) Head speed vs. racket inertia in the tennis serve. *Sports Engineering, 3* (2), 99-110.

Mullins, L. (1969) Softening of rubber by deformation, Rubber Chem. Technol., 42, pp.339–362.

Ogden, R.W. (1984) Non-linear elastic deformations. Dover Publications, New York.

Penn (2009) Penn *[online]*, last accessed on 01/03 2009 at URL: www.pennracquet.com/factory.html

Peterson, W. & McPhee, J. (2008) Shape optimization of golf clubheads using finite element impact models. *The Engineering of Sport 7, 1,* Springer, France, 465-473.

Pratt, G. W. (2000). The interaction of the tennis ball and the court surface. In: Haake, S. j. and Coe, A. O. (eds.). *Tennis Science and Technology.* First ed., Blackwell science Ltd, 163-168.

Price, D.S., Jones, R. & Harland, A.R. (2006) Computational modelling of manually stitched soccer balls. *Journal of Materials; Design and application,* **220** (4), 259-268.

Price, D.S., Jones, R. & Harland, A.R. (2007) Advanced finite-element modelling of a 32-panel soccer ball. *Journal of Mechanical Engineering Science,* **221** (11), 1309-1319.

Price, D.S., Jones, R., Harland, A.R. & Silberschmidt, V.V. (2008) Viscoelasticity of multi-layer textile reinforced polymer composites used in soccer balls. *Journal of Materials Science,* **43** (8), 2833-2843.

Rayleigh, F R S (1877) On the Irregular Flight of a Tennis-Ball, *Vortex Motion,* 14-17.

Rose, P., Coe, A. & Haake, S. (2000) The variation of static and dynamic tennis ball properties with temperature. *Tennis Science and Technology,* **1,** Blackwell Science, London, 169-174.

Spurr, J. & Downing, M. (2007) Good vibrations: the effect of fundamental frequency on tennis. *Tennis Science and Technology 3,* **1,** International Tennis Federation, London, 103-112.

Smith, L.P. (1993). *The Language of rubber.* 1st edn. Butterworth-Heineman.

Smith, L. & Singh, H. (2008) An estimation of cricket bat performance. *The Engineering of Sport 7,* **1,** Springer, France, 475-482.

Walker, P. (1991). *Chambers Science and Technology Dictionary.* W & R Chambers Limited, 1008.

Widing, M. and Moeinzadeh, M. (1989). Nonlinear finite element analysis of a frame stiffened with tension members. *Computers and Structures,* **33** (1), 233-240.

Widing, M. and Moeinzadeh, M. (1990). Finite element modelling of a tennis racket with variable string patterns and tensions. *International Journal of Sport Biomechanics,* **6,** 78-91.

Zhang, Z (1999) Flexible camera calibration by viewing a plane from unknown orientations, *International Conference on Computer Vision* Corfu, Greece, pp. 666-673.

Personal bibliography

Allen, T., Goodwill, S. & Haake, S. (2008) Experimental validation of a FE model of a head-clamped tennis racket. *ANSYS UK Users Conference,* ANSYS, England.

Allen, T., Goodwill, S. & Haake, S. (2008) Experimental Validation of a Finite-element Model of a Tennis Ball Finite-element Model for Different Temperatures. *The Engineering of Sport 7,* **1,** Springer, France, 125-133.

Allen, T., Goodwill, S. & Haake, S. (2008) Experimental Validation of a Finite-element Model of a Tennis Racket String-bed. *The Engineering of Sport 7,* **1,** Springer, France, 115-123.

Allen, T., Goodwill, S. & Haake, S. (2007) Experimental validation of a tennis ball finite-element model. *Tennis Science and Technology 3,* **1,** International Tennis Federation, London, 21-30.

A   Ball model validation

A.1.   Ball model mesh convergence study

A FE model doesn't give an exact solution; it provides an estimation, the accuracy of which is determined by a number of factors. One easily adjustable variable which can have a large influence on the final solution is the mesh density. As the number of elements in the model increases the results should converge towards the exact solution, with increasing process requirements. The aim is not to achieve the most accurate solution, as this would be an inefficient use of the available computational power, but one which can be considered independent of mesh density. The convergence error in the solution can be quantified using Equation 9.1 (Becker, 2004; Kurowski 2004).

$$\text{Convergence error} = \left[\frac{\text{result}(n) - \text{result}(n-1)}{\text{result}(n)} \right]$$

Equation 9.1 Convergence error (Becker, 2004; Kurowski 2004).

An investigation was undertaken to determine the effect of mesh density on the maximum displacement and maximum von Mises stress in the ball. Perpendicular impacts were simulated with an initial velocity of 10 m·s^{-1}. The number of elements in the rigid surface was kept constant at 4800. Initially, an investigation into the effect of element length was undertaken. Firstly, the number of elements around the central circumference of the ball was set at 48 with 6 through the thickness, giving a total of 5184 (Table 1.1). The element length was then halved, quadrupling the total number, for each subsequent analysis, resulting in 20736 in the second and 82944 in the third simulation (Table 1.1). Following the study into element length, a second investigation into the effect of varying the number of elements through the thickness of the ball was undertaken. This involved three further simulations encompassing 4, 8 and 10 elements through the thickness, whilst keeping 96 around the central circumference. This gave a total of 13824, 20736, 27648 and 34560 elements as shown in Table 1.1.

Table 1.1 Mesh convergence study.

Simulation	No. of elements around circumference	No. of elements through the thickness	Total number of elements
1	48	6	5184
2	96	6	20736
3	192	6	82944
4	96	4	13824
5	96	8	27648
6	96	10	34560

The maximum displacement of the ball increased with decreasing element length (Figure 1.1a). The percentage convergence error for displacement was 1.5% between simulation 1 and 2, but only 0.4% between 2 and 3. This indicates that simulation 2 gives a good representation of the true displacement value. Simulation 2 also had a relatively short computation time of 16 minutes. The maximum stress in the ball also converged with the increasing element length and mesh density (Figure 1.1b). However, the percentage convergence error in the results is higher than of displacement, at -8.6% for the second and -2.5% for the third simulation. This indicates the requirement for a denser mesh if precise stress results are to be obtained and analysed.

Increasing the number of elements through the balls thickness from 6 to 8, provided convergence for displacement in agreement with simulation 3 (Figure 1.1a), at a greatly reduced simulation time of 55 minutes. However, increasing the number of elements through the thickness to 10 caused the maximum stress to drop by 0.1%. This apparent drop in accuracy may be due to the brick elements becoming too thin in relation to their length. There was also a large increase in computation time to 323 minutes (5.5 hours). Increasing the number of elements though the thickness also caused the stress to converge, but in a positive direction (Figure 1.1b). The amount of convergence between simulations was reduced in comparison with adjusting the element length. This may be a result of the mesh in simulation 2 being too course to provide accurate stress results, hence limiting the level of convergence possible within the range of elements for the current material models. An ideal simulation, balancing both accuracy and computation time, would consist of about 120 elements around the balls circumference with 8 through the thickness.
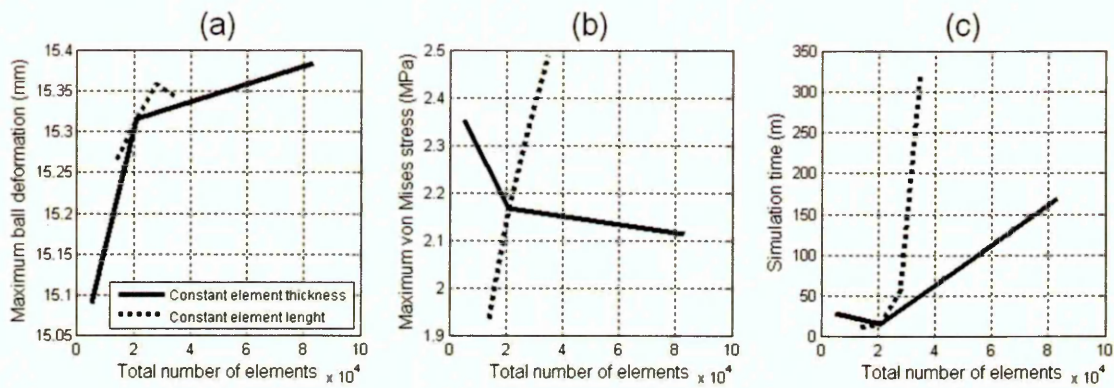
Figure 1.1 Number of elements in the ball model against a) maximum displacement of the ball and b) maximum von Mises stress in the ball.

A.2.   Impact rig validation

A brief validation of the impact rig is detailed in Downing (2007c). However, a more comprehensive validation was undertaken, for inbound velocities in the range from 5 to 30 $m \cdot s^{-1}$, using a *Phantom v4.2* high-speed video camera recording at 4000 fps. The bitmap images obtained from the camera were manually analysed using the bespoke analysis software *Richimas*. The time at the start and end of contact was assumed to be when the vertical location of the geometric centre of the ball equalled the position obtained from a ball resting on the surface. The root mean squared error (RMSE) between the camera and impact rig was 0.20 $m \cdot s^{-1}$ for inbound velocity, 0.26 $m \cdot s^{-1}$ for rebound velocity and 0.4 ms for contact time. The relatively large discrepancy between the two methods of measuring contact time was attributed to errors in using a camera to determine the end of contact, as a result of the deformation of the ball (Goodwill, 2000).

A.3.   Frequency analysis
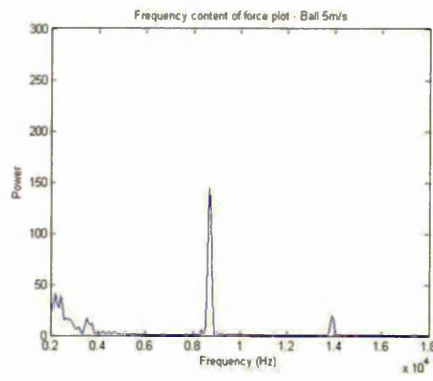

244
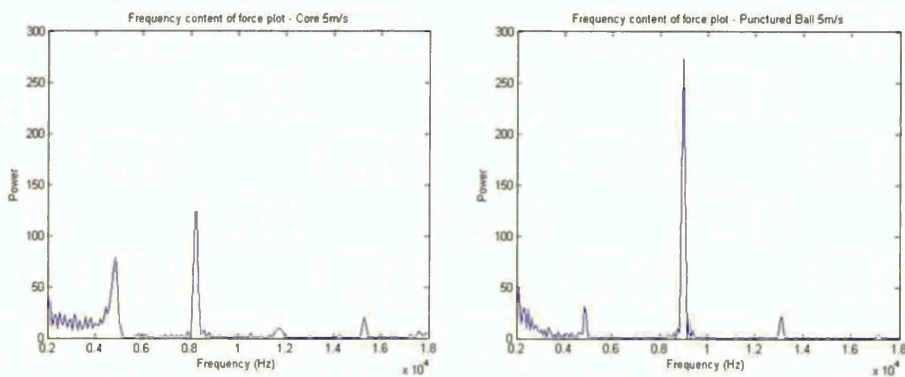
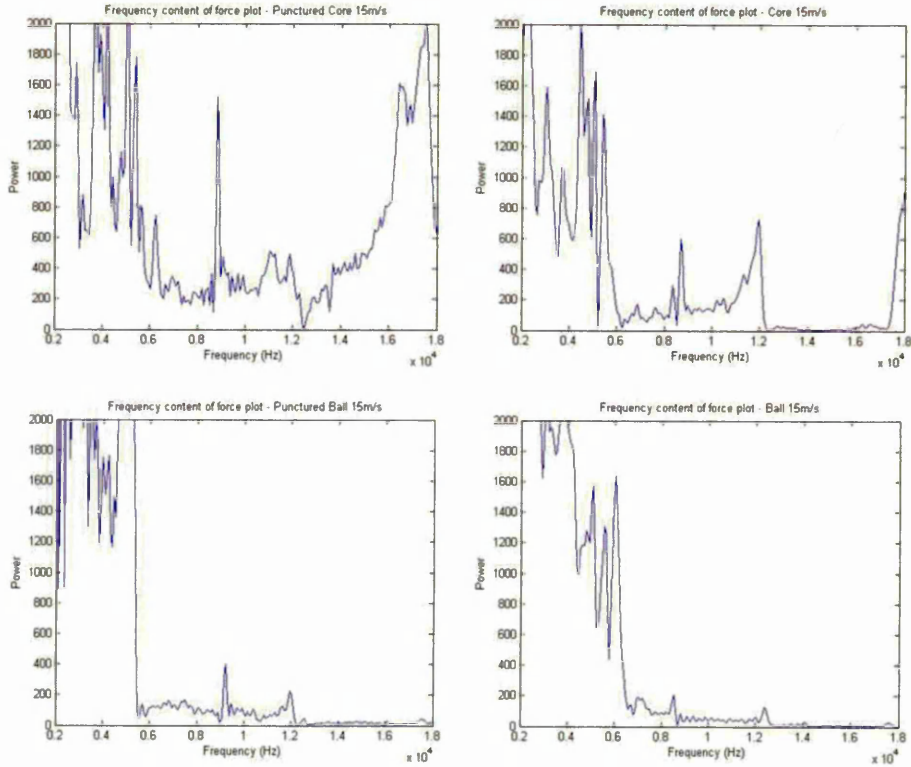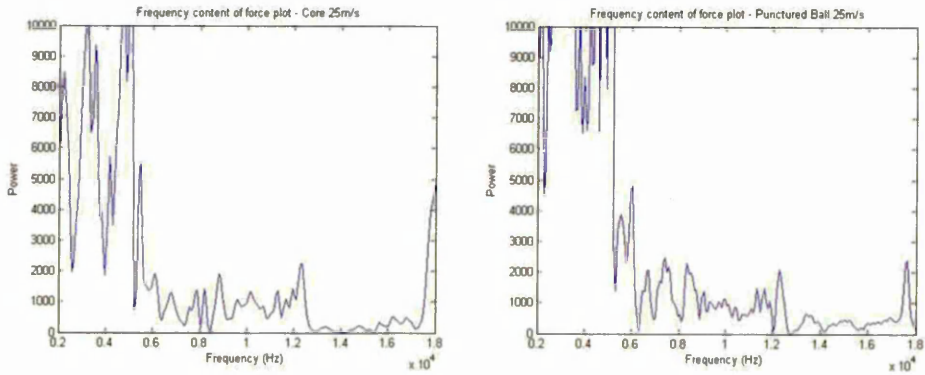**Figure 1.2** Frequency results for a 5 m·s⁻¹ impact on a force plate.

Figure 1.3 Frequency results for a 15 m·s⁻¹ impact on a force plate.
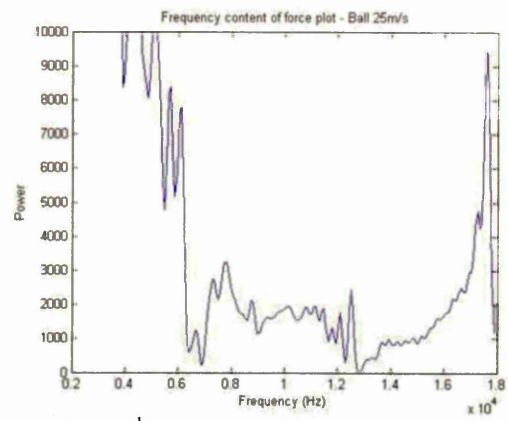

245

Figure 1.4 Frequency results for a 25 m·s^{-1} impact on a force plate.

B   Head-clamped racket model

B.1.   Calculating the impact position on the string-bed

The location of the GSC must be known for the impact distance of the ball from the GSC to be calculated. For the 40° impacts the horizontal position of the GSC was assumed to be the same as that of the impact rig's release pin, whilst the vertical position was obtained from the location of the strings (Figure 1.5). These 2 positions were obtained from the opening image of the first 3 impacts; the mean values were used when calculating the impact position. The impact position, relative to the GSC, was calculated from the initial location of the ball upon exiting the BOLA and its inbound angle, as shown in Figure 4.7, on page 99.

Vertical position of centre of stringbed

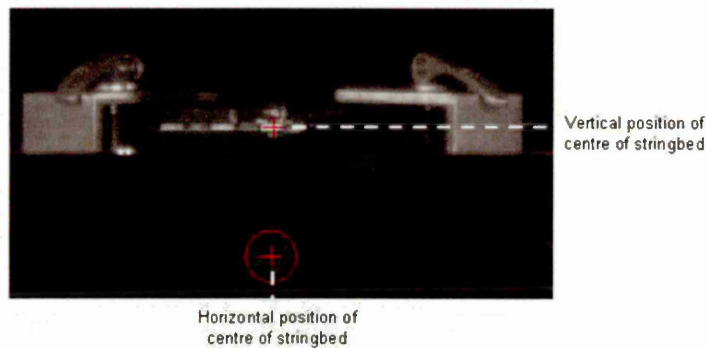Horizontal position of centre of stringbed

Figure 1.5 Horizontal and vertical positions of the centre of the string-bed.

60° Impacts

For an impact angle of 60° the racket was tilted 20° about the pivot, away from the air-cannon (Figure 1.6).

Figure 1.6 Set-up for 60° impacts, showing the location of the release pin and pivot.

The following steps were undertaken to obtain the impact distance of the ball from the GSC;

1. The location of the string-bed centre was obtained.
2. The impact distance along the string-bed from its geometric centre was obtained.

Location of GSC

The horizontal and vertical positions of the release pin and pivot were obtained and used to calculate the location of the centre of the string-bed (Figure 1.6). The positions of these points were obtained from the first 3 images for each set of impacts and the mean values were used in the calculations.

Location of GSC - Horizontal position

X_B in Figure 1.7 denotes the horizontal distance, from the point on the string-bed which was directly above the pivot before it was tilted (Z), to the pivot after tilting. X_B was calculated from the vertical distance from the centre of the pivot to the string-bed, when it was horizontal (r), and the angle (20°) between r and the vertical (Figure 1.7). Following this, the horizontal distance from the GSC to point Z (X_C) was calculated from the angle between the string-bed and horizontal (20°) and the horizontal distance between the release pin and pivot (X_A). Finally, the horizontal distance from the pivot to the GSC (X_D) was calculated from the addition of X_B and X_C.
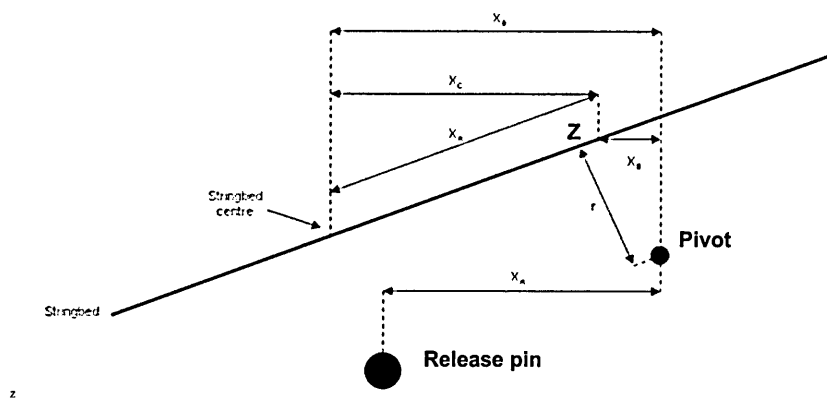
248

Figure 1.7 Calculating the horizontal location of the centre of the string-bed, for 60° impacts.

Location of GSC - Vertical position

The vertical distance (Y_B), from the point Z to the pivot was calculated from r and the angle between r and the vertical (20°) (Figure 1.8). The vertical distance from point Z to the GSC (Y_C) was obtained from X_A and the angle between the string-bed and the horizontal (20°). The vertical distance from the centre of the string-bed to the pivot (Y_D) was calculated, by subtracting Y_C from Y_B.
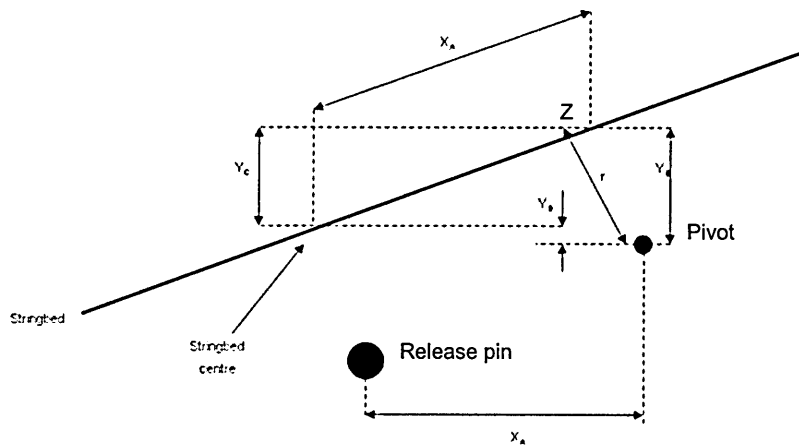

Figure 1.8 Calculating the vertical location of the centre of the string-bed, for 60° impacts.

Impact distance from the GSC

The distance from the GSC to the point of impact on the horizontal plane which passes through the GSC (X_3) was calculated, in the same way as the 40° impact (Figure 1.9) (*A description for 40° impacts is on page 99*).
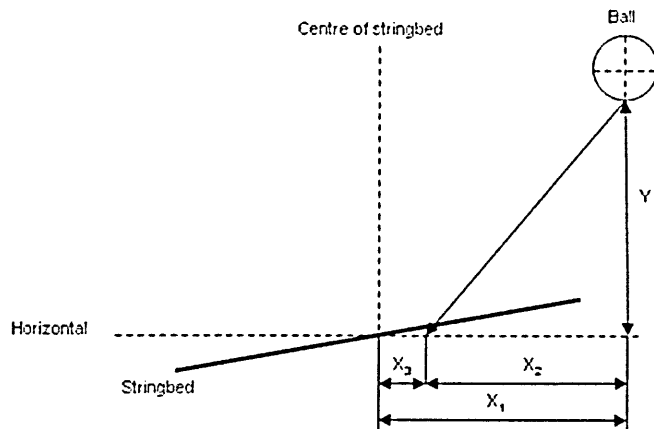
Figure 1.9 Calculating impact position at 60° inbound angle

The distance of the impact along the string-bed from its centre (X_4) (Figure 1.10) was calculated using the sine rule (Equation 1.2) (a = 20°, c = 90 + inbound angle).
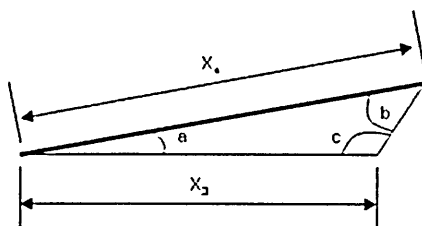
Figure 1.10 Calculating impact position at 60° inbound angle

$$X4 = \frac{X3 \times Sinc}{Sinb}$$

Equation 1.2 Calculating the distance from the impact along the string-bed from its centre, for 60° impacts.

20° impacts

For the 20° impacts the string-bed was tilted about the pivot towards the air-cannon (Figure 1.11). As with the 60° impacts the first stage was to obtain the location of the GSC. Following this the impact distance along the string-bed from its geometric centre was obtained.
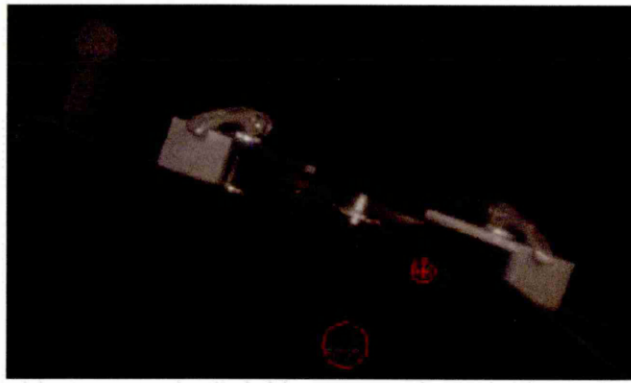
Figure 1.11 Set-up for 20° impacts, showing the location of the release pin and pivot.

Location of GSC - Horizontal position

The horizontal position of the centre of the string-bed was calculated using a similar method to the set-up for 60° impacts (Figure 1.12). The main difference was X_B was subtracted from X_C to obtain X_D, as the setup was tilted in the opposite direction.
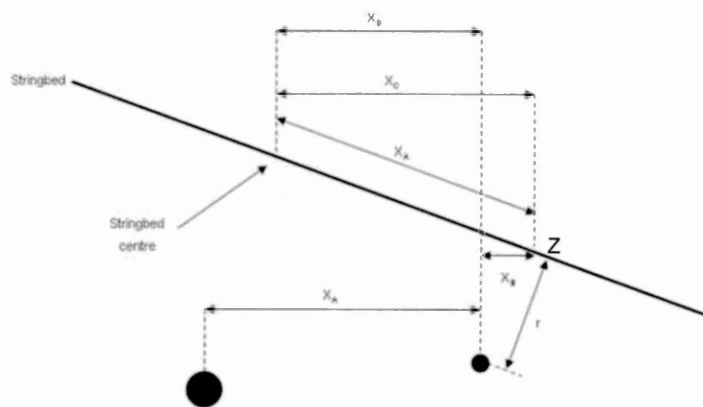
Figure 1.12 Obtaining the horizontal position of the centre of the string-bed for 20° impacts.

Location of GSC - Vertical position

The vertical position of the centre of the string-bed was obtained using a similar method as for the 60° set-up. The main difference was that Y_D was calculated from the addition of Y_B and Y_C (Figure 1.13).
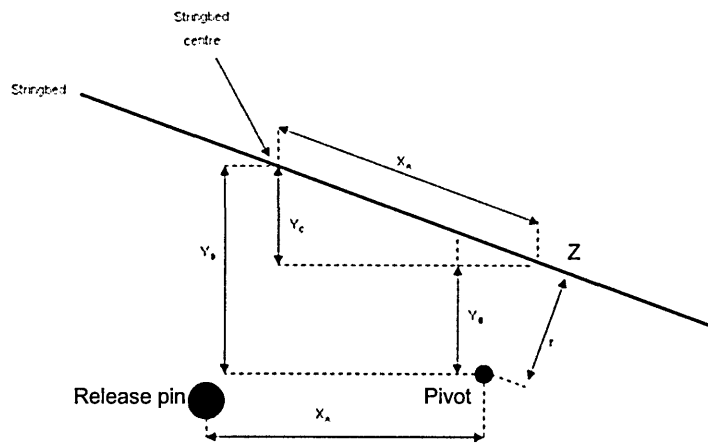
Figure 1.13 Obtaining the horizontal position of the centre of the string-bed for 20° impacts.

The impact distance from the GSC along the horizontal was calculated in the same way as for the 60° impacts (Figure 1.14).
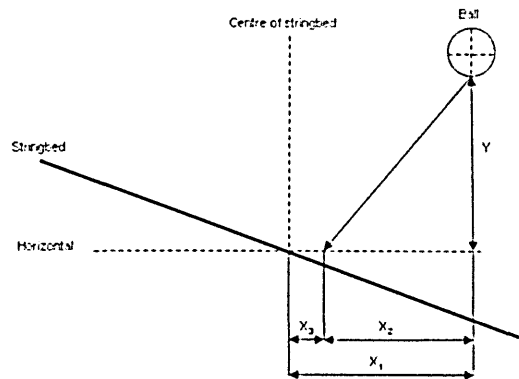
Figure 1.14 Calculating the impact distance from the string-bed along the horizontal axis for the 20° impacts.

The distance of the impact along the string-bed (X_4) (Figure 1.15) was calculated using Equation 1.2 (a = 20°, c = 90 - inbound angle).

Figure 1.15 Calculating impact position at 60° inbound angle.

B.2.   Effect of inbound spin

The inbound velocity, angle and impact location of balls projected onto a head-clamped racket have all been found to be dependent on inbound spin (Figure 4.19, page 118). An investigation was undertaken to determine the effect of any changes in inbound velocity, angle and impact location, as a result of inbound spin. This investigation was undertaken using the impacts at the centre of the string-bed. Linear trend lines were fitted to the experimental data (Figure 1.16). The equations of these line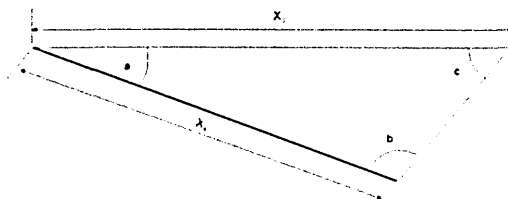s were used to obtain inbound velocities, angles and impact locations for inbound spin rates in the range from 0 to 600 rad·s^{-1} (Table 1.2). FE simulations were undertaken for inbound spins of 0 and 600 rad·s^{-1}, using the conditions in Table 1.2.
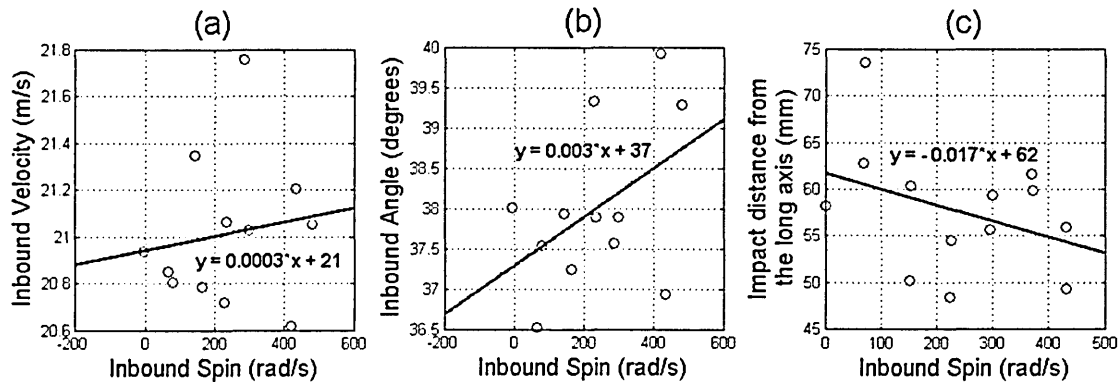
Figure 1.16 Effect of inbound spin inbound on a) velocity, b) angle and c) impact location for the centre impacts

Table 1.2 Calculated inbound velocity and impact location

Inbound spin	FE inbound velocity (m·s^{-1})	FE inbound angle (degrees)	FE impact location (mm)
0	20.94	37.30	33.44
200	21.00	37.90	28.71
400	21.06	38.50	24.83
600	21.12	39.10	20.95
Average	*21.03*	*38.20*	*26.98*
Range	*0.18*	*1.8*	*-12.50*

Figure 1.17 shows that there was very little difference in the results obtained from the model with the updated inbound conditions, in comparison to the original model.

Figure 1.17 Rebound a) velocity, b) angle and c) spin. Inbound velocity = 30 m·s^{-1}, inbound angle = 40°.

B.3.   Difference between string-bed and head-clamped racket model

An investigation was undertaken to determine the cause of the difference in the results obtained from the string-bed and head-clamped racket models. The tip impacts, with an inbound backspin of 600 rad·s^{-1}, were used in the investigation because there was a relatively large difference between the two FE models. It was predicted that the method used to attach the strings to the frame in the head-clamped racket model may be the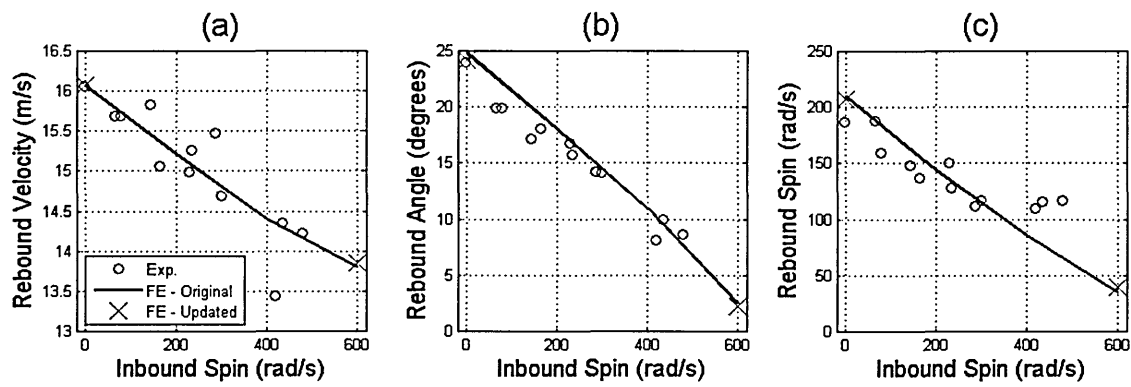 cause of the difference in results. Head-clamped racket model simulations were undertaken with slight modifications. The details of these modifications are listed below;

1. The tied contact was removed and the rigid cylinders were fully constrained for the entirely of the transient phase of the simulation.
2. The same as above except the tied contact was replaced with normal contact with a COF of 0.
3. The thickness of the shell elements which were used for the tied contact was increased from 1 to 2 mm.

It was also predicted that the difference in the convergence of the simulations during the dynamic relaxation phase of the simulations could also have been causing the discrepancy in the results. The following simulations were undertaken.

1. String-bed model with a convergence tolerance for dynamic relaxation of 0.1. This is the same as in the original head-clamped racket model.
2. Head-clamped racket model with a convergence tolerance for dynamic relaxation of 0.07. It was not possible to get the simulation to converge within a realistic time frame using a tolerance of 0.01 as in the original string-bed model.

Figure 1.18 shows none of the modifications made to the models had a noticeable effect on the horizontal rebound velocity of the ball.
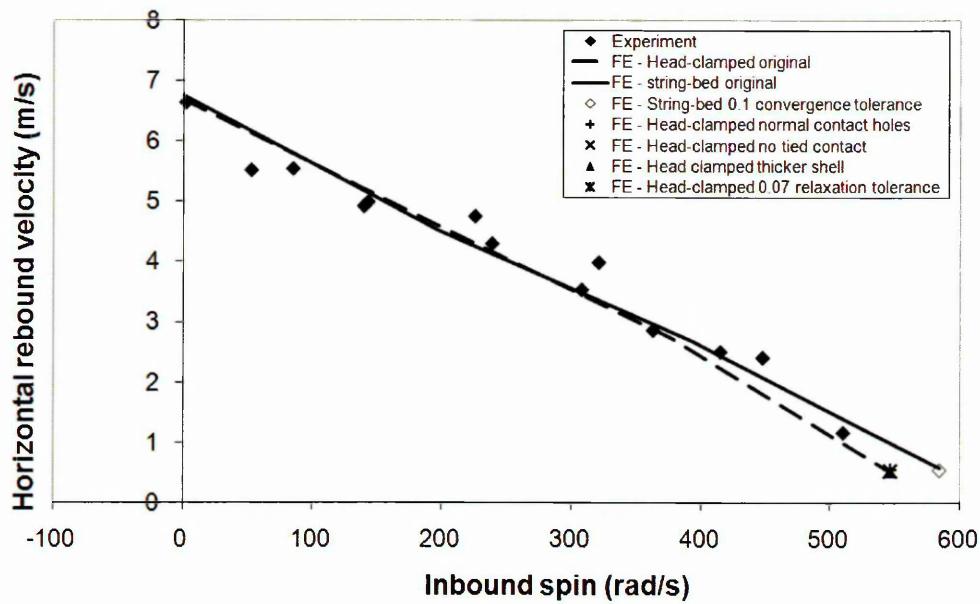
Figure 1.18 Horizontal rebound velocity

Figure 1.19 shows that all of the modifications had an effect on the vertical rebound velocity of the ball. Both of the head-clamped racket simulations with tied contact removed were in good agreement with the results obtained from the string-bed model. The head-clamped racket model with the thicker shell was also in better agreement with the string-bed model. These findings indicate that method used to attach the strings to the racket frame was affecting the results. Adjusting the convergence tolerance also increased agreement between the two models. This implies that the discrepancy in the results could be due to convergence.

255
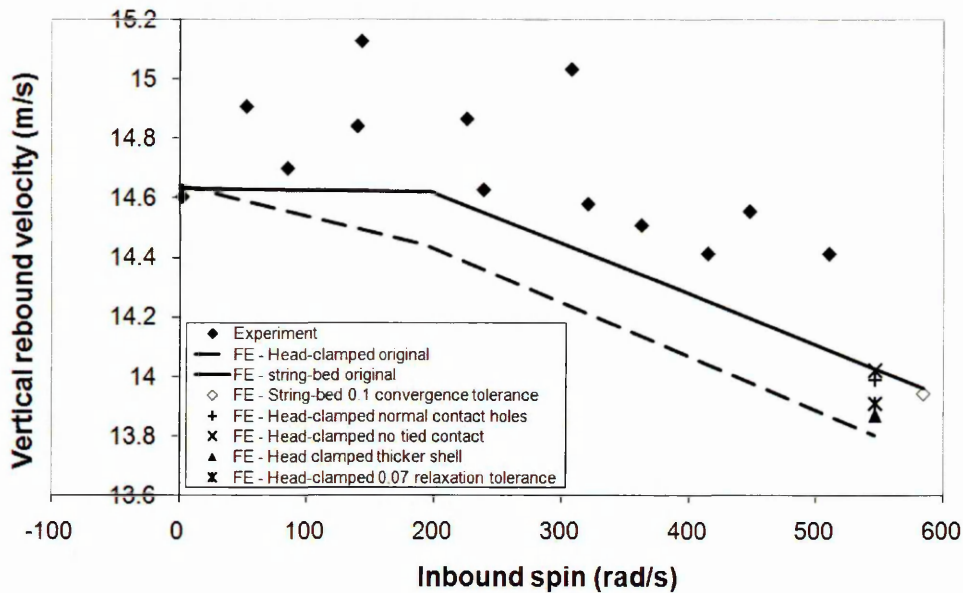
Figure 1.19 Vertical rebound velocity

Figure 1.20 shows that increasing the shell thickness very slightly increased the agreement between the two models. The remaining modifications all slightly decreased the agreement between the two models. This contradicts the results obtained for vertical rebound velocity.
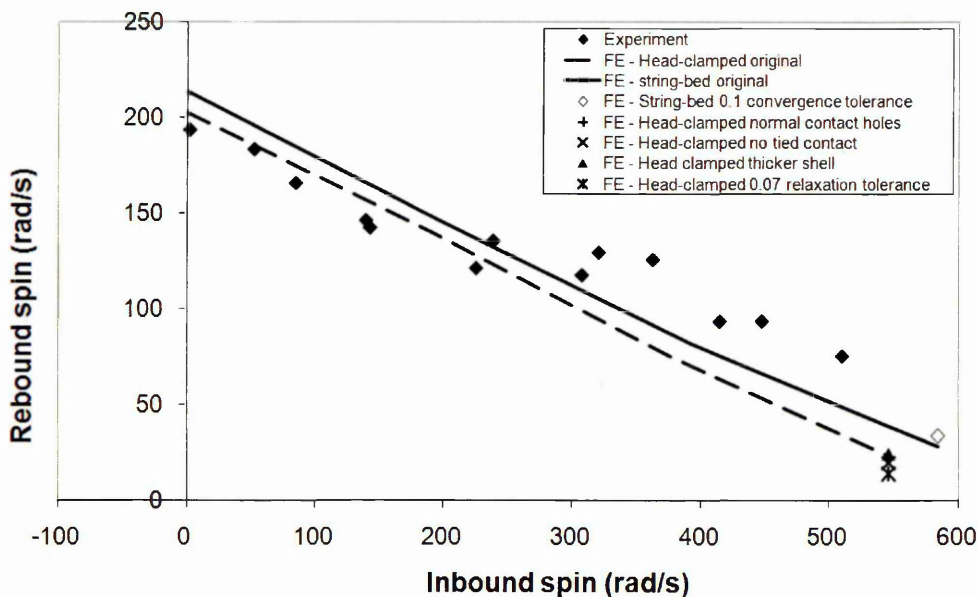
Figure 1.20 Rebound spin

This investigation has highlighted that both the convergence of the models and the tied contact between the racket and strings can have a slight effect on the rebound characteristics of the ball. However, only increasing the shell thickness,

256

in the areas were the strings were tied to the racket frame, improved the agreement between the results obtained from the two models for both rebound velocity and spin. There were apparent contradictions between the results obtained for rebound velocity and spin when the convergence tolerances of the models were adjusted. It is predicted that with this particular model increasing the convergence tolerance may simply lower the accuracy of the simulations. Overall it is predicted that the discrepancy between the two models is likely to be down to differences in convergence, geometry and mesh.

C   Alternative spin calculation

The number of quarter revolutions was counted, assuming the markers to be evenly spaced around the circumference of the ball. The ball had to have rotated at least a half turn for it to be included in the analysis. Figure 1.21a shows there was good agreement between the spin measured from the left and right camera using this method. Although, the right camera appears to produce slightly higher spin rates; the reason for this has been explained previously in section 5.3.1. The RMSE between the spin measured from the two cameras was 28.4 rad·s^{-1}. Figure 1.21b shows a comparison of the spin measured from the two methods. The RMSE between the spin measured from the two methods was 36.4 rad·s^{-1}.
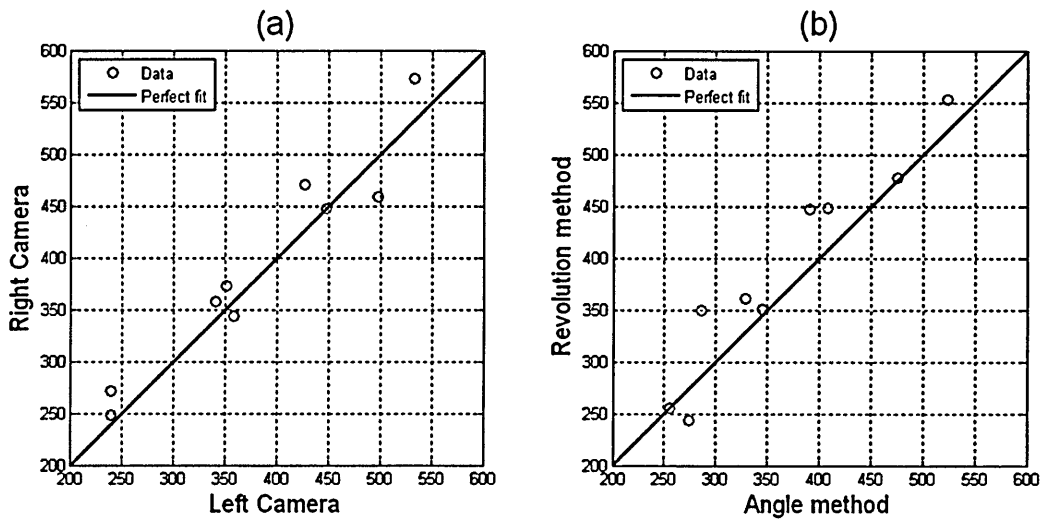

Figure 1.21 a) Comparison of measured spin rates from each camera using the revolution method and b) comparison of spin between the angle and revolution method

D   Material testing of tennis strings

Method

Cross *et al.* (2000) proposed a method for determining the dynamic stiffness (Equation 1.3) of tennis strings. The test involves striking a tensioned string with a hammer and measuring the change in tension and perpendicular displacement. The change in length of the string is calculated from its perpendicular displacement (Figure 1.22). Cross *et al.* measured the impact force using an s-type force sensor. It is predicted that there may be errors as a result of using a force sensor which is designed for measuring quasistatic loads. Therefore, the experiment was undertaken using a *Kistler* piezoelectric force sensor in place of the s-type force sensor.

$$\text{Dynamic stiffness} = \frac{\text{Change in force}}{\text{Change in length}}$$

Equation 1.3 Dynamic stiffness
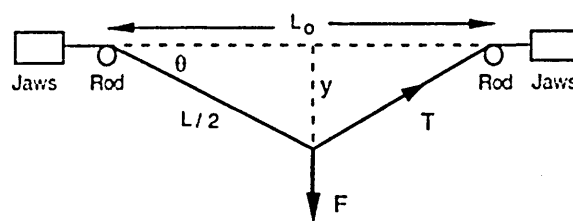
$$L = (L_0^2 + 4y^2)^{1/2}$$

$$T = T_0 + k(L - L_0)$$

Figure 1.22 Calculating tension (T) and extended length (L) (Cross *et al.*, 2000).

The results were compared against results from previous tests using the s-type force sensor (Table 1.3). This was to provide an indication as to whether the type of force sensor influences the results. The Young's modulus was calculated from the dynamic stiffness using the length and cross sectional area of the string (Equation 1.4).

Table 1.3 Previous results

	Displacement y (mm)	Impact force (N)	Dynamic modulus (kN·m⁻¹)	Length before impact (m)	E (GN·m⁻²)
Prince Data	29	146	26.1	0.36	6.8
Lindsey (2006)	-	-	30.8	0.32	7.2

Table header uses superscripts: Dynamic modulus (kN·m^{-1}) and E (GN·m^{-2}).

$$\text{Young's modulus} = \frac{\text{Dynamic stiffness} \times \text{Length}}{\text{Area}}$$

Equation 1.4 Calculating Young's modulus

The method used in this investigation is based on the one detailed by Cross *et al.* (2000) with a few modifications. A modified impact rig was used in this investigation (Figure 1.23). The main difference is that the wooden pendulum was replaced with an aluminium one. Cross *et al.* stated the mass of the hammer head was 0.292 kg and the effective mass of the hammer head, wood beam and optical grid was 0.45 kg. The mass of the hammer head in the modified rig was measured as 0.4 kg. The aluminium beam had a diameter and length of 0.015 and 0.55 m, respectively. Assuming a density of 2800 kg·m⁻³ the mass of the beam was calculated as 1.1 kg. The total mass of the beam and hammer head was 1.5 kg. *It was not possible to measure the mass of the beam as it was securely attached to the impact rig.*

Figure 1.23 Modified impact rig (Hammer head replaced with bolt)

The velocity of the hammer and displacement of the string were measuring using a *Phantom v4.2* high-speed video camera, recording at 400 fps (Figure 1.24). The transverse velocity of the hammer head was calculated from the angular velocity of the pendulum. The distance from the pivot to the string

was 0.6 m. The maximum displacement of the string was calculated from the largest angle which the pendulum reached during impact. To ensure high accuracy, a still image was obtained when the pendulum was resting against a tensioned string. This image was used to obtain the angle of the pendulum relative to vertical at the point of impact. As the velocity and displacement were calculated using angles calibration was not required.

Figure 1.24 Camera set-up

Cross *et al.* held the string at maximum tension (275 N) for 1000 s (16.7 minutes) before subjecting it to 10 impacts from the hammer. The dynamic stiffness was then obtained from the average results of the 10 impacts. In this investigation the string was tensioned to 275 N and impacted with the hammer without a relaxation period. A relaxation phase was not used as it is predicted that drift on the piezoelectric sensor would have resulted in errors in the force readings. The string was impacted 5 times at the original velocity (2.6 $m \cdot s^{-1}$ and 5 times at a higher velocity. The string tension was increased back to 275 N before each impact and the dynamic stiffness was calculated separately for each impact.

The effect of the mass of the pendulum was also analysed. The 0.4 kg hammer head was replaced with a 0.032 kg bolt. The bolt was threaded into the end of the aluminium beam, effectively extending the length of the beam. The total mass of the aluminium beam and bolt was 1.1 kg. The lighter pendulum resulted in a reduced contact time. Therefore, the frame rate of the high speed video camera was increased to 1000 fps. Each of the experiments was repeated three times.

Results

Table 1.4 shows that the quasistatic Young's modulus of the strings was calculated as 1.4 GPa, which is just outside the expected range for Nylon of 2-4 GPa.

Table 1.4 Quasi-static Young's modulus

Force (N)	Cross sectional area (m^2)	Stress ($N \cdot m^{-2}$)	Initial string length (m)	Extension (m)	Strain	Young's modulus ($GN \cdot m^{-2}$)
267.4	1.37×10^{-6}	1.95×10^{8}	0.357	0.05	0.140	1.4

A reliability study was undertaken to determine the level of human error when manually measuring the velocity and displacement of the pendulum, using *Richimas v3*. A single impact was selected and analysed 10 times. The standard deviation (SD) for velocity was 0.1 $m \cdot s^{-1}$ and the SD for displacement was 1.3 mm, for the investigation with the original pendulum. This resulted in a SD of 1.9 $kN \cdot m^{-1}$ for dynamic stiffness and 0.6 GPa for the Young's modulus. For the investigation with the lighter pendulum, the SD for velocity and displacement was 0.1 $m \cdot s^{-1}$ and 1.1 mm, respectively. These are virtually identical to the values obtained in the original investigation. This resulted in a SD for dynamic modulus and Young's modulus of 3.7 and 1.2 GPa, respectively. These are approximately double the values of the original study, which is because the string was displacing less for the impact with the 1.1 kg pendulum. When calculating the Young's modulus of the strings a length of 0.42 m was used. This was the length of all three of the strings, following loading to 275 N from their initial length of 0.375 m.

Table 1.5 shows the results obtained when the strings were impacted at a velocity similar to that used by Cross *et al.* (2000). The velocity used by Cross *et al.* was 2.63 $m \cdot s^{-1}$ and the mean velocity used in this investigation was 2.84 ± 0.1 $m \cdot s^{-1}$ (Table 1.5). The mean impact force at 126 ± 17 N (Table 1.5) was similar, although a little smaller, than the value provided by the manufacturer 146 N (Table 1.3). The mean displacement (y in Figure 1.22) at 29 ± 1 mm was identical to the value of 29 mm provided by the manufacturer (Table 1.3). The mean dynamic modulus obtained in this investigation, at 22.4 ± 3.4 $kN \cdot m^{-1}$, was slightly lower than the value of 26 $kN \cdot m^{-1}$ measured by the manufacturer. The

mean impact force, displacement and dynamic modulus were all in line with the results obtained by Cross *et al.* (2000) for Nylon strings.

Table 1.5 Overall results - original velocity

	Initial force (N)	Max. force (N)	Force (N)	Velocity (m·s⁻¹)	Displacement (mm)	Extension (mm)	Dynamic stiffness (k N·m⁻¹)	E (GPa)
Mean	266.80	392.40	125.60	2.84	29.2	5.6	22.44	6.97
SD	16.24	14.11	16.73	0.10	1.1	0.4	3.40	1.06

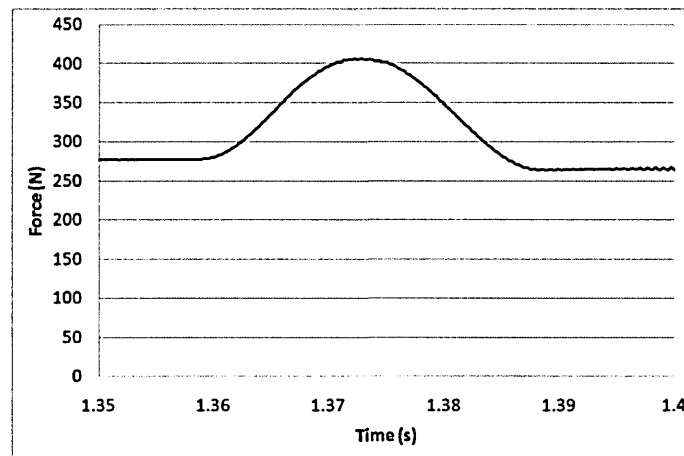Figure 1.25 shows an example of a force plot from an impact at the original velocity (2.8 m·s⁻¹).

Figure 1.25 Force versus time for the original impact velocity.

A sensitivity investigation was undertaken to determine the influence of changing the displacement of the strings on the dynamic modulus. The results from a single impact were selected and the maximum displacement was increased and decreased by 3 mm respectively (Table 1.6). Table 1.6 shows that a small change in the displacement of the string (*approx. 10%*) results in a relatively large change in the dynamic modulus. This indicates that the dynamic modulus is moderately susceptible to errors in the tracking method.

Table 1.6 Displacement sensitivity study - String 1 impact 4 original velocity

	Initial force (N)	Max. force (N)	Force (N)	Velocity (m·s⁻¹)	Displacement (mm)	Extension (mm)	Dynamic stiffness (kN·m⁻¹)	E (GPa)
Original displacement	279	402	123.0	2.9	29.6	5.8	21.2	6.6
- 3mm displacement	279	402	123.0	2.8	32.6	7.0	17.5	5.4
+ 3mm displacement	279	402	123.0	2.9	26.6	4.7	26.2	8.1

Table 1.7 shows the mean results obtained when the string was impacted with the 0.4 kg pendulum, at the higher velocity of 3.6 ± 0.1 m·s⁻¹. The mean dynamic modulus and Young's modulus were both within 3.4% of those obtained at the lower velocity (Table 1.5). This indicates that the strings have linear material properties within the range tested.

Table 1.7 Overall results for the 0.4 kg pendulum at the higher velocity

	Initial force (N)	Max. force (N)	Force (N)	Velocity (m·s⁻¹)	Displacement (mm)	Extension (mm)	Dynamic stiffness (kN·m⁻¹)	E (GPa)
Mean	258.0	445.6	187.6	3.6	35.2	8.1	23.2	7.2
SD	20.0	12.8	11.3	0.1	1.2	0.6	1.8	0.6

Figure 1.26 shows a force plot obtained from an impact on a string at the higher velocity of 3.6 m·s⁻¹. The force plot is similar to one obtained for the impact at the original velocity (Figure 1.25). The contact time for all the force plots is approximately 30 ms, which is similar to the values published by Cross *et al* (2000). A contact time of 30 ms is approximately 6 times longer than the typical contact time between a tennis ball and racket.
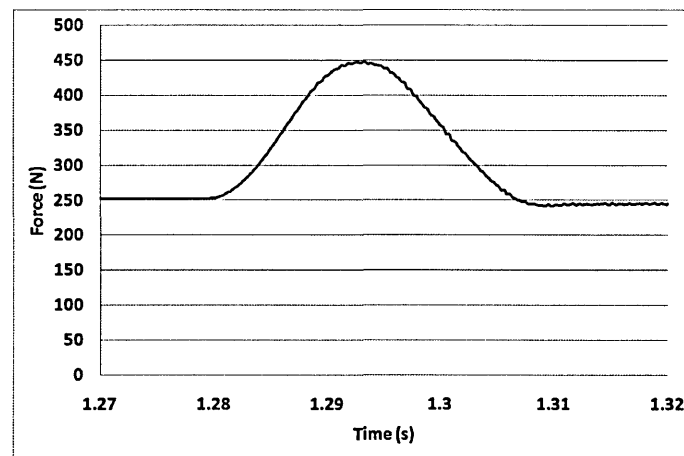
Figure 1.26 Force plot - String 1 impact 5 higher velocity

Table 1.8 shows the overall results for the investigation with the 1.1 kg pendulum. The overall dynamic modulus was 30 ± 3.0 kN·m^{-1}, which was slightly larger than the value of 23 ± 1.8 kN·m^{-1} obtained with the heavy pendulum (Table 1.7, page 264). The Young's modulus was also slightly higher for this investigation at 9.3 ± 0.9 GPa, in comparison to 7.2 ± 0.5 GPa.

Table 1.8 Overall results

	Initial force (N)	Max. force (N)	Force (N)	Velocity (m·s^{-1})	Displacement (mm)	Extension (mm)	Dynamic stiffness (kN·m^{-1})	E (GPa)
Mean	277.5	346.3	68.7	4.0	18.7	2.3	30.0	9.3
SD	5.4	3.7	3.3	0.2	1.0	0.3	3.0	0.9

Figure 1.27 shows a force plot from an impact with the modified pendulum (*hammer head replaced with bolt*). The contact time for the impact is approximately 15 ms, which is around half the value for the impacts with the 1.5 kg pendulum (Figure 1.26). 15 ms is closer to the required contact time of 5 ms.
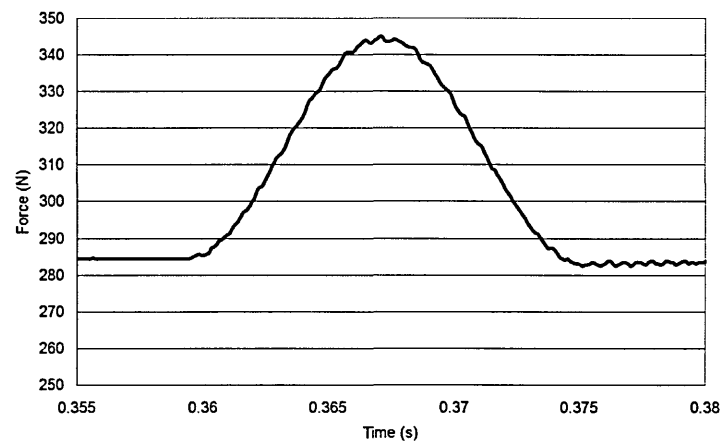
265

Figure 1.27 Force plot for an impact with the hammer head replaced by a bolt

Cross *et al.* (2000) stated that an impact between a tennis ball and racket results in a strain rate of approximately 40 000 $mm \cdot m^{-1}$ (0.67 $m \cdot s^{-1}$). Table 1.9 shows an estimate of the time-averaged strain rates for the three investigations. The impact with the 1.1 kg pendulum had the lowest strain rate at 0.3 $m \cdot s^{-1}$, which was also lower than the value of 0.67 $m \cdot s^{-1}$ stated by Cross *et al.* (2000).

Table 1.9 Estimation of strain rate

Study	Approx. contact time (s)	Extension (m)	Strain rate ($m \cdot s^{-1}$)
1.5 kg pendulum - 2.8 $m \cdot s^{-1}$	0.030	0.0056	0.38
1.5 kg pendulum - 3.6 $m \cdot s^{-1}$	0.030	0.0081	0.54
1.1 kg pendulum - 4.0 $m \cdot s^{-1}$	0.015	0.0023	0.31

Conclusion

The dynamic modulus and Young's modulus obtained using the 1.5 kg pendulum and a piezoelectric force sensor were virtually identical to those obtained from previous investigations. This indicates that an s-type load cell is as suitable as a piezoelectric force sensor for this experiment. The impact duration in this investigation (*approx. 30 ms*) was approximately 6 times longer than when a ball impacts with a racket (*approx. 5 ms*). Using a lighter pendulum (1.1 kg) decreased the contact time to approximately 15 ms, which was closer to the required value. Using a lower mass pendulum increased the Young's modulus of the strings from 7.2 ± 0.6 GPa to 9.3 ± 0.9 GPa. However, there were large SD's in the results, due to uncertainties in the displacement measurements.

In this investigation the contact time was 15 ms which is still three times larger than the required value of 5 ms. The contact time could be decreased by using a pendulum with a lower mass. This could be achieved by using an aluminium bar with a lower diameter. The inbound velocity should also be faster to increase the strain rate and provide more realistic displacement and force results.